

Design, Synthesis and Application
of Novel Disulfide-Intercalation Agents
for the
Site-Selective Modification of
Peptides and Proteins

Dissertation zur Erlangung des Grades „Doktor der Naturwissenschaften“ im Fachbereich
Chemie, Pharmazie und Geowissenschaften der Johannes Gutenberg-Universität in Mainz

vorgelegt von

Christoph Freidel



Mainz, 2017

Dekan:

1. Berichterstatter:

2. Berichterstatter:

Tag der mündlichen Prüfung:

Die vorliegende Arbeit wurde in der Zeit von September 2013 bis Juli 2016 in der Arbeitsgruppe von [REDACTED] und [REDACTED] im Max-Planck-Institut für Polymerforschung in Mainz durchgeführt.

[REDACTED] und [REDACTED]
möchte ich herzlich für die Möglichkeit danken, auf diesem herausfordernden und faszinierenden Projekt arbeiten zu dürfen. Ihre wissenschaftliche und persönliche Unterstützung sowie zahlreiche fruchtbare Diskussionen und Anregungen haben mich stets motiviert.

Für meine Eltern und Geschwister

*Für den gläubigen Menschen steht Gott am Anfang, für den Wissenschaftler am Ende
aller seiner Überlegungen.*

*Die Naturwissenschaft braucht der Mensch zum Erkennen,
die Religion zum Handeln,
weil wir mit unseren Willensentscheidungen nicht warten können,
bis die Erkenntnisse vollständig, und bis wir allwissend geworden sind.*

Max Planck (1858-1947), deutscher Physiker

List of most used abbreviations

A	adenine
ACN	acetonitrile
ACTH	adrenocorticotropic hormone
BOC	tert-butyloxycarbonyl
bp	base pairs
°C	celsius
C	cytosine
CBI	cyclopropabenzindole
Cy5	cyanine 5 dye
Cys	cysteine
CD	circular dichroism
COSY	correlation spectroscopy
CuAAC	copper(I)-catalyzed alkyne-azide cycloaddition
DCM	dichloromethane
DIC	<i>N,N'</i> -Diisopropylcarbodiimide
DIPEA	<i>N,N'</i> -Diisopropylethylamine
DMF	dimethylformamide
DMSO	dimethyl sulfoxide
DNA	deoxyribonucleic acid
DNR	daunorubicin
DOSY	diffusion-ordered spectroscopy
DTT	dithiothreitol
Dox	doxorubicin
DPBS	Dulbecco's Phosphate Buffered Saline
dsDNA	double stranded deoxyribonucleic acid
DTMP	2'-deoxy thymidine 5'-monophosphate
e.g.	exempli gratia
eq	equivalent
EDC	1-Ethyl-3-(3dimethylaminopropyl)-carbodiimide
EGFR	epidermal growth factor receptor
EPR	enhanced permeation and retention effect
EMSA	electrophoretic mobility shift assay
ESI	electrospray ionization
EtOH	ethanol
Et ₂ O	diethyl ether

EtOAc	ethyl acetate
et al.	et alii
F	phenylalanine
FCS	fetal calf serum
FD	field desorption
FDA	food and drug administration
g	gram
G	guanine
GFP	green fluorescent protein
GHIH	growth hormone inhibiting hormone
GPC	gel permeation chromatography
GSH	glutathione
HATU	1-[Bis(dimethylamino)methylene]-1H-1,2,3-triazolo[4,5-b]pyridinium 3-oxid hexafluorophosphate
HMBC	heteronuclear multiple bond correlation
HPLC	high pressure liquid chromatography
HSQC	heteronuclear single quantum coherence
IC ₅₀	concentration of a drug that is required for 50% inhibition
ITC	isothermal titration calorimetry
J	coupling constant (NMR)
JGU	Johannes-Gutenberg Universität
K	lysine
K _a	binding affinity constant
K _d	binding dissociation constant
kDa	kilo Dalton
KGaA	Kommanditgesellschaft auf Aktien
kV	kilo volt
m	milli
M	mol
MALDI	matrix-assisted laser desorption ionization
MeOH	methanol
MDR	multi drug resistance
Milli-Q water	trademark created by Millipore Corporation, ultrapure water
min	minute
MPI	Max-Planck Institute

MS	mass spectrometry
MW	molecular weight
MST	Microscale Thermophoresis
m/z	mass-to-charge ratio
NaOH	sodium hydroxide
n	number
NHS	N-hydroxysuccinimide
NIR	near-infrared
nm	nanometer
NMM	N-Methylmorpholine
NMP	N-methyl-2-pyrrolidone
NMR	nuclear magnetic resonance
2D NMR	two dimensional NMR
NOESY	nuclear overhauser effect spectroscopy
NP	nanoparticle
OD	optical density
PDI	perylene diimide
PMI	perylene monoimide
PEG	polyethylene glycol
PEO	polyethylene oxide
pH	potential hydrogenii
Phe	phenylalanine
PLGA	poly(D,L-lactide-co-glycolide)
ppm	parts per million
Q	quadropol
r.t.	room temperature
RNA	ribonucleic acid
ROESY	rotating-frame nuclear Overhauser effect
RP	reversed phase
s	seconds
SDS-PAGE	sodium dodecyl sulfate polyacrylamide gel electrophoresis
siRNA	silencing RNA
SPR	surface plasmon resonance
SSTR2 and SSTR5	somatostatin type 2 and 5 receptors
t	time
T	threonine

T	thymine
TCEP	tris(2-carboxyethyl)phosphine
TCO	trans-cyclooctene
TFA	trifluoroacetic acid
THF	tetrahydrofuran
Thr	threonine
TLC	thin layer chromatography
TOCSY	total correlation spectroscopy
TOF	time of flight
TRIS	tris(hydroxymethyl)aminomethan
TSTU	<i>N,N,N',N'</i> -Tetramethyl- <i>O</i> -(<i>N</i> -succinimidyl)uronium tetrafluoroborate
UV	ultraviolet
UV-ECD	ultraviolet electronic dichroism
VIP	vasoactive intestinal peptide
W	tryptophan
wt	wild type
μ	micro
α-CHCA	alpha-cyano-4-hydroxycinnamic acid
δ	chemical shift
°	degree

Content

1	Introduction.....	1
1.1	Bioconjugate techniques	2
1.1.1	Amine modification	3
1.1.2	Thiol modification.....	5
1.1.3	Imine, hydrazone and oxime groups	7
1.1.4	Bioorthogonal reactions	9
1.1.5	Crosslinker molecules applied for bioconjugation.....	12
1.2	Disulfide intercalating agents.....	13
1.3	Bioconjugation in the field of tumor targeting.....	17
1.3.1	Passive tumor targeting	18
1.3.2	Active tumor targeting	20
1.3.3	Octreotide.....	21
1.4	References.....	23
2	Motivation and Objectives	29
3	Novel disulfide-based linker platform for site-selective modification of peptides and proteins.....	33
3.1	Synthesis and Characterization	35
3.1.1	Introduction of different functional groups to create a novel linker platform	37
3.1.2	Reduction of octreotide	40
3.1.3	Synthesis of ethynyl- and iodine-modified octreotide conjugates	42
3.1.4	Synthesis of perylenediimide-linker and perylenediimide-octreotide	45
3.1.5	Synthesis of doxorubicin-octreotide conjugates	50
3.2	Glutathione dependent perylenediimide release	59
3.3	Stability and cleavage study of the hydrazone based doxorubicin – octreotide conjugate	62
3.4	Cellular uptake and intracellular distribution.....	63
3.5	Cytotoxicity studies of the doxorubicin – octreotide conjugate.....	66
3.6	Conclusions.....	68
3.7	References.....	70
4	Site-selective modification of peptides and proteins with minimal structural alteration	75
4.1	Computational calculations.....	78

4.2	PEG-octreotide hybrid.....	81
4.2.1	Synthesis.....	83
4.2.2	Circular dichroism studies.....	92
4.2.3	Receptor binding studies	93
4.3	Perylenemonoimide – octreotide hybrid	95
4.3.1	Synthesis.....	96
4.3.2	Microscopy studies.....	99
4.4	Doxorubicin – octreotide hybrid	102
4.4.1	Synthesis.....	102
4.4.2	UV – ECD characterization and receptor binding studies.....	107
4.4.3	pH dependent cleavage study of doxorubicin-octreotide conjugate.....	109
4.4.4	Cell viability and cellular distribution studies of doxorubicin-octreotide conjugate	111
4.5	Conclusion.....	114
4.6	References	116
5	Doxorubicin-Indole conjugates as anticancer agents	121
5.1	Design and Synthesis of Doxorubicin-Indole conjugates.....	122
5.1.1	Synthesis of doxorubicin-indole-NO ₂ conjugate (Doxind-NO ₂)	124
5.1.2	Synthesis of doxorubicin-indole NH ₂ conjugate (Doxind-NH ₂)	126
5.1.3	Synthesis of doxorubicin-indole-indole-NH ₂ conjugate (Doxindind-NH ₂)..	131
5.1.4	Synthesis of doxorubicin-indole guanidyl conjugate (Doxind-G).....	133
5.2	Binding affinity measurements using Microscale Thermophoresis	135
5.2.1	Doxorubicin – DNA intercalation	138
5.3	Toxicity studies of the doxorubicin-indole conjugates.....	139
5.4	References	142
6	Summary and Perspective	145
6.1	References	153
7	Experimental part	155
7.1	General methods.....	155
7.1.1	Chemicals and solvents	155
7.1.2	Chromatography	155

7.1.3	Inert Atmosphere.....	155
7.2	Analytical Techniques.....	156
7.2.1	RP-HPLC	156
7.2.2	Mass spectrometry	156
7.2.3	NMR spectroscopy.....	156
7.2.4	Microscale Thermophoresis	157
7.2.5	SDS-PAGE	157
7.2.6	Circular dichroism spectroscopy.....	158
7.2.7	pH dependent cleavage studies	158
7.2.8	GPC.....	158
7.2.9	Cell cultures	159
7.2.10	Cell viability assay	159
7.2.11	Fluorescence Microscopy	160
7.2.12	Determination of adrenocorticotropic hormone (ACTH) secretion	160
7.2.13	Computational details	161
7.3	Organic synthesis	162
7.3.1	Compounds part 3:	162
7.3.2	Compounds part 4:	186
7.3.3	Compounds part 5:	204
	Appendix.....	223

1 Introduction

Since the beginning of my study of chemistry in 2008, over 54,000 additional publications have appeared in the biological, medical, polymer, material science, and chemistry journals that mention the terms “bioconjugate” or “bioconjugation”. I often asked myself:

What is it that makes this topic so interesting for researchers worldwide from different disciplines?

It has been easy to recognize, that the technology of bioconjugation has affected nearly every discipline in life science. [1] The majority of the research articles of web links in the Internet focuses on new reagents and reactions for the formation of bioconjugates of all types for the application in various fields, as highly sensitive assays, for *in vivo* imaging and diagnosis, therapeutic drug targeting, the capture and purification of biomolecules, catalysis and chemical modification, or for vaccine development and immune modulation. Besides this, the ability to chemically attach small molecules to a biomolecule has caused the birth of billion-dollar biotech companies that are working on discovering the secrets of protein engineering in living cells and revealing new therapeutic targets. In fact, most of the largest biotech and pharmaceutical companies worldwide rely on various bioconjugation techniques to develop future product pipelines and protect a vital edge over the competition. The concepts of “magic bullet” described by Paul Ehrlich and the “targeted drug” delivery to a large extent rely on the creation of highly specific bioconjugates offering therapeutic efficacy towards specific cells or tissues.

On the one hand, the field of bioconjugation has had a deceptively quiet but at the same time an enormous impact on science and technology. The ability to synthesize diverse bioconjugate complexes having unique properties suitable for a wide variety of applications has become the underlying success story of many research endeavors.

Today we have to admit, that there are more options available than ever before to design and chemically create nearly any covalent complex imaginable between two or more molecules of virtually any type.

Bioconjugation – one way to make the impossible possible.

1.1 Bioconjugate techniques

In general, bioconjugation can be described as the chemical derivatization of biomolecules as proteins, DNA, RNA and carbohydrates. To be more precise, it is a chemical strategy to form a stable covalent binding of two or more molecules, at least one of which is a biomolecule, to form a novel complex. The final product is called a bioconjugate, having the combined properties of its individual components.

Forming a bioconjugate involves the reaction of two molecules and often a crosslinking agent that links the two molecules A and B together. Sometimes an activation agent is used that results in linking of the two molecules without an intervening cross-bridge between them.



Figure 1: Formation of a bioconjugate

For an example, a molecule (e.g. drug **A**) able to interact discreetly with a target inside the cell (e.g. DNA) can be conjugated with a reporter molecule (e.g. a biomolecule like a peptide **B**), which functions as the delivery agent to form a bioconjugate (Figure 1). It is important that the coupling does not affect the biological function of the two molecules.

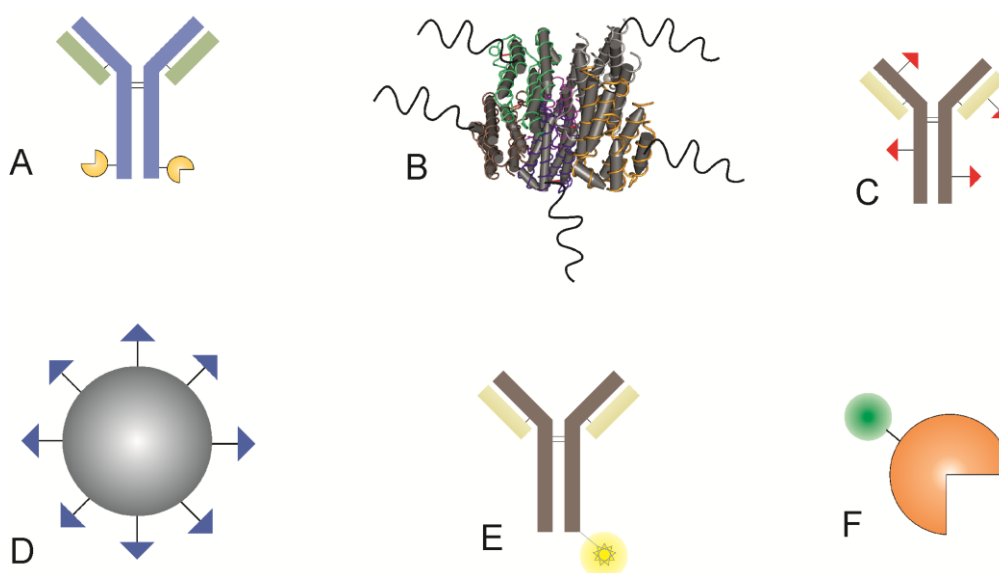


Figure 2: Common bioconjugates used in life science applications include (A) antibody-enzyme conjugate, (B) PEGylated proteins, in this case interferon, (C) an antibody-drug conjugate, (D) an immobilized affinity ligand on a particle, (E) antibody-dye conjugate, (F) a biotinylated enzyme. [1]

Figure 2 shows several examples of the enormous possibilities of bioconjugation applications such as labelling molecules with chromophores to study the natural environment of antibodies, peptides or proteins, preparing antibody-toxin conjugates for use as targeted therapeutic agents in cancer therapy or producing polymer conjugates to modulate bioactivity or stability of biomolecules, as for instance the PEGylation of interferon. [1] Finally, bioconjugate techniques are responsible for the discovery of new biomolecules, the elucidation of complex biological processes, and the spawning of entire industries within the medical, diagnostics, life sciences, microelectronics, and material sciences fields.

Conjugation techniques utilized to prepare bioconjugates are diverse and depend on the functional groups intrinsically present in the respective molecules. There are hundreds of reagents described in literature and offered commercially, but most utilize common principles of organic chemistry that can be reduced to a few primary reactions. The following section is giving a short overview of examples of typical reactions in the field of bioconjugate chemistry applied to couple a biomolecule with another molecule to form bioconjugates. [1]

1.1.1 Amine modification

The natural abundance of amino groups in biomolecules is markedly high and coupling reactions with amine-reactive molecules is by far the most common, where such processes can be used to conjugate nearly all available biomolecules. The primary coupling reactions for modification of amines are mainly performed by one of two routes: either acylation or alkylation. The advantages of both routes and for amine coupling reactions in general, are fast reaction times coupled with high yields that lead to the formation of a stable primary or secondary amine bond. [1]

Referred to the modification of peptides, the ϵ -amino group of lysine and the N-terminal amine of the peptides play a key role. Most of the amino-groups are situated on the peptide's surface in solution and are available for further modification steps and coupling processes. Whereas the pK_s -value of the lysine amine is around 9.0-9.5, the pK_s value of the N-terminus is lower (7.5-8.0). To obtain good coupling yields without affecting or changing the peptides structure, reactions are generally performed at pH 7-9, enabling the modification of amines with isocyanates, NHS-esters or sulfonyl chlorides (Figure 3).

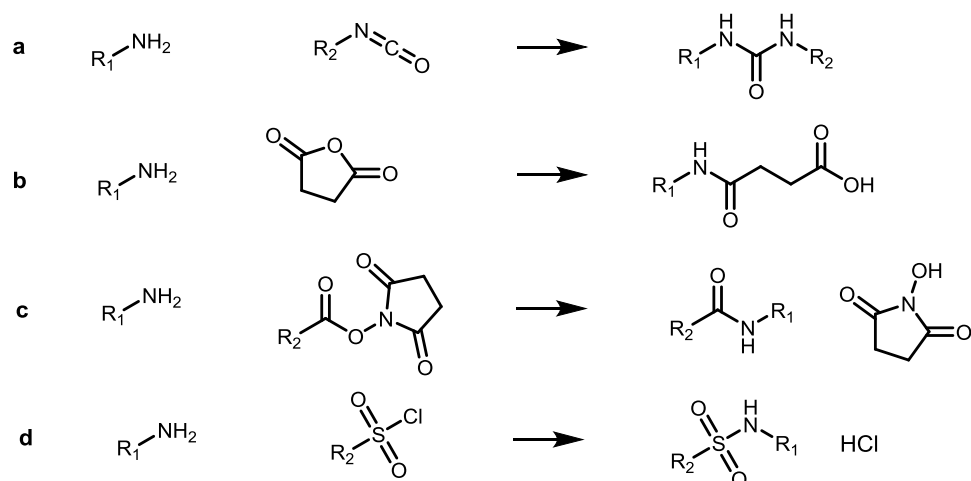


Figure 3: Chemical modification techniques for amino-groups of biomolecules [1] a) isocyanate group to form an urea bond, b) succinic anhydride to form an amide bond, c) NHS ester derivative to form an amide bond, d) sulfonyl chloride derivative to form a sulfonamide bond

Especially amide bond formation is an important reaction in organic synthesis and plays a major role in the structure of biological systems. Amide bonds possess high stability due to its resonance stabilization and can also be cleaved in the body by enzymes such as proteases. The building blocks of amide bonds are typically carboxylic acids and amines; however the unification of these two does not occur spontaneously at ambient temperatures. The necessary elimination of water in the reaction only takes place at high temperatures ($>200^{\circ}\text{C}$), which are incompatible with many living systems and biomolecules. For this reason, the formation of an amide bond is often assisted through “activated esters” of the carboxyl group, which react with a free amino group.

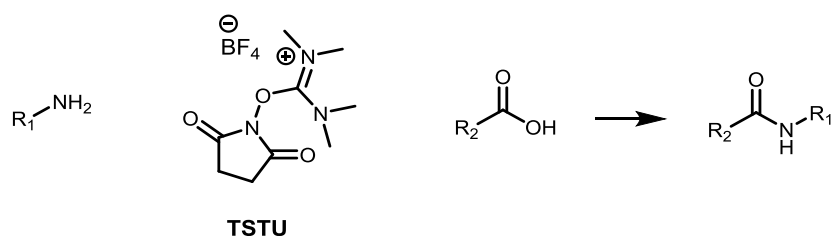


Figure 4: Amide bond formation between an amine and a carboxylic group using TSTU as a coupling reagent

As depicted in Figure 4 O-(N-succinimidyl)-1,1,3,3-tetramethyluronium tetrafluoroborate (TSTU) can be employed for an effective and fast formation of carboxamides by previous transformation of the carboxyl group into the corresponding hydroxysuccinimido ester, having the advantage to be less sensitive to water compared to common reagents as carbodiimides. [2] Nowadays, scientist are mainly focusing on *in situ* activation with

reagents like HATU, PyBOB or HBtO belonging to the next generation of amide coupling reactions in order to enhance the reactivity and yield of the reaction.

Despite these advances, the choice of base is also important in amide coupling reactions. Especially tertiary amines such as *N,N*-diisopropylethylamine (DIPEA) and *N*-methylmorpholine (NMM) have been considered as practically useful bases due to their non-nucleophilic property. Because of the shielded nitrogen by two isopropyl groups and an ethyl group, DIPEA is a good base but a poor nucleophile. Thus, side reactions such as a nucleophilic attack to the activated carboxyl group by the base are not possible. [1]

1.1.2 Thiol modification

Besides amino-groups, sulfhydryl-groups are probably the second most common functional group present on biomolecules. In case of using the free thiol group of a biomolecule, the coupling reactions proceed by one of the two routes: either alkylation or disulfide interchange. In both cases, the formed bonds are stable in aqueous environments and allow further coupling steps with other functional groups in a two-step conjugation strategy. Again, these reactions are rapid and occur in high yield to give stable disulfide or thioether bonds. [1]

Cysteine is the only proteinogenic amino acid containing a thiol group. Under physiological conditions this group is either present in the protonated thiol form (pK_s 8.8-9.1) or even more often in its oxidized disulfide form, which often plays a key role in preserving the spatial structure. Nevertheless, both forms are still reactive and used for more than 100 years for peptide and protein modification in different ways, as it is shown on the following figure and described in the next section. [3] [4]

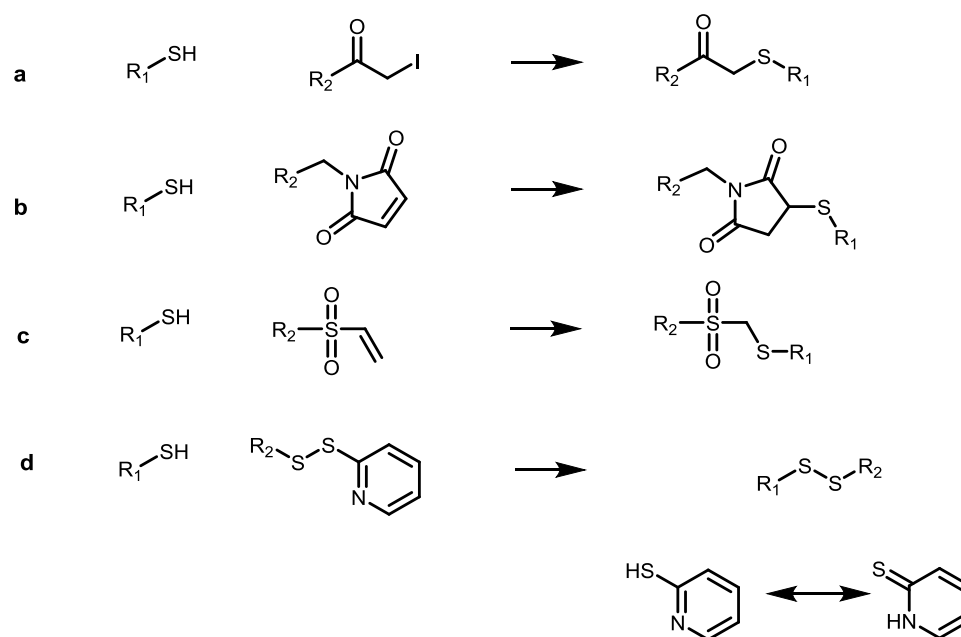


Figure 5: Chemical modification techniques for thiol-groups of biomolecules; a) iodoacetyl derivative to form a thioether bond, b) maleimide derivative to form a thioether bond, c) vinylsulfone reactive group to form β -thiosulfonyl linkage (thioether bond), d) pyridyl disulfide derivative to form a disulfide bond [1]

The sulfhydryl group is among the most highly reactive nucleophiles found in biomolecules and thus enables rapid conjugation with electrophilic functional groups, such as acyl or alkyl group, N-ethyl maleimide or iodoacetate derivatives, as well as pyridyl disulfide containing derivatives (Figure 5). Reversible protection can be done through disulfide formation, susceptible to be cleaved by reduction (e.g. glutathione (GSH)) in the cytosol. Activation of thiols with such derivatives enables further coupling-reactions with other free thiol groups, as pyridine-2-thione is a good leaving group. The advantage of e.g. 2,2'-dithiopyridine towards other permanent thiol protecting agents such as sodium tetrathionate or S-methyl methanethiosulfonate is the absorption of the leaving group pyridine-2-thione at 343 nm, which can be applied to monitor the progress of the subsequent reaction with thiols (Figure 5 - d). [7].

An additional example for thiol modification of peptides was demonstrated by Shiu *et al.*, where electron poor terminal alkynes can also react with thiol groups, but only under basic conditions, which are not tolerated by all biomolecules. [5] Jones *et al.* were able to reduce the disulfide bond of salmon calcitonin with water-soluble phosphines (e.g. TCEP) to form two thiol groups, which were coupled to PEG-methacrylate by Michael addition (Figure 6). [6]

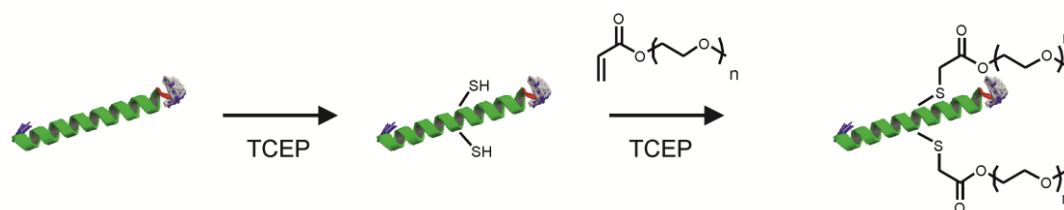


Figure 6: Disulfide reduction and modification based on Michael addition reaction for the peptide salmon calcitonin

Pyridine disulfides are the most common reactive group for initiating disulfide exchange reactions. They are used to temporarily protect or to activate thiol groups, respectively.

1.1.3 Imine, hydrazone and oxime groups

The functionalization of ketones and aldehydes with amino groups continues to play an important role in the field of bioconjugation. Especially the facile synthesis of carbon-nitrogen double bonds via condensation of the previously mentioned functional groups in aqueous solution under neutral pH without the addition of any coupling reagents render them attractive for bioconjugation. [8] The introduction of aldehydes and ketones into proteins site specifically is attributed to chemical, enzymatic, and genetic methods, which include periodate oxidation of N-terminal serine or threonine residues, addition of ketone-containing small molecules to protein C-terminal thioesters generated by expressed protein ligation or genetically encoded incorporation of unnatural amino acids containing ketones via amber stop codon suppression. [9]

In general, reactions between ketones and primary or secondary amines form a Schiff base, a dehydration reaction yielding an imine. Imines can undergo hydrolysis in aqueous solutions, meaning a reversible reaction which is not always suitable for modifications. Therefore, the labile Schiff base can be chemically stabilized by reduction (e.g. using cyanoborohydride) creating a secondary amine linkage between the two molecules and, thus, a convenient modification technique. [1]

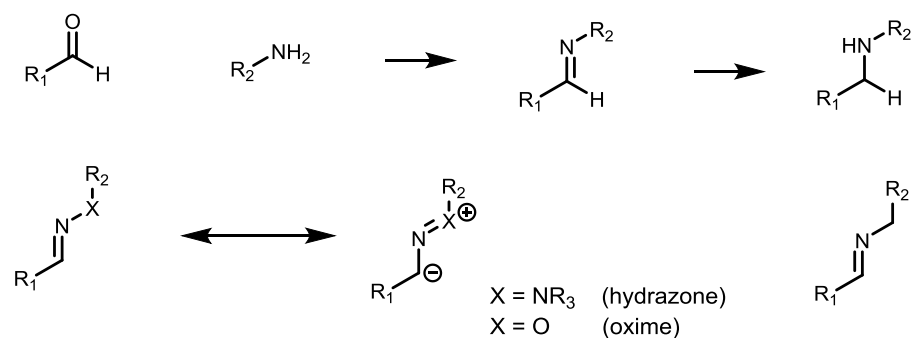


Figure 7: Reaction of carbonyl groups with amine nucleophiles to form reversible Schiff base intermediates as well as the resonance forms of carbon-nitrogen double bond conjugates of the oxime and hydrazone bond formation (R = aryl or alkyl group)

In contrast, hydroxylamines or hydrazine-groups will react with ketones via oxime or hydrazone bond formation, which are much more stable than imines under similar conditions. This greater hydrolytic stability invokes the participation of the additional heteroatom in electron delocalization compared to a simple amine. The additional resonance form increases the negative-charge density on the carbon atom and hence reduces its electrophilicity (Figure 7).

The comparative stability of hydrazones and oximes was investigated by Kalia and Raines and established oximes as the linkage of choice for the stable conjugation of molecules via carbon-nitrogen double bond. [8] The explanation for this effect is the resistance to protonation based on the higher electronegativity of oxygen in the oxime versus nitrogen in the hydrazone. On the other hand, hydrazone bonds are frequently used in drug delivery areas, as this bond is stable at pH 7, but undergoes hydrolysis in acidic environments.

The possibility to use aldehydes and ketones for modification purposes have been demonstrated in different experiments. For instance, Bertozzi and coworkers demonstrated that certain keto sugars are metabolized by cells and integrated into cell-surface glycans, where they can be coupled with aminoxy and hydrazone probes. [9] Furthermore, our group has recently shown the potential of an oxime bond as part of a cross-linking reagent to couple the cytotoxic drug doxorubicin, which in this case contains the keto group, to the tumor targeting vector octreotide. [10]

1.1.4 Bioorthogonal reactions

As described in the previous section, conventional covalent chemical attachment methods focus on the targeting of primary amines, thiols or carboxylic acids of proteins using commercially available reagents such as hydroxysuccinimide esters, isocyanates or maleimides. The critical drawback of this technique is the resulting heterogeneity of the modified products, which occurs due to the lack of selectivity of the targeted functional groups. [11]

In contrast, bioorthogonal reactions are defined as reactions with a very high selectivity for certain functional groups and high overall yields, in which side reactions are almost eliminated completely. Furthermore, these reactions are achievable in aqueous solutions, under soft reaction conditions, and even in presence of other functional groups (Figure 8). [11]

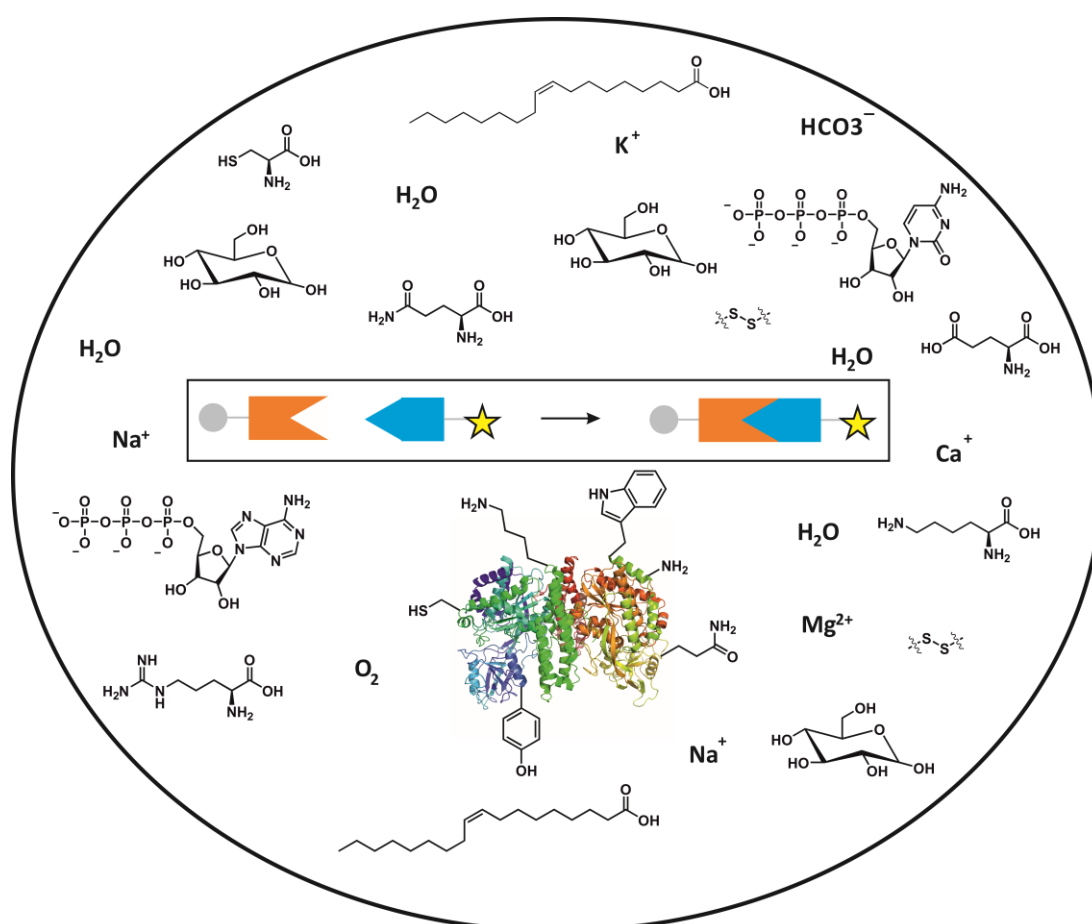


Figure 8: Schematic overview of the vast complexity of functional groups in living systems and the schematic principle of a bioorthogonal reaction in the middle

As an example, the discovery of the genetically encoded green fluorescent protein (GFP) is based on a bioorthogonal technique (genetic engineering) that has dramatically increased our understanding of cellular processes. Nevertheless, this principle remains restricted to biomolecules that can be genetically engineered. The same is true for the work of Nobel Prize winner Roger Y. Tsien, who invented this α -helical motif, composed of mainly four cysteines (sequence Cys-Cys-Xaa-Xaa-Cys-Cys, where Xaa is a non-cysteine amino acid), which binds organoarsenic compounds selectively and could be used for bioorthogonal coupling reactions. The special amino-acid sequence is genetically fused to or inserted within the protein, where it can be specifically recognized by a membrane-permeant fluorescein derivative with two As(III) substituents. [13]

In the last decade different techniques of bioorthogonal reactions have been developed and applied for the modification of various biomolecules *in vitro* as well as *in vivo*, which will be discussed below with few examples.

Back in the 1950s, Huisgen and coworkers were the first to report the [2+3]-cycloaddition between azides and alkynes. [12] However, since this reaction is typically very slow under ambient conditions, high temperatures or pressure was required to obtain high yields of the corresponding triazol product, conditions which are not compatible with biomolecules. Because of the remarkable work of Sharpless and Medal, who independently proved that Cu(I) salts can be used to dramatically increase the reaction rate between azides and alkynes at biocompatible conditions, the copper-catalyzed azide-alkyne cycloaddition (CuAAC) has achieved a widespread application in the field of bioorthogonal chemistry. [11] [13] For example, the profiling of enzymes with fluorescent tags using CuAAC has already been reported by Cravatt and co-workers more than 10 years ago. [14] Due to the cytotoxicity of the Cu(I) catalyst, which can lead to oxidative damage in living cells through the formation of reactive oxygen species such as hydroxyl radicals, these reactions were mainly used *in vitro*. [15] Therefore, Blomquist *et al.* first suggested in 1953 the use of strained alkyne rings to circumvent copper catalysts, but its potential as a bioorthogonal reaction was first recognized by Bertozzi *et al.* in 2004 with the application of a cyclooctyne ring as an activated reaction partner for azides. [16]

An alternative conjugation technique that does not require the addition of a catalyst or rely on complex cyclooctyne molecules is the inverse electron-demand Diels-Alder reaction (IEDDA). In 2008, Fox and co-workers reported the efficient, irreversible coupling reaction between the strained molecule *trans*-cyclooctene (TCO) and the electron-deficient

biaryltetrazine in a [4+2]-cycloaddition under the loss of nitrogen, that proceeds in aqueous solutions and does not interfere with other biomolecules (Figure 9). [11] [17]

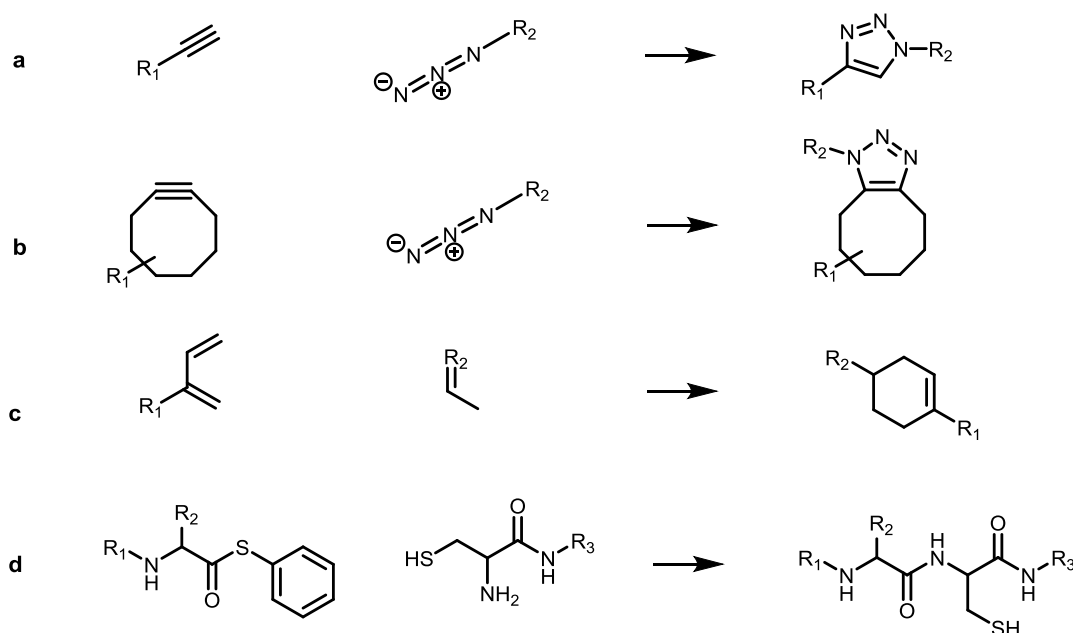


Figure 9: Schematic representation of typical bioorthogonal reactions a. CuAAC, b. SPAAC, c. IEDDA, d. native chemical ligation [11]

Further examples of bioorthogonal reactions include Staudinger Ligation between azides and triarylphosphines, (hetero)-Diels-Alder-Reaction between a diene and a dienophile in [4+2]-cycloaddition, Pictet-Spengler Ligation for the modification of reactive carbonyl groups with hydrazine, alkyl/arylhydrazine or aminoxy nucleophiles or the Native Chemical Ligation between peptide segments, one containing a C-terminal thioester and the other containing an N-terminal cysteine residue that leads to the formation of stable amide bond. [11]

The field of bioorthogonal techniques is increasing dramatically and illustrates a crucial part of the aforementioned journey of taking advantage of bioconjugation to create novel tools for research, diagnostics, and therapeutics.

1.1.5 Crosslinker molecules applied for bioconjugation

Next to the type of coupling reactions, which were previously outlined, bioconjugate crosslinkers are also significant to the field of bioconjugation. They play an important role in the formation of bioconjugates, as they are often responsible for the connection of both molecules. Thereby, bioconjugate crosslinkers must possess high stability in aqueous solutions and can be subdivided in zero-length, homo- and heterobifunctional, as well as trifunctional types. Their application mainly depends on the functional groups in the different molecules, which should be linked. Crosslinkers are extensively applied in drug modifications and their utilization has proven to be very important for the attachment of diverse carriers, such as monoclonal antibodies [18], proteins [19], polymers [20] and peptides [21] to drugs or dyes. [22]

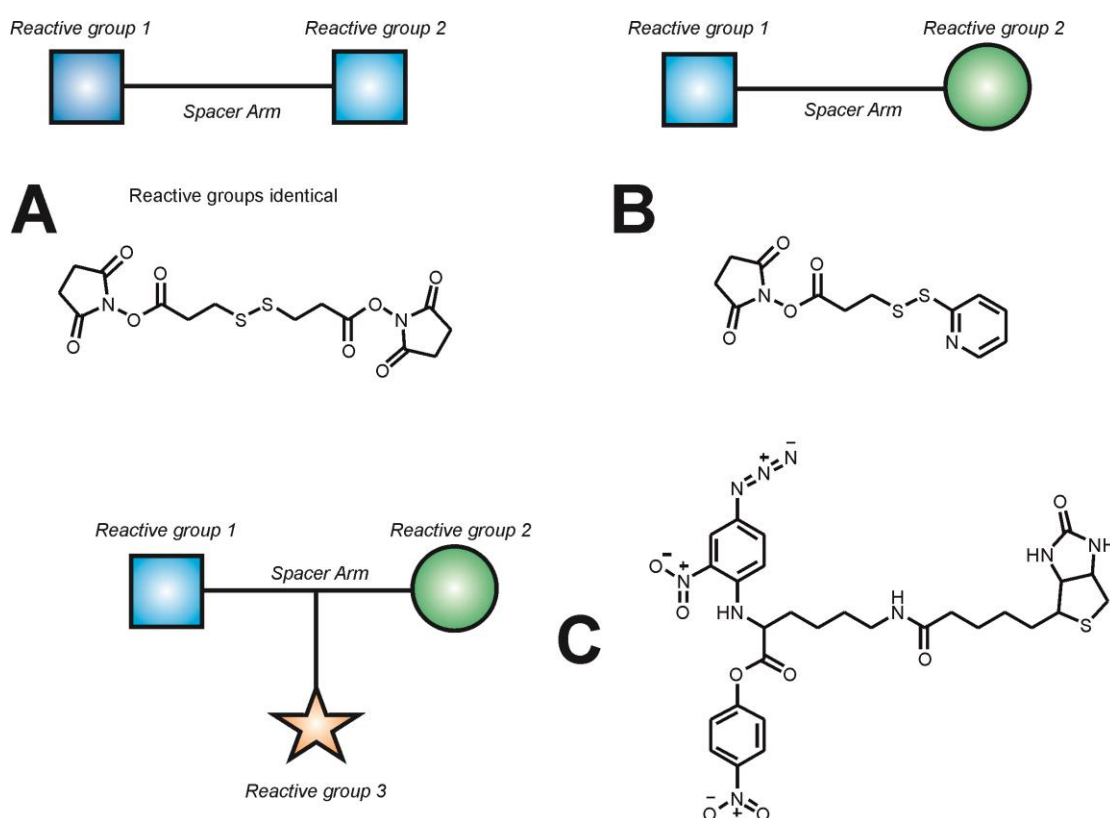


Figure 10: Overview of the different linker types, A: DSP = Dithiobis(sulfosuccinimidylpropionate), B: SPDP = N-succinimidyl-3-(2-pyridyldithio)propionate, C: ABNP = 4-Azido-2-nitrophenylbiocytin-4-nitrophenyl ester

The smallest available reagent systems for bioconjugation are the so-called zero-length linkers. The coupling techniques in the aforementioned section belong to this class of bioconjugation reagents, as one atom of a molecule is covalently attached to an atom of a second molecule with no intervening linker or spacer. Examples for the other types of

crosslinkers are shown on Figure 10, which can be subdivided in homo- (A) or heterobifunctional (B) reagents and heterotrifunctional (C) reagents.

The main disadvantage, however, of using homobifunctional reagents is the potential for creating a broad range of poorly defined conjugates, as the probability of coupling two times the same molecule in contrast to two different molecules, all possessing identical functional groups, is increased (Figure 10, A). In contrast, heterobi- or heterotrifunctional conjugation reagents (Figure 10, B and C) contain different reactive groups that can couple to different functional targets on proteins and other macromolecules, thus garnering better control over the conjugation process.

In the last decade, researchers have been focusing intensively on coupling reactions involving thiol groups of reduced disulfide bonds. Examples of such crosslinkers are *N*-Succinimidyl-3-(2-pyridyldithio)-propionate, having the advantage of fast and efficient coupling reactions, as well as the introduction of a disulfide bond between the conjugates, which is cleavable inside the cell under reducing conditions (e.g. intracellular glutathione). Further details about crosslinkers focusing on thiol coupling reactions are highlighted in the following chapter.

1.2 Disulfide intercalating agents

Most thiol groups are present as disulfide bonds in peptides and proteins, as they are essential for its stability and function. Therefore, a reduction of the disulfide bond to form two free thiol groups in a first step is necessary to enable any type of modification at the disulfide bond in a second step. The crucial point is that the peptide or protein can lose its activity due to the conformational changes in the secondary or tertiary structure. Thus, it is important to introduce techniques which do not influence the actual activity of the biomolecule.

Disulfide-intercalating agents belong to a relatively young subclass, which is gaining increasing interest in the field of bionconjugated chemistry and is therefore discussed in this section part separately. The advantage of this structural instrument is the site-selective modification of complex peptides and proteins at its disulfide bond, neither changing its structure nor function. Brocchini *et al.* pioneered this field with his work published in 2006 with a novel designed and synthesized bissulfone linker system for disulfide intercalation reactions after a soft reduction step to form two thiols in the first step. Thereby the disulfide

bond of the biomolecule is cleaved and re-bridged, yielding the respective bis-sulfide bioconjugate while the function and stability is maintained, as there is almost no change in the secondary structure (Figure 11).

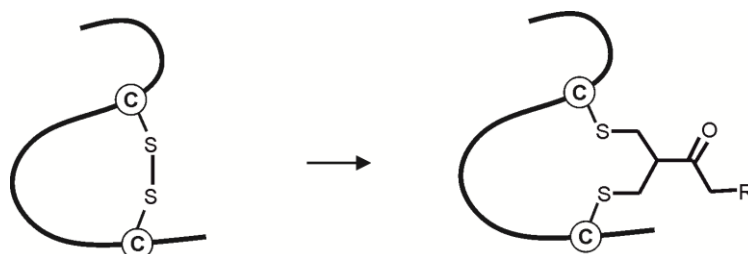


Figure 11: Schematic disulfide intercalation process of somatostatin using the bis-sulfone linker system

Up to now, this linker system has been used in different studies for the modification of peptides, most frequently the cyclic peptide somatostatin, which contains one disulfide bond only. Brocchini himself, and his group accomplished the PEGylation of cytokines, enzymes, antibody fragments as well as peptides, without destroying the biomolecule's tertiary structure or abolishing its biological activity. [24, 25] Weil and coworkers reported different modifications of somatostatin for a targeted drug delivery, but also on a versatile toolbox of such bis-alkylation reagents offering improved solubility and multiple functionalities at predefined positions of peptides and proteins. [26-28]

However, many time consuming and extensive synthesis steps have to be carried out in advance and the final peptide modification needs long reaction times with relatively low yields (Figure 12).

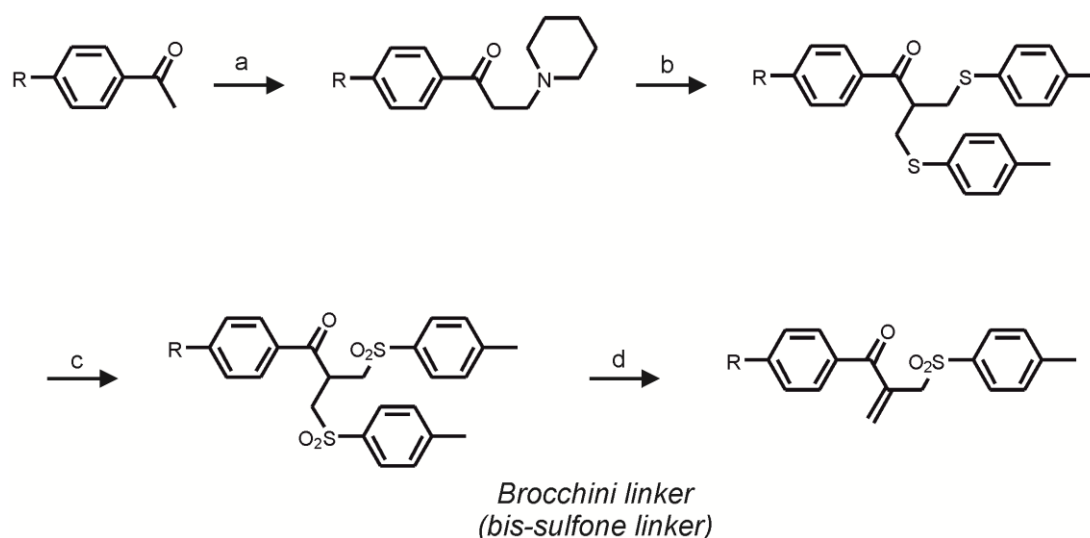


Figure 12: Synthetic pathway for the bis-sulfone linker introduced by Brocchini

An additional way of disulfide intercalation and, thus, modification of peptides was described by Smith *et al.*, using 2,3-dibromomaleimides. [29] In the first step the biomolecule's disulfide bond is reduced, afterwards both bromo atoms are replaced by the peptide's thiol groups in a double nucleophilic substitution reaction forming two stable thioether bonds. The advantage of this linker system is the fast coupling rate and high yield compared to the bis-sulfone linker, which takes up to 24 h for a complete disulfide intercalation. Furthermore, the number of atoms which are introduced between the two sulfur atoms are reduced to two atoms only, which is a positive side effect concerning possible structural changes of the biomolecule after the modification. Literature describes many successful examples using dibromomaleimides, for instance, it was utilized for cysteine modification as illustrated on the SH2 domain of the Grb2 adaptor protein (L111C) and for the insertion of disulfide bonds as illustrated on the peptide hormone somatostatin via PEGylation (Figure 13). [29] [30]

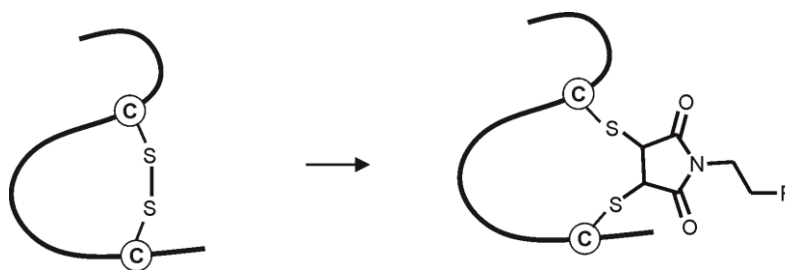


Figure 13: Schematic disulfide intercalation process of somatostatin using 2'3-Dibromomaleimide

Both reagents have been successfully used for the site-selective modification of peptides by disulfide intercalation generating two stable thioether bonds not affecting the biomolecules stability or activity. However, these frequently used reagents are stable and cannot be cleaved controlled under physiological conditions. For instance, the dibromomaleimide needs up to 100 eq of glutathione to be cleaved to release the drug, conditions which are far away from the reality inside the cell. [29] Thereby, they cannot be applied for the release of a toxic freight admittedly, which is a crucial drawback in the field of drug delivery. [10]

Recently our group has introduced a new approach to overcome the aforementioned limitation in the field of targeted drug delivery (Figure 14). A novel disulfide-intercalating cross-linking reagent was used to couple the cytotoxic drug doxorubicin to the tumor-targeting vector octreotide. The cornerstone of this linker system are two activated thiol groups, which react with both thiol groups of octreotide by the formation of two disulfide

bonds to keep the cyclic structure of the peptide active. Furthermore, those two disulfide bonds allow the efficient release of the toxic cargo within the reducing environment in cancer cells, as it was shown in different experiments by the addition of cellular concentrations of glutathione.

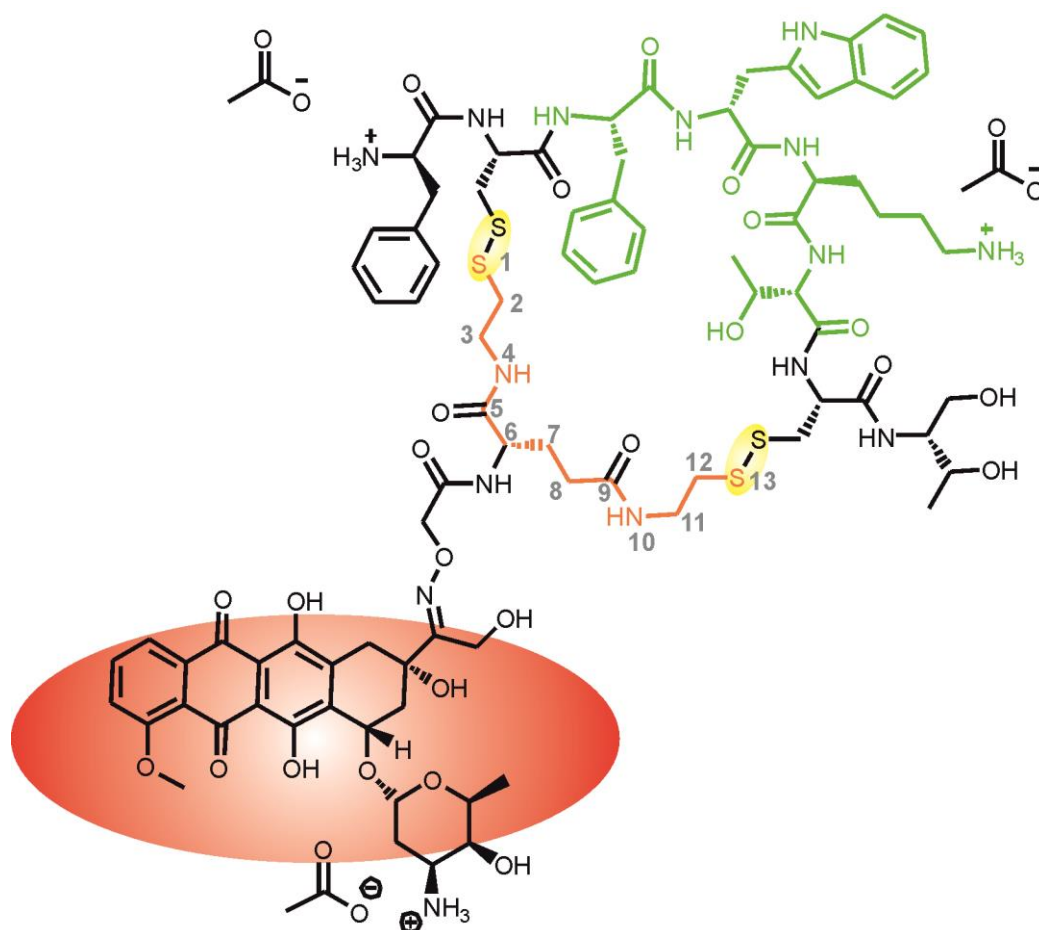


Figure 14: Doxorubicin-octreotide conjugate for a targeted drug delivery with additional cleavage potential under reducing conditions inside the cell synthesized in our group by [10], orange: 11 linker atoms are introduced between the initial disulfide bond, green: active centre of the peptide, yellow: reducible disulfide bonds, red: toxic cargo Doxorubicin

The synthesis of this novel reducible linker is also quite time-consuming and elaborate, as it needs six steps to synthesize the linker and two more to couple the drug to the peptide. Furthermore, the linker itself, which is introduced between the sulfur atoms of the disulfide bond, is relatively large compared to the structure of bis-sulfone and dibromomaleimide linkers. As this can influence the structure of the biomolecule and thus the function, the linker should be as small as possible. Nevertheless, this novel disulfide based linker type has

the big advantage over all other disulfide linker types in that it is cleavable under physiological conditions.

Although there was much work done in this interesting field of disulfide intercalation as a part of bioorthogonal peptide and protein modification, open questions still remain concerning important facts, which are listed below and will be a main part of this work:

- 1) **the size** of the linker, which is introduced between the sulfur atoms,
- 2) the synthetic **effort and yield** of the linker,
- 3) **efficacy and coupling yield** of the reaction,
- 4) as well as the possible **cleavage** of a delivered cargo at the place of interest.

1.3 Bioconjugation in the field of tumor targeting

In the field of chemotherapeutic agents, unavoidable side effects are mainly caused by the poor targeting of the highly toxic agents. Therefore, especially in the field of cancer therapy, drug delivery research aims in helping patients by developing clinically useful formulations to minimize the aforementioned limitation.

Within the last decades, drug delivery technology in general has advanced significantly. Current technologies include the development of various clinical formulations allowing the delivery of drugs at desired locations and controlled release kinetics. [31] The clinically significant impact of targeted drug delivery depends on the ability to specifically target a drug and to minimize the drawback of drug-originated systemic toxic effects. [32, 33] Therefore, targeted drug delivery can be defined as the predominant drug accumulation within a targeted area, which is independent of the method and route of drug administration. [34]

Tumor targeting, in particular, is mainly possible due to the slightly different composition and metabolism of tumor tissue and healthy tissue, a concept which has already been introduced by the Nobel Prize winner Paul Ehrlich more than 100 years ago and is still applied in the development of drug formulations nowadays. [35] To achieve a targeted delivery and release in cancer therapy, there are different strategies described in literature, which have frequently been divided into two categories, “passive” or “active” tumor targeting. In the following section part both terms will be described separately.

Nevertheless, improving and overcoming the challenges of developing a successful targeted drug delivery strategy requires deeper knowledge of the events involving the transport of drugs or drug carriers to a targeted site after application – that is what it makes a highly interesting and interdisciplinary research field.

1.3.1 Passive tumor targeting

Passive targeting is mostly connected with the enhanced permeation and retention (EPR) effect. When a solid tumor reaches a given size, the normal vasculature present in its close vicinity is not sufficient to provide all nutrients and oxygen supply required for its further proliferation. [31] [36] Thus, cells start to die in this area, but there are growth factors, which trigger the budding of new blood vessels from the surrounding capillaries - a process, which is called angiogenesis. [37] As blood vessels are needed for the tumor cells to survive, this process promotes the rapid development of new, irregular blood vessels, that present a discontinuous epithelium and lack the basal membrane of normal vascular structures. [38] Depending on the tumor type, the localization and general environment, the resulting fenestrations in those capillaries can reach sizes ranging from 200 – 2000 nm. As these fenestrations offer little resistance to extravasation to the tumor interstitium, nanoparticles or any type of blood components are able to reach the abnormal, discontinuous vascular bed and can accumulate, a process which represents the enhanced permeation component of the EPR effect (Figure 15).

In comparison, the extracellular fluid is constantly drained to the lymphatic vessels at a mean flow velocity around 0.1 – 2 $\mu\text{m/s}$ in normal tissue causing the continuous draining and renewal of interstitial fluid and colloids back to the circulation. [39] Furthermore, this mechanism and the lymphatic function are defective in tumors resulting in minimal uptake of the interstitial fluid. Therefore, molecules which are smaller than 4 nm can diffuse back to the blood circulation and are reabsorbed. In contrast, the diffusion of macromolecules or nanoparticles (NPs) is hindered by their large hydrodynamic radii. In conclusion, NPs which have reached the perivascular space will not be cleared efficiently and accumulate in the tumor interstitium, a process which represents the enhanced retention component of the EPR effect.

Thus, NPs such as dendrimers, micelles or liposomes can be used as delivery system for drugs due to its size between 10 – 100 nm, which is intended to selectively accumulate in the tumor tissue. For example, the PEGylated liposome-encapsulated form of doxorubicin,

which is distributed under the trade name Doxil, has to be mentioned here as it is the first FDA-approved nano-drug. [40]

For more than 30 years, since the early works of Matsumura and Maeda in the mid-1980s, the EPR effect has not only been comprehensively investigated and documented using various tumor types and animal models, but it has also been successfully used to treat and fight cancer. Nevertheless, as many factors such as extravasation, tumor vasculature as well as its environment, the diffusion and convection in the interstitium, tumor biology and physicochemical parameters in general, the EPR effect is much more complex than initially defined and going to be revealed by researchers. [31]

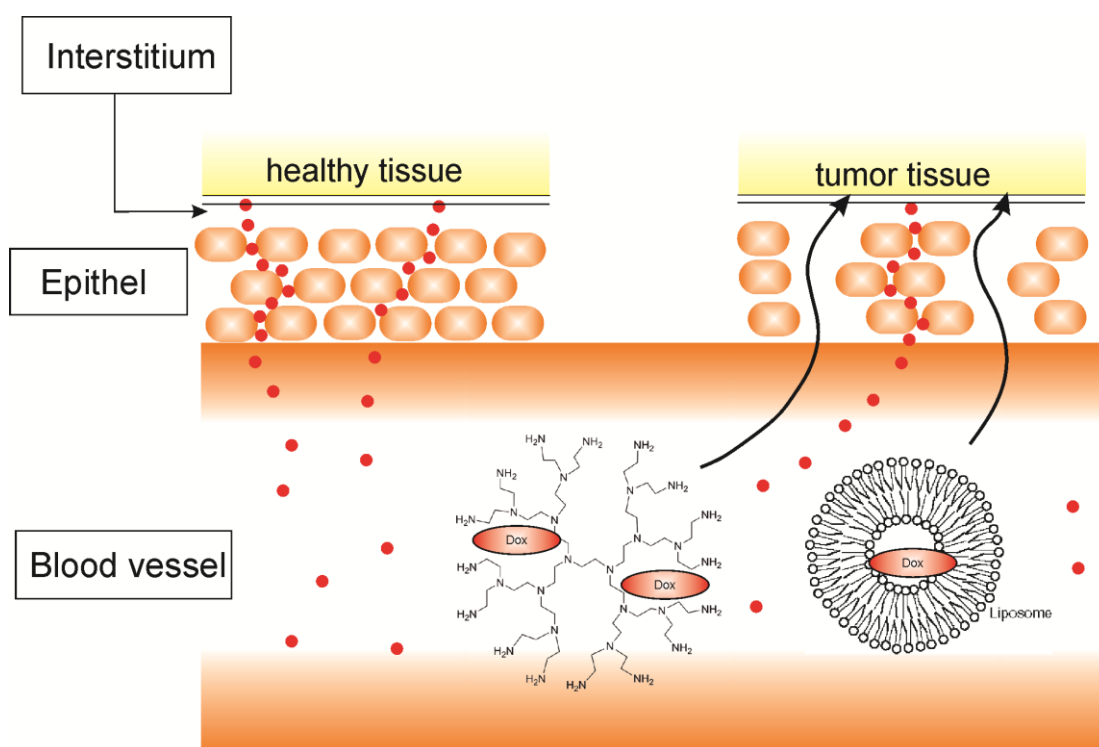


Figure 15: Difference between the composition of healthy tissue versus tumor tissue and a schematic example how NPs as dendrimers or liposomes loaded with doxorubicin can permeate the tumor tissue.

1.3.2 Active tumor targeting

In contrast to “passive targeting”, the so called “active targeting” does not depend on the constitution of the tumor tissue, but relies on the different metabolism of cancer cells compared to healthy cells. In general, the term is used to describe the specific interaction between the drug, its carrier system, respectively, and the cancer cell itself, usually through specific ligand-receptor or ligand-surface molecule interactions. This interaction is based on a close proximity between the two components and thus the system also depends on the blood circulation and extravasation followed by intra-tumoral retention and distribution. The efficiency of targeting and delivery depends on the availability of the selective receptor on the cell surface and its frequency of occurrence compared to non-target cells. Furthermore, other factors like the administration route, physicochemical properties like ligand density and the choice of targeting ligand as well as the architecture and ligand conjugation chemistry have been shown to have a huge influence. [41-43]

Cell receptors can interact with different kinds of ligands, as for instance antibodies, proteins or peptides. In turn, these biomolecules can also act as the drug itself, as for instance the monoclonal antibody Cetuximab, which is an epidermal growth factor receptor (EGFR) inhibitor used for the treatment of metastatic colorectal cancer, metastatic non-small cell lung cancer and head and neck cancer. It is distributed under the trade name Erbitux by the drug companies Bristol-Myers Squibb and Merck KGaA. [44] [45] Another example is the octapeptide and somatostatin analogue octreotide, which is distributed under the trade name Sandostatin by Novartis Pharmaceuticals, which is described in the following section. [46] Nevertheless, biomolecules acting as ligands without any further function can be used for the accumulation of a drug inside the desired tissue after the internalization of the whole complex due to strong interactions with the receptors or molecules overexpressed at tumor cell. [47] For instance, glycoproteins as transferrin and lectin were used for an efficient accumulation of doxorubicin in cancer cell. [48] [49] Even octreotide itself can be used as a ligand to achieve receptors selectively and enable an internalization of the drug to tumor cells. [50] In this context, both, tumor and endothelial cells, can be addressed with the drug-ligand conjugates to achieve a selective uptake, but in the end the toxic effect depends on the drug.

1.3.3 Octreotide

Octreotide is a cyclic peptide which is known chemically as L-Cysteinamide, D-phenylalanyl-L-cysteinyl-L-phenylalanyl-D-tryptophyl-L-lysyl-L-threonyl-N-[2-hydroxy-1-(hydroxymethyl)-propyl]-, cyclic (2→7)-disulfide; [R-(R*, R*)] acetate salt. It is distributed by Novartis Pharmaceuticals under the trade name Sandostatin and mimics the natural hormone somatostatin pharmacologically. It is even a more potent inhibitor of growth hormone, glucagon, and insulin than somatostatin and has been used to treat the symptoms associated with metastatic carcinoid tumors (flushing and diarrhea) and Vasoactive Intestinal Peptide (VIP) secreting adenomas (watery diarrhea). Octreotide is administered as an injection as a clear sterile solution in a buffered lactic acid solution by deep subcutaneous or intravenous injection. [51]

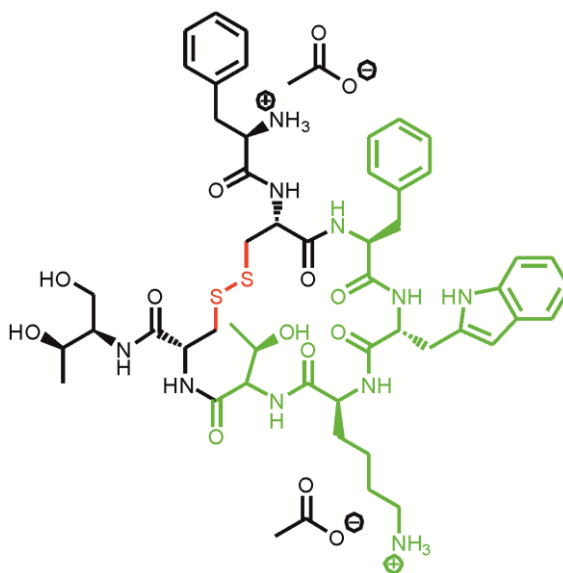


Figure 16: Structure of octreotide diacetate, the disulfide bond is highlighted in red and the tetrameric amino acid motif FWKT (Phenylalanine-Tryptophan-Lysine-Threonine) is marked in green

Somatostatin itself is a cyclic tetradecapeptide with an internal disulfide bond and is known as growth hormone-inhibiting hormone (GHIH). Its main function is similar to octreotide and associated with the regulation of the endocrine systems as well as cell proliferation via interaction with G protein-coupled somatostatin receptors. The cyclic peptide is mainly produced in the small intestine and endocrine pancreas. [52] The drawback of somatostatin is its short half-life (1-3 min) which limits its clinical use. Synthetic somatostatin analogues as lanreotide, octreotide or vapreotide achieve much longer circulation half-lives due to shorter sequences and the right integration of D-amino acids within the cyclic structure of the peptide. Somatostatin and its analogues all possess the cyclic structure enabled by the formation of a disulfide bond as well as the tetrameric amino acid motif FWKT

(Phenylalanine-Tryptophan-Lysine-Threonine), which is responsible for the interaction with the somatostatin receptors (Figure 16). [53]

Next to its intrinsic function; somatostatin as well as octreotide possesses a high affinity towards somatostatin receptors 2 and 5, which are overexpressed in different tumor cells. [54] Therefore, these peptides are frequently used as a tumor targeting peptides, which have been successfully coupled to drugs, polymers [25] and chromophores to achieve tumor targeting for drugs and tumor visualization by the chromophore. [10, 28]

1.4 References

1. Hermanson, G.T., *Bioconjugate Techniques*. Copyright © 2013 Elsevier Inc., 2013. **Third Edition**.
2. Han, S.Y. and Y.A. Kim, *Recent development of peptide coupling reagents in organic synthesis*. Tetrahedron, 2004. **60**(11): p. 2447-2467.
3. Goddard, D.R. and L. Michaelis, *Derivatives of keratin*. Journal of Biological Chemistry, 1935. **112**(1): p. 361-371.
4. Chalker, J.M., et al., *Chemical Modification of Proteins at Cysteine: Opportunities in Chemistry and Biology*. Chemistry-an Asian Journal, 2009. **4**(5): p. 630-640.
5. Woghiren, C., B. Sharma, and S. Stein, *Protected Thiol Polyethylene-Glycol - a New Activated Polymer for Reversible Protein Modification*. Bioconjugate Chemistry, 1993. **4**(5): p. 314-318.
6. Shiu, H.Y., et al., *Electron-Deficient Alkynes as Cleavable Reagents for the Modification of Cysteine-Containing Peptides in Aqueous Medium*. Chemistry-a European Journal, 2009. **15**(15): p. 3839-3850.
7. Jones, M.W., et al., *Phosphine-mediated one-pot thiol-ene "click" approach to polymer-protein conjugates*. Chemical Communications, 2009(35): p. 5272-5274.
8. Kalia, J. and R.T. Raines, *Hydrolytic stability of hydrazones and oximes*. Angewandte Chemie-International Edition, 2008. **47**(39): p. 7523-7526.
9. Agarwal P, v.d.W.J., Sletten EM, Rabuka D, Bertozzi CR, *A Pictet-Spengler ligation for protein chemical modification*. Proc Natl Acad Sci USA, 2013. **110**(1):**46-51**.
10. Bertozzi, E.M.S.a.C.R., *Bioorthogonal Chemistry: Fishing for Selectivity in a Sea of Functionality*. Angew. Chem. Int. Ed. 2009, 48, 6974 – 6998, 2009.
11. Lelle, M., et al., *Octreotide-Mediated Tumor-Targeted Drug Delivery via a Cleavable Doxorubicin-Peptide Conjugate*. Mol Pharm, 2015. **12**(12): p. 4290-300.
12. Freidel, C., S. Kaloyanova, and K. Peneva, *Chemical tags for site-specific fluorescent labeling of biomolecules*. Amino Acids, 2016.
13. Stephen R. Adams, R.E.C., Larry A. Gross, Brent R. Martin, Grant K. Walkup, Yong Yao, Juan Llopis and Roger Y. Tsien, *New Biarsenical Ligands and Tetracysteine Motifs for Protein Labeling in Vitro and in Vivo: Synthesis and Biological Applications*. Journal of the American Chemical Society, 2002. **124** (21), pp 6063-6076.

14. Blomquist, A.T. and L.H. Liu, *Many-Membered Carbon Rings .7. Cyclooctyne*. Journal of the American Chemical Society, 1953. **75**(9): p. 2153-2154.
15. Kolb, H.C., M.G. Finn, and K.B. Sharpless, *Click chemistry: Diverse chemical function from a few good reactions*. Angewandte Chemie-International Edition, 2001. **40**(11): p. 2004-+.
16. Speers, A.E., G.C. Adam, and B.F. Cravatt, *Activity-based protein profiling in vivo using a copper(I)-catalyzed azide-alkyne [3+2] cycloaddition*. Journal of the American Chemical Society, 2003. **125**(16): p. 4686-4687.
17. Kele, P., et al., *Clickable fluorophores for biological labeling-with or without copper*. Organic & Biomolecular Chemistry, 2009. **7**(17): p. 3486-3490.
18. Agard, N.J., J.A. Prescher, and C.R. Bertozzi, *A strain-promoted [3+2] azide-alkyne cycloaddition for covalent modification of biomolecules in living systems*. Journal of the American Chemical Society, 2004. **126**(46): p. 15046-15047.
19. Blackman, M.L., M. Royzen, and J.M. Fox, *Tetrazine ligation: Fast bioconjugation based on inverse-electron-demand Diels-Alder reactivity*. Journal of the American Chemical Society, 2008. **130**(41): p. 13518-+.
20. Greenfield, R.S., et al., *Evaluation In vitro of Adriamycin Immunoconjugates Synthesized Using an Acid-Sensitive Hydrazone Linker*. Cancer Research, 1990. **50**(20): p. 6600-6607.
21. Kratz, F., et al., *Transferrin conjugates of doxorubicin: Synthesis, characterization, cellular uptake, and in vitro efficacy*. Journal of Pharmaceutical Sciences, 1998. **87**(3): p. 338-346.
22. Duncan, R. and R. Gaspar, *Nanomedicine(s) under the Microscope*. Molecular Pharmaceutics, 2011. **8**(6): p. 2101-2141.
23. Schlage, P., et al., *Anthracycline-GnRH derivative bioconjugates with different linkages: Synthesis, in vitro drug release and cytostatic effect*. Journal of Controlled Release, 2011. **156**(2): p. 170-178.
24. Lelle, M., et al., *Novel cleavable cell-penetrating peptidedrug conjugates: synthesis and characterization*. Journal of Peptide Science, 2014. **20**(5): p. 323-333.
25. Shaunak, S., et al., *Site-specific PEGylation of native disulfide bonds in therapeutic proteins*. Nature Chemical Biology, 2006. **2**(6): p. 312-313.
26. Balan, S., et al., *Site-specific PEGylation of protein disulfide bonds using a three-carbon bridge*. Bioconjugate Chemistry, 2007. **18**(1): p. 61-76.

27. Wang, T., et al., *A Disulfide Intercalator Toolbox for the Site-Directed Modification of Polypeptides*. Chemistry-a European Journal, 2015. **21**(1): p. 228-238.
28. Wang, T., et al., *Bis-sulfide bioconjugates for glutathione triggered tumor responsive drug release*. Chemical Communications, 2014. **50**(9): p. 1116-1118.
29. Wang, T., et al., *Receptor selective ruthenium-somatostatin photosensitizer for cancer targeted photodynamic applications*. Chem Commun (Camb), 2015. **51**(63): p. 12552-5.
30. Mar E. B. Smith, F.F.S., Chris P. Ryan and James R. Baker, *Protein Modification, Bioconjugation, and Disulfide Bridging Using Bromomaleimides*. 2010.
31. Schumacher, F.F., et al., *In situ maleimide bridging of disulfides and a new approach to protein PEGylation*. Bioconjug Chem, 2011. **22**(2): p. 132-6.
32. Bertrand, N., et al., *Cancer nanotechnology: The impact of passive and active targeting in the era of modern cancer biology*. Advanced Drug Delivery Reviews, 2014. **66**: p. 2-25.
33. Bae, Y.H. and K. Park, *Targeted drug delivery to tumors: myths, reality and possibility*. J Control Release, 2011. **153**(3): p. 198-205.
34. Hoffman, A.S., *The origins and evolution of "controlled" drug delivery systems*. Journal of Controlled Release, 2008. **132**(3): p. 153-163.
35. Torchilin, V.P., *Drug targeting*. European Journal of Pharmaceutical Sciences, 2000. **11**: p. S81-S91.
36. Strebhardt, K. and A. Ullrich, *Paul Ehrlich's magic bullet concept: 100 years of progress*. Nature Reviews Cancer, 2008. **8**(6): p. 473-480.
37. Ghaz-Jahanian, M.A., et al., *Application of Chitosan-Based Nanocarriers in Tumor-Targeted Drug Delivery*. Molecular Biotechnology, 2015. **57**(3): p. 201-218.
38. Bergers, G. and L.E. Benjamin, *Tumorigenesis and the angiogenic switch*. Nature Reviews Cancer, 2003. **3**(6): p. 401-410.
39. Jain, R.K., *Delivery of Novel Therapeutic Agents in Tumors - Physiological Barriers and Strategies*. Journal of the National Cancer Institute, 1989. **81**(8): p. 570-576.
40. Heldin, C.H., et al., *High interstitial fluid pressure - An obstacle in cancer therapy*. Nature Reviews Cancer, 2004. **4**(10): p. 806-813.

41. Barenholz, Y., *Doxil (R) - The first FDA-approved nano-drug: Lessons learned*. Journal of Controlled Release, 2012. **160**(2): p. 117-134.
42. Monopoli, M.P., et al., *Biomolecular coronas provide the biological identity of nanosized materials*. Nature Nanotechnology, 2012. **7**(12): p. 779-786.
43. Gu, F., et al., *Precise engineering of targeted nanoparticles by using self-assembled biointegrated block copolymers*. Proceedings of the National Academy of Sciences of the United States of America, 2008. **105**(7): p. 2586-2591.
44. Valencia, P.M., et al., *Effects of ligands with different water solubilities on self-assembly and properties of targeted nanoparticles*. Biomaterials, 2011. **32**(26): p. 6226-6233.
45. Messersmith, W.A. and D.J. Ahnen, *Targeting EGFR in colorectal cancer*. New England Journal of Medicine, 2008. **359**(17): p. 1834-1836.
46. Administration, U.S.F.a.D., *Class Labeling Changes to anti-EGFR monoclonal antibodies, cetuximab (Erbix) and panitumumab (Vectibix): KRAS Mutations*. 2010-01-11.
47. *Official manufacturer website for up-to-date dosing & safety information: <http://www.sandostatin.com>*. 2016.
48. Kirpotin, D.B., et al., *Antibody targeting of long-circulating lipidic nanoparticles does not increase tumor localization but does increase internalization in animal models*. Cancer Research, 2006. **66**(13): p. 6732-6740.
49. Minko, T., *Drug targeting to the colon with lectins and neoglycoconjugates*. Advanced Drug Delivery Reviews, 2004. **56**(4): p. 491-509.
50. Daniels, T.R., et al., *The transferrin receptor part II: Targeted delivery of therapeutic agents into cancer cells*. Clinical Immunology, 2006. **121**(2): p. 159-176.
51. Huang, C.M., Y.T. Wu, and S.T. Chen, *Targeting delivery of paclitaxel into tumor cells via somatostatin receptor endocytosis*. Chemistry & Biology, 2000. **7**(7): p. 453-461.
52. Novartis,
https://www.pharma.us.novartis.com/sites/www.pharma.us.novartis.com/files/sandostatin_inj.pdf. 2016.
53. Lamberts, S.W.J., E.P. Krenning, and J.C. Reubi, *The Role of Somatostatin and Its Analogs in the Diagnosis and Treatment of Tumors*. Endocrine Reviews, 1991. **12**(4): p. 450-482.

54. Moller, L.N., et al., *Somatostatin receptors*. *Biochimica Et Biophysica Acta-Biomembranes*, 2003. **1616**(1): p. 1-84.

55. De Martino, M.C., L.J. Hofland, and S.W.J. Lamberts, *Somatostatin and somatostatin receptors: from basic concepts to clinical applications*. *Neuroendocrinology: Pathological Situations and Diseases*, 2010. **182**: p. 255-280.

2 Motivation and Objectives

Gaining deeper knowledge of function and possible utilization of proteins in living organism is an increasing necessity in many fields like biology, chemistry and medicine. The widespread use of bioconjugated techniques provides researchers with an ever expanding toolbox to take advantage of the functionalities of different proteins either in using such molecules as potential drugs or as targeting moiety for addressing specific cells or tissues.

However, the critical drawback of conventional covalent, chemical techniques is the resulting heterogeneity of the modified proteins caused by the lack of selectivity of the chosen functional groups. In contrast, bioorthogonal techniques that enable the selective modification of proteins at pre-defined positions hold a central role in this regard and offer the opportunity to design biopharmaceuticals with increased efficacy as well as superior pharmacokinetic properties to tackle therapeutic challenges that are left unmet by the current modification methods. Thereby, a key requirement to ensure optimal efficacy of protein therapeutics is the preservation of the native function of the protein upon conjugation of the synthetic component. Performing such a chemoselective reaction on a protein and preserving its integrity is a very challenging task, due to the intrinsic sensitivity of biomolecules against heat, presence of organic solvents as well as high concentrations of salts or other chemical reagents.

Naturally, such selectivity and preservation of the integrity can be achieved by targeting one of the most distinguished canonical amino acid on proteins, namely cysteine. The thiol group of cysteine is an excellent soft nucleophile, rarely present as a free amino acid on the protein surface and usually found in disulfide bonds.

As mentioned and discussed in the previous section, different cross-linkers enabling the disulfide modification of proteins have been published within the last decade comprising different advantages and disadvantages such as stability under physiological conditions, conversion time, reaction yield or simply the molecular size of the cross-linker and necessary synthetic effort.

Therefore, the main goal of this work is to develop novel disulfide intercalating agents combining the advantages of the aforementioned approaches, while overcoming the disadvantages of previously reported cross-linkers. Applications like the PEGylation of peptides, visualization of biomolecules inside the cell and a targeted drug delivery towards tumor cells could benefit from the chemical properties of novel, efficient conjugates, thus, these concepts will be investigated in this work (Figure 17).

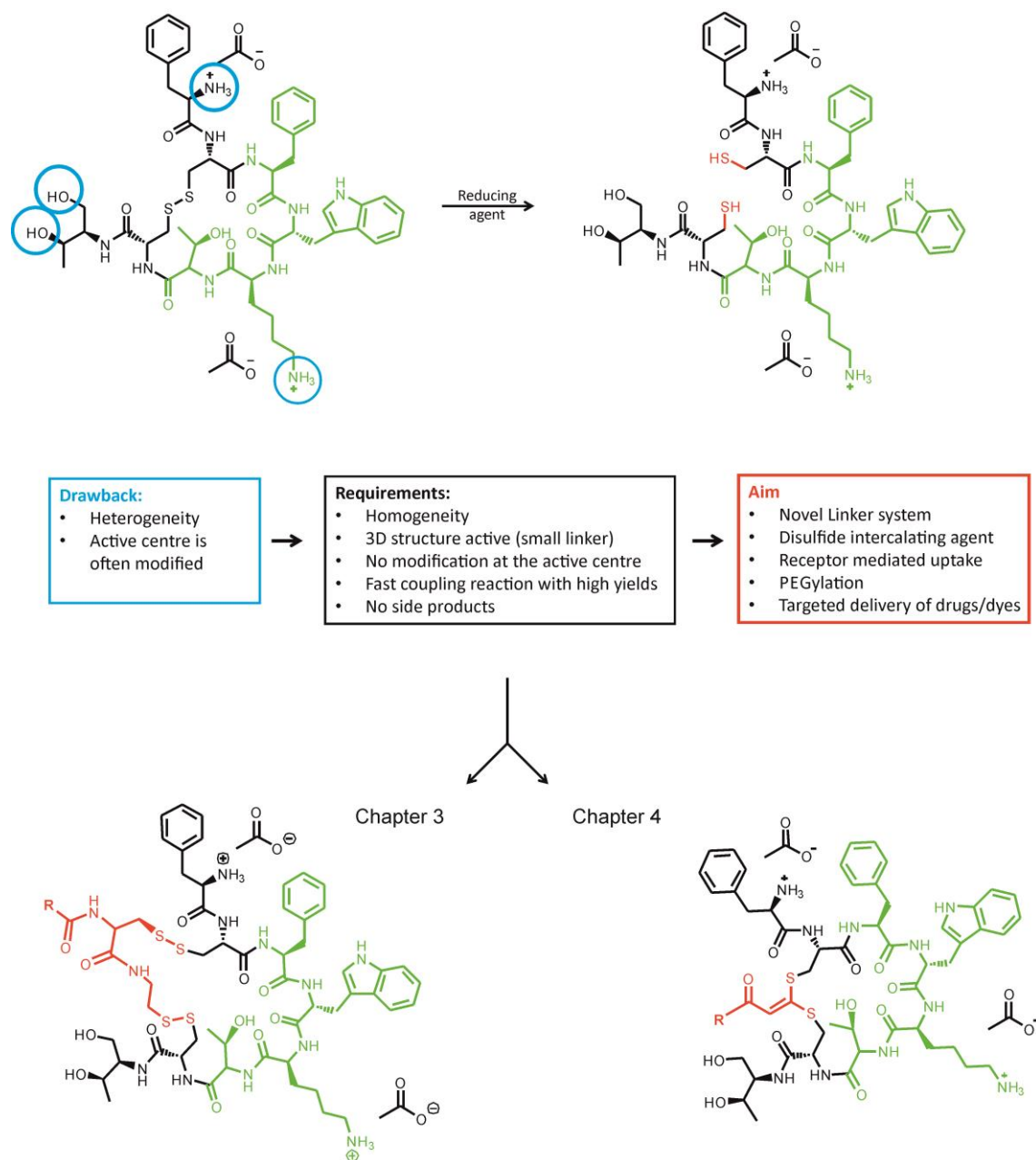


Figure 17: Aim, requirements and drawbacks in the field of peptide modification (octreotide was chosen as the model peptide, in which blue circles indicate general possible modification sites of the peptide and the green highlighted part of the peptide indicates the receptor binding motif of octreotide)

In the first part of this work (Chapter 3) the main focus is on the development of an improved cleavable cross-linker, based on an approach previously described in our group by [REDACTED]. The advantage to this conjugate is that the number of atoms between the sulfur atoms of the initial disulfide bond was reduced from 11 to 6 atoms. In addition, compared to previously reported bis-sulfone and maleimide based conjugates, the delivered cargo can be released inside the cell.

After the successful synthesis that started from the amino acid cysteine, peptide modification was tested first with a model peptide, namely octreotide, possessing a high binding affinity towards cell surface somatostatin receptors 2 and 5, which are overexpressed on tumor cells (e.g. lung cancer). Different perylenediimide-based dyes were synthesized and coupled to the peptide to visualize the conjugates inside cells. In the next step, this approach was extended to the targeted delivery of the anticancer drug doxorubicin within cancer cells. Furthermore, functional groups like hydrazine, hydroxylamine, iodo- or ethynyl-groups were introduced to octreotide based on the novel intercalation cross-linker, to enable bioorthogonal-coupling reactions with different types of substituents.

In Chapter 4, a completely novel conjugate was designed and synthesized focusing on the molecular size as well as fast and high coupling efficiencies. The goal is to create a cross-linker, which combines the advantages of previously reported examples while only needing one atom for the re-bridging of the disulfide bond after the reductive cleavage. A cross-linker like this has not been reported in literature and possesses the unique advantage that the spatial structure of modified peptide is perturbed as little as possible. Peptide modification using the 2, 3-dibromomaleimide, as performed by Baker and coworkers, is achieved by a double addition-elimination reaction of the bromines with the thiol groups of the reduced peptide's disulfide bond. After the addition of the thiolate to the bromo-carrying carbon atom, the elimination of the bromine is favored by the constitution of the maleimide and the corresponding mesomeric effect inside the five membered rings, as the carbon atoms carrying the halogens are partially positively charged. In contrast to this approach, 3,3-dichloroacrylic acid was chosen in this work as the cornerstone of a novel cross-linker that inserts only one carbon atom between the two thiol ends by retaining the cyclic structure of the peptide. Within the modification process of a peptide at the disulfide-bond, both chlorines are substituted stepwise by the sulfhydryl groups of the reduced peptide (two subsequent addition-elimination reactions).

First, the effect of the insertion of the novel cross-linker was investigated by computational studies as well as circular dichroism and receptor binding studies with AtT-20 pituitary tumor cells, which is endogenously expressing somatostatin receptor subtypes. In the following steps the novel conjugate was used as the cornerstone for three different topics:

- 1) PEGylation of octreotide in order to improve the plasma half-life of the peptide,
- 2) Tumor imaging based on a dye-octreotide conjugate and
- 3) Targeted drug delivery based on a drug-octreotide conjugate.

Among others, microscopy and cell viability studies were performed to prove the intended application after having successfully finished the synthesis of all the desired conjugates.

The anticancer drug doxorubicin was chosen as the model drug within this work, because it is highly toxic and possesses an intrinsic fluorescence. Furthermore, doxorubicin belongs to the class of DNA intercalation agents and it is used in the clinical treatment of different cancer types (e.g. solid breast cancer). Therefore, Chapter 5 focuses on the possibility to increase the toxicity of this drug by the addition of different indole units, as they are known to be strong minor groove binders of the DNA. The motivation of this work is to combine both ways of DNA binding in one molecule: DNA intercalation and minor groove binding. The target molecule should possess a higher binding affinity to DNA, which would result in a higher toxicity compared to single doxorubicin or indole derivatives alone, as well as reduced doses reducing side effects during treatments. Furthermore, Microscale Thermophoresis, a relatively new technique to determine binding affinities between biomolecules, was applied to evaluate the binding of doxorubicin-derivatives with DNA. The advantage of MST compared to other techniques such as isothermal titration calorimetry, electrophoretic mobility shift assay) or surface plasmon resonance based techniques are the easy sample handling, small sample amount, short measuring time and that there is almost no limitation of the size or molecular weight of the bound conjugates for MST.

Finally, chapter 6 summarizes the results obtained and outlines future applications and utilization of bioorthogonal cross-linkers, doxorubicin, peptides as well as proteins in medicine.

3 Novel disulfide-based linker platform for site-selective modification of peptides and proteins

As already mentioned in the introduction chapter, Brocchini *et al.* pioneered the field of disulfide-intercalating agents with his work published in 2006 with a novel designed and synthesized bis-sulfone linker system (Figure 18, compound a). [1] For the first-time disulfide bonds were used for the PEGylation of peptides by the introduction of two thioether bonds, keeping the cyclic structure of somatostatin intact. However, time consuming and extensive synthesis steps have to be carried out in advance and the final peptide modification needs long reaction times (~24 h) with relatively low yields depending on the attached cargo. [2] In contrast, functional bis-bromomaleimides are easier to synthesize and enable fast peptide modification with higher yields as it was shown by Baker *et al.* (Figure 18, compound b). [3] Nonetheless, all intercalating reagents described in the literature based on these two techniques generate two widely stable thioether bonds with the biomolecule, which cannot be cleaved under physiological conditions and thereby could not be applied for the controlled release of a toxic freight yet.

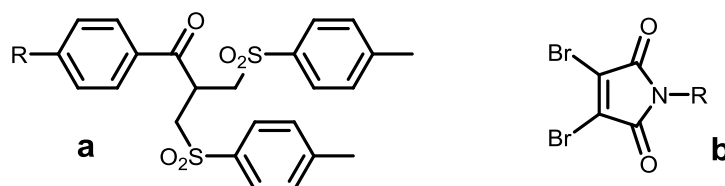


Figure 18: a) Bis-sulfone linker, b) bis-bromomaleimide linker

Overcoming the aforementioned limitations, the focus of this chapter is set on the design and synthesis of a novel cleavable disulfide-intercalating cross-linking reagent for the site-selective modification of peptides. This linker reagent is similar to the one introduced by our group before (Figure 19, compound **c**), with the advantage to be smaller in size (Figure 19, compound **d**). A decrease of the number of atoms between the sulfur atoms of the initial disulfide bond from 11 atoms to 6 atoms is a crucial point as the peptide structure is less influenced by the shorter spacer after modification (Figure 19). Octreotide was chosen as a model peptide for accessing the potential of the novel linker **d**, because only one single disulfide bond is present for chemical modification in this peptide. [4, 5]

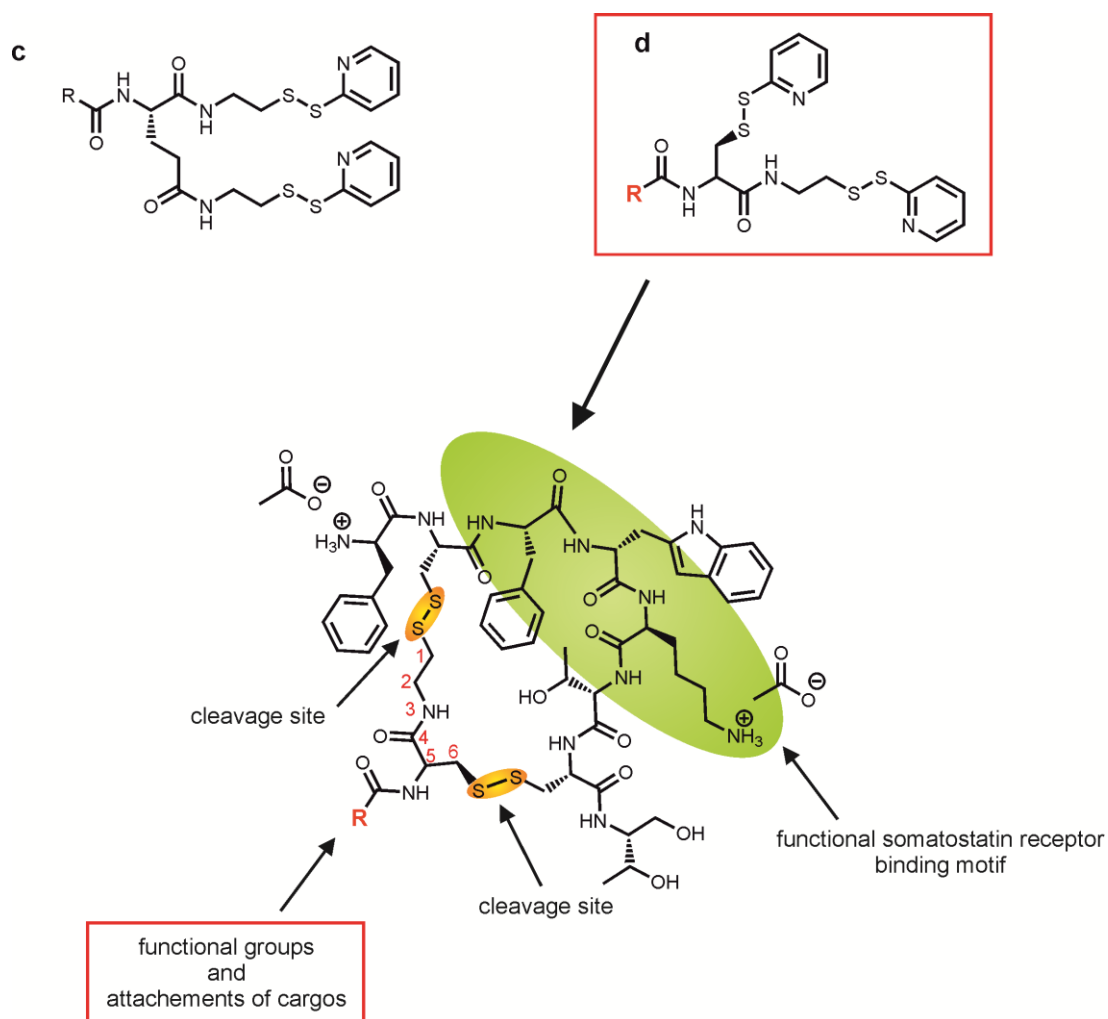


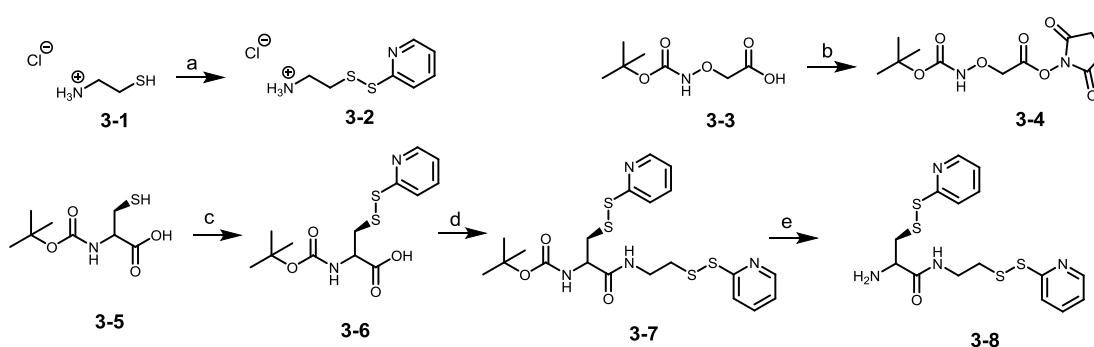
Figure 19: Disulfide-based intercalating agent, c) old version, d) novel version, the red R is going to be replaced by the different functional groups going to be attached to the linker in this work

Furthermore, there is an increasing interest in the development of chemically modified peptides, which enable bioorthogonal-coupling reactions with different types of substituents. Therefore, next to the design of the novel linker, the main aim of this section is to extend the linker's application by the introduction of a huge variety of functional groups suitable for the attachment of different molecules to the peptide. Finally, the novel linker platform was used to create new bioconjugates by attaching different molecules as a drug or chromophore to octreotide, having the combined properties of its individual components.

3.1 Synthesis and Characterization

Amino acids offer a high potential for bioorthogonal reaction due to its diversity as they are small molecules which typically bear several different reactive sites. Therefore, as main scaffold for the synthesis of the novel linker mentioned in the previous passage (compound **d**, Figure 19) cysteine-derivative N-(tert-Butoxycarbonyl)-cysteine **3-5** was selected. It enables the introduction of different functionalities to construct the desired linker and further modification opportunities.

The straightforward synthetic route toward the novel linker **3-7** is shown on Scheme 1. It starts with an activation of the thiol group of the cysteine for further disulfide coupling reactions by stirring **3-1** overnight in methanol with a 6-fold excess of 2,2'-Dithiodipyridine. [6] Purification was accomplished by precipitation in hexane and a subsequent filtration. To synthesize the final disulfide-intercalating agent **3-7**, the carboxylic acid was reacted with 2-(2-pyridyldithio)-ethylamine hydrochloride (**3-2**), while *N,N,N,N*-tetramethyl-*O*-(*N*-succinimidyl)uronium tetrafluoroborate (TSTU) was used as a coupling reagent to form the amide bond. The product was washed with brine to remove unreacted educts. Afterwards, silica column chromatography was used to obtain the final pure compound **3-7** as yellow oil with high yields (86 %). With compound **3-7** in hand, a novel, smaller and cleavable disulfide intercalation reagent was successful synthesized (Scheme 1). It possesses two activated thiol groups for the formation of two new disulfide bonds during the peptide intercalation process and the number of atoms, which is introduced between the peptides sulfur atoms, is reduced to 6 atoms only.



Scheme 1: Synthesis of 2-amino-3-(pyridin-2-yl)disulfaneyl-N-(2-(pyridin-2-yl)disulfaneyl)ethylpropanamide (**3-8**): a) 2,2'-Dithiodipyridine (6 equiv), methanol, argon, overnight, r.t., quantitative yield. b) *N*-Hydroxysuccinimide (1.05 equiv), *N,N'*-diisopropylcarbodiimide (1.15 equiv), dry DCM, argon, 4 h, r.t., 93%. c) 2,2'-Dithiodipyridine (6 equiv), methanol, argon, overnight, r.t., quantitative yield. d) **3-2** (1.15 equiv), TSTU (1.15 equiv), DIPEA (4 equiv), dry DMF, argon, 5 h, r.t., 86%. e) dry DCM/TFA (1:1), 1 h, r.t., quantitative yield.

In order to prove the successful coupling and the existence of both 2-pyridyldisulfides, compound **3-7** was analyzed by MALDI-TOF MS as well as NMR. The corresponding NMR spectrum of **3-7** exhibits well-separated and clearly assignable signals as depicted on Figure 20. The intensity ratios of all peaks agree with the theoretically expected integrals of all protons, as for instance of the 2-pyridyl groups (8 protons) or the two amide-bonds (2 protons).

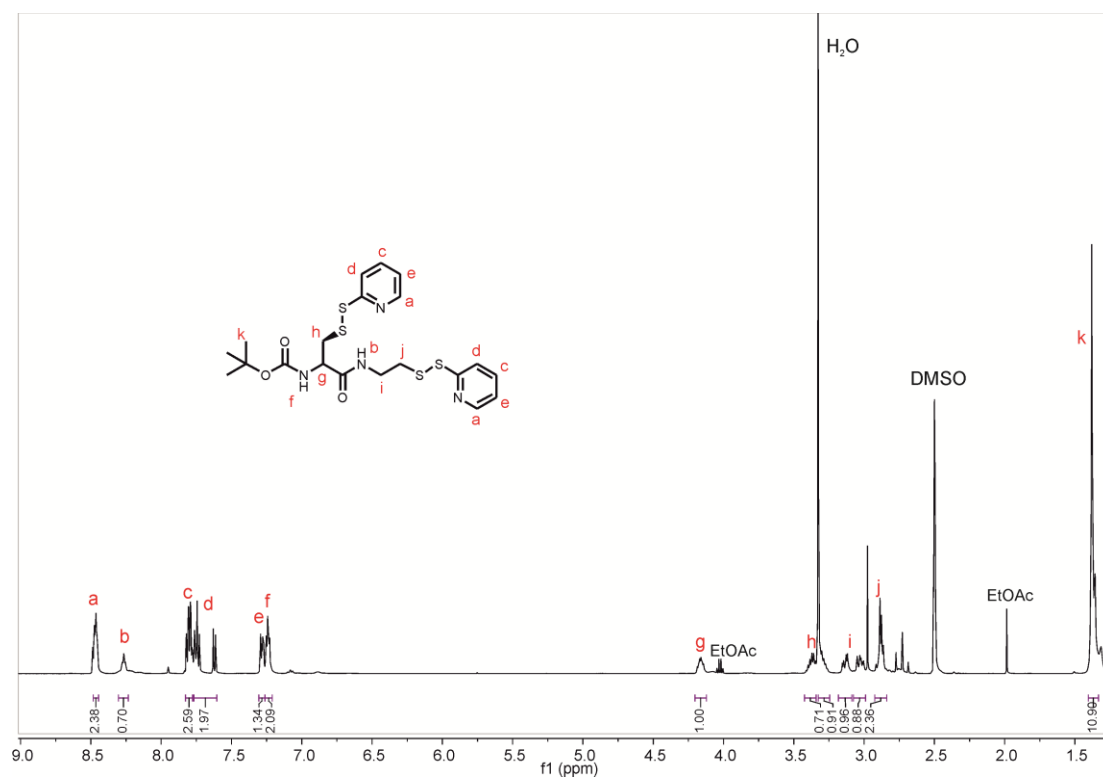


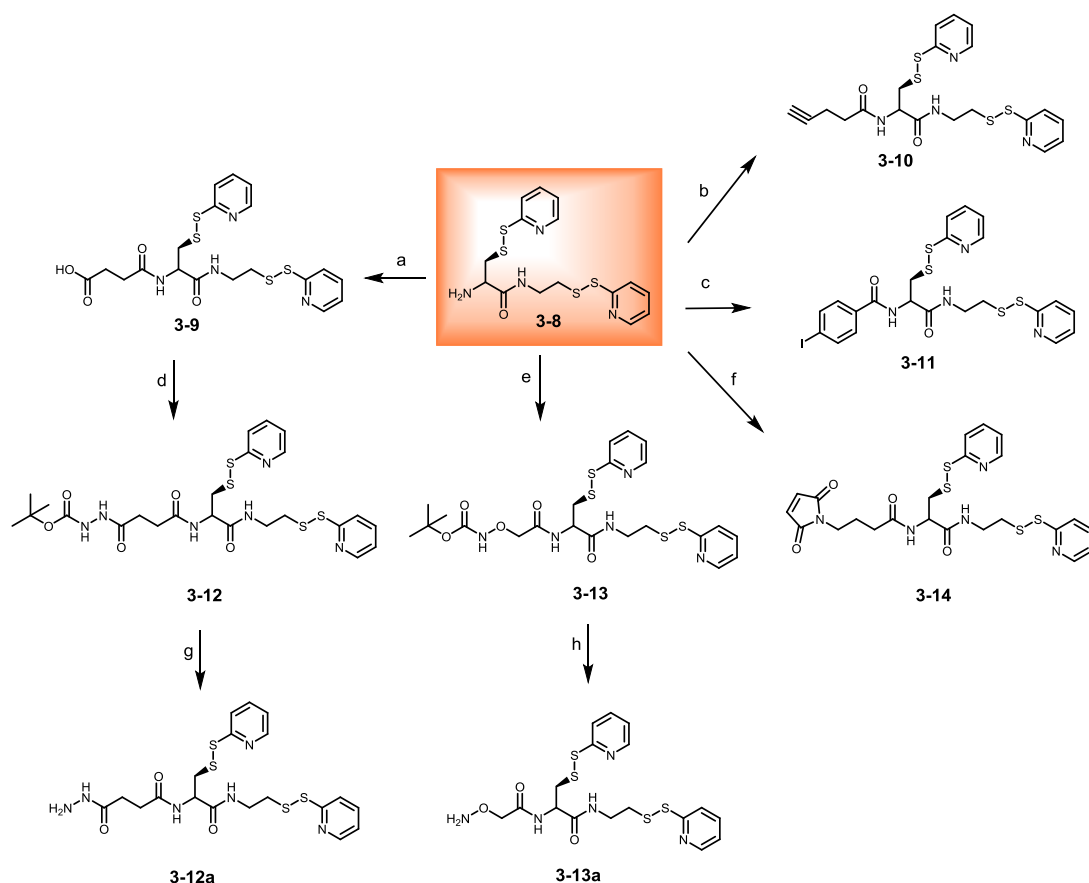
Figure 20: ¹H-NMR spectrum of compound **3-7** in DMSO-d₆ (300 MHz)

3.1.1 Introduction of different functional groups to create a novel linker platform

The intention of this section is the extension of the portfolio of chemically modified octreotide with different functional groups based on the novel linker **3-7**, as this strategy offers a broad range of alternatives for the bioorthogonal modification with different molecules.

Besides the frequently used amine and carboxyl groups we focused on the introduction of iodo- and ethynyl - substituents, enabling subsequent coupling reactions such as palladium(0)-catalyzed cross coupling reactions (e.g. Heck, Suzuki or Sonogashira reactions) as well as [2+3] cycloaddition “click” reactions. [4] For instance, dyes containing an azide bond can be easily attached to a peptide in a [2+3] cycloaddition “click” reaction with the introduced ethynyl group at the linker. Additionally, further functional groups as a hydrazine as well as a hydroxylamine group were introduced to the novel linker allowing the attachment of aldehyde or ketone carrying molecules *via* an oxime or pH sensitive hydrazone bond.

As main scaffold for the introduction of different unnatural functional groups to octreotide, the novel disulfide intercalating linker **3-7** was selected. The straightforward synthetic route towards the different linker molecules is shown on Scheme 2. In all cases it starts with the deprotection of **3-7** to obtain compound **3-8** bearing a free amine. This reaction was performed under acidic conditions with equal amounts of dichloromethane and trifluoroacetic acid and allowed quantitative yield within 1 h. [7] In the following steps **3-8** was either directly coupled to an carboxyl bearing compound or modified with different linker molecules to achieve an introduction of the desired ethynyl-, iodo-, acid-, hydrazine- or hydrazone- functional groups as described in Scheme 2.



Scheme 2: Synthesis of the different 2-amino-3-(pyridin-2-ylsulfaneyl)-N-(2-(pyridin-2-ylsulfaneyl)ethyl)propanamide - derivatives: a) succinic anhydride (6 eq), DIPEA (6 eq), NMP, argon, 2 h, r.t., 68%. b) 4-pentynoic acid (1.02 eq), HATU (1.02 eq), DIPEA (1.2 eq), dry DMF, argon, 2 h, r.t., 87%. c) 4-iodobenzoic acid (1.05 eq), HATU (1.25 eq), DIPEA (1.25 eq), dry DMF, argon, 2 h, r.t., 79%. d) HATU (1.15 eq), DIPEA (1.2 eq), tert-butyl carbazate (1.1 eq), dry DMF, argon, 1.5 h, r.t., 85%. e) 4 (1.2 eq), DIPEA (1.5 eq), dry DMF, argon, 3 h, r.t., 50%. f) 4-maleimidobutyric acid (1.1 eq), HATU (1.15 eq), DIPEA (1.2 eq), dry DMF, argon, 2 h, r.t., 54%, g) dry DCM/TFA (1:1), 1 h, r.t., quantitative yield, h) dry DCM/TFA (1:1), 1 h, r.t., quantitative yield

After the successful deprotection of **3-7**, both solvents (DCM and TFA) were removed under reduced pressure. Compound **3-8** was dissolved in DMF and DIPEA was added as base to conduct the following reactions under slightly basic conditions. For the synthesis of **3-9**, the Boc-protected **3-8** was stirred in NMP with an excess of succinic anhydride for 2 h. Afterwards EtOAc was added to the reaction mixture, which was washed with brine to obtain the pure product. The introduction of an oxime as well as a hydrazine functional group to the linker was accomplished by an amide bond formation by adding tert-butyl carbazate to **3-9** and **3-4** to **3-13** (Scheme 2). The active ester **3-4** was prepared as described before in Scheme 1. After removal of DMF under reduced pressure compounds **3-12** and **3-13** were purified by silica column chromatography. Finally, an attachment of a maleoyl-

ethynyl- and iodo-functionality to the linker cornerstone **3-8** was achieved by the reaction with 4-maleimidobutyric acid, 4-pentynoic acid or 4-iodobenzoic acid. In all cases DMF was used as the solvent, HATU as a coupling reagent and DIPEA as the base to enable a slightly basic pH of the reaction solution (Scheme 2).

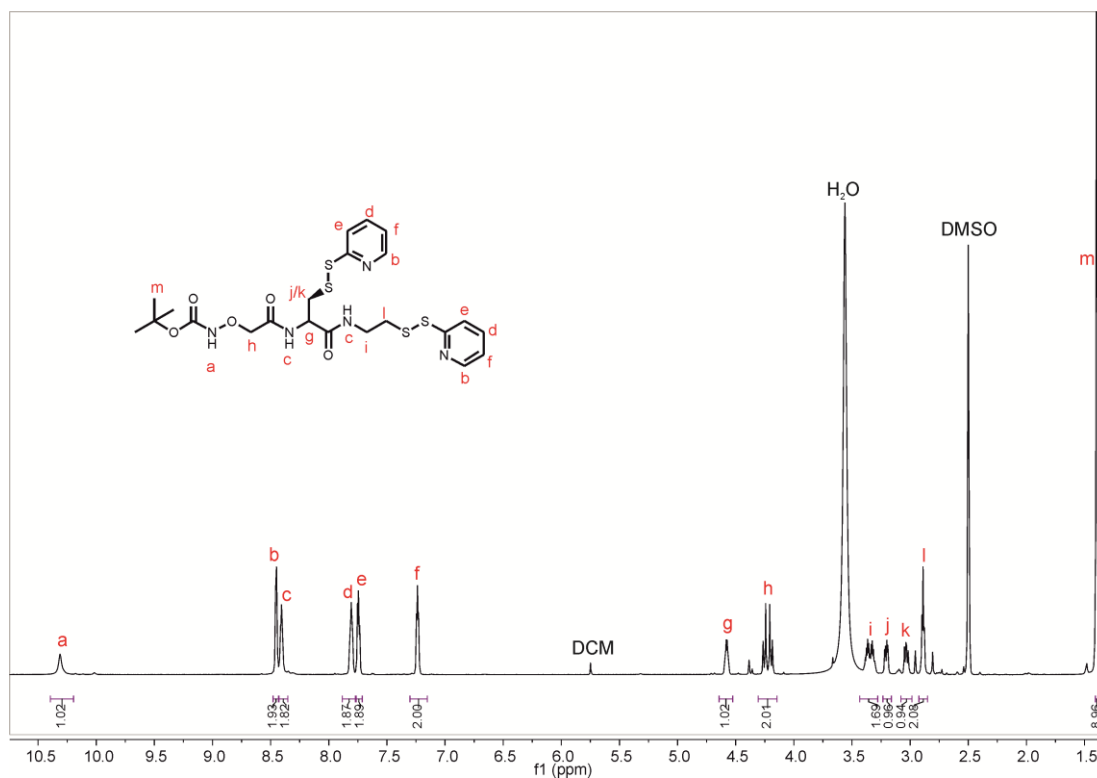
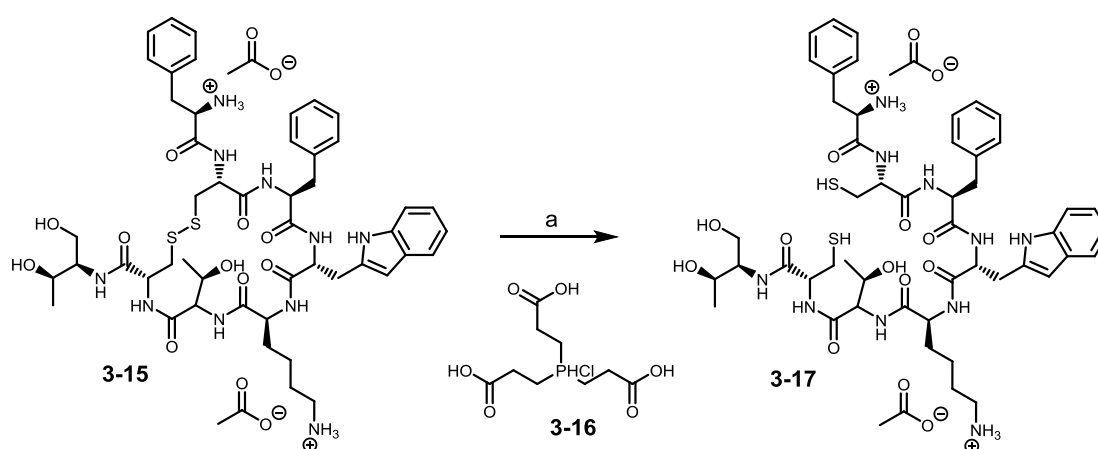


Figure 21: ¹H-NMR spectrum of compound **3-13** in DMSO-d₆ (300 MHz)

All compounds were analyzed and identified by means of NMR spectroscopy and mass spectrometry (MALDI-TOF). As an example **3-13** was chosen and the corresponding characteristic ¹H NMR spectrum together with the peak assignment is shown on Figure 21. The integrated signals of the 2-pyridyl disulfides as well as the amide protons were utilized for the confirmation of the structure. Furthermore, the existence of the protected aminoxy-functionality can be proven by both singlets at 10.32 ppm and 1.42 ppm as well as the additional two methyl-protons *h*, giving a quartet at 4.25 ppm. All other signals are as expected identical to compound **3-7**. Traces of the solvents as DCM and EtOAc could not be removed completely even after intensive drying steps at the vacuum line (10⁻³ mbar, 48 h), which is probably caused by the oily characteristic of product **3-13**.

3.1.2 Reduction of octreotide

After the successful synthesis of the different disulfide intercalation agents described in the previous section, the model peptide octreotide was modified in the following steps. The disulfide bond of the peptide was reduced to make the sulfur atoms accessible; otherwise an intercalation would not be possible. The reduction of the cyclic peptides, bearing one disulfide bond, is known in literature and is generally performed with equimolar amounts of either dithiothreitol (DTT) or *tris*(2-Carboxyethyl)phosphine-hydrochloride (TCEP) **3-16**, within 1 h (Scheme 3). [1] [8] [9]



Scheme 3: Reduction of octreotide using TCEP as the reducing agent, a) TCEP (**3-16**, 4 eq), phosphate buffer pH 6.2, argon, r.t., 1 h, 90 %

The above-mentioned reducing agent has no thiol groups in contrast to DTT and was therefore used in this reaction to avoid any side reactions with the linker conjugates. Due to the analogy of somatostatin and octreotide the conditions described in literature, reduction with 1.5 eq of TCEP in a phosphate buffered solution (pH 6.2) was applied here and followed by analytical RP-HPLC. [3, 10] Figure 22 shows the reduction of octreotide to its reduced version within 1 h. The detection of the peptide was performed at 280 nm, the characteristic UV-absorption area of the aromatic amino acids phenylalanine and tryptophan, which are part of octreotide amino acid sequence. Interestingly, there is always a small peak (26 min) with shorter retention time present in the chromatogram, next to the main peak of the product at 27 min. This fact is caused by the favorable ring closure of the peptide in absence of TCEP, as both substances are separated on the column as soon as the reaction solution is in the HPLC system. The ring closure on the HPLC could be verified by a comparison of the retention times, as the small peak has the same retention time as

octreotide. Furthermore, octreotide as well as its reduced form could be detected by MALDI-TOF MS.

Reduction of octreotide and the additional purification by preparative HPLC is performed before each coupling step to guarantee that the reduced form of the peptide is present, thus, the fractions collected were used directly for subsequent coupling steps.

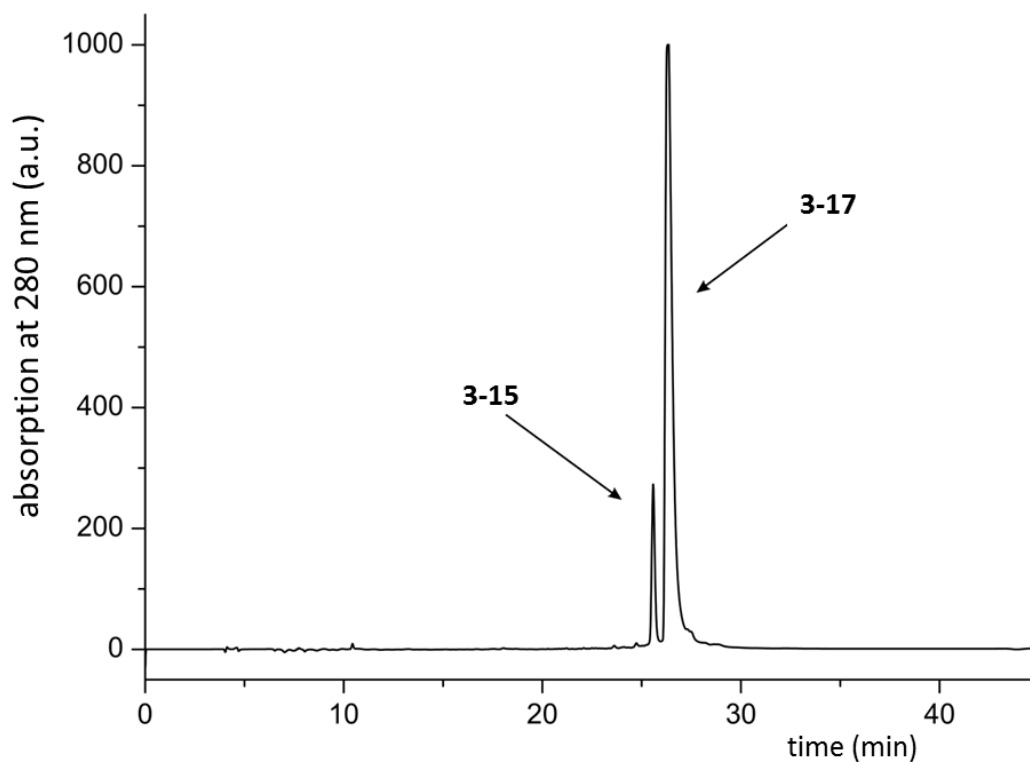
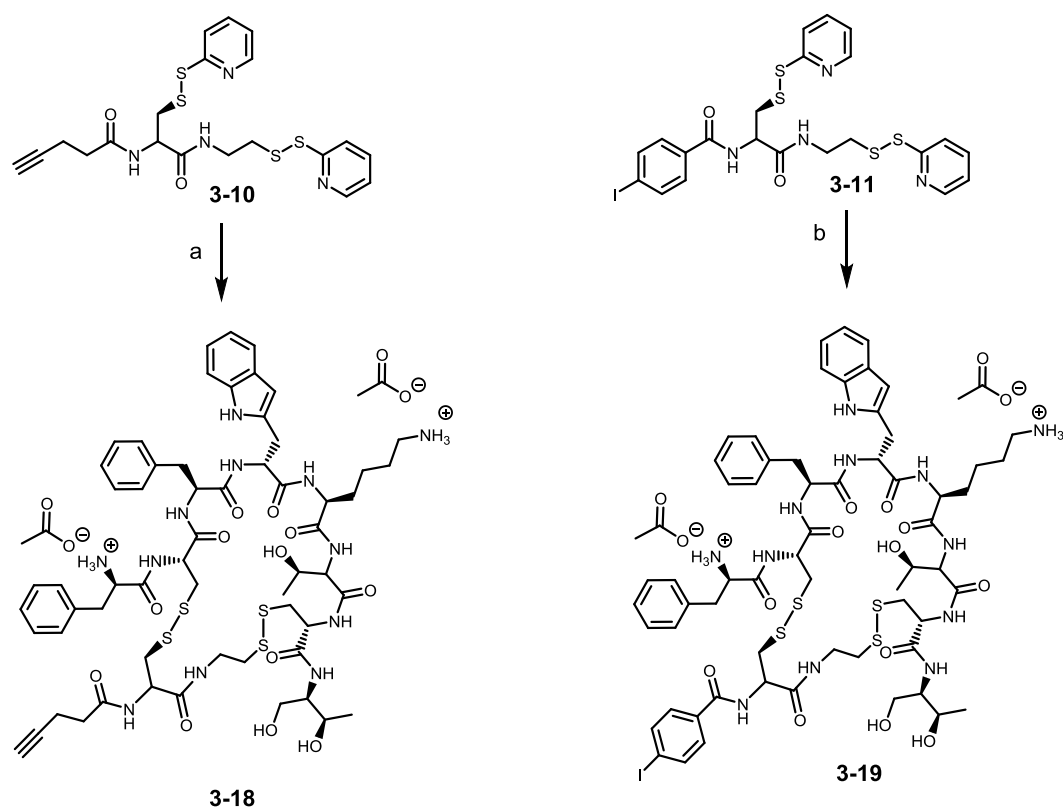


Figure 22: Reduction of native octreotide **3-15** using TCEP as the reducing agent to form **3-17** after 1h of reaction time

3.1.3 Synthesis of ethynyl- and iodine-modified octreotide conjugates

Extending the portfolio of chemically modified octreotide with different functional groups is one of the main interests of this study offering alternatives for the bioorthogonal modification of this peptide. Especially the introduction of functional groups which are not present in nature as iodo- and ethynyl – substituents are very attractive, as bioorthogonal coupling reactions as palladium(0)-catalyzed cross coupling reactions (Heck, Suzuki or Sonogashira) as well as [2+3] cycloaddition “click” reactions are rendered possible. [4]

The synthesis of the bifunctional linkers **3-10** and **3-11** as well as the reduction of the peptide was already described, enabling the final modification of octreotide. Accordingly, compounds **3-10** and **3-11** were added to an excess of the reduced peptide octreotide (**3-17**) and reacted for 1 h in phosphate buffer pH 7.4 (Scheme 4). The reaction mixture was analyzed by analytical HPLC at different time points.



Scheme 4: Synthesis of ethynyl- and iodo-functionalized octreotide **3-18** and **3-19**, a) **3-17** (1.2 eq), DMF, DPBS, Argon, 1 h, r.t., 83 %, b) **3-17** (1.2 eq), DMF, DPBS, Argon, 1 h, r.t., 72 %

The chromatograms of octreotide, reduced octreotide and the modified octreotide were recorded and visualized in Figure 23 for the synthesis of **3-18**. The reduced octreotide (red

curve, b) has a prolonged retention time (28 min) compared to octreotide (black curve, a). The peak at 27 min of the red curve with lower absorbance intensity belongs to octreotide. The prolonged retention time of the modified octreotide *c* compared to octreotide *a*, suggests that the conjugate is getting more hydrophobic, as the interaction with the unpolar column material is increased. Full conversion of the reduced peptide is not possible, as it was used in excess, which explains the peak of the reduced octreotide at around 28 minutes in the HPLC run of compound *c*.

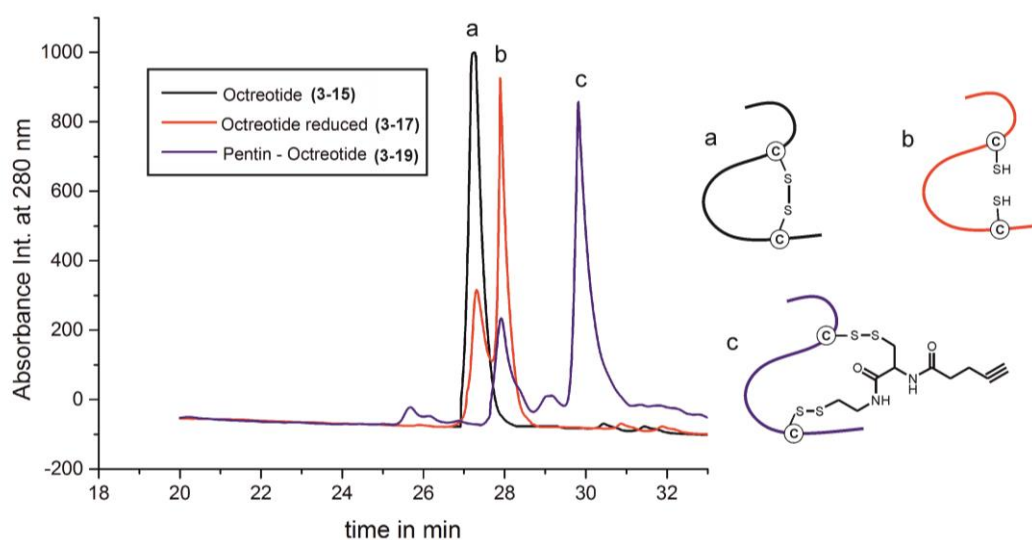


Figure 23: HPLC chromatogram of octreotide **3-15** a (black), reduced octreotide **3-17** b (red) and Iodo-octreotide **3-19** c (blue)

After purification by preparative RP-HPLC the collected fractions were analyzed by MALDI-TOF MS as shown on Figure 24 to confirm the presence of the products **3-18** and **3-19**.

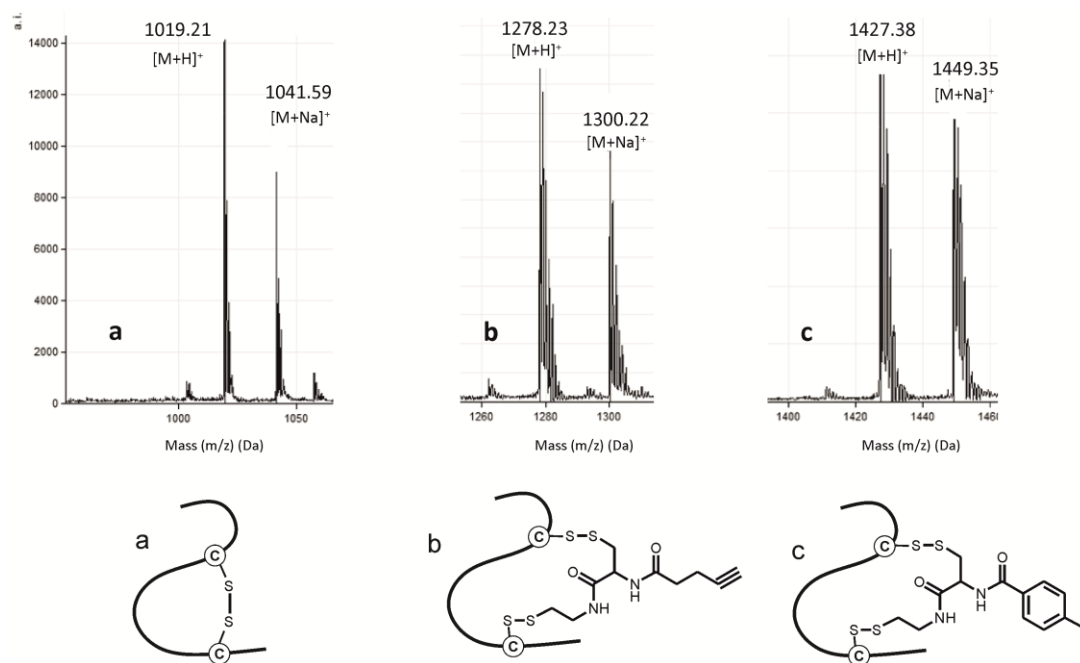
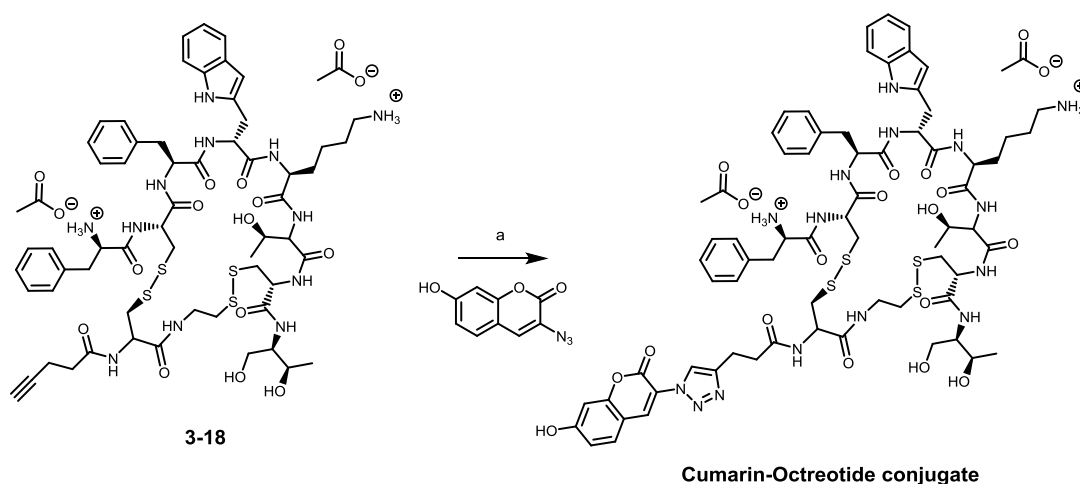


Figure 24: MALDI-TOF MS spectrum of octreotide **3-15** (a), ethynyl-octreotide **3-18** (b) and iodo-octreotide **3-19** (c), (matrix: α -CHCA)

Examples how to take advantage of the herein introduced functional groups as ethynyl and iodo groups for peptide modifications were already discussed and proven by Pfisterer *et al.* with the model peptide somatostatin using the bis-sulfone linker, for instance the cycloaddition of 3-azido-7-hydroxycumarin. The same is feasible using octreotide as the peptide and the herein introduced linker agents (Scheme 5). Furthermore, all these conjugates described here have the additional advantage over the bis-sulfone linker to be cleavable, meaning if a cargo is transported (e.g. dye or drug) it can be released inside the cytosol of the cell. [4]



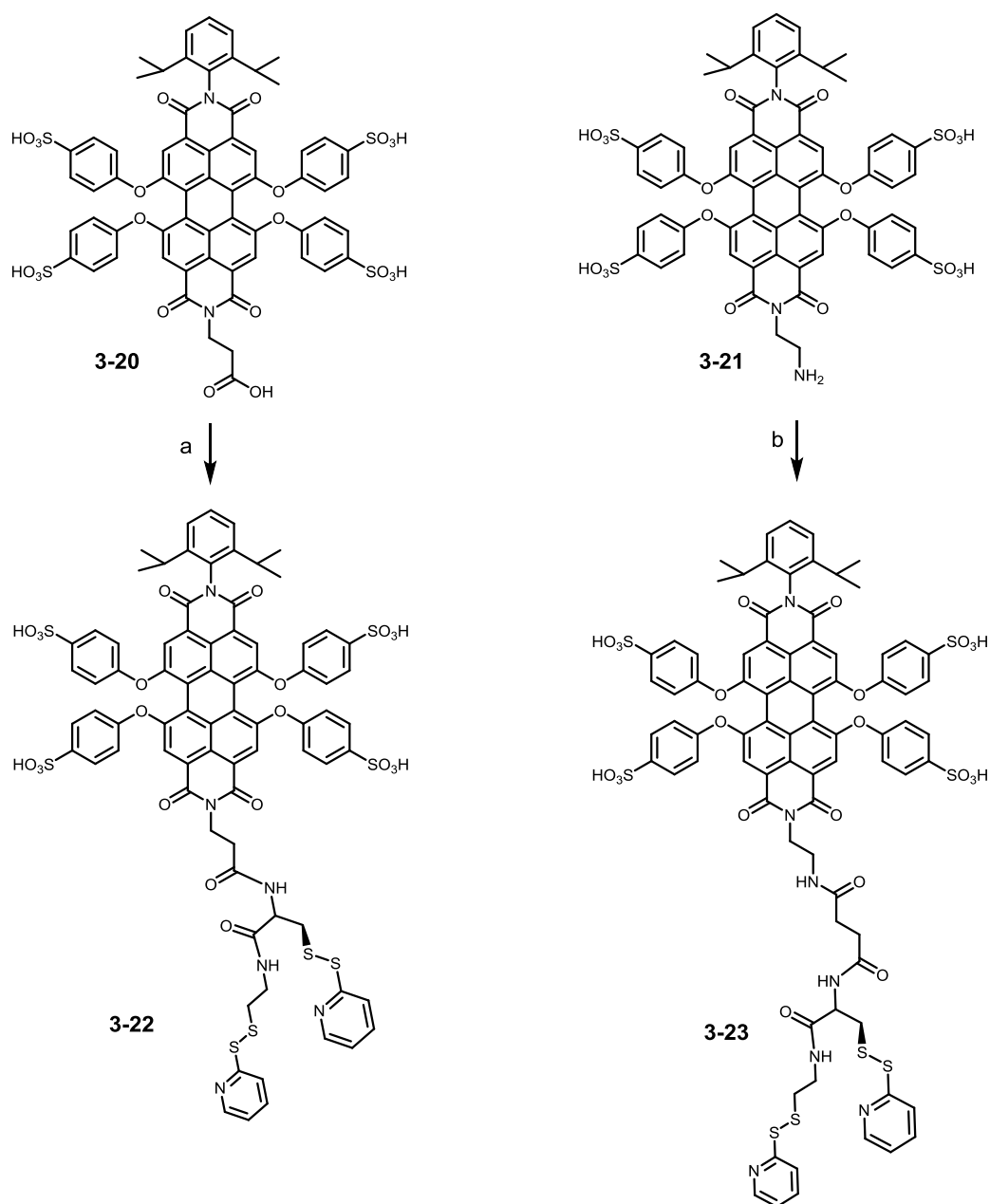
Scheme 5: Example: synthesis of a cumarin-octreotide conjugate, a) 3-azido-7-hydroxy-cumarin, CuSO_4 [3]

3.1.4 Synthesis of perylenediimide-linker and perylenediimide-octreotide

We investigated the performance of the synthesized linkers for the labeling of peptides, in this case octreotide. The purpose of this strategy is to get a better understanding of the biomolecule inside the cell. Octreotide-dye conjugates are suitable components to prove whether the biologically active conformation of the peptide is retained after the intercalation and to investigate the cell-uptake characteristics of modified octreotide-conjugates. The concept of a targeted delivery to tumor cells and the release of the cargo inside the cell under reducing conditions was investigated in a following chapter separately.

Rylene chromophores have proven to be a remarkable class of dyes that are characterized by an exceptional thermal and photochemical stability as well as having fluorescence quantum yields close to unity in organic solvents. [11] [12] Especially sulfonated PDIs have been reported to show good water solubility (10^{-2} M) and high fluorescence quantum yields in water as shown by Kohl. [13] All of the above mentioned demanding studies could benefit from the extraordinary properties of the rylene dyes. The herein used sulfonated PDI chromophores were synthesized as described by Peneva *et al.* [11] The molecular structures and purity of the sulfonated asymmetric perylene chromophores were confirmed by ^1H and ^{13}C -NMR spectroscopy and MALDI-TOF analysis.

After the successful synthesis of the dyes, the dye-linker conjugates were obtained by the coupling of the two different functionalized PDI chromophores **3-20** and **3-21** to either the amine or acid modified disulfide intercalating linker **3-8** or **3-9** within 2 h, while HATU was used as a coupling reagent to form the amides (Scheme 6). Interestingly, the amide bond formation did not work using any other coupling reagent as TSTU or DCC/DIC in combination with NHS. A reason for this could be that the reaction solution contains parts of water bound to the sulfone groups of the dye, although dry DMF is used as the solvent and the reaction is performed under argon. As water can prevent the formation of the activated NHS ester of the used acid, which is going to be formed with the different coupling reagents, the coupling will not be possible. The reason for the water in the reaction solution are probably the sulfonated PDI conjugates **3-20** and **3-21**, as the sulfo groups strongly bind water molecules.



Scheme 6: Synthesis pathway for compounds **3-22** and **3-23**, a) HATU (1.25 eq), DIPEA (1.5 eq), **3-8** (1.1 eq), dry DMF, argon, 2 h, r.t., 84 %. b) HATU (1.25 eq), DIPEA (1.5 eq), **3-9** (1.1 eq), dry DMF, argon, 1.5 h, r.t., 81%.

Reaction control and purification of the final conjugates was conducted by analytical and preparative RP-HPLC. In the following steps the solvents were removed and the product was precipitated in diethyl ether, after resolving it in a small amount of methanol, to give the final product as violet powder in high yields. Without precipitation, the salt content of final product would be too high, as triethylammonium acetate was used as HPLC solvent during the purification. Complete analysis of **3-22** and **3-23** was carried out by ^1H NMR and

MALDI-TOF MS, whereas the ^1H and TOCSY NMR of **3-22** are shown on Figure 25 to verify the successful synthesis. This NMR spectrum exhibits well-separated and clearly assignable signals and their intensity ratios of all peaks agree with the theoretically expected.

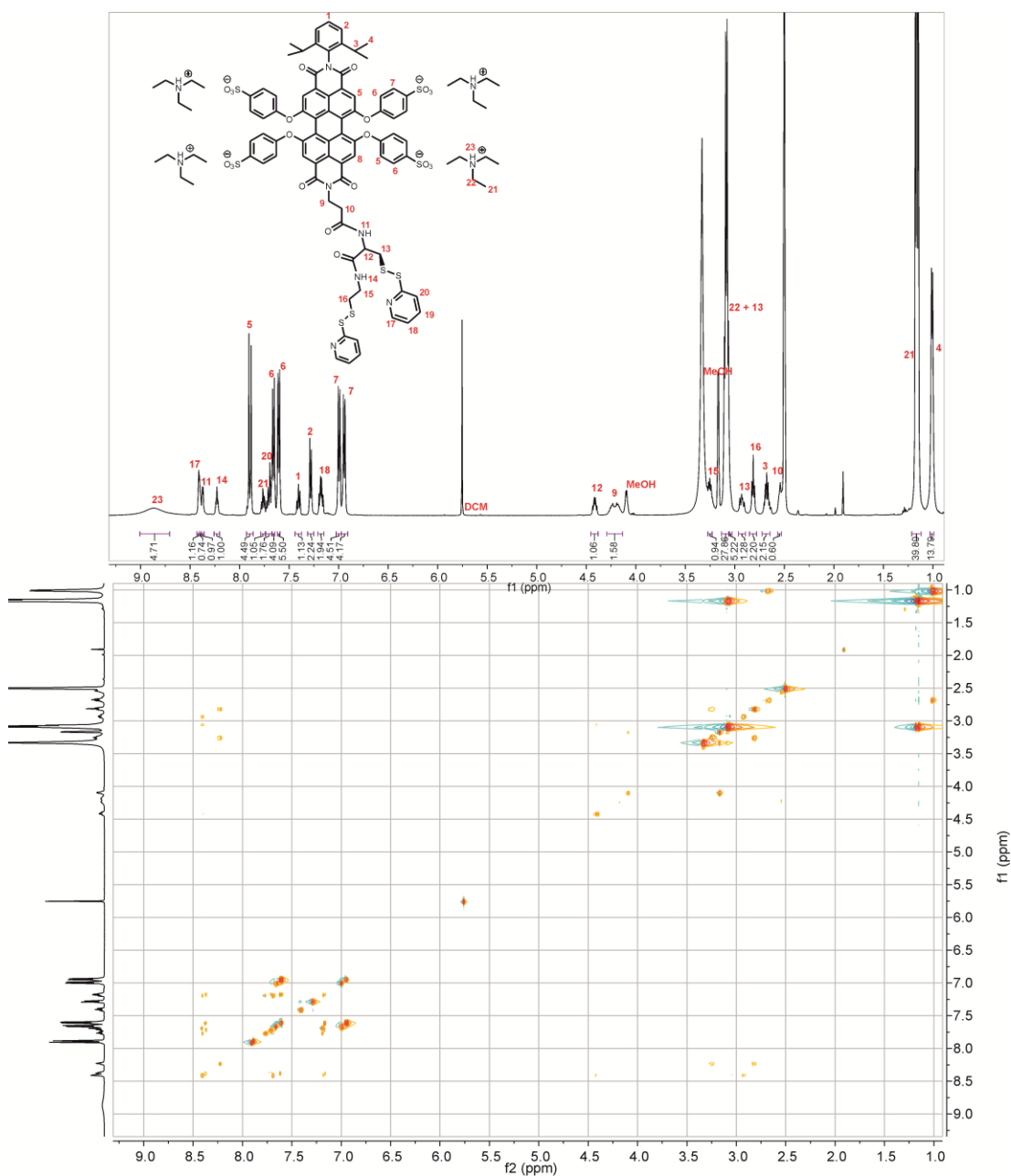
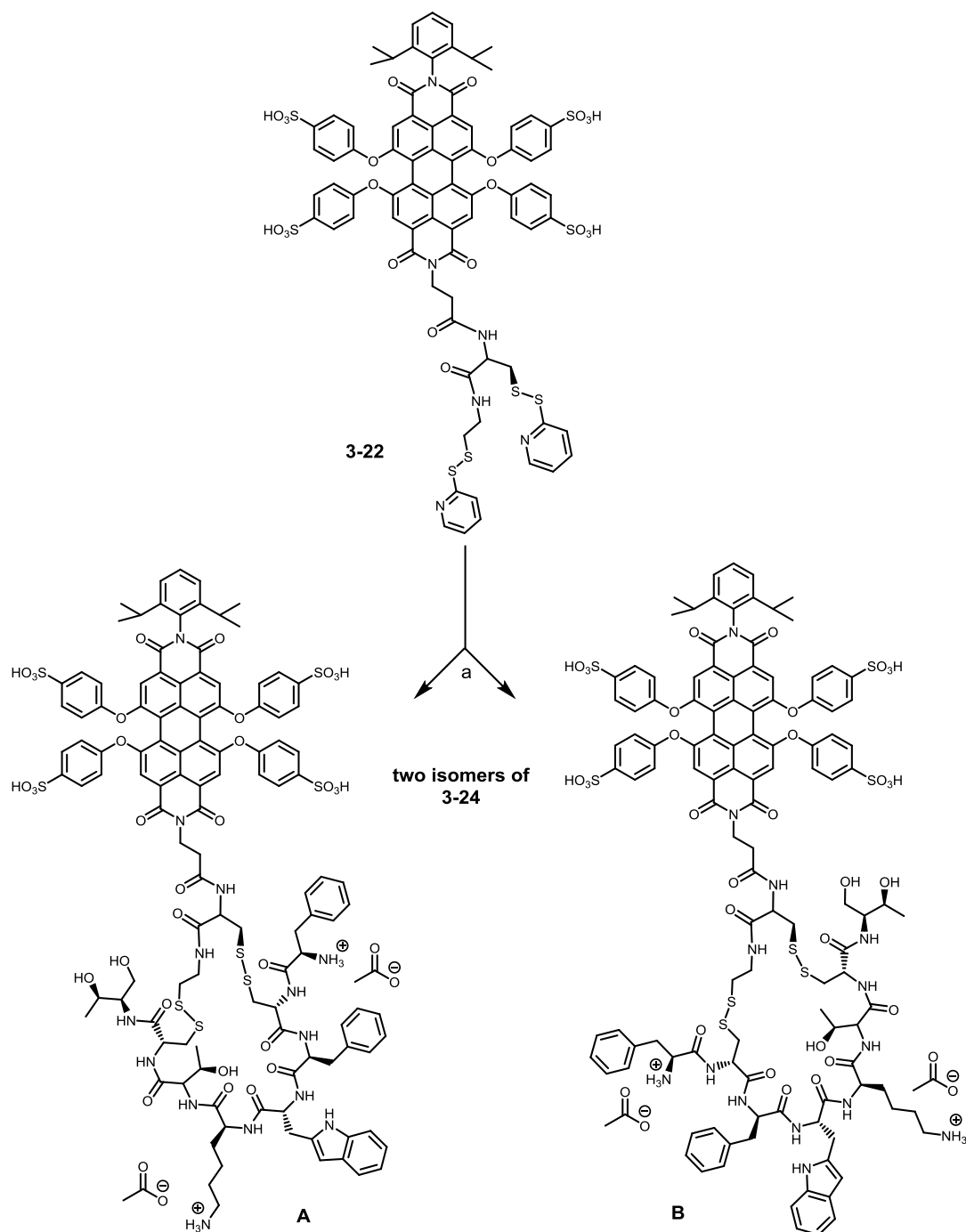


Figure 25: ^1H ,H-TOCSY-NMR spectrum of compound **3-22** in $\text{DMSO-}d_6$ (500 MHz)

After the successful synthesis of the dye-linker conjugates, the final coupling to octreotide was performed. Therefore, octreotide was reduced first as described before in presence of an excess of the reducing agent TCEP and purified by preparative RP-HPLC. This purification step is necessary as the reducing agent can influence the following coupling reaction of the

peptide and the dye-linker conjugates. The isolated fractions of the reduced peptide were then directly conjugated to the pyridyl disulfide carrying reagents **3-22** and **3-23** to yield the pure products **3-24** and **3-25** after purification by reversed-phase chromatography (Scheme 7). Monitoring of the reaction process was possible by HPLC, because pyridine-2-thione is released during the formation of the two disulfide bonds, which has a characteristic absorbance at 343 nm. [14]



Scheme 7: Synthesis of the PDI-octreotide hybrid **3-24**, a) **3-17** (1.2 eq), DMF, DPBS, argon, 1 h, r.t., 85 %

Interestingly, two new peaks appeared in the HPLC chromatogram (reaction control), although only one product was expected to be formed. To analyze the formed products, purification was performed by preparative HPLC to collect both peaks separately. Because of the close proximity of the peaks in the chromatogram, clear base-line separation was not achievable and only one fraction was collected containing both peaks. The solvent was removed under reduced pressure, resolved in methanol and precipitated in diethyl ether to yield the product as a violet powder. The sample was analyzed by MALDI-TOF MS to identify the two products. Figure 26 shows the corresponding spectrum and clearly verifies the existence of only one product without any side products or educts. The agreement between the calculated (m/z calculated = 2559.20) and experimentally determined m/z ratios (m/z observed = 2559.13) confirms the existence of this monofunctional water soluble dye-linker conjugates. Due to the equal reactivity of both pyridyl disulfides and both thiols, two isomers (**3-24a** and **3-24b**) were formed during the reaction for each of the final conjugates explaining the two peaks in the chromatogram.

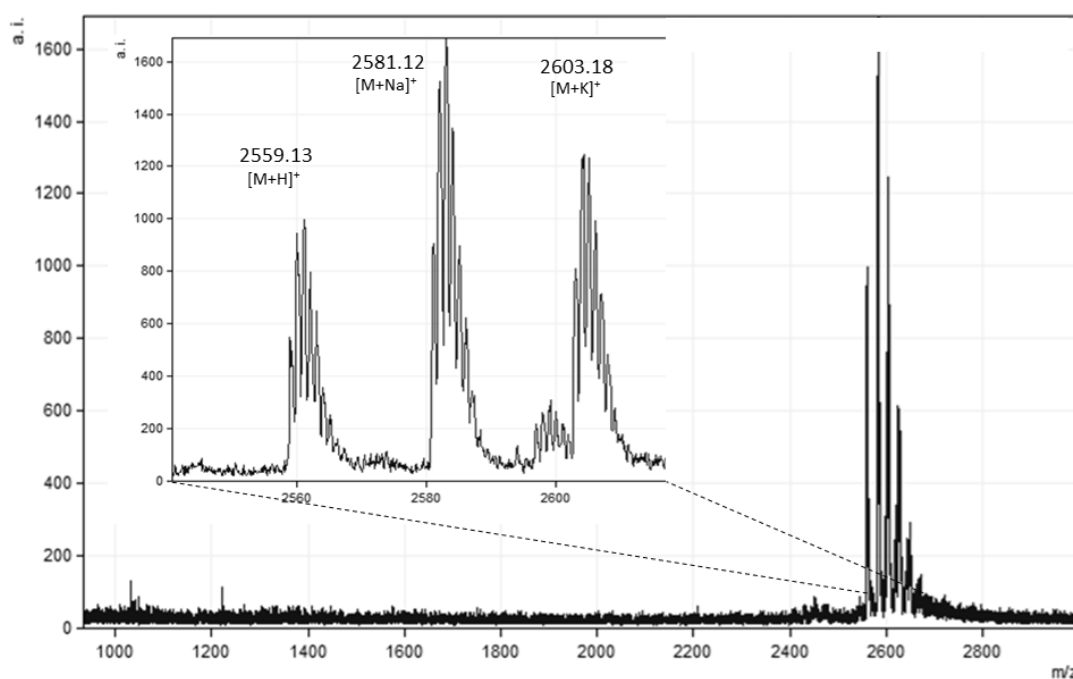


Figure 26: MALDI-TOF MS spectrum of **3-24** additionally showing five different sodium and potassium adducts of the product (matrix: α -CHCA), in the zoom at the top left the single sodium and potassium adduct is given only.

The described PDI-octreotide conjugates **3-24** and **3-25** confirmed the potential of the novel linker system in the field of site-selective peptide modification. The numbers of atoms, which are introduced between the sulfur atoms of the peptide during the intercalation, were

reduced to six atoms compared to the cleavable linker system which has been developed by our group in the past. [5] This reduced length can be crucial for retaining the biological function of peptides active after modification. As already mentioned before, another advantage of this linker system is that the delivered cargo, in this case the dye-chromophore, can be released after the receptor mediated cell uptake inside cells in the presence of increased levels of glutathione, which will be discussed in a following chapter. This is an important characteristic, which is not achievable with other linker systems used in literature for instance by Brocchini *et al.* or Baker *et al.* [3, 15]

3.1.5 Synthesis of doxorubicin-octreotide conjugates

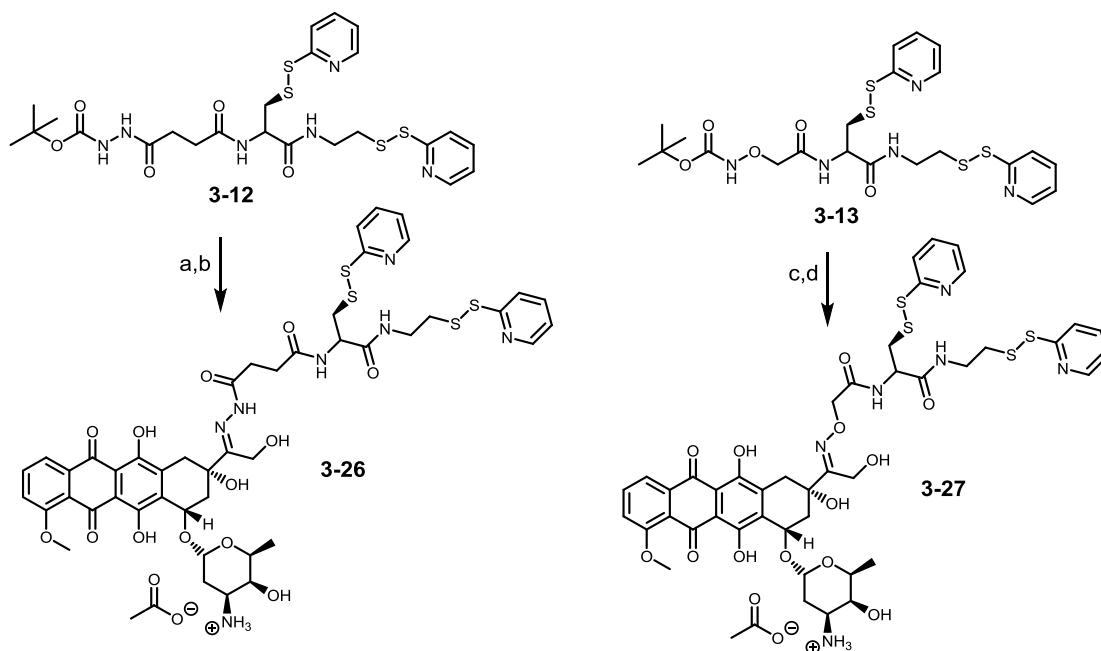
Nowadays, chemotherapeutic agents are applied often as first line of treatment of cancer disease. Among others there are many active drug molecules available with outstanding characteristics and toxicity, for instance doxorubicin, but their application in patients is limited due to low therapeutic efficacy or side effects as systemic toxicity. To bypass these limitations, doxorubicin, for instance, has already been encapsulated in liposomes or micelles so that the accumulation of the drug in the tumor tissue is facilitated by the EPR-effect (passive targeting of tumor cells). [16-18]

Another technique to circumvent these limitations is to use drug delivery systems that enables activate targeting of tumor cells. Therefore, anticancer drugs have been modified with highly specific ligands (e.g., gonadotropin-releasing hormone, transferrin, folic acid) for cell surface associated receptors to overcome limitations as crucial side effects of the drug caused by poor tumor selectivity. [19-21]

In general synthetic somatostatin analogs, such as lanreotide, octreotide or vapreotide, have a much longer half-life due to the incorporation of D-amino acids compared to somatostatin, which makes them more stable against peptidases and thereby interesting for therapeutic applications. The strong interaction of somatostatin and its analogs to the corresponding cell surface receptors is enabled by two factors, on the one hand the cyclic structure of the peptide due to the formation of the disulfide bond between two cysteines, and on the other hand the tetrameric amino acid motif FWKT (Phenylalanine-Tryptophan-Lysine-Threonine, Figure 19), which is responsible for the receptor interaction. So far the application of doxorubicin-somatostatin bioconjugates is not considered in clinical application studies mainly due to the low half-life of the peptide (half-life somatostatin 1-3 min). [22] Nevertheless, there are few doxorubicin-somatostatin-analog conjugates described in literature. [23, 24] Nagy *et al.* established a coupling between the drug and the peptide based

on glutaric acid, in which the primary alcohol of the drug and the amine of the N-terminus were conjugated *via* an ester bond. [25] The drawback is that ester bonds are known to be cleaved under physiological conditions by hydrolysis and the drug will be set free at any place causing undesired side effects as destroying healthy tissue by killing the cells. Weil and coworkers prepared a doxorubicin-somatostatin conjugate using the already introduced bis-sulfone linker system. [26, 27] This system is again limited by the short half-life of somatostatin and the absence of a release mechanism for the drug molecule. [27] In contrast, the potential of octreotide as a stable targeting moiety with prolonged half-life has been shown by Reubi *et al.* by the attachment of the peptide to the surface of doxorubicin loaded liposomes or micelles. [28, 29]

We compiled in our group the formation of a doxorubicin-octreotide conjugate based on the aforementioned linker system, which is stable against hydrolysis, but cleavable under reducing conditions in the cytosol. Therefore, the main goal of this chapter is to synthesize drug-octreotide conjugates based on the novel, cleavable cysteine based linkers. First, doxorubicin was attached to the novel aminoxy- or hydrazine-functionalized linker derivatives **3-12** and **3-13**. In the next step the coupling and modification of octreotide was performed in a similar way as already discussed for the PDI dyes in the previous part (chapter 3.1.4).



Scheme 8: Synthesis of the disulfide intercalating doxorubicin derivatives **3-26** and **3-27**, a) dry DCM/TFA (1:1), 1 h, r.t., quantitative yield; b) doxorubicin-hydrochloride (1 eq), 0.4 M sodium acetate buffer (pH 5.0), DMF, 40 h, r.t., 54 %, c) dry DCM/TFA (1:1), 1 h, r.t., quantitative yield; d) doxorubicin-hydrochloride (1 eq), 0.4 M sodium acetate buffer (pH 4.8), DMF, 40 h, r.t., 78 %

In analogy to previously described synthesis of linker-cargo conjugates the Boc-protective group of **3-12** and **3-13** were cleaved to unmask the desired aminoxy-/ hydrazine-group. The product was dried under reduced pressure to remove the solvents residues. The addition of the disulfide-intercalating cross-linking reagent to the aliphatic keto-group of doxorubicin was followed by analytical RP-HPLC, in which both condensation reactions between the two components were carried out under slightly acidic conditions in sodium acetate buffered solution (pH 4.8 for oxime bond formation, respectively pH 5.0 for hydrazone bond formation). After few hours an additional peak next to the peak of doxorubicin (18 min) with a retention time of 19 min could be detected in the HPLC chromatogram at the wavelength 490 nm, indicating the existence of a doxorubicin derivative. The same peak was still present after two days, but with much higher absorption intensity. In contrast, the peaks of the linker derivatives **3-12** and **3-13** were gone, indicating that the reaction was completed successfully. Afterwards preparative RP-HPLC was used for purification and all solvents were removed under reduced pressure. The residues were dissolved in methanol and precipitated in diethyl ether to obtain product **3-26** and **3-27** as a red powder in high yields (Scheme 8). The removal of any remains of the triethylammoniumacetate buffer used for the HPLC purification was successful performed by the precipitation in diethyl ether. Besides analytical RP-HPLC, both drug-linker conjugates were analyzed by MALDI-TOF MS as well as proton and carbon NMR.

The novel formed doxorubicin-derivatives have a longer retention time compared to doxorubicin, which was expected, since an unpolar molecule is attached to the drug. The corresponding m/z ratios of the products were detected by MALDI-TOF MS analysis. Additionally, both products were analyzed by NMR spectroscopy for a complete structural characterization based on 2D experiments using COSY, NOSY and TOCSY. The corresponding H, H – TOCSY spectrum is depicted in the following Figure 27. The aromatic area was used as the reference. In total, the integration of the aromatic signals was in sum 13, which fits to the expected three protons of doxorubicin (“c” and “d”), the eight protons of the two pyridyl-groups (“a”, “d”, “e” and “f”) as well as the two amide protons (“a” and “b”). Furthermore, the acetate anion of the daunosamine is present (integral 3 of “v”), which is important as this group is responsible for the water solubility of the product. Based on the 2D signals all aromatic signals could be clearly assigned and the including methyl- and ethyl-groups (“r, n, o and s”) could be identified. As assumed, the aliphatic protons in close proximity to the chiral carbon atom of “i” are separated in the ^1H NMR, but could be clearly differentiated due to the long range coupling of the different protons in the TOCSY spectrum.

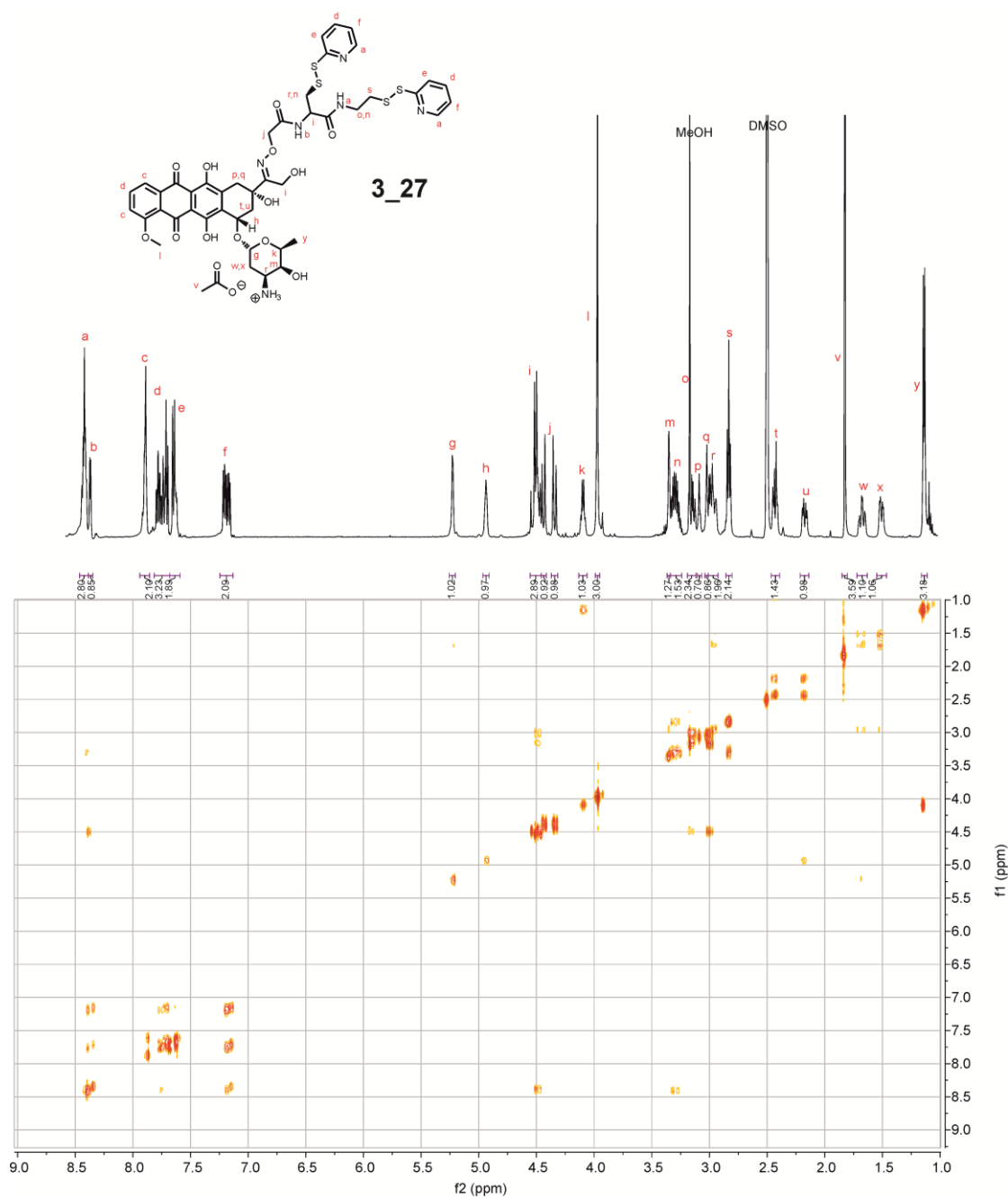
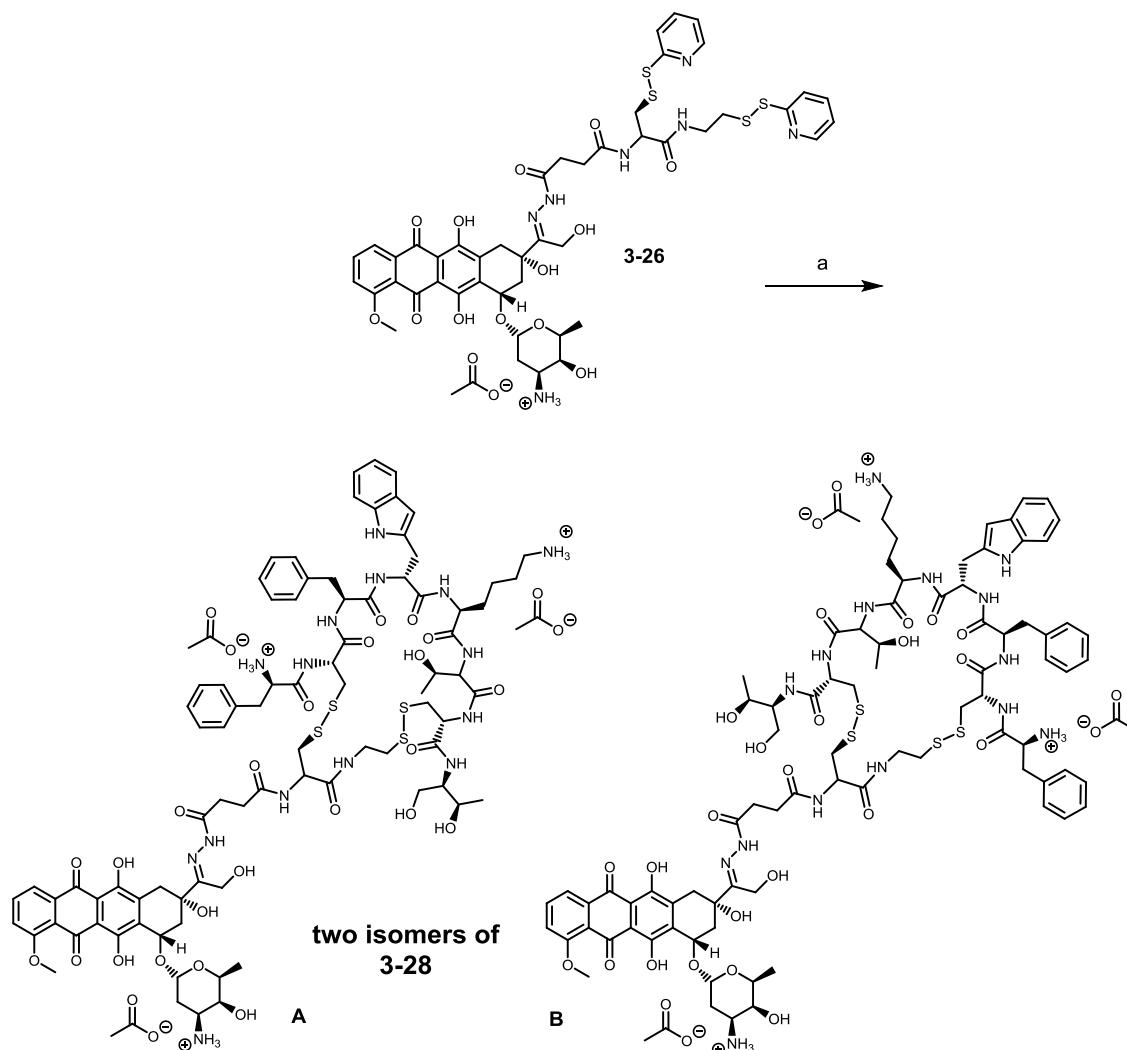


Figure 27: H,H-TOCSY-NMR spectrum of **3-27** in DMSO-*d*₆ (700 MHz)

In order to couple the doxorubicin linker conjugates **3-26** and **3-27** with the peptide, octreotide was first reduced using TCEP as the reducing agent and then purified by preparative HPLC. The reaction process of the final peptide modification was determined by means of analytical RP-HPLC. After one hour reaction time, the cyclisation was completed successfully as indicated by the existence of one peak in the chromatogram absorbing at the

characteristic doxorubicin wavelength 490 nm and the missing peak of the educts **3-26** and **3-27**.



Scheme 9: Synthesis of the doxorubicin-octreotide hybrid **3-28**, a) **3-17** (1.2 eq), DMF, DPBS, Argon, 1 h, r.t., 80 %

A pyridyl disulfide has the advantage to readily undergo an interchange reaction with a free sulfhydryl to yield a single mixed disulfide product; otherwise the activated thiol is stable. This is due to the fact that the pyridyl disulfide is easily transformed into a non-reactive compound (2-pyridinthion) not capable of participating in further mixed disulfide formation. Therefore, the formation of a peak absorbing at 343 nm could be detected during the reaction process, which is the corresponding signal of 2-pyridinthion, the cleavage product of the coupling process. Purification of the final drug-octreotide hybrids were accomplished by preparative RP-HPLC as already described for the dye-octreotide hybrids to yield the **3-28** and **3-29**, which were analyzed by analytical HPLC and MALDI-TOF MS. Although only

one peak could be detected during the purification, the following analytical HPLC run shows two signal peaks. The reason for this can be found in the nature of the cyclisation reaction, as two different isomers can be formed during this reaction step as shown on Scheme 9. In order to prove this assumption, the purified sample was analyzed by MALDI-TOF MS (Figure 28). On the basis of this it can be clearly proven that only one product is formed with the expected cyclic structure, otherwise the m/z would not fit. Thus, compound **3-28** is present in both isomers, which can be separated by analytical HPLC due to their slightly different chemical characteristics.

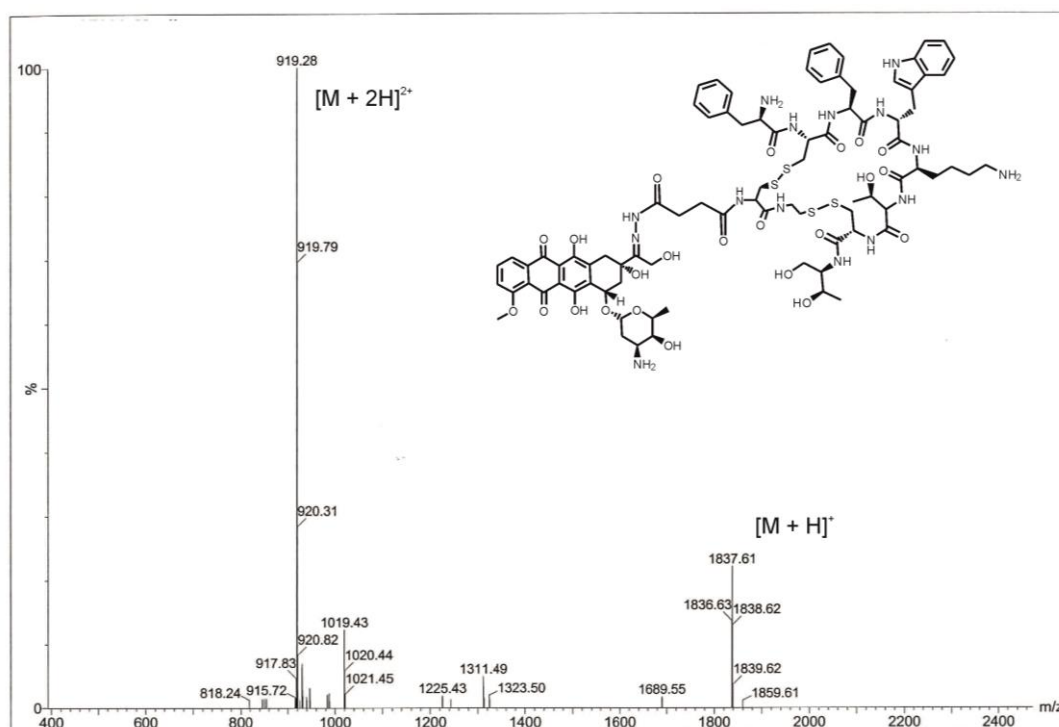
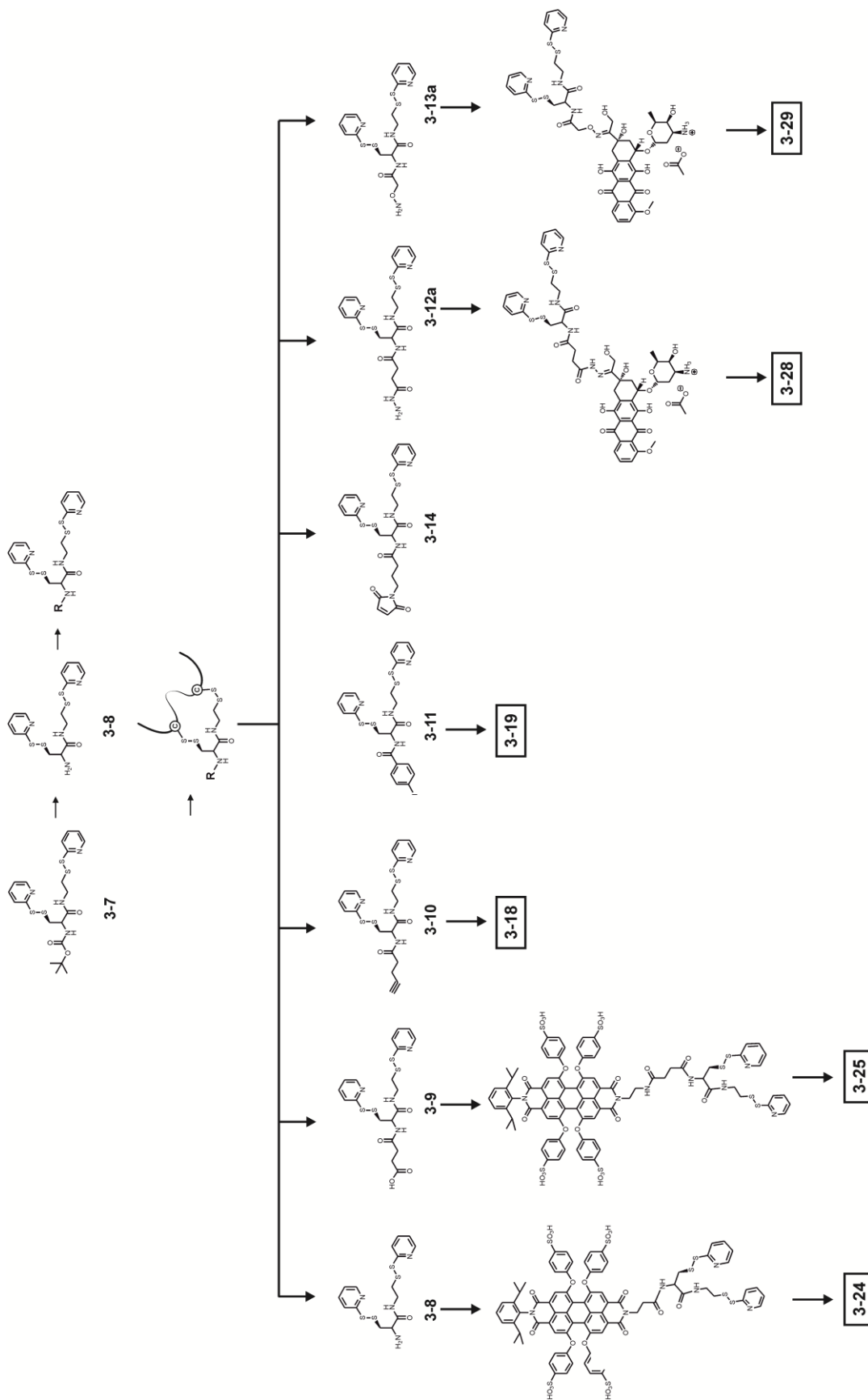


Figure 28: ESI-TOF MS spectrum of **3-28**

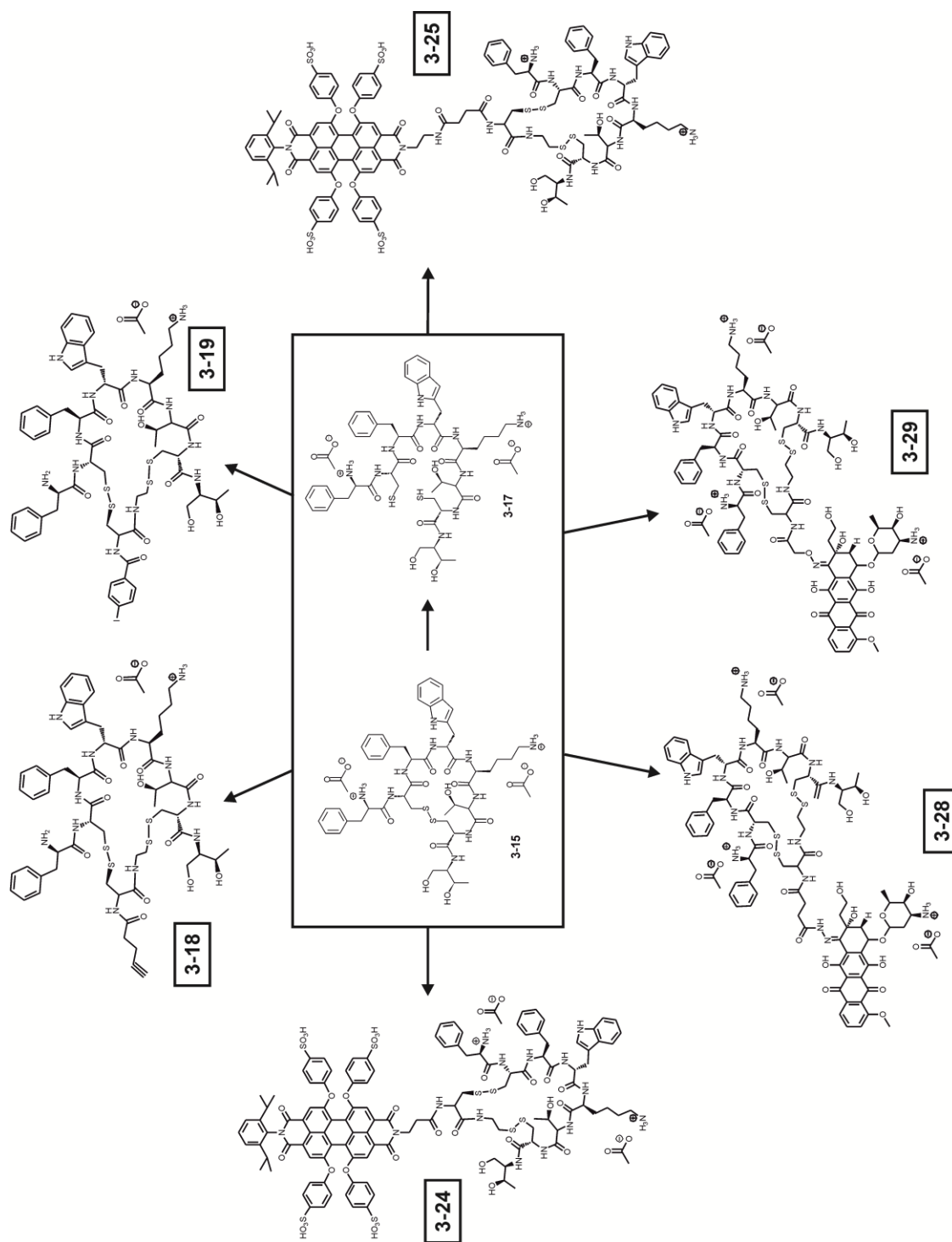
Finally, both novel conjugates are expected to have high potential in the field of targeted drug delivery, as they allow a safe and stable transport of the drug to the place of interest. In the following sections of this chapter different experiments are described to confirm the controlled release mechanism of the novel linker under reducing conditions and to prove the targeting effect of octreotide based on the interaction with overexpressed receptors on tumor cells.

Scheme 10 and Scheme 11 give a final overview of all synthesized products and octreotide conjugates. For the final coupling, the disulfide bond of octreotide acetate **3-15** was first reduced in a short period of time by adding a small excess of *tris*(2-carboxyethyl)phosphine hydrochloride (TCEP HCl) to form reduced octreotide **3-17**. The excess of the reducing agent was removed by RP-HPLC and the isolated product fraction of the reduced peptide was then conjugated to the different pyridyl disulfides carrying reagents **3-10**, **3-11**, **3-22**, **3-23**, **3-26** and **3-27** to yield the pure products **3-18**, **3-19**, **3-24**, **3-25**, **3-28** and **3-29** after purification by reversed-phase chromatography. Due to the equal reactivity of both pyridyl disulfides and both thiols, two isomers were formed during the reaction for each of the final conjugates.

The advantage of this novel linker type over the before mentioned linker systems used for site-selective peptide modification by disulfide intercalation is its smaller size as well as its ability to be cleaved under reducing conditions inside the cell, which will be discussed in the following section. [30] [31] Additionally, based on the high interaction of octreotide with somatostatin receptors, which are overexpressed on certain tumor cells and primary tumor tissue, a targeted delivery of the dye and drug towards tumor cells is achieved (e.g. MCF 7, Mia-Paca 2). [28, 29, 32]



Scheme 10: Overview of the different linker molecules



Scheme 11: Overview of the final octreotide conjugates

3.2 Glutathione dependent perylenediimide release

One of the major goals in modern cancer chemotherapy is the design of multi-functional drug conjugates aiming at not only cell type specific drug uptake, but also at intracellular cleavage to liberate the drug molecules based on various stimuli. [33] [27] Such intracellular release mechanisms are e.g. based on pH changes in some cellular compartments or on the reductive conditions inside the cytosol. Glutathione (GSH) is present in a concentration range of 0.5-10 mM in the cytosol; while its concentration in plasma is considerably lower (ca. 2-20 μ M). [34] Furthermore, increased intracellular glutathione concentrations have been reported for different cancer cells, thus offering potential for the controlled, cell-type selective drug release.

In this study the potential of the novel linker system was investigated focusing on a controlled cleaving process of the drug in presence of glutathione. Therefore, PDI functions as a model molecule due to its intensive UV absorbance which is necessary for the following HPLC-UV/MS study. The advantage of this analysis method is that the different cleavage products can be separated by HPLC and analyzed by UV absorbance as well as MS simultaneously in one step. Thereby, the different cleavage products were first identified by their m/z ratio (ESI-MS) and afterwards assigned to the UV absorbance peaks in the HPLC chromatogram. It has to be emphasized that this cleavage procedure is only possible for the herein used disulfide based linker system. Such exceptional properties are not achievable for peptide modifications as using the formation of stable thioether bonds.

To evaluate and confirm the efficient release of the cargo under reducing conditions present in the cytosol, compound **3-24** was incubated with the tripeptide glutathione, the most prevalent cellular thiol, which mainly serves as an indispensable reducing agent in mammalian cells. [35] A 0.5 mM solution of **3-24** was incubated with a 10 mM GSH solution at 37°C for 24 h and analysis of the mixture was performed by analytical HPLC-ESI-MS at hourly intervals to separate the different fractions and allow a distinct characterization in one step. Additionally, the characteristic absorbance of the PDI dye at 560 nm and octreotide at 280 nm was used to monitor the reduction process. Identification of the cleavage products was conducted by mass spectrometry. Figure 29 summarizes the measured chromatograms and Figure 30 shows the detected and identified cleavage products.

After 10 h the initial conjugate was almost completely reduced and the major cleavage products are molecules *b* and *d*, in which the two thiols of the PDI-linker were oxidized to

build a disulfide bond with themselves (*b*) or with two different glutathione molecules. Substance *d* consists of two isomers, similar to **3-24**, as there is no preference for reformation of the disulfide bonds. However, it seemed that *b* is converted to *c* over time, as this compound is visible with higher intensity after 24 h. Due to the complexity of the products formed during this cleavage step, the assignment of the peaks was only possible using a coupled HPLC-UV/MS system.

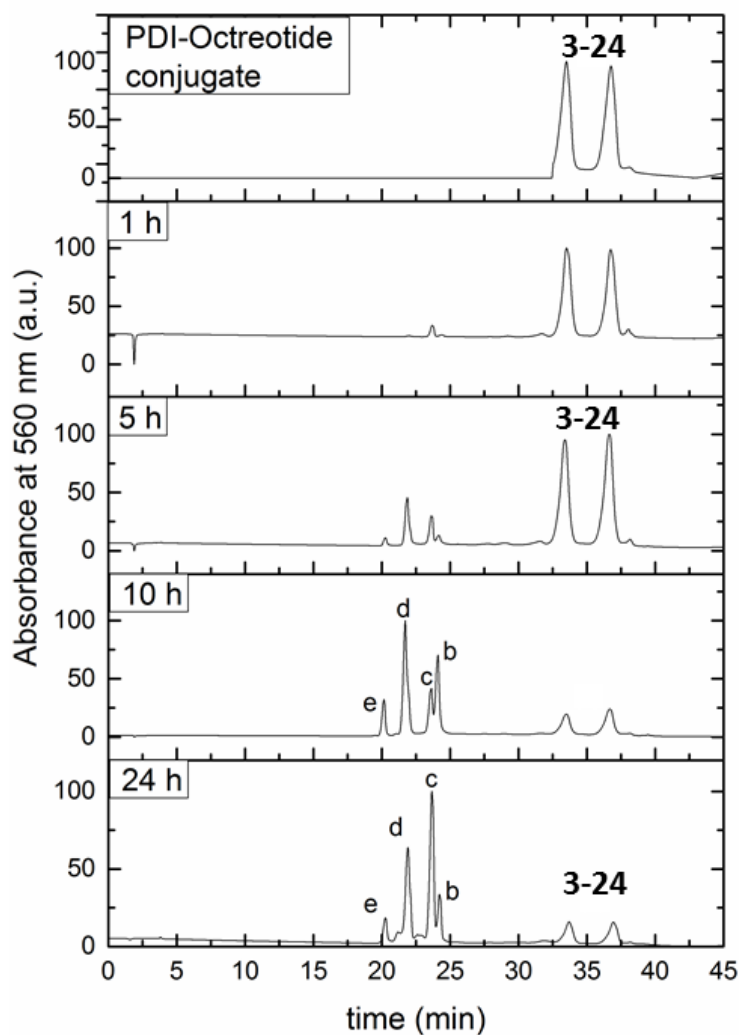


Figure 29: Glutathione-mediated degradation of the peptide-drug conjugate. (A) RP-HPLC analysis of the degradation of **3-24** (0.5 mM) in the presence of 10 mM glutathione in DPBS (pH 7.4) at 37 °C.

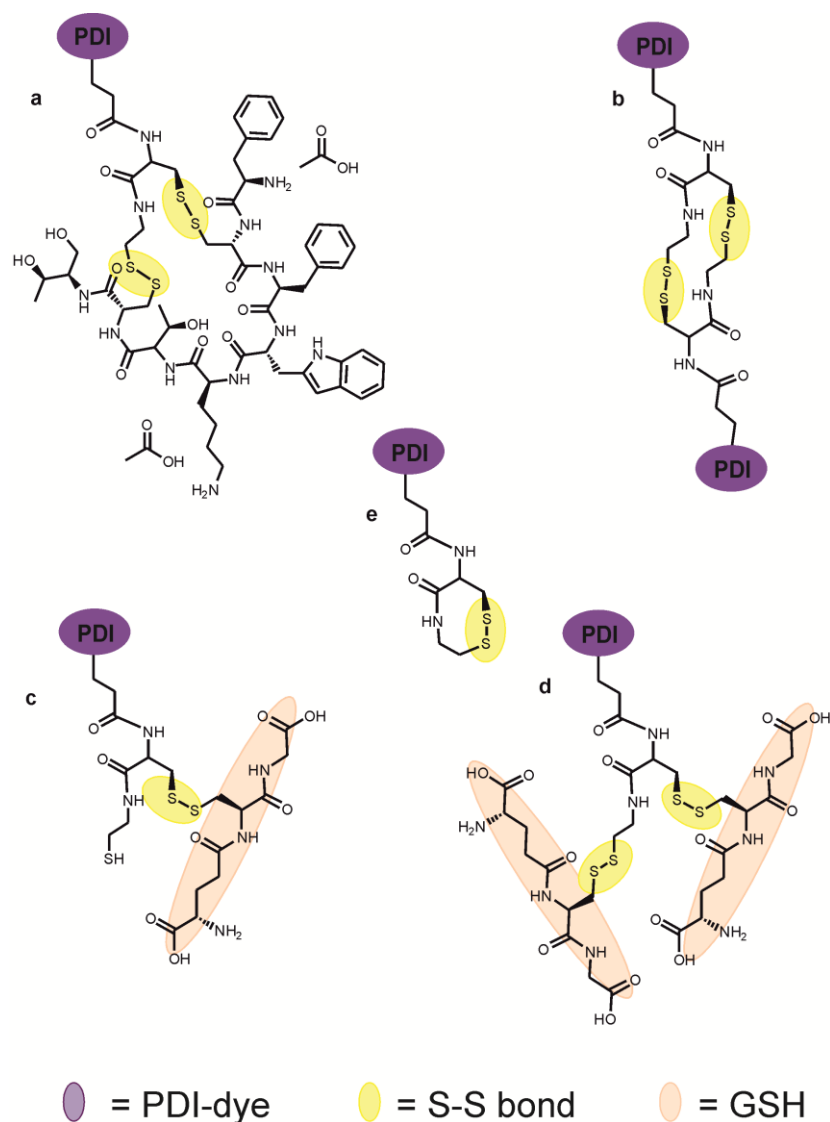


Figure 30: Corresponding structures of the cleavage products of the glutathione-mediated degradation of the peptide-drug conjugate **3-24**

In conclusion, this experiment proved our hypothesis, that the dye is released from the peptide in presence of GSH under physiological conditions. As the dye functions as a model, this experiment can be seen as the proof of concept and therefore true for any type of cargo. In this context, it has to be mentioned, that the linker has a high potential to couple drugs or other active substance to octreotide or other peptides containing disulfide bonds.

3.3 Stability and cleavage study of the hydrazone based doxorubicin – octreotide conjugate

The main aim of targeted drug delivery is not only that the cytotoxic cargo is delivered inside the cell, but also released in its active form following the uptake. However, transferring the knowledge gained in the previous cleavage study towards the synthesized doxorubicin-octreotide conjugates **3-28** and **3-29**, it has to be stated, that there will be no native doxorubicin formed. As GSH only reduces the disulfide bonds, there is always at least a linker part or even GSH attached to doxorubicin, similar to the structures shown on Figure 30, which can reduce the drug's toxicity. [5] In case of anthracyclines like doxorubicin a complete release of the cargo is a crucial and necessary advantage, since its main action is recognized as DNA intercalation. Thereby, it hinders the enzyme topoisomerase 2 to function, which in the end causes cell death of the tumor cells. This means, if a drug can only act in its native form or the toxicity is hindered by modifications of its molecular structure, solutions have to be found to improve this linker system.

Therefore, an additional bond has to be introduced allowing the native drug to be set free inside the cell. Commonly described techniques enabling a drug release of cytotoxic agents into the cytosol or even the nucleus after receptor-mediated endocytosis are based on the coupling between the drug and the delivery or targeting agent *via* a hydrazone bond. This bond is known to be stable at neutral pH, but starts to hydrolyze in an acidic environment, which is typically found in tumor tissue in general and especially the late endosomes. Thus, doxorubicin could be cleaved inside the cell after being taken up by the cells. To investigate the stability of the chemotherapeutic agent at neutral pH, followed by the final release caused by hydrolysis, the drug-peptide conjugate **3-28** was dissolved in DBPS (pH 7.4) as well as in a sodium acetate buffered solution (pH 5) for 24 hours at 37°C and the mixtures were analyzed by analytical RP-HPLC (Figure 31). The characteristic absorbance of doxorubicin at 494 nm was used to monitor the process of drug release and the identification of the free doxorubicin was achieved by running a control standard (0.5 mM doxorubicin HCl in water).

This study demonstrated the expected and highly desired release of native doxorubicin in an acidic environment of the tumor milieu. After 3 h most of the initial doxorubicin-octreotide conjugate **3-28** was cleaved and doxorubicin was released. Finally, after 24 h there was no conjugate left, only free doxorubicin was detected. Consequently, the novel linker system is not only able to intercalate disulfide bonds for a site selective modification, but also enables the desired drug release inside the cell to achieve an unlimited DNA intercalation. In

contrast, there is no cleavage at all at pH 7.4 indicating the stability of the conjugate in blood serum.

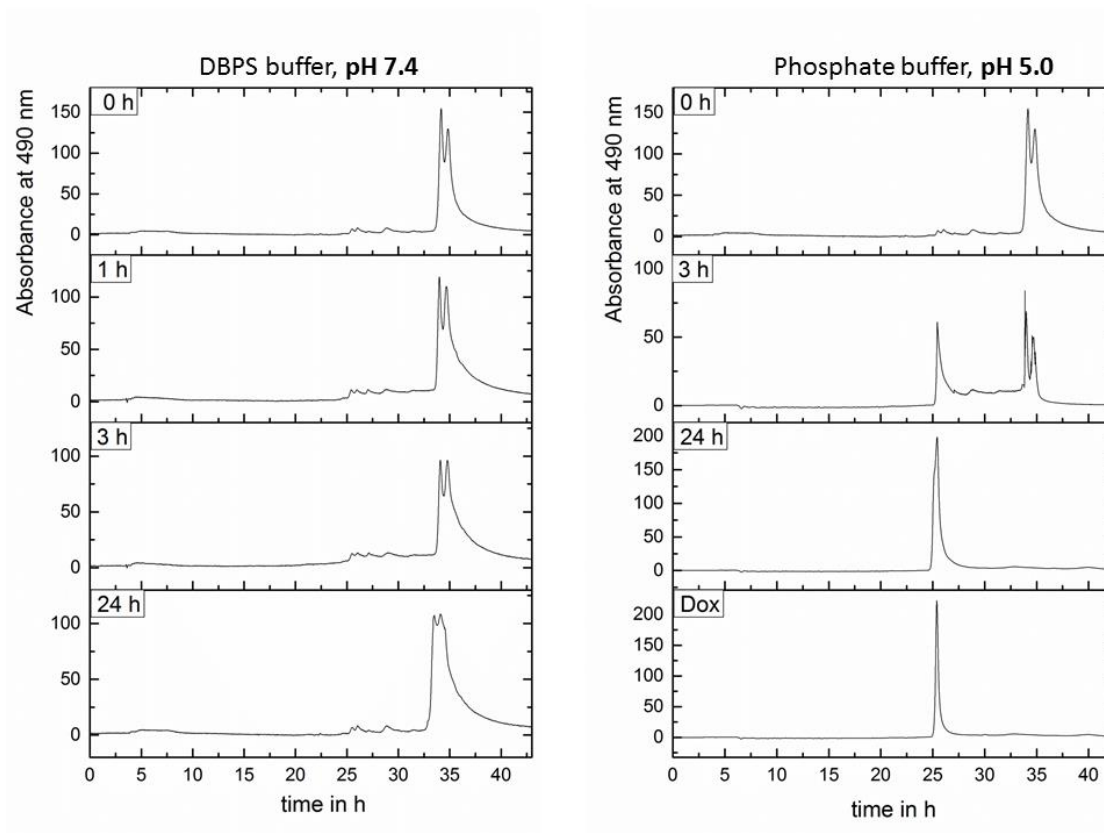


Figure 31: Analytical HPLC chromatograms of the pH dependent cleavage study of **3-28** at pH 7.4 and pH 5.0 over 24 h at 37 °C

3.4 Cellular uptake and intracellular distribution

In the following study, the main focus of attention is given to the intracellular distribution of conjugate **3-28**, the cellular visualization of doxorubicin inside the cell and finally demonstrating the targeted receptor mediated cell uptake, which is necessary for a successful tumor targeting. [36] The intracellular distribution of the oxime containing compound **3-27** was not analyzed in this study, as native doxorubicin is only supposed to be set free for the hydrazine based conjugate **3-28** as shown in the previous stability study. Two different cell lines were chosen, human pancreatic carcinoma cell line MIA PaCa-2 cells as a control cell line that overexpress somatostatin receptors and adenocarcinomic human alveolar basal epithelial cells A549 cells as negative control cell lines as these cells almost lack these receptors completely.

Both cell lines were incubated with a 10 μM solution of **3-28** and the anthracycline derivative was monitored by fluorescence microscopy at 24 h and 48 h. The application of this concentration ensures imaging of live cells, even after prolonged incubation (48 h). The initial interaction of octreotide with the somatostatin receptors on the cell surface causes the internalization of the ligand receptor complexes *via* endocytosis. [37] The distinct binding of the ligand to somatostatin receptors on the cell surface of MIA PaCa-2 cells after a short incubation time is also visible in Figure 32. Here, the overlay of the brightfield and the fluorescence microscopy image clearly indicates that anthracycline fluorescence is present at the membrane. Furthermore, after 24 h of incubation with the drug, intracellular doxorubicin associated fluorescence (red) was already visible in MIA PaCa-2 cells by exhibiting fluorescence in the endosome/lysosomes as well as the cytosol (Figure 32). [38] After 48 h the fluorescence in the cytosol and at the membranes was even more widespread.

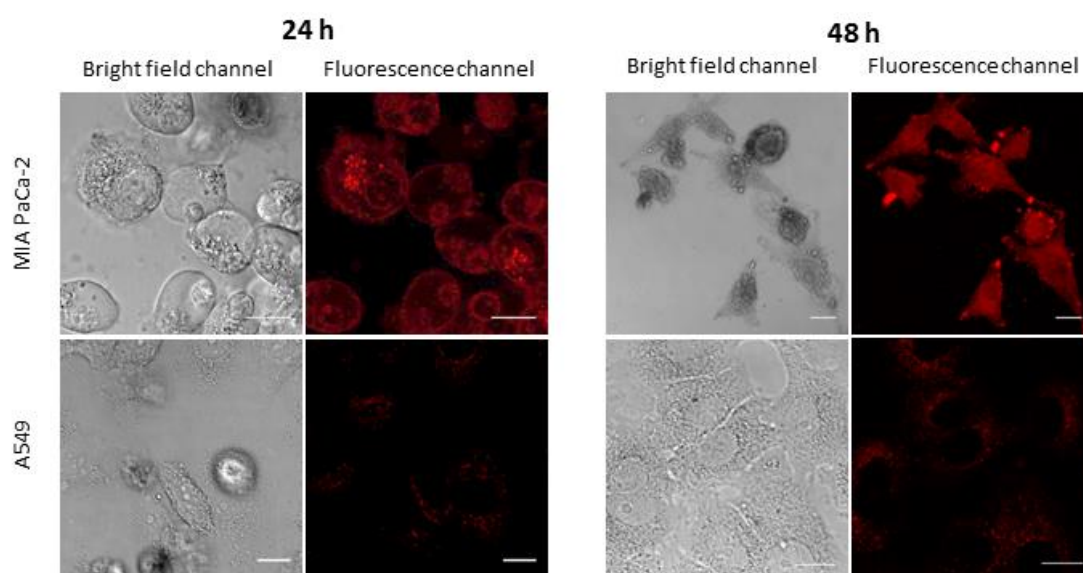


Figure 32: Intracellular trafficking of the doxorubicin–octreotide hybrid **3-28** in MIA PaCa-2 and A549 cells imaged by confocal laser scanning microscopy and fluorescence widefield microscopy at various time points. All cell lines were incubated with 10 μM of **3-28** at 37 $^{\circ}\text{C}$. Red color illustrates doxorubicin fluorescence. Scale bars represent 15 μM .

The advantage of **3-28** is that the drug is attached to the linker *via* a hydrazone bond in comparison to **3-27** using an oxime bond for the attachment of doxorubicin to octreotide. Oxime bonds are in general stable under physiological conditions, even in slightly acidic milieu with pH 5. In contrast, hydrazone bond is stable under neutral pH, but undergoes hydrolysis at such low pH values as they are present in the endosomes. Therefore, the

internalization of the conjugate **3-28** *via* endocytosis is favorable for the delivery of cytotoxic substances like doxorubicin that exhibit their anticancer activity predominantly in the cell nucleus through DNA intercalation and subsequent inhibition of DNA topoisomerases. [39] To prove the localization of the anthracycline in the cell nucleus, MIA PaCa-2 cells were stained with DRAQ5 nuclear stain prior to microscopy. The colocalization with the drug **3-28** is unambiguous because of the obtained violet color from the overlay of both channels. (Figure 33)

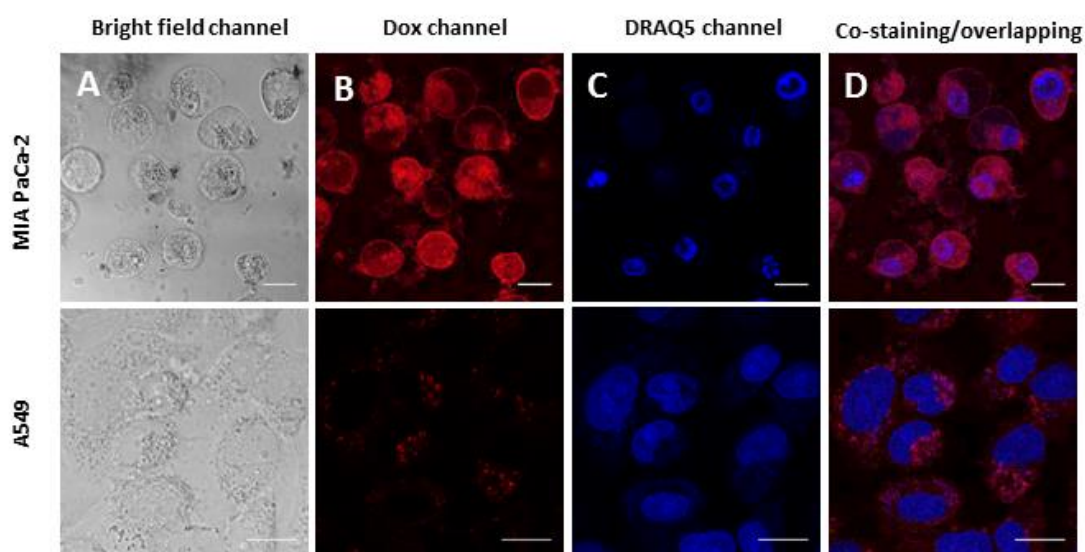


Figure 33: Determination of the nuclear localization of the anthracycline drug in MIA PaCa-2 and A549 cells by microscopy, 48 h after the incubation with 10 μ M of **3-28**. (A) Bright field image. (B) Confocal fluorescence microscopy image of the doxorubicin derivative. (C) Nuclei staining *via* incubation with 5 μ M DRAQ5, carried out 5 min prior to microscopy. (D) Overlay of the drug-associated fluorescence (red) and the fluorescence of the nuclear stain (blue). The corresponding colocalization is represented by violet color. Scale bars represent 15 μ M.

The endocytotic cell entry can be followed by a translocation to perinuclear regions accompanied by release of the ligand as already reported in previous reports. [32] [40] This pathway is crucial for the herein described peptide–drug conjugate to mediate cleavage in acidic environment and subsequent action of the anthracycline in the nucleus. Incubation for 48 h proves that the drug reaches the nucleus of MIA PaCa-2, by the overlay of the red and blue pseudocolor forming a violet color (Figure 33, part D). In contrast, the same overlay is missing for the A549 cells. The few red dots of doxorubicin in close proximity to the blue color of the nuclei are assumed to be aggregates sticking to the cell membrane. Endosomes containing the drug-peptide conjugate could be another explanation, but in this case we would expect the drug to become cleaved and set free by endosomal escape as for observed

for the Mia-Paca 2 cell line. The only difference between both tumor cells is the amount of somatostatin receptors on the surface, which is responsible for the receptor-mediated cell uptake by endocytosis. The result of the nuclei staining experiment is also supporting the previous discussed microscopy pictures of **3-28** and the somatostatin receptor mediated uptake in the cellular distribution experiment (Figure 32).

The performed intracellular trafficking experiments once more supported our hypothesis of selective delivery of hybrid **3-28** to cancer cells overexpressing somatostatin receptors subtypes 2 and 5 and additionally setting free the native tumor drug. The co-localization with the drug is unambiguous because of the obtained violet color from the overlay of both channels and proves the presence of the drug in the nuclei.

3.5 Cytotoxicity studies of the doxorubicin – octreotide conjugate

The *in vitro* toxicity of the doxorubicin-conjugates **3-27** and **3-28** described before was investigated by quantification of the cell viability using the CellTiterGlo™ cell viability assay. Mia Paca-2 cells were chosen as a “positive control” due to the overexpression of the corresponding somatostatin receptors and A549 cells as a “negative control”.

In the first study the focus was set on the cell toxicity determination of the novel synthesized doxorubicin-octreotide conjugates **3-27** and **3-28** as well as the direct comparison of the hydrazone and oxime. For this purpose Mia Paca-2 cells were chosen only.

Table 1: *In Vitro* Cytotoxic effects of the doxorubicin-octreotide conjugate **3-27** and **3-28**, as well as native doxorubicin on MIA PaCa-2 (data expressed as IC_{50} Values in μM , $n \geq 3$, Mean \pm Standard Deviation)

	Doxorubicin – Hydrazone - Octreotide (3-28)	Doxorubicin – Oxime - Octreotide (3-27)	Doxorubicin
IC_{50} Mia Paca-2 cell line (μM) 72 h	2.56	14.21	0.80

The obtained toxicity values herein are almost 7-times higher on Mia Paca-2 cells for the hydrazone based conjugate **3-28** ($IC_{50} = 2.56 \mu M$), compared to the oxime based conjugate **3-27** ($IC_{50} = 14.21 \mu M$). The big difference in the IC_{50} values are caused by the fact, that

there is only free doxorubicin present inside the cell in case of the hydrazone based doxorubicin octreotide conjugate **3-28**. In contrast, in case of the doxorubicin-oxime-octreotide conjugate it is not possible to release native doxorubicin, because the linker molecule contains a bond not cleavable at low pH. A doxorubicin derivative is formed, which is still carrying a small cross-linker residue, similar to the PDI-derivative formed in the GSH cleavage study in **section 3.2** of this work. Those types of molecules are still capable of mediating their cytotoxic properties as reported in previous studies, but to a lesser extent. [41] [42]

Doxorubicin antiproliferative action on Mia Paca-2 cells after an incubation of 72 h was slightly stronger ($IC_{50} = 0.80$) compared to the herein tested conjugate, which can be explained by a different cellular uptake mechanism (

Table 1). The doxorubicin-octreotide conjugate is taken up by a receptor-mediated endocytosis followed by an endosomal escape, while doxorubicin is taken up quickly by passive diffusion (direct transcytosis).

In the second study the focus was set on the cell toxicity determination of **3-28** on the two different cell lines Mia Paca-2 and A549. Therefore, both cell lines were incubated for 24 h and 72 h with the hydrazone based conjugate.

Table 2: *In Vitro* cytotoxic effects of the doxorubicin-octreotide conjugate **3-28** on MIA PaCa-2 and A549 Cells (Data Expressed as IC_{50} Values in μM , $n \geq 3$, Mean \pm Standard Deviation)

Compound	IC_{50} Mia Paca-2 cell line (μM)		IC_{50} A549 cells line (μM)	
	24 h	72 h	24 h	72 h
Doxorubicin – Hydrazone - Octreotide (3-28)	4.57	2.56	14.28	7.25

The tested conjugate **3-28** shows a three times higher toxicity for the MIA PaCa-2 cells ($IC_{50} = 4.57$, 24 h) with an overexpression of somatostatin receptors compared to the basal epithelial cells A549 ($IC_{50} = 14.28$, 24 h). In turn, the IC_{50} value for the last mentioned cell line is around three times higher after 24 h as well as 72 h compared to Mia Paca-2 cells (Table 2). Furthermore, for both cell lines the IC_{50} value after 72h is half of the value for 24 h. This result proves the expected higher toxicity of the synthesized doxorubicin-octreotide on the somatostatin overexpressing cell line Mia Paca-2, which is supposed to be caused by a receptor mediated cell uptake mechanism.

3.6 Conclusions

Based on our successful experience before in making conjugates for targeted tumor delivery we have designed and prepared a linker molecule that works even better because of its smaller size and still possessing the potential to be cleaved under reducing conditions inside the cell. The number of atoms, which are introduced between the sulfur atoms of the peptide during the intercalation could be almost halved, which is a crucial factor and important for keeping the function of peptides active after modification.

Additionally, we have expanded the initial idea of modifying biomolecules with the novel linker by the introduction of a high diversity of different reactive unnatural substituents into peptides and proteins while the bioactive structure is obtained. Thereby, a new platform was build enabling a high portfolio of different coupling reactions to take place to octreotide. For instance, derivatives of the peptide hormone octreotide bearing a single iodo or ethynyl group were synthesized *via* the novel linker by the intercalation into the disulfide bridge. The iodo and ethynyl bioconjugation reagents **3-10** and **3-11** presented herein could be applied for introducing such substituents into alternative peptides and proteins.

All different intercalating reagents synthesized in this work allow a covalent modification of native disulfide bonds through reductive liberation of the cysteine thiol groups followed by the formation of two new disulfide bonds. The successful intercalation was demonstrated by the application of octreotide, which contains a single disulfide bridge, by means of RP-HPLC, NMR spectroscopy and MALDI-TOF MS experiments

Besides the synthesis of the different linker reagents, the potential of those in the field of site-selective peptide modification could be confirmed by the synthesis of dye- and drug-octreotide conjugates showing high overall yields and fast coupling steps (1h). In contrast, similar coupling steps using a bis-sulfone linker need much more time (24 h). [43] This is in important aspect, as time can be crucial for many peptides that are sensitive and difficult to handle.

The advantage of the novel linker to be cleavable under reducing conditions was proven for the PDI-octreotide conjugates **3-24** and **3-25**. Furthermore, these dye-octreotide conjugates are assumed to have high potential for tumor imaging experiments, due to the exceptional thermal and photochemical stability as well as fluorescence quantum yields of the chosen PDI dye.

Regarding a targeted delivery of drugs towards tumor cells we also created a pH responsive group that enables the controlled release of the drug doxorubicin in tumor tissue. Stability experiments of the synthesized doxorubicin-octreotide conjugate by RP-HPLC confirmed the controlled release of native doxorubicin in acidic solutions only. The cytotoxicity assays conducted for the herein synthesized doxorubicin-octreotide conjugates **3-27** and **3-28** with the two tested cell lines demonstrated that the hybrids can be applied as potent and selective antitumor agents. The performed microscopy and intracellular trafficking experiments once more supported our hypothesis of a selective delivery of hybrid **3-28** to cancer cells and additionally setting free the native tumor drug.

Based on this novel, smaller and cleavable linker type as well as the introduction of different functional groups the field of bioconjugate chemistry will be extended to new fields and applications not known before. In principle, the different molecules presented herein could facilitate the efficient design of a broad variety of artificial protein and peptide analogues with previously unknown bioactivities.

3.7 References

1. Brocchini, S., et al., *PEGylation of native disulfide bonds in proteins*. Nature Protocols, 2006. **1**(5): p. 2241-2252.
2. Pfisterer, A., *Ortsgerichtete Modifikationen von Somatostatin-14 zur Darstellung von maßgeschneiderten Biohybridkonjugaten*. Dissertation, MPIP Mainz, 2012.
3. Mar E. B. Smith, F.F.S., Chris P. Ryan and James R. Baker, *Protein Modification, Bioconjugation, and Disulfide Bridging Using Bromomaleimides*. 2010.
4. Pfisterer, A., et al., *Bioactive unnatural somatostatin analogues through bioorthogonal iodo- and ethynyl-disulfide intercalators*. Chemistry, 2011. **17**(35): p. 9697-707.
5. Lelle, M., et al., *Octreotide-Mediated Tumor-Targeted Drug Delivery via a Cleavable Doxorubicin-Peptide Conjugate*. Mol Pharm, 2015. **12**(12): p. 4290-300.
6. van der Vlies, A.J., et al., *Synthesis of pyridyl disulfide-functionalized nanoparticles for conjugating thiol-containing small molecules, peptides, and proteins*. Bioconjug Chem, 2010. **21**(4): p. 653-62.
7. *Protective groups in organic synthesis. Proceedings of a symposium/workshop. Stockholm, October 13, 1986*. Acta Pharm Suec, 1986. **23**(6): p. 321-417.
8. Balan, S., et al., *Site-specific PEGylation of protein disulfide bonds using a three-carbon bridge*. Bioconjugate Chemistry, 2007. **18**(1): p. 61-76.
9. Brocchini, S., et al., *Disulfide bridge based PEGylation of proteins*. Advanced Drug Delivery Reviews, 2008. **60**(1): p. 3-12.
10. Youziel, J., et al., *Bromo- and thiomaleimides as a new class of thiol-mediated fluorescence 'turn-on' reagents*. Org Biomol Chem, 2014. **12**(4): p. 557-60.
11. Peneva, K., et al., *Water-soluble monofunctional perylene and terylene dyes: Powerful labels for single-enzyme tracking*. Angewandte Chemie-International Edition, 2008. **47**(18): p. 3372-3375.
12. Dubois, A., et al., *Photostability of dye molecules trapped in solid matrices*. Applied Optics, 1996. **35**(18): p. 3193-3199.
13. Kohl, C., *Dissertation*. Johannes-Gutenberg University (Mainz), 2013.

14. Carlsson, J., H. Drevin, and R. Axen, *Protein thiolation and reversible protein-protein conjugation. N-Succinimidyl 3-(2-pyridyldithio)propionate, a new heterobifunctional reagent*. *Biochem J*, 1978. **173**(3): p. 723-37.
15. Sibubalan, A.G.a.S.B., *Site-Specific PEGylation of Protein Disulfide Bonds Using a Three-Carbon Bridge*. 2006.
16. Zou, A., et al., *In vivo studies of octreotide-modified N-octyl-O, N-carboxymethyl chitosan micelles loaded with doxorubicin for tumor-targeted delivery*. *J Pharm Sci*, 2013. **102**(1): p. 126-35.
17. T. Ishida, Y.O., T. Kobayashi, H. Kiwada, *Int. J. Pharm.*, 2006. **309**, **94**.
18. Huo, M.R., et al., *Somatostatin receptor-mediated tumor-targeting drug delivery using octreotide-PEG-deoxycholic acid conjugate-modified N-deoxycholic acid-O, N-hydroxyethyl chitosan micelles*. *Biomaterials*, 2012. **33**(27): p. 6393-6407.
19. Szabo, I., et al., *Development of an oxime bond containing daunorubicin-gonadotropin-releasing hormone-III conjugate as a potential anticancer drug*. *Bioconjug Chem*, 2009. **20**(4): p. 656-65.
20. Kratz, F., et al., *Transferrin conjugates of doxorubicin: synthesis, characterization, cellular uptake, and in vitro efficacy*. *J Pharm Sci*, 1998. **87**(3): p. 338-46.
21. Leamon, C.P. and J.A. Reddy, *Folate-targeted chemotherapy*. *Advanced Drug Delivery Reviews*, 2004. **56**(8): p. 1127-1141.
22. Novartis,
https://www.pharma.us.novartis.com/sites/www.pharma.us.novartis.com/files/sandostatin_inj.pdf. 2016.
23. Theodoropoulou, M. and G.K. Stalla, *Somatostatin receptors: from signaling to clinical practice*. *Front Neuroendocrinol*, 2013. **34**(3): p. 228-52.
24. Roosterman, D., et al., *Distinct agonist-mediated endocytosis of cloned rat somatostatin receptor subtypes expressed in insulinoma cells*. *Journal of Neuroendocrinology*, 1997. **9**(10): p. 741-751.
25. Nagy, A., et al., *Synthesis and biological evaluation of cytotoxic analogs of somatostatin containing doxorubicin or its intensely potent derivative, 2-pyrrolinodoxorubicin*. *Proc Natl Acad Sci U S A*, 1998. **95**(4): p. 1794-9.
26. Wang, T., et al., *Receptor selective ruthenium-somatostatin photosensitizer for cancer targeted photodynamic applications*. *Chem Commun (Camb)*, 2015. **51**(63): p. 12552-5.

27. Wang, T., et al., *Bis-sulfide bioconjugates for glutathione triggered tumor responsive drug release*. Chemical Communications, 2014. **50**(9): p. 1116-1118.
28. Reubi, J.C., *Peptide receptors as molecular targets for cancer diagnosis and therapy*. Endocrine Reviews, 2003. **24**(4): p. 389-427.
29. Schaer, J.C., et al., *Somatostatin receptor subtypes sst(1), sst(2), sst(3) and sst(5) expression in human pituitary, gastroentero-pancreatic and mammary tumors: Comparison of mRNA analysis with receptor autoradiography*. International Journal of Cancer, 1997. **70**(5): p. 530-537.
30. Schumacher, F.F., et al., *In situ maleimide bridging of disulfides and a new approach to protein PEGylation*. Bioconjug Chem, 2011. **22**(2): p. 132-6.
31. Zloh, M., et al., *Identification and insertion of 3-carbon bridges in protein disulfide bonds: a computational approach*. Nature Protocols, 2007. **2**(5): p. 1070-1083.
32. Sun, L.C. and D.H. Coy, *Somatostatin receptor-targeted anti-cancer therapy*. Curr Drug Deliv, 2011. **8**(1): p. 2-10.
33. Cheng, R., et al., *Dual and multi-stimuli responsive polymeric nanoparticles for programmed site-specific drug delivery*. Biomaterials, 2013. **34**(14): p. 3647-57.
34. Schafer, F.Q. and G.R. Buettner, *Redox environment of the cell as viewed through the redox state of the glutathione disulfide/glutathione couple*. Free Radic Biol Med, 2001. **30**(11): p. 1191-212.
35. Deneke, S.M. and B.L. Fanburg, *Regulation of cellular glutathione*. Am J Physiol, 1989. **257**(4 Pt 1): p. L163-73.
36. De Martino, M.C., L.J. Hofland, and S.W. Lamberts, *Somatostatin and somatostatin receptors: from basic concepts to clinical applications*. Prog Brain Res, 2010. **182**: p. 255-80.
37. Amherdt, M., Y.C. Patel, and L. Orci, *Binding and Internalization of Somatostatin, Insulin, and Glucagon by Cultured Rat Islet Cells*. Journal of Clinical Investigation, 1989. **84**(2): p. 412-417.
38. Huang, C.M., Y.T. Wu, and S.T. Chen, *Targeting delivery of paclitaxel into tumor cells via somatostatin receptor endocytosis*. Chem Biol, 2000. **7**(7): p. 453-61.
39. Nadas, J. and D. Sun, *Anthracyclines as effective anticancer drugs*. Expert Opin Drug Discov, 2006. **1**(6): p. 549-68.

40. Hornick, C.A., et al., *Progressive nuclear translocation of somatostatin analogs*. Journal of Nuclear Medicine, 2000. **41**(7): p. 1256-1263.
41. Schlage, P., et al., *Anthracycline-GnRH derivative bioconjugates with different linkages: synthesis, in vitro drug release and cytostatic effect*. J Control Release, 2011. **156**(2): p. 170-8.
42. Orban, E., et al., *In vitro degradation and antitumor activity of oxime bond-linked daunorubicin-GnRH-III bioconjugates and DNA-binding properties of daunorubicin-amino acid metabolites*. Amino Acids, 2011. **41**(2): p. 469-483.
43. Wang, T., et al., *A Disulfide Intercalator Toolbox for the Site-Directed Modification of Polypeptides*. Chemistry-a European Journal, 2015. **21**(1): p. 228-238.

4 Site-selective modification of peptides and proteins with minimal structural alteration

Literature describes three linker systems for the disulfide intercalation of biomolecules so far, which have been discussed in the introduction of this work. The first linker belongs to the group of disulfide-based disulfide intercalation and was first described by our group in the last year (compound **4-1**). [1] An improved derivative of this linker system was described in the previous Chapter 3, in which the number of atoms used for the disulfide intercalation could be halved (compound **4-2**). However, the common advantage of these two linker systems is its ability to undergo a controlled cleavage process inside the cell, thus enabling a targeted delivery of the cargo.

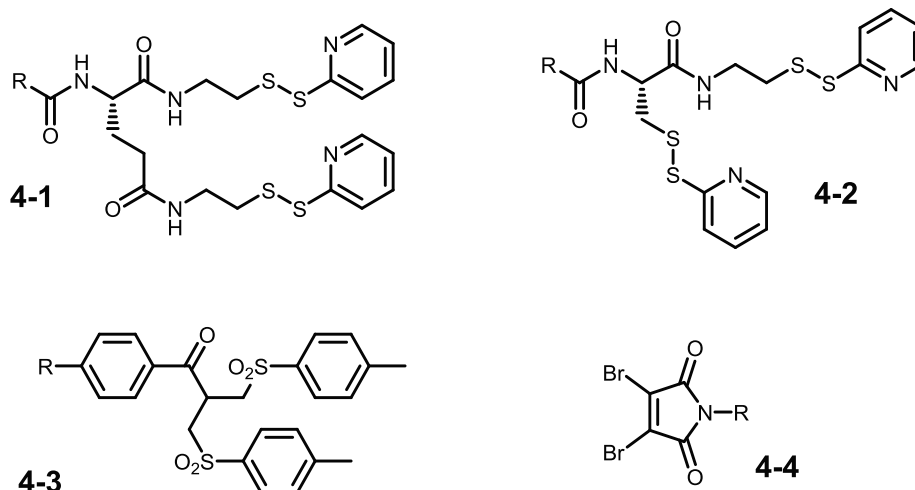


Figure 34: Peptide modification reagent for disulfide intercalation described in literature

In contrast, cleavable linker systems are only useful for the transport of those drugs, which should be set free inside the cell. If one wants to attach a polymer or to label a peptide, the linker system has to be stable under physiological conditions, which is not the case for the disulfide based linker systems. In turn this is an advantage of the bis-sulfone or 2, 3-dibromomaleimide based linker systems (**4-3** and **4-4**) due to the formation of stable thioether bonds. Furthermore, these two linker systems are relatively small when talking about the number of atoms, which are inserted during the intercalation between the disulfide bonds for the desired modification. The bis-sulfone based linker systems consists of three carbon atoms and the dibromomaleimide linker system contains two carbon atoms. [1-3] Finally, the small size is an additional advantage of the linker systems **4-3** and **4-4** (Figure

34). The following chapter will point out the missing piece of the puzzle in the field of bioconjugation techniques.

Although the last mentioned two systems have been used successfully in different projects, they either lack fast and high coupling reactions or even more important the required stability in physiological conditions, even though they form stable thioether bonds. It has been previously reported that maleamic acids are labile in acidic pH and maleimide derived conjugates are known to be susceptible to exchange reactions with endogenous proteins. [4] [5] In the case of PEGylation, meaning the attachment of the polymer PEG to the biomolecule, the exchange reactions result in deconjugation of the protein from polymer. Finally, as PEGylation endows proteins with many favorable characteristics such as enhanced water solubility, reduced immunogenicity, improved circulating half-life *in vivo* due to and improved thermal and mechanical stability, this will lead to a rapid, uncontrolled clearance of the protein and a reduction in efficacy (Figure 35).

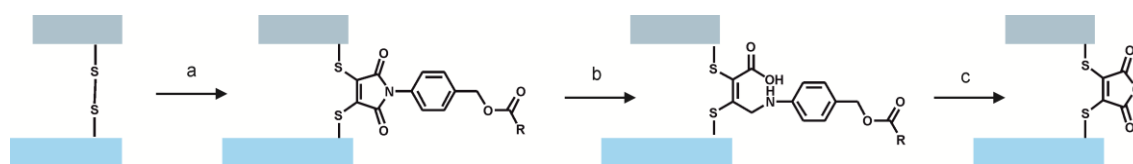


Figure 35: Assembly/cleavage of a disulfide (e.g. from Fab ADC) modified with a dibromomaleimide linker, a) TCEP, pH 8.0 37 °C, 1.5 h, addition of the linker, 37°C, 1h; b) pH 7.4, 20 h; c) pH 4.5, 72 h

The same is true for the bis-sulfone linker, as it has been reported that reagents that undergo conjugation by a Michael addition reaction are susceptible to retro Michael reactions leading to deconjugation of the PEG or the labeling unit (e.g. dyes) from the protein. In cases of bis-sulfones this problem can only be circumvented by an additional reduction of the electron-withdrawing carbonyl group. [6] However, such reduction steps in presence of the therapeutically active proteins are often inappropriate as the biomolecule will easily lose its function.

In the end, we do have a portfolio of different linker systems for disulfide modification in hand, but none is fulfilling all of the requirements given in the introduction of this work. The ideal conjugation strategy for the site-directed modification of peptides or proteins should possess the following prerequisites:

- ideally no additional atoms are introduced between the sulfur atoms
- high coupling yields and fast reaction kinetics
- stability under physiological conditions
- easy introduction of responsive groups for controlled release of therapeutically active molecules

The intention of this work is to present a novel linker platform based on 3,3-dichloroacrylic acid for the site-selective covalent modification of therapeutic peptides and proteins, fulfilling the aforementioned prerequisites. This linker system enables the introduction of one carbon atom between the sulfur atoms only and is therefore the smallest disulfide linker system reported so far. The reaction proceeds in two steps: (1) disulfide reduction of the protein to release two free thiols, and (2) two subsequent addition/elimination reactions.

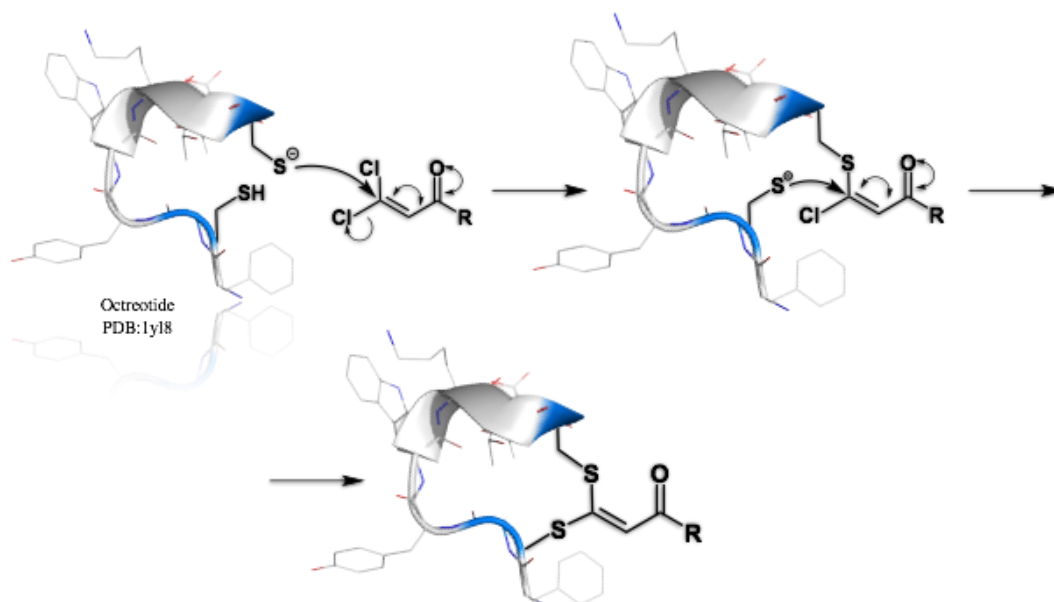


Figure 36: 3,3-dichloro-acrylic acid as a novel cornerstone for the disulfide intercalation of peptides and the suggested reaction principle with thiol groups of reduced disulfide bond of octreotide

Due to the carbonyl group as well as the electron withdrawing chlorine atoms, the β -carbon of the acrylic acid is partially positively charged, allowing the nucleophilic attack of both thiol groups at the same carbon atom (Figure 36). The two subsequent addition/elimination reactions involve the attack of one thiol on the double bond of the acrylic acid first followed by the elimination of one chlorine atom. The intermediate is susceptible to further nucleophilic attack due to the reformation of the double bond. After the addition of the second thiol group, the second chlorine atom is eliminated. The coupling principle is supposed to allow an efficient bioconjugation with high coupling yields, fast reaction times and without the loss of biological activity. [7]

Herein, 3,3-dichloroacrylic acid (**4-5**) was tested as the smallest possible disulfide-intercalating cross-linking reagent for the selective and stable modification of therapeutic peptides and proteins. The high potential and versatility of the novel linker system to modify such biomolecules was investigated for the first time. Similar reactions proving that this linker is able to react with two different thiol groups have been reported in literature. [8-10] Advantages over known linker systems in literature would be its small size and ease of synthesis, which would be especially important for future applications in pharmacy, as well as its stability under physiological conditions. The potential of the novel linker platform was evaluated by the PEGylation and labeling of octreotide as well as the targeted delivery of the anticancer drug doxorubicin.

4.1 Computational calculations

Before first test reaction were started, the idea to use 3,3-dichloroacrylic acid as a new linker reagent was validated by computational calculation studies in cooperation with the group of Prof. Till Opatz from Johannes-Gutenberg University, Mainz.

In order to study the general effect of the insertion of an acrylamide-based linker system into a disulfide bond in silico, the impact on the C-S-S-C dihedral angle as well as the C-C distance, as these should be the primary relevant geometric factors, were investigated first. It is known that the disulfide bond in proteins is characterized by a preferred C-S-S-C dihedral angle of about (\pm) 90° , typically referred to as χ_3 . Using dimethyl disulfide as a test compound, relaxed surface scan using different computational levels was performed:

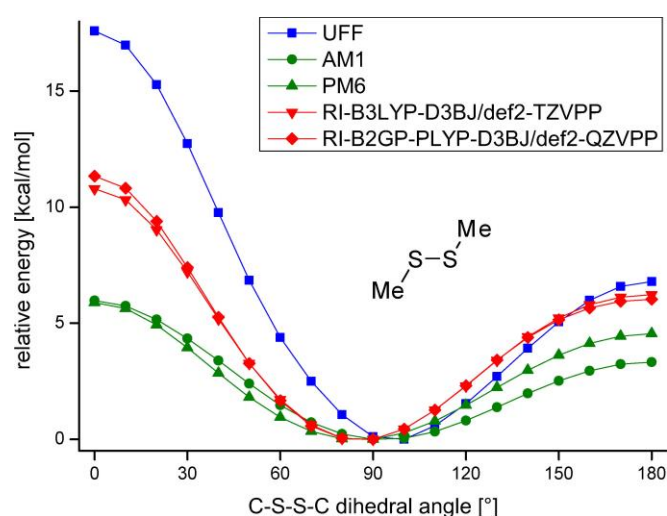


Figure 37: Relatively energy in dependence to the dihedral angle of a model structure $\text{CH}_3\text{-S-S-CH}_3$

The double-hybrid DFT calculation with a large basis set is used as a reference. It is obvious that the force field overestimates and the semi-empirical methods underestimate the torsional barriers. However, the hybrid DFT calculation at a triple-zeta level is more computationally feasible and yields good results. Therefore, this method was chosen to study the following model compound:

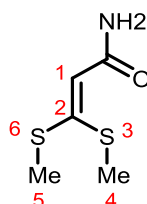


Figure 38: Structure of the model compound $(\text{MeS})_2\text{CCH-CONH}_2$ for the computational study

The $(\text{MeS})_2\text{CCH-CONH}_2$ single bond was constrained to be *s-cis*, as the nitrogen atom carries a sterically demanding substituent in the synthesized compounds. A two-dimensional surface scan was performed (scanning the 1-2-3-4 and 1-2-5-6 dihedral angles; red and blue mark regions of high or low electronic energy, respectively; asterisks correspond to local minima):

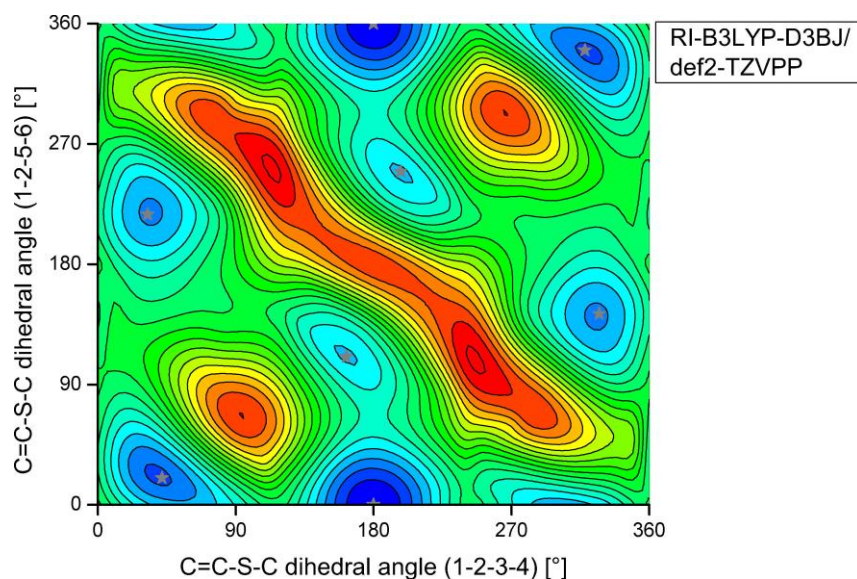


Figure 39: Two-dimensional surface scan, red = high energy, blue = low energy

The following stationary points were found after re-optimization (mirror images are omitted as the potential energy surface shows inversion symmetry):

Conf. No.	C-C-S-C dihedral angle (1-2-3-4) [°]	C-C-S-C dihedral angle (1-2-5-6) [°]	ΔE [kcal/mol]	ΔG [kcal/mol]
1	179.4	359.9	0.00	0.00
2	42.0	19.9	1.18	0.54
3	32.5	217.2	1.81	1.07
4	162.2	110.7	2.40	1.69

All conformations are within an energetically accessible range concerning the Gibbs free enthalpies, especially considering ring strain effects in large cyclic proteins that could alter the order found here. The minima correspond to the following C-S-S-C dihedral angles as well as methyl-methyl distances:

Conf. No.	C-S-S-C dihedral angle (4-3-5-6) [°]	C-C distance (4-6) [Å]
1	179.2	4.74
2	86.1	3.60
3	101.4	4.58
4	85.0	3.52

These values can be compared with the data for Me_2S_2 (dihedral angle = 85.8° , distance = 3.76 \AA). It can be seen that conformation 2, 3, and 4 also possess C-S-S-C dihedral angles around 90° . Especially for conformations 2 and 4, no significant change of the C-C distance is observed. Only conformation 1 gives a dihedral angle of around 180° , which corresponds to a local maximum for a classical disulfide bond (albeit it is not as energetically disfavored as an angle of 0°). This “new” conformation is caused by the conjugation between the lone

pairs on both sulfur atoms and the unsaturated amide group. The only really disallowed (red) regions in the potential energy surface correspond to C-S-S-C dihedral angles of approximately 0° or 180° that are also disfavored for a normal disulfide bond.

In conclusion, the incorporation of an acrylamide moiety in the disulfide bond of a protein should principally be possible without a significant change of the structure, as conformations 2 and 4 closely resemble a classical disulfide bond.

4.2 PEG-octreotide hybrid

With the computational calculations data in hand, the outlined linker systems 3,3-dichloroacrylic acid was applied first to a possible modification of a peptide with a polymer. In this case PEG was used as the polymer and octreotide as the peptide.

PEGylation describes the modification of most typically peptides, proteins or antibody fragments by attaching the strands of the polymer PEG, having turned such molecules into important new biopharmaceuticals for more than 40 years, when Frank. F. Davis came up with the idea to develop a process to render usable bioactive biomolecules of potential medical value. [11] [12] Different studies have proven that the modification of peptides with PEG causes an optimization of the pharmacokinetic and pharmacodynamic properties as well as the water solubility of the conjugate. For a given molecular weight PEG has a 5-10 time bigger volume in water compared to a peptide with similar molecular weight. The reason for this is the binding of 2-3 water molecules for each repetition unit of PEG. In turn the increased hydrodynamic volume enables a longer circulation in the blood, as the renal clearance depends on the size of the molecule. [13] Furthermore, the PEG chains function as a protective shield hindering enzymes as peptidases proteases to digest the native peptide molecule and showing no toxicity. [14] Therefore, such techniques are well-known nowadays to overcome problems related to therapeutic applications of peptides as reduced immunogenicity, proteolytic degradation and rapid clearance from blood circulation.

First generation techniques in the field of PEGylation mainly focus on attaching the PEG chain to ϵ -amino group of lysines. [15] Due to the huge amount of possible active reaction centers the peptide was modified multiple times and the whole process was not reproducible. Thus, evading such drawbacks, the approaches of the second generation aimed to other shortcut methods which ensure for example a selective modification of the N-terminus of a peptide. An additional opportunity includes the genetically engineered introduction of

cysteines at precisely defined locations in the biomolecule, leading to a monofunctional modification. [16] Furthermore, branched as well as higher molecular PEGs have been used to improve the pharmacokinetic properties. [17] The last mentioned technique has the drawback of being very time consuming and inconvenient, as it is not feasible with every peptide or protein.

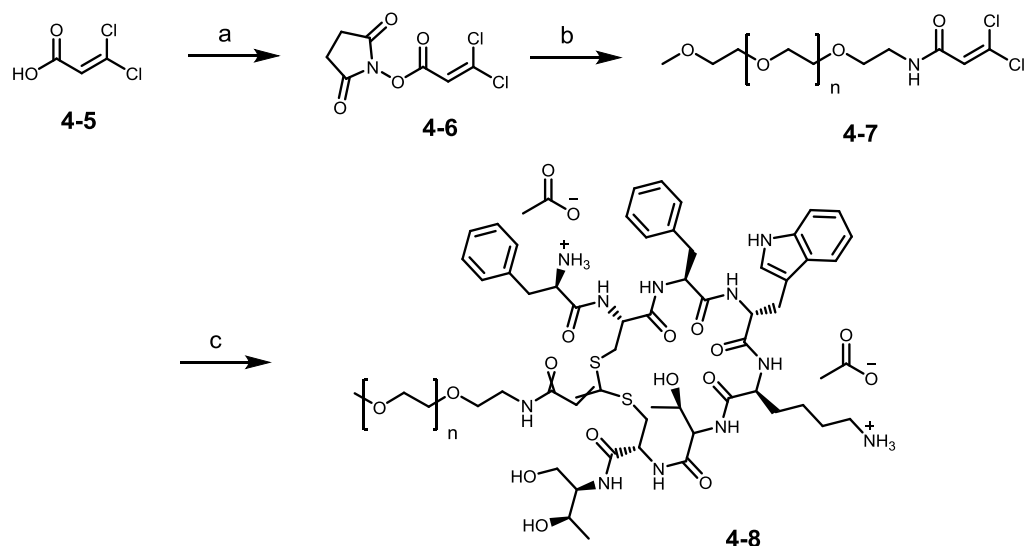
Octreotide is clinically used for the treatment of acromegaly and certain endocrine tumors. [18, 19] The commercial formulation is based on in poly(D,L-lactide-co-glycolide) (PLGA) microspheres (Sandostatin LAR depot, Novartis Pharma, Basel, Switzerland) and is applied for subcutaneous administration by injection. After injection, octreotide is absorbed rapidly and completely from the injection site. Compared with the elimination half-life from plasma of the natural hormone with 1-3 minutes, octreotide stays with an apparent half-life of 1.7 to 1.9 hours much longer in the blood plasma. [20]

PEG-octreotide hybrids are known to have greater circulation half-life and stability toward octreotide, as it was shown by DeLuca and co-workers. [21, 22] Interestingly, in this work PEGylation of octreotide was performed at the N-terminus of the peptide *via* an amide bond formation with PEG-(2000) as well as PEG-(5000). However, the problem in this study was, that side products were formed, as octreotide also possesses an ϵ -amino group, which will also be modified. In order to obtain the mono-functionalized peptide an additional purification step would be needed. Nevertheless, as it was stated in this study, the attachment of PEG-(5000) to octreotide significantly improved the pharmacokinetic properties compared to PEG-(2000), which only showed similar properties to native octreotide.

Herein, a new method of octreotide PEGylation was tested involving a mild reduction of disulfide bond in the first step, followed by the intercalation and back-closing of the disulfide bond due to the reaction with the 3,3-dichloroacrylic part of our novel synthesized linker system in the second step. This novel method combines fast and efficient coupling reactions with a single and site-specific modification of the peptide overcoming the aforementioned disadvantages. Thereby, octreotide's half-life and efficiency would be extended as proteolytic degradation would be decreased and renal clearance would be delayed.

4.2.1 Synthesis

The required bis-thiol alkylating reagent was in all cases prepared from the commercially available 3,3-dichloroacrylic acid (**4-5**) in one or two steps only, depending on the cargo. In case of the PEGylation agent, PEG-(5000) amine could be directly attached to the NHS ester of 3,3-dichloroacrylic acid (**4-6**), which was synthesized in presence of NHS and DIC in very good yields (90 %, Scheme 10). Therefore, **4-6** was used in excess to enable a complete conversion of the PEG-(5000)-NH₂ and to simplify the following purification step by size-exclusion chromatography. Additionally, any side reaction of the amine with the chlorine atoms of the linker system were avoided by using adjusted stoichiometric amounts. For the modification of octreotide with the linker-modified PEG-(5000), the peptide's disulfide bond had to be reduced first in order to enable the addition-elimination reaction of both free thiol groups at the 3,3-dichloro-acrylamide part of **4-4**. Reduction of the peptide's disulfide bond was achieved by means of TCEP (1.5 eq) in a phosphate buffered solution (pH 6.4) at room temperature. Finally, the coupling of the PEG-Linker system (**4-7**) and the reduced octreotide was accomplished by stirring both reagents in Milli-Q water/DMF under slightly basic conditions for 3-4 h (c (**4-7**) = 8 mg/ml). Interestingly, this coupling process did not work without the addition of 8 eq KOH in MeOH to the reduced peptide, dissolved in a mixture of Milli-Q water and DMF, prior to the addition of the linker dissolved in an identical amount of solvents. [9] Like this, the thiol groups will be deprotonated forming the more reactive thiolate groups for the desired addition-elimination reaction. Different other conditions with DPBS, EtOH or ACN were tested as it is also described in literature, but none of them worked at all. [8, 10] All reactions were conducted at room temperature, which is particularly important for many temperature-sensitive proteins such as antibodies, which should be addressed in future applications.



Scheme 10: (a) N-hydroxysuccinimide (1.15 eq), N,N'-Diisopropylcarbodiimide (1.2 eq), dry dichloromethane, argon, overnight, r.t., 92% (b) PEG-(5000)-NH₂ (0.9eq), dry DMF, argon, 4 h, r.t., 88% (c) reduced octreotide (1.5 eq), KOH in methanol (8 eq), DMF, Milli-Q water, argon, 4 h, r.t., 86%

To prove the successful coupling between the PEG-(5000) amine and octreotide, the different molecules and conjugates were investigated by gel-electrophoresis (SDS-PAGE, Figure 40), as different macromolecules will be separated and analyzed based on their size and charge. In this experiment it is expected that octreotide moves faster and migrates for a longer distance in the electric field applied than the bigger PEG-(5000)-NH₂ as well as compound **4-8**. The left panel displays the obtained protein bands after staining with Coomassie Brilliant blue, which is known to stain molecules containing free amine groups. This is the case for the octreotide molecule only as it possesses a free lysine amine as well as the free N-terminal amine of the phenylalanine. A characteristic staining of the amine of the PEG-(5000)-NH₂ compound would be desirable, but was not expected due to the high amount of ethylene glycol units in relation to one amine group only. In addition, barium iodide solution was used to stain PEG bands as shown on the right panel (Figure 40). In all cases the gels were first stained with barium iodide solution and afterwards with Coomassie Brilliant blue, but a separate picture was taken after each staining step to allow a direct comparison and evaluation of the coupling process. Furthermore, two appropriate protein ladders for the accomplished SDS-PAGE were applied in different lanes and the corresponding molecular weights are shown next to the gel (Kaleidoscope Prestained Standard and the polypeptide SDS-PAGE Molecular Weight Standard).

Both, line 2 and line 6, show a clear signal after Coomassie staining in the left panel of the unmodified peptide indicating a molecular mass around 1.4 kDa (MW octreotide = 1.021 kDa). In comparison, there is no octreotide band detectable at line 3 and 7 after the Coomassie staining (compound **4-8**, PEG-5000-octreotide). It can be stated that the coupling between the peptide and polymer was successful, as there is only the final conjugate detectable at a molecular mass around 6.5 kDa at line 3 and 7 in the left panel (MW conjugate = 6.2 kDa). This observation is supported by the fact, that **4-8** (line 3 and 7) shows a shorter migration compared to PEG-(5000)-NH₂ (line 5 and 8) after staining with barium iodide solution in the right panel, which indicates a higher molecular mass due to the coupled peptide. Different concentrations of the conjugates were tested in advance to improve the resolution of the relatively weak spot of **4-8** in comparison to the spot of native octreotide after the Coomassie staining. The problem is similar to the already mentioned failed Coomassie staining of PEG-(5000)-NH₂ (left panel, lines 5 and 8). The high amount of ethylene glycol units in relation to one amine group only, respectively two amine groups in case of the PEG-octreotide conjugate, avoids a clear staining at the concentration used. Of course, a higher concentration of **4-8** would have been possible and has been tested, but the drawback was, that the peak in the right panel was far too intensive after the barium iodide staining. In the end, the concentrations utilized here have been identified to be the most suitable. Interestingly, **4-8** not only shows the expected band around 7.6 Da, but also three bands with lower intensity and shorter migration length. These bands are probably caused by the aggregation of the conjugates, forming molecules with higher molecular masses. A reason for the potential aggregation could not be found, but has been reported in different works using different peptides. [23]

To conclude, the molecular weights of the corresponding standard peptides verify the successful coupling process between peptide and polymer based on our novel linker system 3,3-dichloroacrylic acid. In addition, the conjugates were analyzed by GPC in DMF using a PEG-(5000) molecule as the standard as well as by MALDI-TOF MS, confirming the results presented here (Appendix 2).

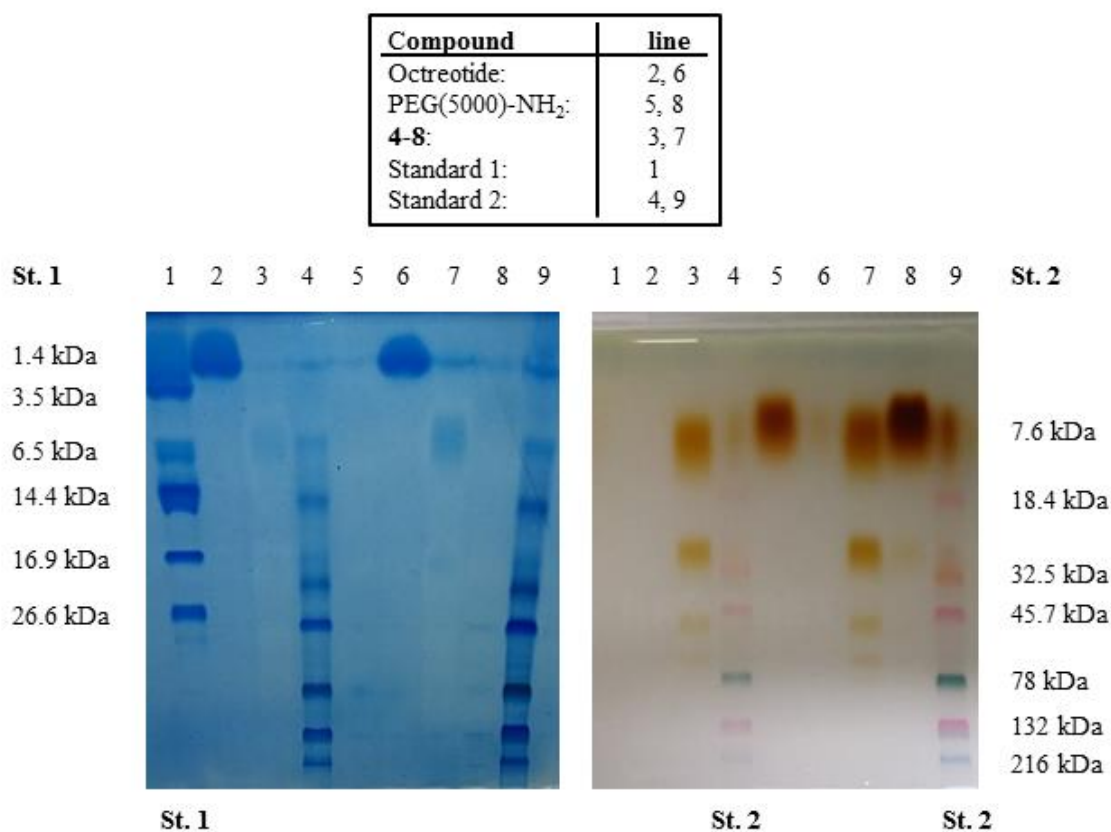
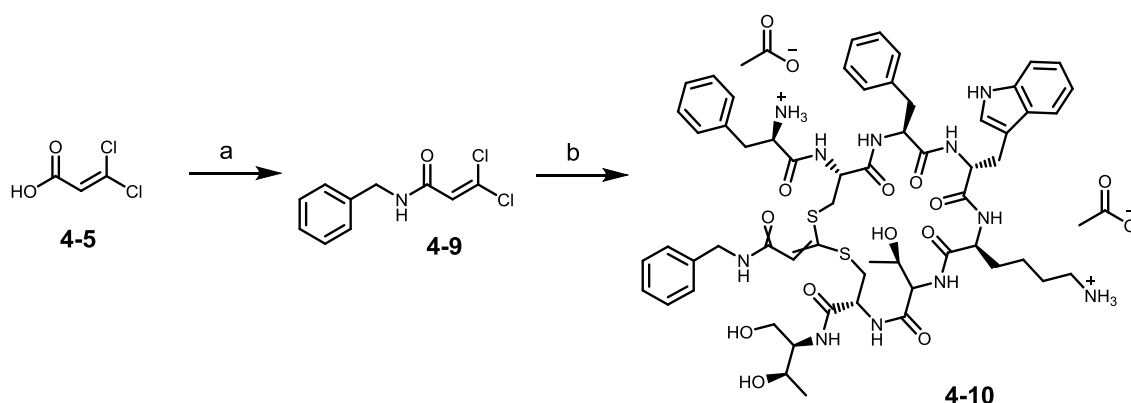


Figure 40: Comparative study of the PEG-(5000)-octreotide (**4-8**), PEG-(5000)-NH₂ and native octreotide by SDS-PAGE. Peptide bands were visualized by Coomassie staining (left panel) and PEG bands were visualized by barium iodide solution (right panel).

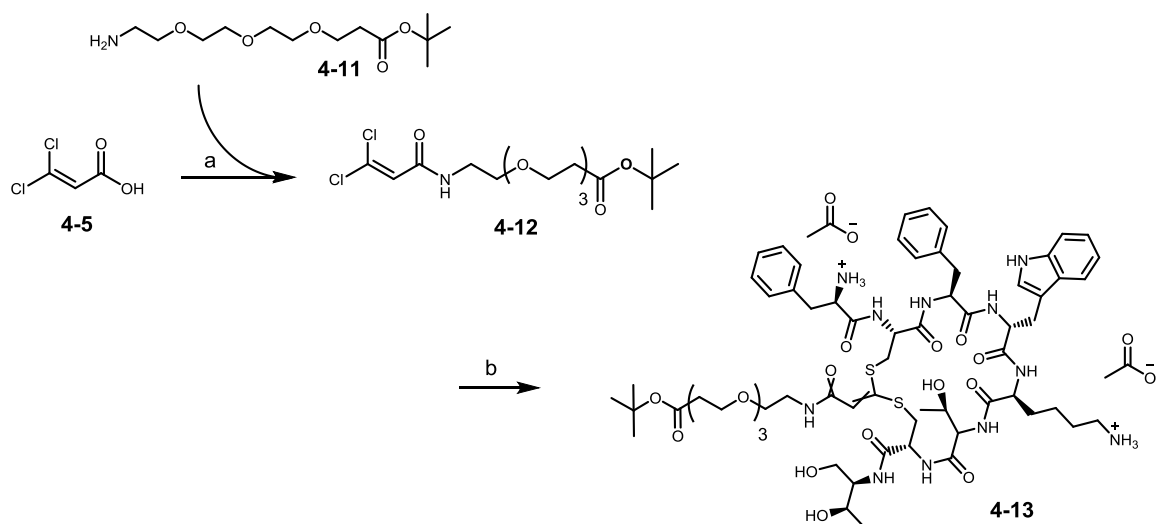
Furthermore, the suggested coupling procedure had to be proven, in which both thiols of the reduced octreotide are assumed to attack at the 3,3-dichloroacrylic group aiming in the closing back towards the cyclic structure of the peptide. Therefore NMR spectroscopy was chosen as a suitable method. ¹H NMR as well as the corresponding COSY, HSQC and HMBC measurements of the PEG-(5000)-octreotide conjugate (**4-8**) were performed in different solvents and concentrations due to solubility problems, but the final spectra were not analyzable. Neither a clear assignment of the aromatic protons nor an interaction of the protons in the 2D NMR measurements was possible in presence of the long PEG chain, as the ethylene protons absorb most of the energy due to frequency of occurrence in the hybrid molecule. Utilization of different solvents as well as increasing the concentration of the conjugate until the deuterated solution was saturated gave no improvement.

Therefore two simple model compounds with similar characteristic to the PEG-octreotide conjugate were synthesized with smaller size. Benzylamine was chosen as it is a simple alkyl-carrying amine allowing an easy peak assignment in the NMR and *tert*-butyl 12-amino-4,7,10-trioxadodecanoate (PEG-277-NH₂) was selected due to its similarity to the PEG-(5000)-NH₂. The assumed and described intercalation mechanism was proven by NMR with a benzylamine-octreotide (**4-10**) as well as a PEG-(277)-octreotide conjugate (**4-13**), consisting of three polyethylene glycol repeating units only (Scheme 11 and Scheme 12). In both synthetic cases, either benzylamine or *tert*-Butyl 12-amino-4,7,10-trioxadodecanoate were first coupled with 3,3-dichloroacrylic acid in presence of HATU or TSTU, in which the last mentioned one causes the formation of an additional unknown side product complicating the purification by silica column chromatography. The coupling of both linker-intermediates with octreotide was accomplished under similar conditions as already described before.



Scheme 11: Synthesis of benzylamine-octreotide hybrid **4-10**. a) benzylamine (0.9), HATU (1.3 eq), DIPEA (2 eq), dry DMF/DMSO, argon, 3 h, r.t. 68% b) reduced octreotide (1.5 eq), KOH in methanol (8 eq), DMF, Milli-Q water, argon, 4 h, r.t., 90%

Validation of the successful synthesis was accomplished by analytical HPLC, mass spectrometry as well as NMR spectroscopy. As an example the MALDI-TOF MS spectrum of **4-10** is depicted in Figure 41 showing the existence of the protonated product as well as the sodium and potassium adducts.



Scheme 12: Synthesis of PEG-(277)-octreotide hybrid **4-13**. a) HATU (1.3 eq), DIPEA (2 eq), **4-11** (0.9 eq), dry DMF, argon, 3 h, r.t. 85%. b) reduced octreotide (1.5 eq), KOH in methanol (8 eq), DMF, Milli-Q water, argon, 4 h, r.t., 90%

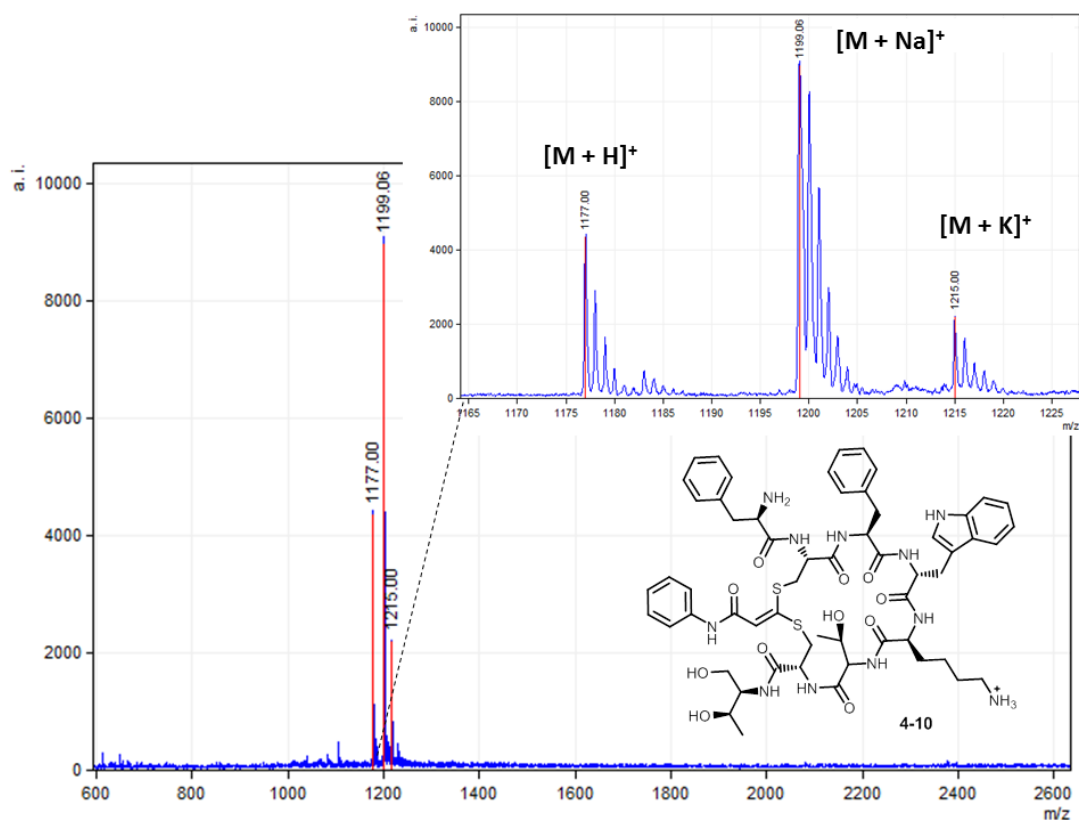


Figure 41: MALDI-TOF MS spectrum of **4-10** (matrix α -CHCA)

The final coupling to octreotide was visualized in both cases by means of analytical RP-HPLC as a reaction control. Interestingly two different peaks were formed for both products **4-10** and **4-13** during the reaction, a conspicuousness which was realized in cases of octreotide modification in chapter 3 as well. However, as shown above in the MALDI-TOF MS spectrum, only on single product could be detected, besides the sodium and potassium adducts (Figure 41). Consequentially it is assumed, that two isomers are formed during the reaction of the final conjugate. The detected masses of both species fit to the calculated mass, which is a first clear hint for the successful modification of the peptide with the novel linker system. Nevertheless, NMR spectroscopy was chosen as the method of choice, as 2D analysis of compounds **4-10** and **4-13** will give us the desired structural information.

In the first step, the ^1H NMR spectrum in Figure 42 together with the peak assignment clearly shows the successful synthesis of the intermediate **4-12**, the short PEG-(277) modified with the novel linker functionality. The most important proton belongs to number 11, as this olefinic proton will have a crucial part in the following 2D ROESY NMR experiment. In this spectrum here, number 11 gives one single singlet signal with the intensity of one in the proton spectrum. What we would like to see in the 2D NMR experiment is, that this acrylic proton shows cross peaks with the amide proton as well as the cysteine protons which are in close proximity. Exactly this would be the clear prove wanted to verify the assumed intercalation process.

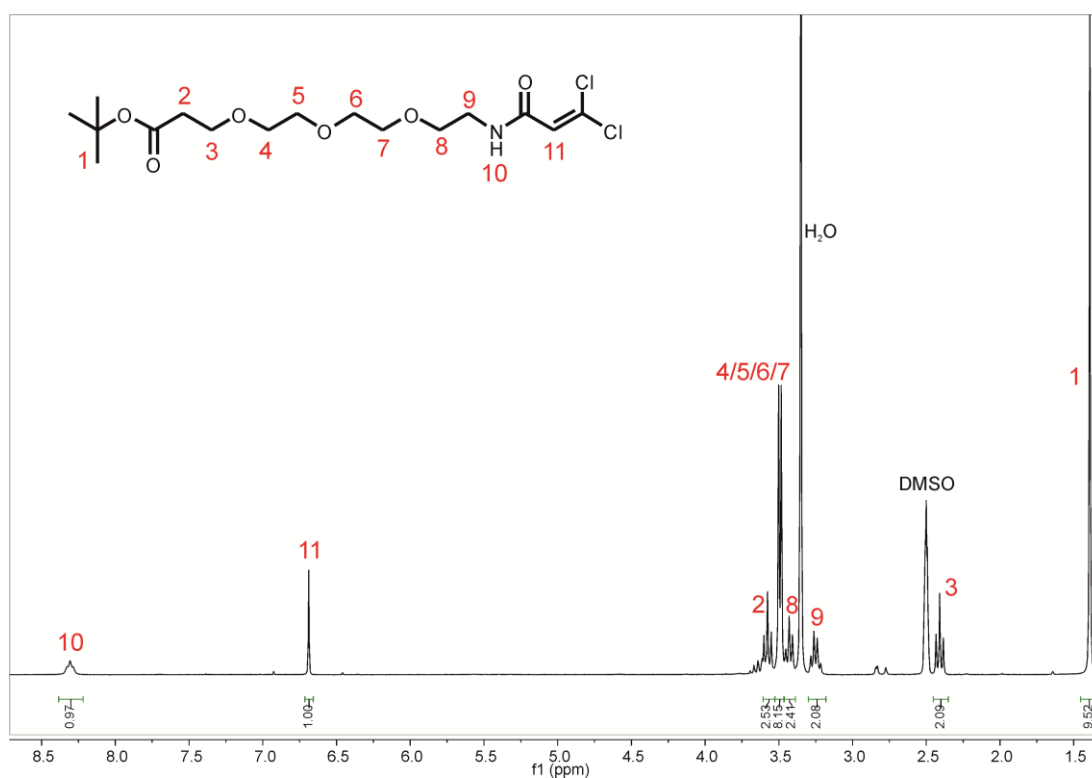


Figure 42: ^1H -NMR spectrum of compound **4-12** in DMSO-d_6 (500 MHz)

The ROESY spectrum of **4-12** is shown on Figure 43. Interestingly, the same olefinic proton is divided into two singlets with an intensity of 0.60, respectively 0.40, after the coupling of **4-12** to octreotide, which indicated the formation of two different preferred isomers. Furthermore the expected cross peaks between the olefinic protons and cysteines as well as amide protons are marked with black circles proving the drawn structure and the existence of the desired product. The concomitance of two isomers of **4-13** can be easily explained by the two different proton signals of the acrylic linker proton as highlighted with the green circle. This observation is caused by the spatial arrangement of the green marked proton causing the two cis/trans isomers; the proton is either directed towards the Thr or Phe. Thus the number of ROESY signals between the acrylic proton and the amide proton as well as the cysteine protons, which are in close proximity is doubled (black circles in the 2D spectrum).

One possible problem of the novel linker system could be the formation of side reactions like the reaction with amines instead of thiols. For instance, octreotide possess a free amine at the side chain of the amino acid lysine. However, no side reactions could be observed so far indicating the attachment of this amine to the dichloro-acrylamide linker system. An explanation for this fact can be given by referring to the HSAB concept, also known as the Pearson acid base concept. The main point of this theory is that soft acids react faster and form stronger bonds with soft bases, whereas the same is true for hard acids and hard bases, all other factors being equal. Whereas the ammonia of the lysine can be seen as hard base, the thiol group can be assigned to the group of soft bases. In general it is known, that only soft bases add to the C-C double bond. Furthermore, in order to avoid side reactions during the amide bond formation in the first step, 3,3-dichloroacrylic acid containing was always used in excess (0.9 eq of the amine containing molecule).

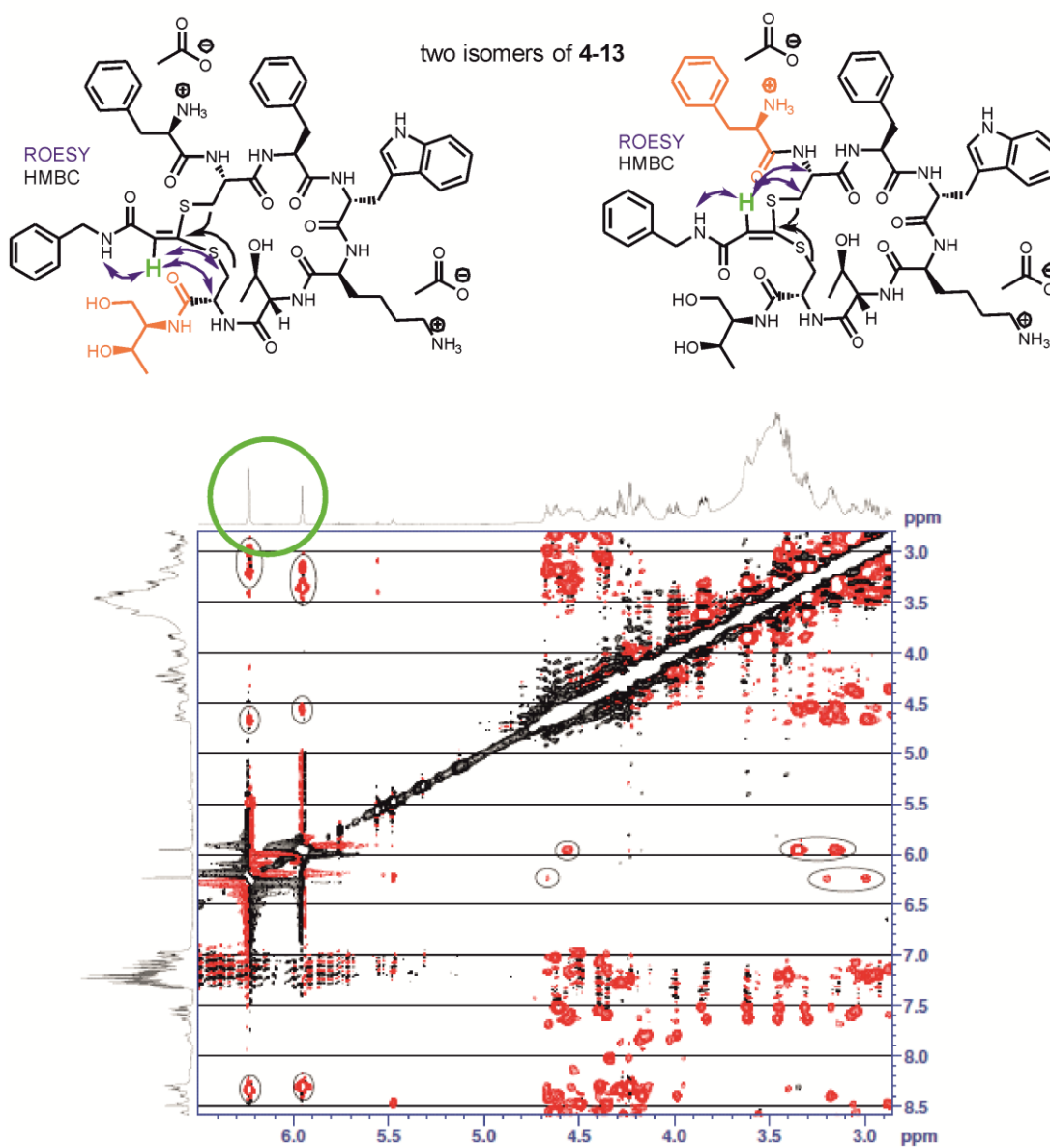
Benzylamine - Octreotide towards *Thr*Benzylamine - Octreotide towards *Phe*

Figure 43: Part of the ROESY spectra of the benzylamine-octreotide conjugate **4-12** (cis/trans isomers) showing the crosspeaks between the olefinic protons and cysteines as well as amide protons as marked.

4.2.2 Circular dichroism studies

Circular dichroism (CD) spectroscopy is an excellent tool for rapid determination of the secondary structure and folding properties of peptides and proteins. Thereby it is one of the most widely used applications focus on the change of the peptide's or protein's structure after chemical modifications. Besides this, this technique can also be used for the study of protein interactions as well as the determination whether an expressed, purified protein is folded correctly or if a mutation affects the conformation or stability. [24]

Herein, CD was used to evaluate possible structural changes of the peptide octreotide after the chemical modifications described in the previous parts to obtain the conjugates **4-8**, **4-10** and **4-13**. As already described in the introduction, octreotide possesses a strong interaction with somatostatin receptors 2 and 5, which is mainly based on the sequence of the four amino acids Phe³-Trp⁴-Lys⁵-Thr⁶. Exactly this receptor affinity is crucial for the peptide's function on cellular level. Accordingly, any change in the structure, which for instance can be caused by a chemical modification of the peptide, will affect the initial function of the peptide.

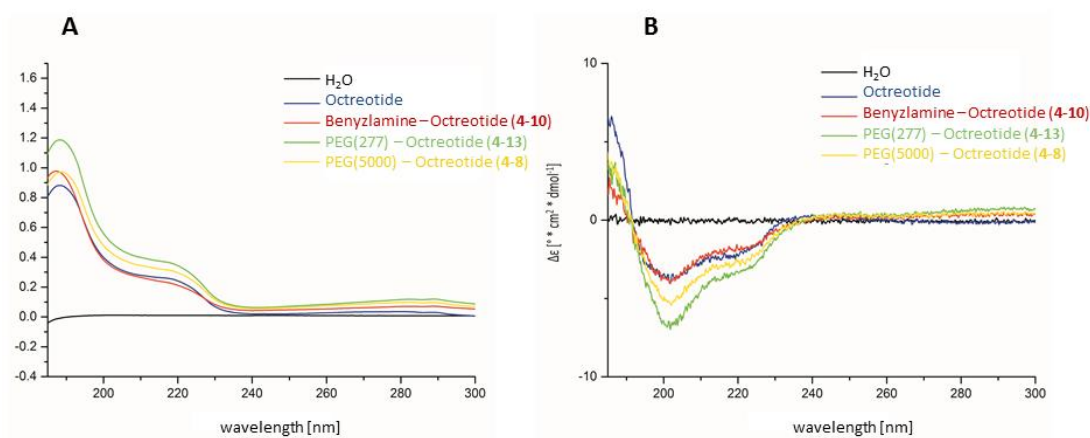


Figure 44: Absorbance (picture A) and circular dichroism spectra (picture B) of octreotide (blue), benzylamine-octreotide **4-10** (red), PEG-(277)-octreotide **4-13** (green) and PEG-(5000)-octreotide **4-8** (yellow)

Analysis of the CD spectra shown on Figure 44 of intact octreotide (blue) and the synthesized conjugates have similar UV absorbance bands in the ultraviolet wavelength region and are almost superimposing in the range of 190 – 250 nm, which indicates complete structure recovery after the peptide modification. DeLuca and coworkers found similar results for the structural study of PEGylated octreotide by circular dichroism, with the difference, that PEGylation was either performed on the phenylalanine or lysine amine. [22]

Interestingly modification at the lysine amine showed spectral changes indicating conformational modifications. This observation can be easily explained by the fact, that lysine is part of the peptide's receptor binding motif and the amino group has an important function in the formation of the spatial structure. [22] Furthermore as the sequence Phe³-Trp⁴-Lys⁵-Thr⁶ in the structure of octreotide is known to be essential for biological activity, modifications will impede the interaction with the somatostatin receptors. [25]

In conclusion, modifications at the peptide's disulfide bond with the novel acrylamide based linker system indicated no changes in the structure. Additionally, the receptor affinity properties of octreotide are assumed to be not affected at all, which will be investigated in the following experiment.

Pharmacokinetic properties of peptides and proteins have been successfully improved by PEGylation due to the increased molecular size and providing protection against proteolytic enzymes. [26] Herein, we abstained from the investigation of the influence of the PEGylation of octreotide on its pharmacokinetic properties, as DeLuca and coworkers have already determined the optimal polyethylene glycol (PEG)-conjugate of octreotide by evaluating the effects of PEGylation chemistry on the pharmacokinetic properties. The results of the subcutaneous administration of different conjugates to rats prove that PEG-(5000)-octreotide showed significantly improved pharmacokinetic properties compared with PEG-(2000)-octreotide as well as native octreotide. Based on these results we expect our conjugates to show similar effects as increased serum half-life by decreasing the glomerular filtration rate and increasing the resistance to proteolytic digestion. [26] Furthermore the great benefit of our novel strategy to modify octreotide is, that we will obtain homogenous products, the structure of octreotide is not altered and the receptor binding motif of the peptide is not changed at all.

4.2.3 Receptor binding studies

The intention of PEGylating octreotide was to increase the water solubility, decrease renal clearance as well as to reduce the susceptibility to digestive enzymes of the modified peptide. However, it is significant that the ability of the peptide to interact with the corresponding receptors remains intact after such modification, otherwise PEGylation is nonsense.

To evaluate changes concerning receptor affinity between the synthesized peptide-conjugates and the unmodified peptide, a cell line was chosen, which is endogenously expressing somatostatin receptor subtype 2. The AtT-20 pituitary tumor cells respond to the synthetic ligands of this receptor by decreasing the adrenocorticotrophic hormone (ACTH) secretion. This effect is applied to assess receptor interactions of different conjugates compared to the unmodified octreotide in the following study.

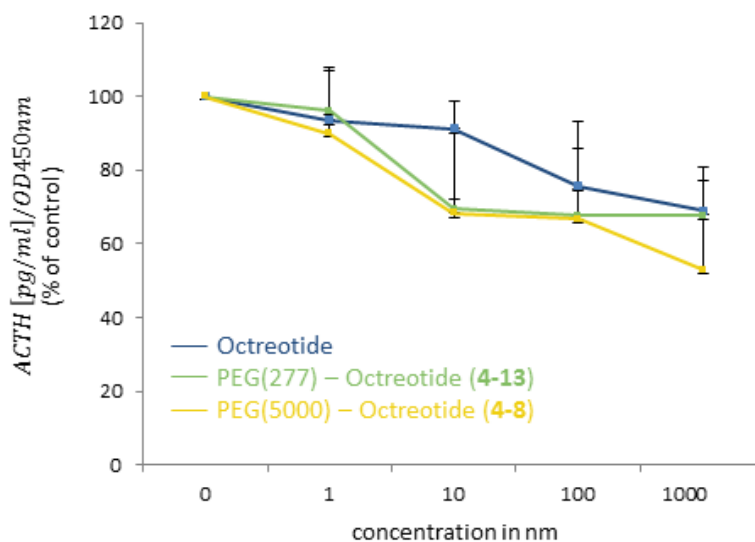


Figure 45: Functional assays in AtT-20 cells, effect of octreotide compounds on ACTH secretion as determined by a specific radioimmunoassay after 72 hours of treatment. Data are represented as the ratios of ACTH (pg/ml) to cell viability values (WST-1 colorimetric assay; OD450nm) and shown as percentage of untreated control. The graph shows the means of 2 measurements, with each treatment condition accomplished in triplicates (per measurement). Compounds tested were native octreotide (blue), PEG-(277)-octreotide **4-13** (green) and PEG-(5000)-octreotide **4-8** (yellow, “PEGylated”).

The treatment of AtT-20 cells with the different peptide conjugates **4-8** and **4-13** as well as octreotide for 72 h suppressed the ACTH secretion in the expected dose-dependent manner (Figure 45). Interestingly, the ACTH secretion is even decreased for the modified peptide hybrids compared to the unmodified octreotide peptide. This observation clearly indicates that the tumor targeting peptide is still functional after the modifications and can interact with the somatostatin receptors. Furthermore, the interaction of the hybrids is even slightly increased after the modification related to these results. As dead cells could influence the determination of the hormone suppression, the data obtained from the ACTH secretion assay were normalized to cell viability determined by the WST-1 antiproliferative assay.

After proving that chemical modification does not affect the peptide's structure, receptor binding studies successfully reveal no loss of receptor affinity and interaction of the modified octreotide conjugates compared to the native peptide.

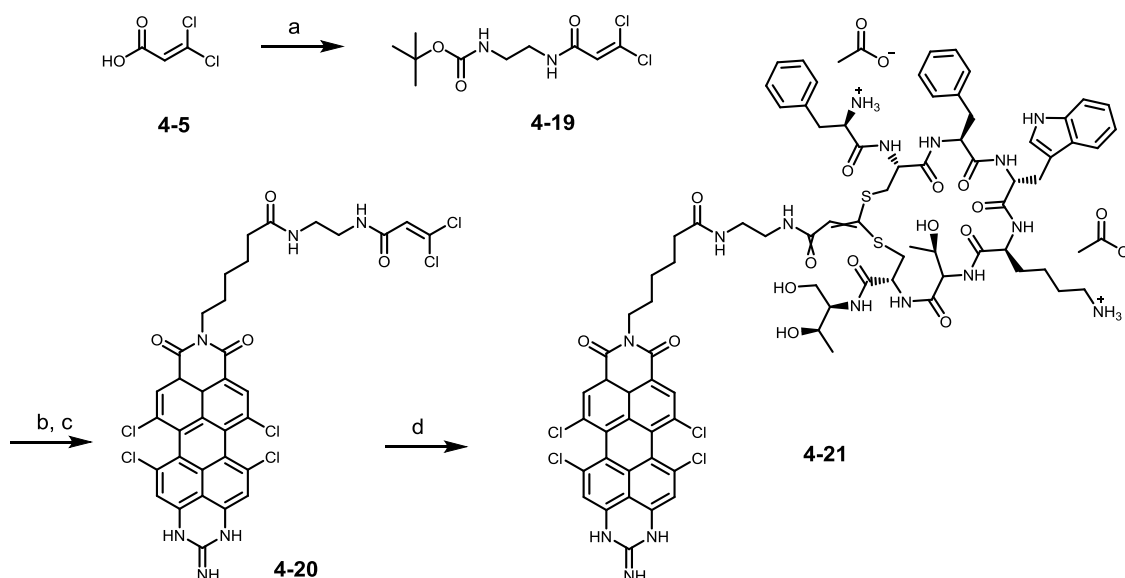
4.3 Perylenemonoimide – octreotide hybrid

Understanding the function and possible utilization of biomolecules, especially peptides and proteins, in living organism is an increasing necessity in many fields like biology, chemistry or medicine. [27] Among the existing optical imaging methods, fluorescence imaging, which uses near-infrared (NIR) light (650-900 nm) has found widespread application both *in vitro* and *in vivo*. [28] [29] [30] Biocompatible organic dyes emitting in the near-infrared are highly desirable in such areas as fluorescence imaging techniques. Its advantages are among others the low absorption and autofluorescence compared to biological structures in this spectral range. Organic dyes such as indocyanine green, have been in clinical use for more than 50 years, as they have proven to be highly specific and sensitive molecular reporters. [31] However, conventional NIR organic chromophores usually suffer from poor hydrophilicity as well as photostability, low quantum yields, low detection sensitivity and insufficient stability in biological systems. In the last decade great effort has been invested in improving the aforementioned characteristics, but none of them could be applied in biological systems so far. For instance, rylene dyes have been reported to show exceptional photochemical stability, but failed due to their large size, intrinsic hydrophobicity and tendency to show aggregation. Kaloyanova *et al.* have recently published a synthetic approach for building novel small peri-guanidine-fused perylene monoimide chromophores, the first low-molecular weight, water-soluble, NIR-absorbing members of the rylene family, which are a cornerstone of the herein introduced NIR dye-peptide conjugate. [30]

The initial idea of this study was to couple this novel NIR dye to the tumor targeting peptide octreotide *via* the novel disulfide intercalating linker system. Incorporation of such dyes to octreotide would enable a selective and targeted uptake of the dye in order to trace and visualize tumor cells. The development of such multifunctional agents for simultaneous tumor targeting and near infrared (NIR) fluorescence imaging is expected to have significant impact on future personalized oncology. [32] The investigation of multifunctional hybrids combining targeting, imaging and even therapeutic routes is the ambition of research in this field.

the PEG-Linker conjugate already described before. Finally, the desired PMI modified octreotide conjugate **4-21** was obtained as a blue powder.

Figure 46 shows the ^1H NMR spectrum of **4-20** together with a peak assignment proving the existence of the desired PMI-linker conjugate. Interestingly, traces of the reaction solvent DMF are still present although the product was purified by silica column chromatography after the removal of DMF under reduced pressure over night as well as an extra precipitation in diethyl ether. An additional extraction of the product with EtOAc and diethyl ether to remove DMF was not possible due to the high polarity of the product **4-20**. Nevertheless, the protons of the characteristic functional groups as the guanidyl (signals 1 and 2) and 3,3-dichloroacrylamide group (signal 14) could be identified by 2D NMR spectroscopy.



Scheme 14: Synthesis of PMI-octreotide hybrid **4-21**. a) HATU (1.3 eq), DIPEA (2 eq), *N*-Boc-ethylenediamine (0.9 eq), dry DMF, argon, 3 h, r.t. 48%, b) dry DCM/TFA (1:1), 1 h, r.t., quantitative yield, c) HATU (1.15 eq), **4-18** (1.0 eq), DIPEA (1.5 eq), dry DMF, argon, 2 h, r.t. 81%, d) reduced octreotide (1.5 eq), KOH in methanol (8 eq), DMF, Milli-Q Water, argon, 4 h, r.t., 81%

Physical data (RP-HPLC, MALDI-TOF MS, ^1H NMR and ^{13}C NMR spectra) confirmed the proposed structure of the compound **4-21**. NMR spectroscopy was the most convenient method to verify the identity of the attachment of **4-20** to **4-21**. A comparison of the NMR spectra of **4-20** with **4-21** gives another hint for the successful coupling. The spectrum after the coupling exhibits chemical shifts at $\delta = 5,89$ ppm and $\delta = 6,17$ ppm for the olefinic proton of the linker, whereas the same proton (proton 14 of the previously shown NMR spectrum) showed only one peak with the intensity of one before the coupling to the peptide.

The reason for this is the expected formation of the two cis/trans isomers. Hence, a complete assignment of all atoms in the corresponding NMR spectra was rather difficult as two isomers were formed due to the different intercalation ways either towards phenylalanine or threonine, which was already discussed for compounds **4-10** and **4-13**. Nevertheless an appropriate assignment and detailed explanation is given in the appendix (Appendix 5). The stability of hybrid was proven by analytical RP-HPLC in DPBS over 24 h at 37 °C, an important property for the intended tumor imaging agent. Furthermore, the MALDI-TOF MS spectrum shows the m/z ratio of the protonated product as well as the sodium adduct and is given in Figure 47.

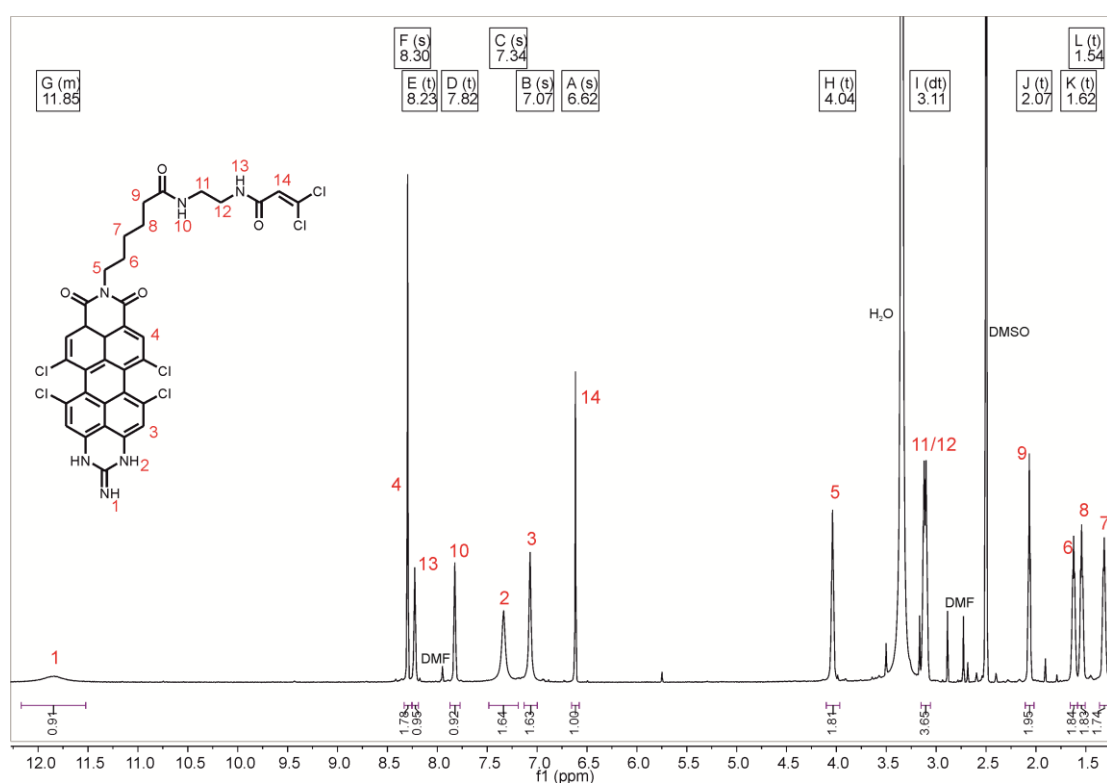


Figure 46: ¹H-NMR spectrum of compound **4-20** in DMSO-d₆ (700 MHz)

The final yield of the reaction is with 48 % relatively low compared to the previously described coupling reactions, in which the yield was around 90 %. During the reaction no side products were formed and the educt peak disappeared over time as it could be observed by means of RP-HPLC. In contrast, only the desired product was detected. Therefore it is assumed that the reason for the reduced yield can be attributed to the purification step. Cleaning runs after the preparative HPLC runs showed a colored solvent, which indicates, that product stayed on the column due to the affinity of the perylene dye to the column material.

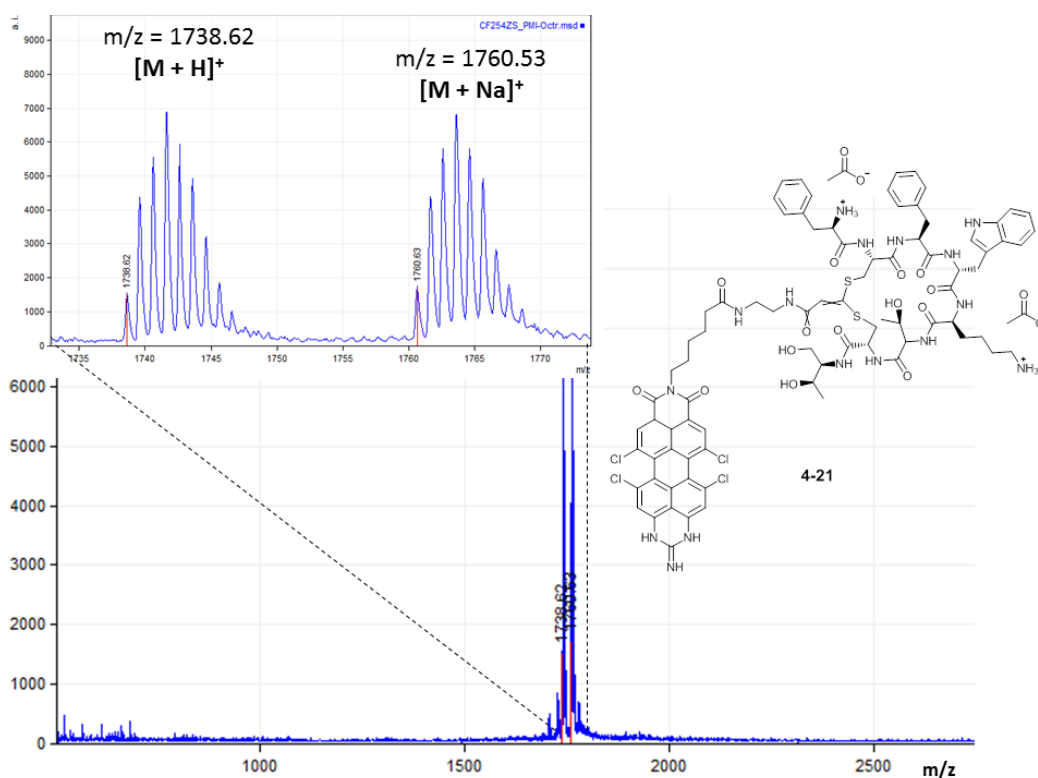


Figure 47: MALDI-TOF MS spectrum of **4-21** (matrix α -CHCA)

4.3.2 Microscopy studies

By the incorporation of the octreotide to PMI, we would like to combine the selective uptake of the dye towards tumor cells with the excellent photochemical properties of the rylene dye **4-18**. It is intended to trace and label tumor cells overexpressing the somatostatin receptors 2 and 5. Visualization of tumor cells by NIR fluorescent dyes would provide important information in the detection of tumor tissue.

After the successful synthesis of the desired dye-peptide hybrid, the cellular uptake and staining ability of the novel PMI chromophore was investigated in this study by fluorescence microscopy on two different cell lines (MIA PaCa-2 as well as A549), which have been introduced before in chapter 3.

Finally, the corresponding microscopy study is summarized in Figure 48. Pictures were taken for both cell lines after treatment with **4-21** after 2h, 6h and 24h *via* a bright field as well as a fluorescent channel. After 2h there is almost no dye detectable in both cell lines. In contrast, after 6 h of incubation and washing with DPBS buffer a selective staining with low background appeared for the MIA PaCa-2 cells only. The red pseudo color represents the

NIR absorbing PMI dye. It is assumed that there is almost no dye detectable even after 24 h of incubation in case of the human lung carcinoma cell line A549. This cell line lacks the somatostatin receptors, which are responsible for the cell uptake. During the measurements, the cells did not exhibit any structural changes, indicating good biocompatibility and no toxicity. In addition the PMI dye showed good photostability and prolonged fluorescence imaging without significant photobleaching, as there is still a significant staining present after 24 h for the receptor positive cell line MIA-PaCa-2, overexpressing somatostatin 2 receptors.

In summary, the PMI-octreotide conjugate takes advantage of the unique characteristics of this new type of PMI dye, which are small size, water solubility, high extinction coefficients and quantum yields as well as absorption and emission maxima beyond 700 nm. Coupling of this dye to functional peptides based on our novel synthesized disulfide-intercalation linker shows high potential in the application in trafficking studies of tumor cells. Furthermore, the receptor mediated uptake of the PMI towards tumor cells due to peptide-receptor interaction could be proven. Currently, the PMI-octreotide conjugate is under investigation in *in vivo* experiments with mice for the imaging of tumors.

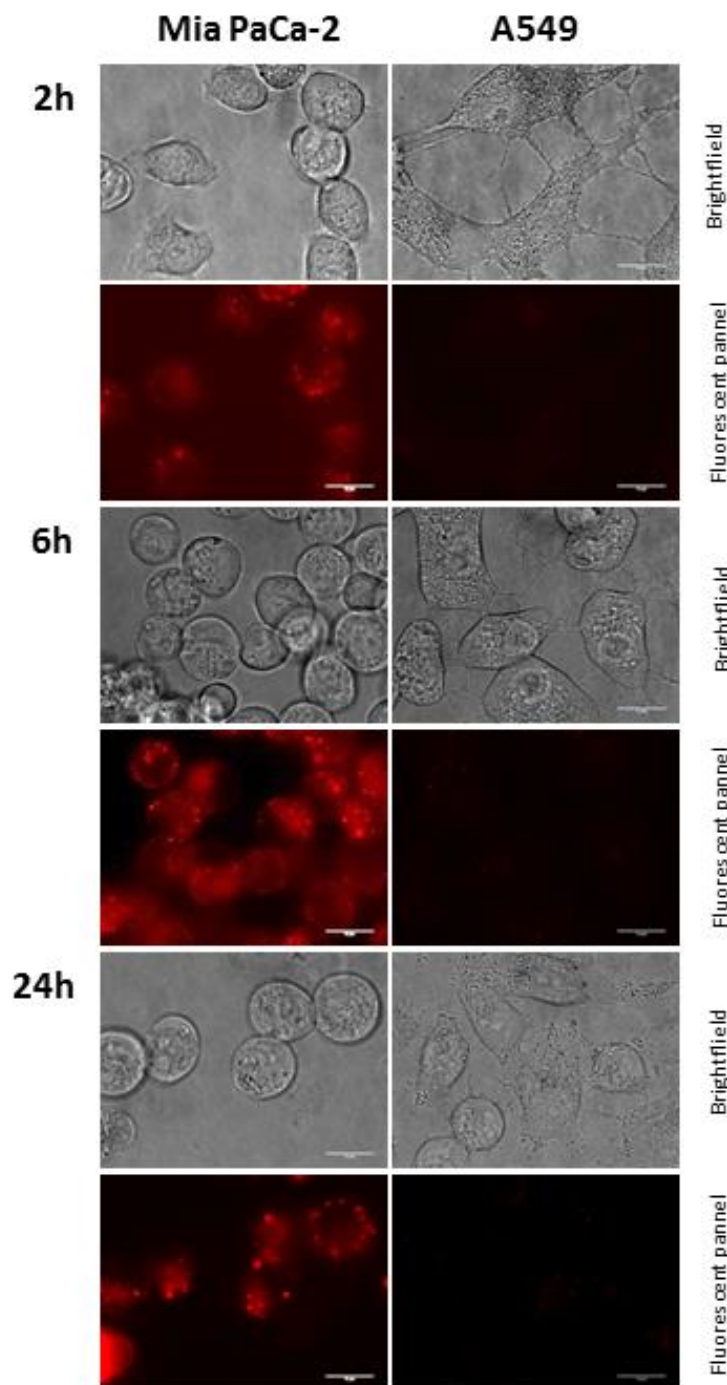


Figure 48: Intracellular traffic of PMI-octreotide conjugate **4-21** imaged by fluorescence widefield microscopy in MIA PaCa-2 (Human pancreatic carcinoma) and A 549 (Human lung carcinoma) cell lines. A549 cells do not express the SST2 receptors. All cell lines were incubated with 15 μM of the compound and the uptake was followed at different time points: 2h, 6h and 24h (cells were washed several times with PBS before imaging). A) bright-field images and B) the corresponding fluorescent images (red pseudo color represents fluorescence of the conjugate); after 6h - C) bright-field images and D) fluorescent images; after 24h – E) bright-field images and F) fluorescent images. Scale bars 15 μm . As negative control non-treated cells from both cell lines were imaged by the same conditions (pictures not shown).

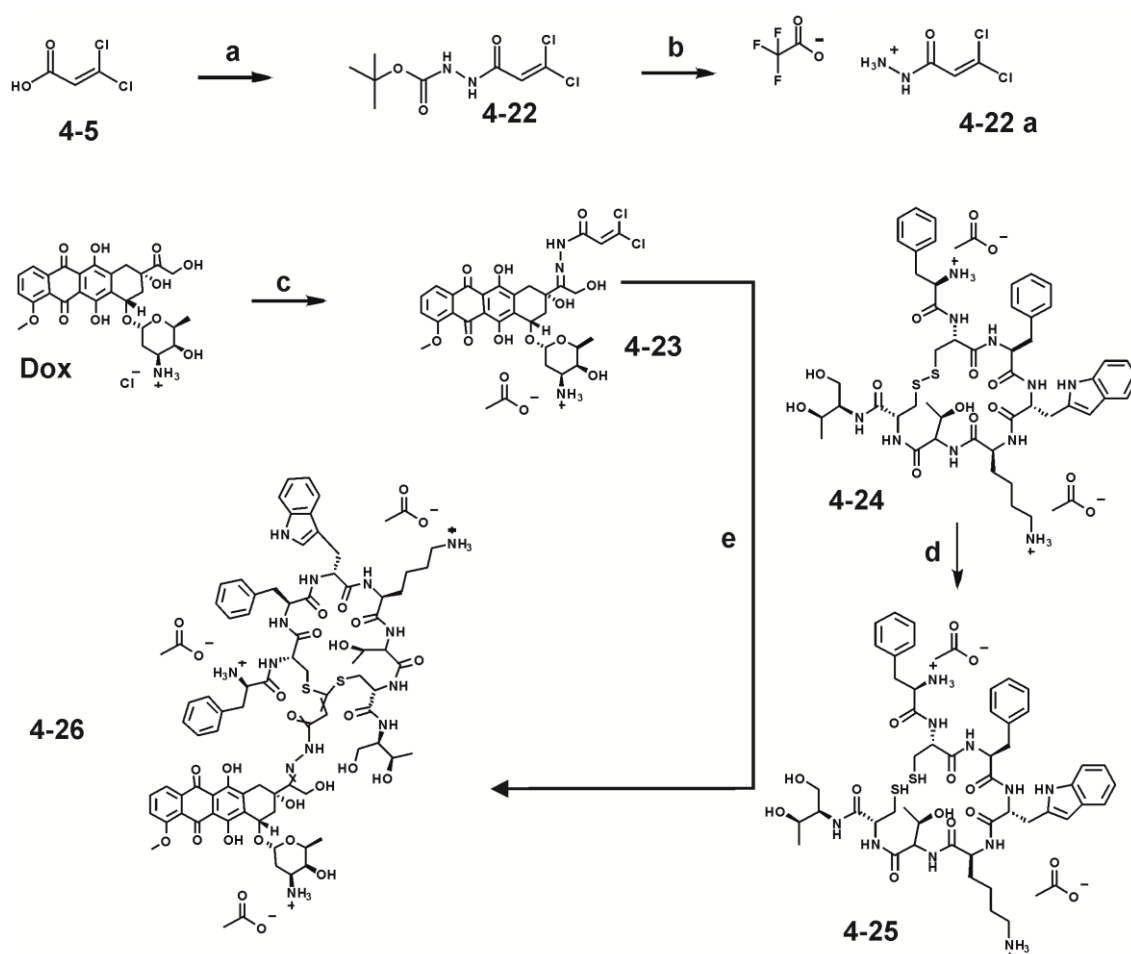
4.4 Doxorubicin – octreotide hybrid

A first introduction of different ways of fighting cancer including passive and active targeting was already given in Chapter 1 of this work. As the therapeutic efficacy of drugs is often limited by poor tumor selectivity, the modification with highly specific ligands as octreotide is an attractive target for somatostatin receptor-mediated anticancer therapy. This effect is based on the complex forming interaction of such ligands with receptors like peptides or antibodies overexpressed on tumor cells. [34] Such complexes enable the translocation to perinuclear regions after a rapid internalization by endocytotic processes, which is favorable for the delivery of cytotoxic substances acting in the cell nucleus. [35] In this study doxorubicin will be used as the drug. The advantage of doxorubicin compared to other drugs is its intrinsic fluorescence facilitating the fluorescence tracing of the drug inside the cell. Its anticancer activity is predominantly caused by the DNA intercalation and subsequent inhibition of DNA topoisomerase in the nucleus. [36] [37]

With the convincing performance of the novel linker system 3,3-dichloroacrylic acid in the synthesis and application of PEG-octreotide and PMI-octreotide hybrids in mind, the present work focused on new approach to synthesize doxorubicin-octreotide conjugates based on 3,3-dichloroacrylic acid.

4.4.1 Synthesis

There are different chemically reactive functional groups present on both molecules, doxorubicin as well as octreotide, which have been used in different ways to synthesize different types of conjugates as described in the literature. [1] [21] [38] The most suitable groups to create a drug-peptide conjugate are the keto group of the drug doxorubicin and the disulfide bond of octreotide. Therefore, a novel cross-linking reagent is required, that possesses two different functionalities. For that reason, 3,3-dichloroacrylic acid (**4-5**) was chosen as a cornerstone in the preparation of the linker, as this molecule allows the covalent modification of native disulfide bonds through the reductive liberation of the cysteine thiol groups. Thus, this cornerstone allows the closing of the reduced octreotide back to a cyclic structure by the introduction of only one carbon atom. This means in particular, that the chlorine atoms can be used for a doubled addition-elimination reaction both thiol groups of the reduced octreotide and the carboxylic acid can be directly used for further coupling reactions. In case of the coupling of doxorubicin to octreotide a hydrazine component for the condensation with the aliphatic ketone of doxorubicin had to be introduced to the linker system at its carboxylic acid group (Scheme 15).



Scheme 15: Synthesis of the doxorubicin-octreotide conjugates **4-26**. (a) 3,3-Dichloroacrylic acid (1eq), HATU (1.15 eq), DIPEA (1.3 eq), tert-butyl carbazate (0.9 eq), dry DMF, argon, 2h, r.t., 46% (b) DCM/TFA (1:1), 1 h, r.t., quantitative yield; (c) doxorubicin hydrochloride, **4-22 a** (1.2 eq), dry methanol, argon, 24h, r.t., 57%; (d) octreotide acetate **4-24**, TCEP (2eq), Phosphate buffer pH 6.2, 1h, r.t., quantitative yield; (e) reduced octreotide **4-25** (1.5 eq), KOH in methanol (8 eq), DMF, Milli-Q Water, argon, 4 h, r.t., 86%

In the end the linker reagent creates an additionally hydrazone bond with the drug having a characteristic pH-responsive behavior allowing the efficient release of the toxic cargo within the slightly acidic endo-lysosomal system of cells. This is an advantage compared to oxime bonds, which are stable under similar conditions. [39] Furthermore, the coupling of the linker to the peptide forms two stable thioether bonds, which are responsible for keeping the cyclic structure of the peptide active after the modification and showing no susceptibility to hydrolysis.

The linker was synthesized by the addition of tert-butyl carbazate to 3,3 dichloracrylic acid in presence of HATU. Thereby, the desired compound **4-22**, containing a protected hydrazine group, was obtained, although the yield of this reaction was lower than expected. The reason for this is the formation of a side product, which could not be identified although it was visualized by TLC at the base line, indicating a highly polar substance. The yield could not be improved using other coupling reagents as TSTU or DIC/NHS. The necessary hydrolytic stability of the hydrazone bond at neutral pH coupled with possible hydrolysis at acidic pH is a key feature for the drug delivery approach utilized here, which allows a selective release of the drug inside cancer cells. In contrast to oxime bonds, the hydrazone bond is susceptible to hydrolysis in the late endosome due to the reduced pH values present in this environment. [40] In the following steps, first the Boc-protective group of **4-22** was cleaved to unmask the desired hydrazide group and to attach the linker system to doxorubicin afterwards. The hydrazone condensation between both components was achieved in methanol without the addition of TFA. The required slightly acidic conditions (pH around 5.2, catalytic amounts of TFA) for this coupling could be obtained by the 1 eq of TFA which is still present after the BOC cleavage in the previous step. Nevertheless this reaction is only possible, if **4-22a** is tried under reduced pressure (10^{-3} mbar) over night. Otherwise the amount of TFA present is too much and no coupling at all to doxorubicin occurs. In contrast this reaction showed very low yields using a slightly acidic buffer system (acidic acetate buffer pH 5.2) as it is also described in literature and was used in the previous chapter for a similar hydrazone-bond formation (chapter 3.1.5). [41] Complete analysis of the final compound was achieved by analytical RP-HPLC as well as NMR spectroscopy and mass spectrometry. As an example Figure 49 is depicted showing the MALDI-TOF MS spectrum of **4-23**. Although the m/z ratio of the initial protonated product is missing, the sodium as well as the potassium adducts of the product can be detected proving the existence of the desired molecule. Concerning the NMR analysis it has to be mentioned, that two isomers (cis/trans isomers) could be detected due to the formation of the hydrazone double bond. The acrylic proton was divided into two singlets in the proton NMR. In contrast, the RP-HPLC chromatogram only showed one single product peak, indicating that the two isomers were not separable with the used column.

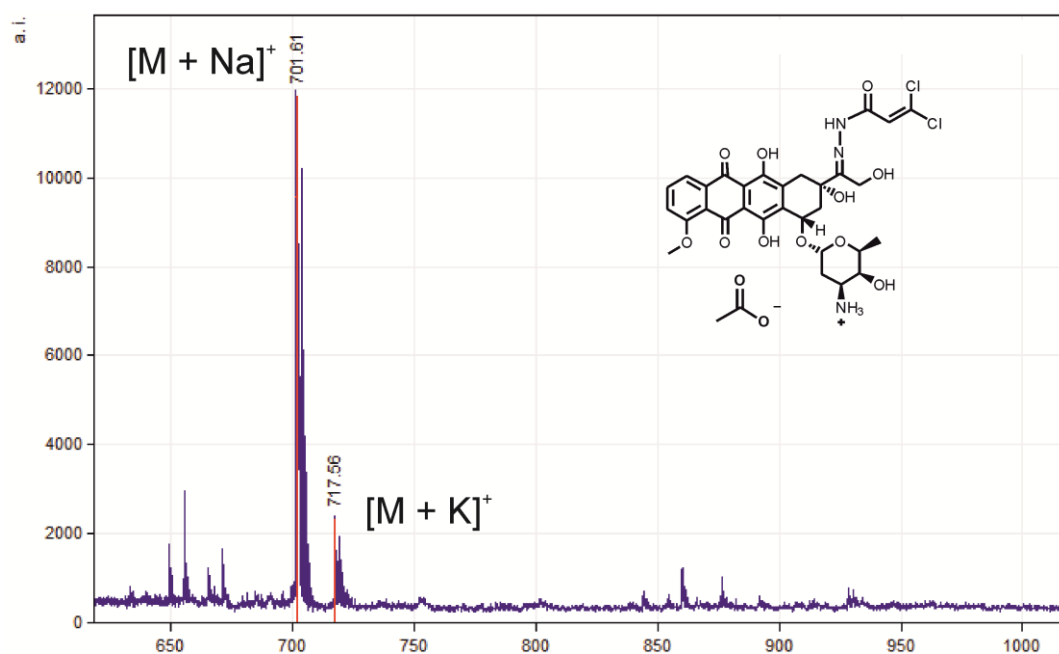


Figure 49: MALDI-TOF MS spectrum of **4-23** (matrix α -CHCA)

In the second step the disulfide bridge of the peptide **4-24** was reduced by adding tris(2-carboxyethyl)phosphine hydrochloride (TCEP HCl) to form reduced octreotide (**4-25**), which was purified by RP-HPLC and afterwards added to the 3,3-dichloroacryloylhydrazone carrying doxorubicin derivative **4-23** at a concentration of roughly 11 $\mu\text{mol/ml}$. Due to the equal reactivity of the two chlorines and both thiol groups of **4-25**, two novel isomers of **4-26** are formed during the reaction, which could be followed by RP-HPLC this time. Both fractions were collected together by RP-HPLC and first analyzed by ESI-TOF MS to prove the existence of two isomers of the final peptide-drug conjugate showing the same m/z ratio (Figure 50). Next to the initial m/z ratio of the desired protonated molecule, there is only the m/z ratio of the double protonated product present. This additional observation can be explained by the nature of the product, as it possesses different functional groups (mostly amines, in this case three amine groups are available), which can be easily protonated. However, this characteristic has not been seen for any of the previous compounds, but it is often related to ESI measurements compared to MALDI measurements, due to the different ionization mechanism.

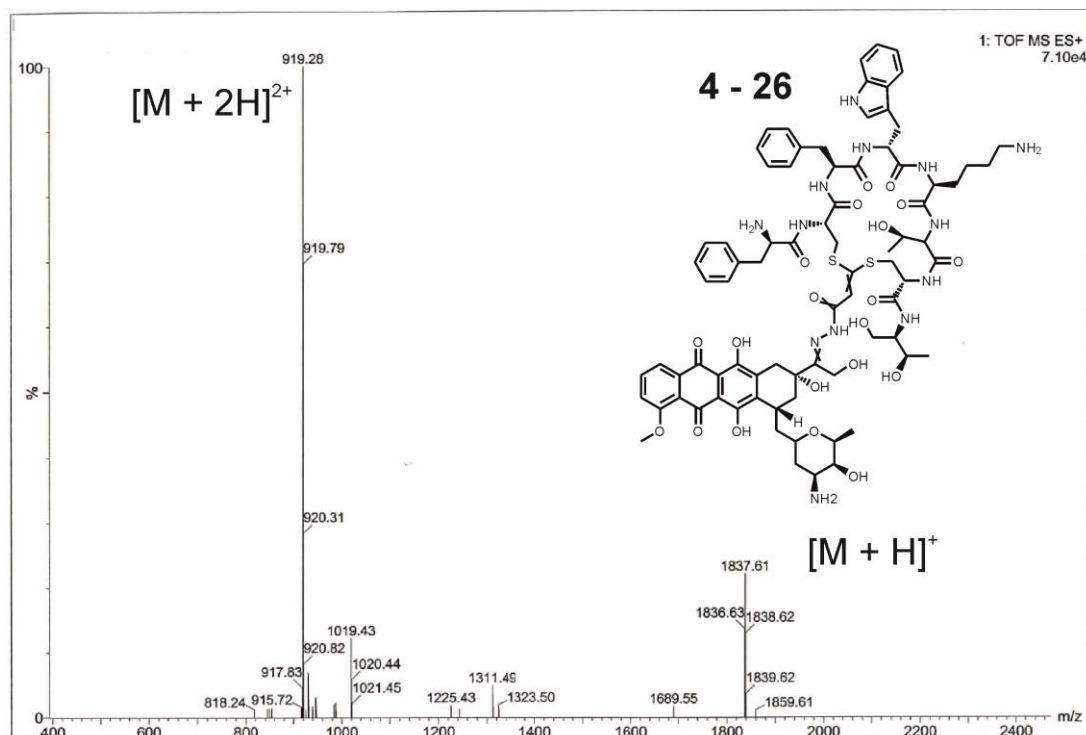


Figure 50: ESI-TOF MS spectrum of **4-26**

In addition, the covalent bond between doxorubicin and octreotide was verified by DOSY NMR as a clear peak assignment by ^1H NMR was not possible due to the existence of four possible isomers of the final conjugate. Next to the formation of two isomers (acrylic proton can be directed towards Phenylalanine as well as Threonin), two more double bond isomers are possible during the formation of the hydrazone bond, which was already detected for **4-23**.

The analysis of three characteristic signals from the doxorubicin-linker conjugate **4-23** (blue; 8.00-7.78 [aromatic protons], 5.67-5.49 [acetalic position] and 4.06-4.00 ppm [methoxy group]) and octreotide (black; 7.30-7.22 [phenyls from Phe], 5.31-5.27 [α -protons of Cys] and 0.77-0.65 ppm [γ -protons of Lys]) show the same diffusion constants $2.735 \times 10^{-10} \text{ m}^2/\text{s}$ (red, doxorubicin-octreotide conjugate **4-26**). These diffusion constants are different from the diffusion constants found for octreotide $3.665 \times 10^{-10} \text{ m}^2/\text{s}$ (7.39-7.23 [phenyls from Phe], 5.31-5.22 [α -protons of Cys] and 0.65-0.51 ppm [γ -protons of Lys]) and doxorubicin-linker $4.182 \times 10^{-10} \text{ m}^2/\text{s}$ (7.96-7.78 [aromatic protons], 5.50-5.46 [acetalic position] and 4.06-4.00 ppm [methoxy group]). Thereby the successful coupling of the drug-peptide hybrid could be proven (Figure 51).

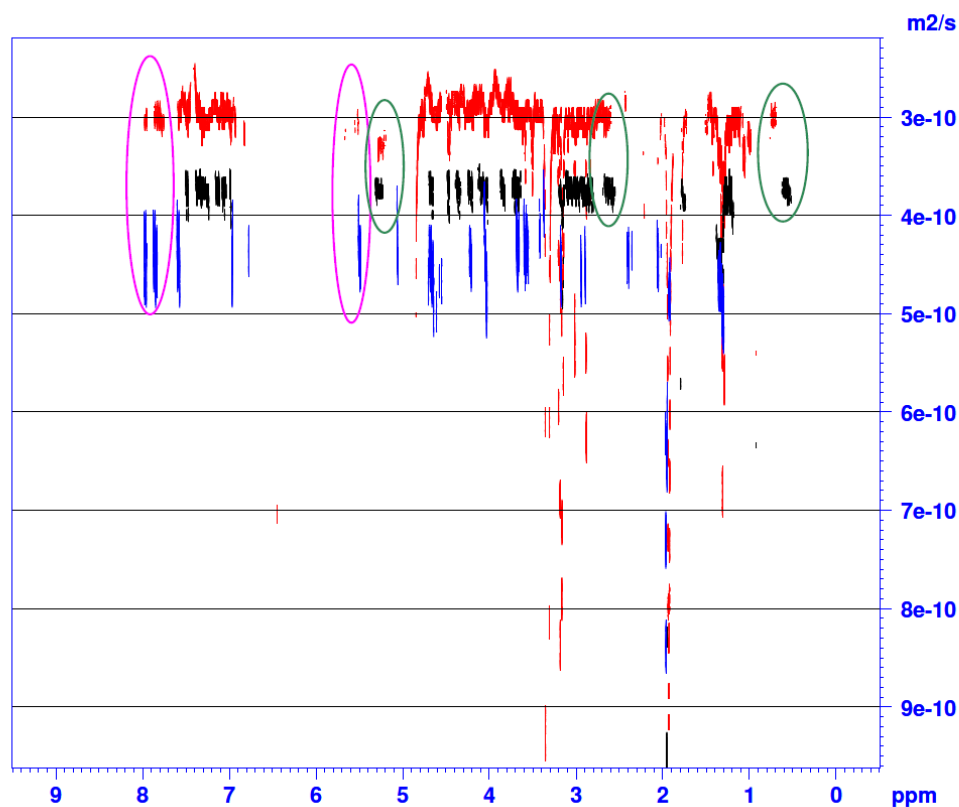


Figure 51: DOSY NMR experiment of doxorubicin-octreotide (**4-26**, red), doxorubicin-linker (**4-23**, blue) and octreotide acetate (**4-24**, black)

4.4.2 UV – ECD characterization and receptor binding studies

As already shown for the PEG-octreotide conjugate, UV-ECD analysis was utilized to verify the complete structure recovery of octreotide after the coupling with doxorubicin, as this is crucial for the desired interaction of the peptide with the corresponding receptors. First the characteristic CD spectrum of each compound is shown alone (Figure 52, A-D). Afterwards an overlay of all spectra proves that the native octreotide and the conjugate **4-26** are nearly superimposed in the range of 195 – 250 nm, suggesting that the modification had no significant effect on the spatial structure of the peptide. Furthermore the characteristic absorption of doxorubicin is also maintained as there is no difference compared to pure, unmodified doxorubicin.

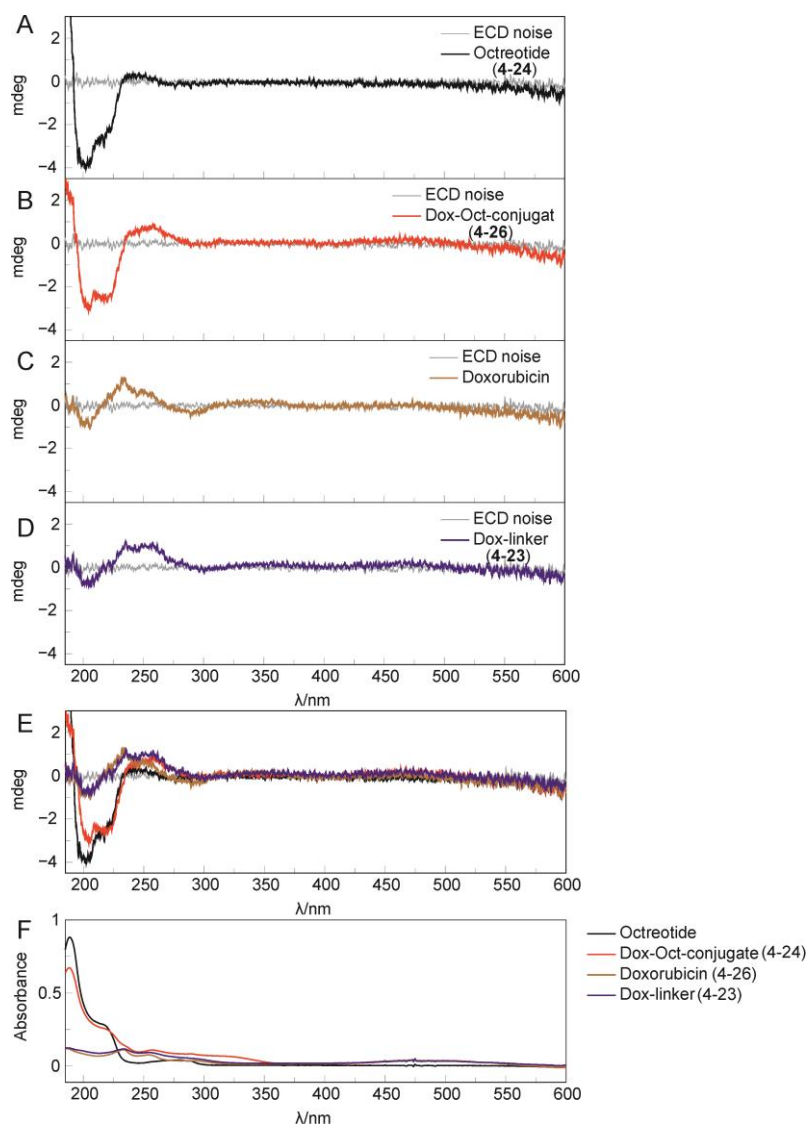


Figure 52: UV-ECD (A - E) and absorbance spectra (E): A: octreotide (**4-24**, black), B: doxorubicin-octreotide (**4-26**, red), C: doxorubicin (brown), D: doxorubicin-linker (**4-23**, blue) F: Overlay UV-ECD (A-D), Absorbance (A-F)

After proving complete structure recovery of the peptide upon modification, direct receptor binding studies of the drug-peptide conjugate was investigated in a separate experiment, which was done in cooperation with the MPI of Psychiatry in Munich. The final results of these studies indicated the desired effect, namely the tumor targeting peptide octreotide remains intact after the coupling with the antitumor drug doxorubicin. Interestingly, this interaction of the conjugates with the corresponding receptors is even higher compared to octreotide based on the data shown on Figure 53, as the ACTH secretion is decreased. In conclusion, the synthesized conjugates is taken up by a receptor mediated endocytosis based on the still intact interaction of the modified octreotide and the corresponding somatostatin receptors, the first step towards a novel tumor targeting drug delivery.

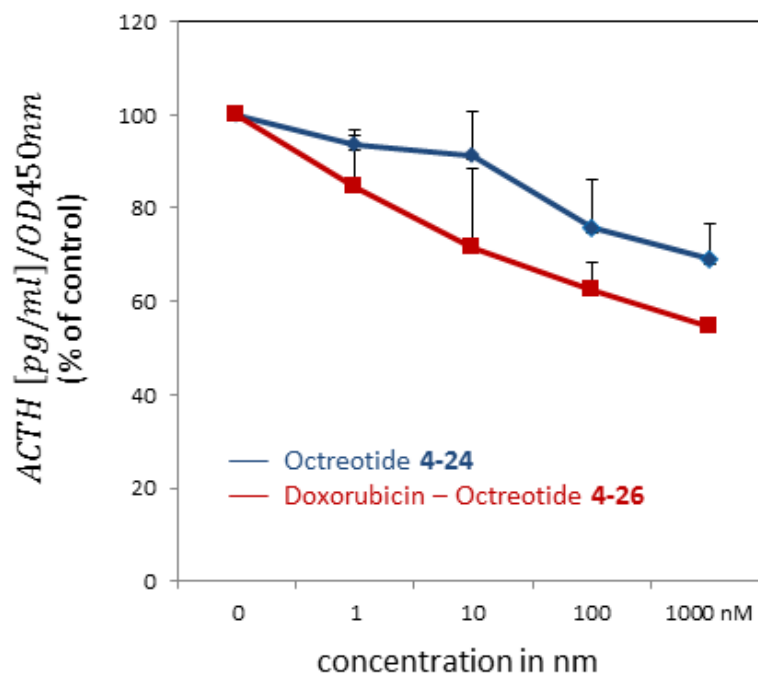


Figure 53: Functional assays in AtT-20 cells, effect of octreotide compounds on ACTH secretion as determined by a specific radioimmunoassay after 72 hours of treatment. Data are represented as the ratios of ACTH (pg/ml) to cell viability values (WST-1 colorimetric assay; OD450nm) and shown as percentage of untreated control. The graph shows the means of 2 measurements, with each treatment condition in triplicates (per measurement). Tested compounds are octreotide **4-24** and the doxorubicin-octreotide conjugate **4-26** (“hybrid”).

4.4.3 pH dependent cleavage study of doxorubicin-octreotide conjugate

The main action of doxorubicin is attributed to DNA intercalation as well as inhibition of the enzyme topoisomerase 2, which in the end causes cell death of the tumor cells. Common techniques enabling a drug release of cytotoxic agents (e.g. doxorubicin) into the cytosol or even the nucleus are based on the coupling between the drug and the delivery/targeting agent *via* hydrazone bonds, as this bond is known to be stable at neutral pH, but starts to hydrolyze in acidic environment. Therefore, doxorubicin is supposed to be cleaved from the peptide octreotide at acidic milieu, which is present in tumor tissue in general and especially the late endosomes.

To investigate the stability of the chemotherapeutic agent at neutral pH, followed by the final release caused by hydrolysis, the drug-peptide conjugate **4-26** was dissolved in DPBS (pH 7.4) as well as in a acetic acid/acetate buffer (pH 5) for 24 hours at 37°C. The cleavage process of both mixtures was analyzed by analytical RP-HPLC (Figure 54). The

characteristic absorbance of doxorubicin at 480 nm was used to monitor the process of drug release and the identification of the free doxorubicin was achieved by running a control standard (0.5 mM doxorubicin HCl in water).

In conclusion, the study demonstrated the expected release of doxorubicin in acidic environment. After 3 h most of the initial doxorubicin-octroetide conjugate **4-26** is cleaved and doxorubicin is set free. After 24 h there is no conjugate left, which means only free doxorubicin is present and no further drug derivatives are present. Consequently, the novel linker system is not only able to intercalate disulfide bonds for a site-selective modification, but also enables the desired drug release inside the cell. In order to support this statement, cell viability and cell distribution studies were performed, which will be discussed in the following section 4.4.4.

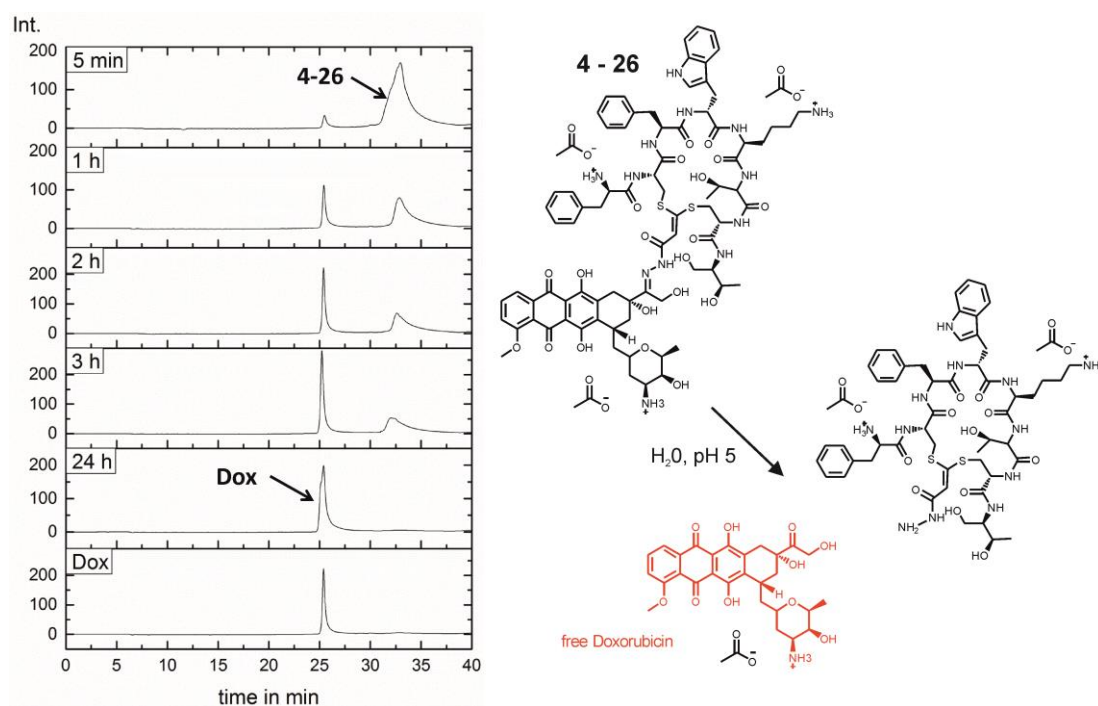


Figure 54: pH dependent cleavage of the peptide-drug conjugate **4-26**, RP-HPLC analysis of the degradation of **4-26** (0.5 mM) in an acetic acid/acetate buffered pH 5 solution at 37°C for 24 h as well as the chemical structures and the acid mediated drug release..

4.4.4 Cell viability and cellular distribution studies of doxorubicin-octreotide conjugate

The toxic effects of the conjugate were tested on two selected cell lines, which differ in the amount of somatostatin receptors on the surface to prove the receptor mediated uptake of the conjugates. Therefore, as already described in section 3.4., the human pancreatic carcinoma cell line MIA PaCa-2 as well as the adenocarcinomic human alveolar basal epithelial cells A549 was chosen. To determine the toxicity, the IC₅₀ values were determined *via* a luminescence-based cell visibility assay for both cell lines (Table 3).

Table 3: *In vitro* cytotoxic effects of doxorubicin on MIA PaCa-2 and A549 cells (data expressed as IC₅₀ values in μM , $n \geq 3$, mean \pm standard deviation, appendix 8)

Compound	IC ₅₀ MIA Paca-2 cell line (μM)	IC ₅₀ A549 cells line (μM)
Doxorubicin-Octreotide conjugate (4-26)	2.29 \pm 0.21	14.35 \pm 1.89
Doxorubicin	0.80 \pm 0.13	-
Octreotide	> 150	> 150

The fascinating result is, that the cytotoxic effects of the conjugate, expressed as half maximal inhibitory concentration, was with a factor 7 stronger for MIA PaCa-2 cells compared to A549 cells. The characteristic feature of **4-26** is attributed to the overexpression of somatostatin receptors on MIA PaCa-2 cell line, which in turn enables a higher uptake of the drug-peptide conjugate. Thus there are more doxorubicin molecules inside the cell, which finally causes a higher toxicity. In contrast, A549 cells serve as negative control and underline the direct connection between receptor expression and cytotoxicity, respectively. In comparison doxorubicin antiproliferative action on MIA PaCa-2 cells after an incubation of 72 h was slightly stronger ($IC_{50} = 0.80 \pm 0.13 \mu\text{M}$), which can be explained by a different cellular uptake mechanism (passive diffusion vs. receptor mediated uptake). The toxicity of doxorubicin on A549 was not needed in this comparison study and therefore not determined and the peptide octreotide showed almost no toxicity. However, the doxorubicin-octreotide conjugate is taken up selectively by tumor cells with an overexpression of somatostatin receptors, finally the desired targeted drug delivery system.

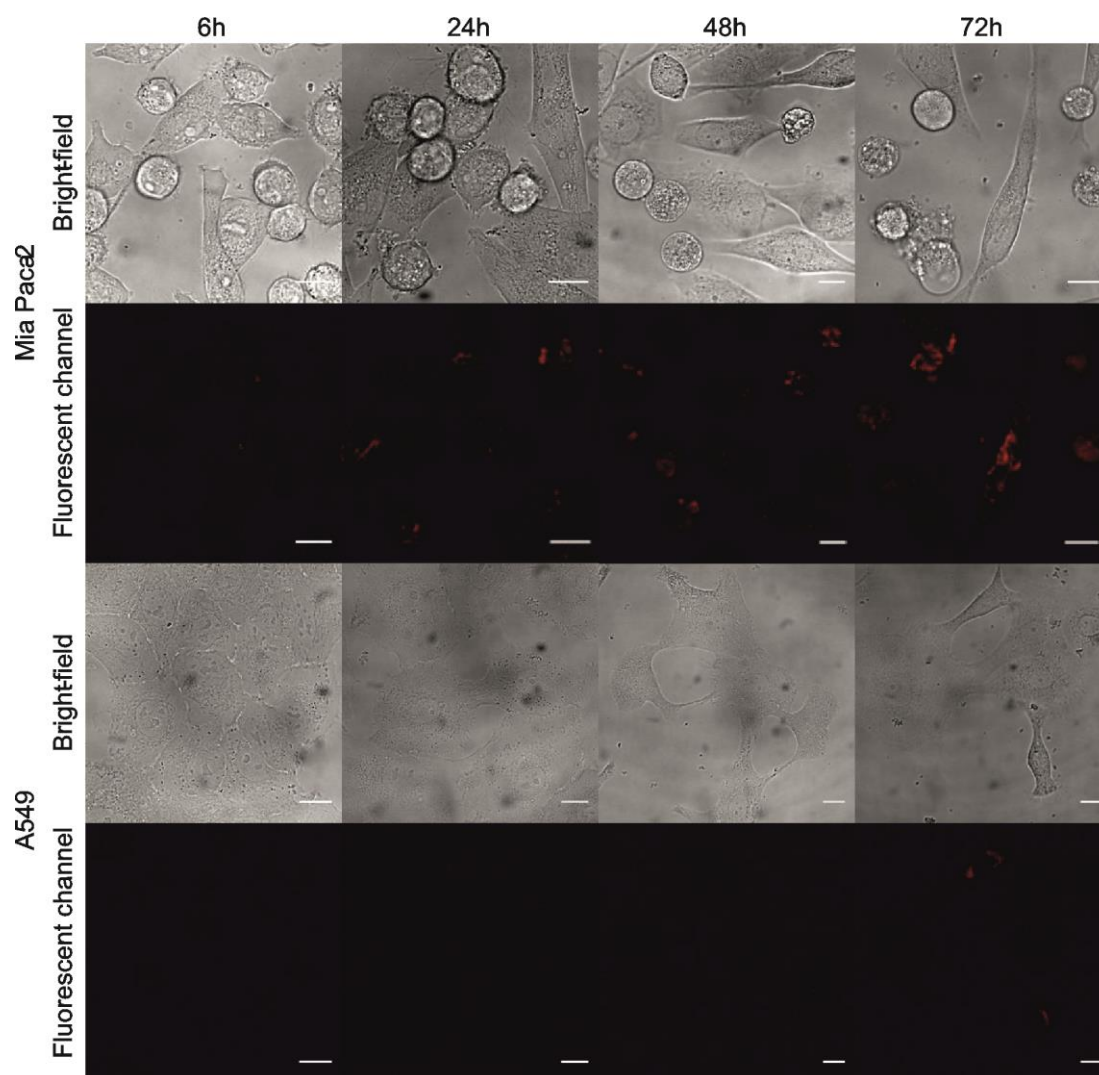


Figure 55: Confocal microscopy images of MIA PaCA-2 and A549 cells treated with 10 μ M doxorubicin-hydrazone-octreotide conjugate **4-26** at 37°C and different incubation times (6 hours - 72 hours). MIA PaCa-2 cells were used as a model system of overexpressed Somatostatin type 2 and 5 receptors (SSTR2 and SSTR5) to study the effect of internalized conjugate and the cleaved doxorubicin based on the fluorescence intensity (of doxorubicin). As negative control A549 cell line was used, which does not express the SST2 receptors. Scale bars represent 15 μ m.

To highlight the subcellular distribution, the receptor binding properties as well as the cytotoxic effects of the hybrid, both aforementioned cell lines were incubated with the conjugate at 37 °C for 72 h and analyzed by fluorescence microscopy at different time points (Figure 55). A relatively low concentration of 10 and 5 mM doxorubicin-octreotide solution ensures the imaging of live cells, even after prolonged incubation. Doxorubicin associated fluorescence was clearly visible only for the positive cell line MIA PaCa-2 in a time dependent manner, while the detected fluorescence signal in the negative A549 cells was comparatively weak, even after 72 h of incubation. This observation supports the results

from the cell viability studies, where **4-26** was much more toxic in MIA PaCa-2 cells compared to the A549 cell line due to lack of somatostatin receptors. [42]

As doxorubicin intercalates the DNA, its main location to function is assumed to be the nucleus. Cleavage of the hybrid setting free the pure drug was already proven in an acidic environment, but clear evidence *in vitro* is missing. To prove the estimation that doxorubicin is also cleaved from the conjugate and reaches the nucleus *in vitro*, MIA Paca-2 cells were stained with DRAQ5 nuclear stain prior to microscopy (counterstaining - Figure 56). Microscopy images highlight the unambiguous colocalization with the drug as a violet color is obtained from the overlay of both channels.

In conclusion, next to the interaction of our conjugates with the corresponding receptors and the possible cleavage in acidic environment, the performed intercellular trafficking experiments encouraged our hypothesis of a selective uptake of conjugate **4-26** to cancer cells overexpressing somatostatin receptors subtypes 2 and 5.

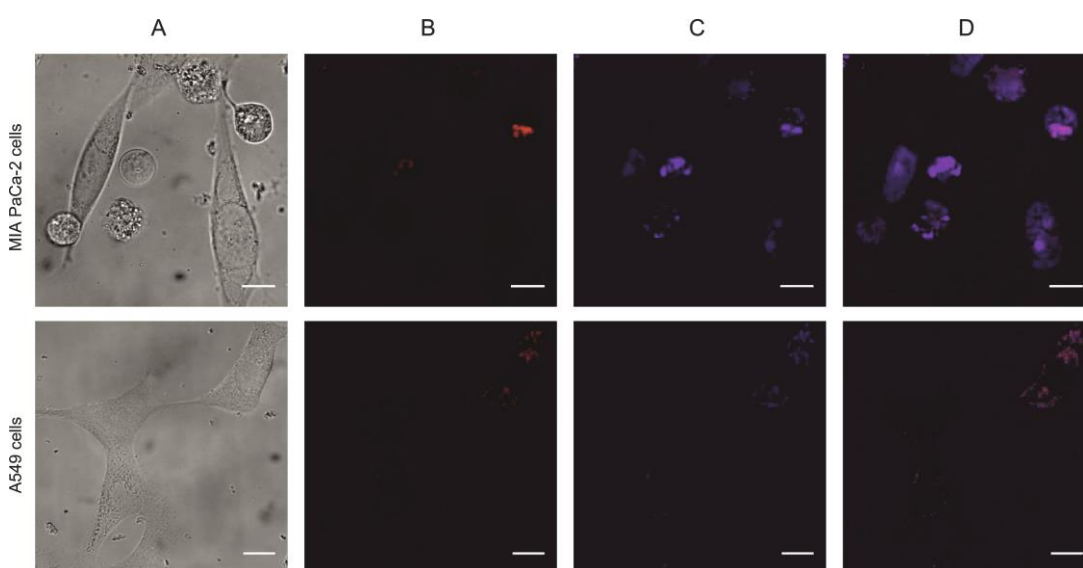


Figure 56: Confocal microscopy images of MIA PaCA-2 and A549 incubated with 10 μM doxorubicin-hydrazone-octreotide conjugate **4-26** at 37°C for 72 hours – nuclear accumulation of cleaved Dox is demonstrated with co-staining with 5 mM of DRAQ5 dye: **A**. Brightfield images. **B**. Confocal fluorescence microscopy images of the doxorubicin conjugate (red pseudo color). **C**. Nuclei staining after incubation with DRAQ5, carried out 5 min prior to imaging (blue pseudo color). **D**. Overlay of the drug-associated fluorescence and the fluorescence of the nuclear stain, co-localization is shown with violet pseudo color. Scale bars represent 15 μm.

4.5 Conclusion

In summary, we have presented a novel platform for the chemical modification of peptides, using a small readily available molecule based on 3,3-dichloroacrylic acid. This linker introduces only one carbon atom between a disulfide bond, thus represent the smallest crosslinker for site-selective modification of peptides reported so far. The successful intercalation of this novel linker was demonstrated by the application of octreotide, as it contains a single disulfide bridge, by different experiment as 2D NMR spectroscopy, circular dichroism experiments and binding assays of cell lines overexpressing receptors selective to octreotide. This chemical approach can find widespread application in the modification of therapeutic proteins with polymers, dyes and drugs with high potential in future pharmaceutical applications.

The results of the computational calculations and circular dichroism studies indicated complete secondary structure recovery after the incorporation of an acrylamide moiety in the disulfide bond of octreotide. Furthermore the successful interaction of the novel synthesized octreotide conjugates with the corresponding somatostatin receptors at the cell surface, which as a positive consequence enables tumor targeting, could be proven by the suppression of the ACTH secretion in AtT-20 pituitary cells to a similar extent as the unmodified peptide.

Initially, 3,3-dichloroacrylic acid **4-5** was used to modify the somatostatin analog octreotide with a PEG chain, a vibrant research area for years, confirmed by the fact that different PEGylated proteins have been approved by the FDA. [43] [44] [45] After proving the successful coupling of PEG-5000 to octreotide (**4-8**) by 2D NMR studies and SDS-PAGE analysis, receptor binding studies revealed no loss of receptor affinity and interaction of the modified octreotide conjugates compared to the native peptide.

Another aim of this work was the modification of octreotide with a low-molecular weight, NIR-absorbing perylene monoimide dye, as fluorescent imaging has emerged as a promising non-invasive, real-time and high-resolution technique for the visualization of biomolecules and its processes in living cells [30, 34]. The successful synthesis of the PMI-octreotide conjugate **4-21** based on 3,3-dichloroacrylic acid was among others confirmed 2D NMR studies. Furthermore the high potential of the conjugate in the application in trafficking studies of tumor cells and enables future imaging of proteins could be proven with different cell experiments.

As the therapeutic efficacy of doxorubicin is often limited by poor tumor selectivity, the modification with highly specific ligands as octreotide was an attractive target for somatostatin receptor-mediated anticancer therapy. Therefore, the cytotoxic drug doxorubicin was coupled to the tumor targeting octreotide *via* our novel disulfide-intercalating cross-linking reagent. The structure of the conjugate **4-26** was investigated using 2D NMR, as well as DOSY NMR, whereas circular dichroism studies were used to demonstrate the complete structural recovery of octreotide upon conjugation. The pH dependent cleavage of the drug was confirmed by using buffer solution with pH 5 and monitoring the cleavage process using analytical HPLC. Furthermore, confocal fluorescence microscopy studies were conducted to gain deeper insight into the subcellular distribution and additional co-staining of the cells with DRAQ-5 highlighted the unambiguous co-localization with the drug in the nucleus. Finally the cytotoxic effect of the drug-peptide conjugate was tested on A549 and Mia Paca-2 cells demonstrating the receptor mediated uptake.

Based on this novel, smaller and cleavable linker type the field of bioconjugate chemistry will be extended to new fields and applications not known before. It combines efficient conjugation, high coupling yields with fast reaction times and it can preserve the biological function of the octreotide. Thus, 3,3-dichloroacrylic acid enables the development of the next generation therapeutics and novel conjugation methods that allow the “almost” traceless introduction of payloads to biomolecules.

Up to now, the focus was set to novel linker-systems for the site-selective modification of peptides with different cargos. In both cases the highly toxic anticancer agent doxorubicin was used as a drug. The following chapter addresses different possibilities to even improve the toxicity of doxorubicin by increasing its binding affinity towards dsDNA, the initial mechanism toxicity is based on. Besides the explanation of the synthesis of such conjugates, novel ways of determining their binding affinities towards DNA will move to the fore.

4.6 References

1. Lelle, M., et al., *Octreotide-Mediated Tumor-Targeted Drug Delivery via a Cleavable Doxorubicin-Peptide Conjugate*. *Mol Pharm*, 2015. **12**(12): p. 4290-300.
2. Tedaldi, L.M., et al., *Bromomaleimides: new reagents for the selective and reversible modification of cysteine*. *Chem Commun (Camb)*, 2009(43): p. 6583-5.
3. Brocchini, S., et al., *PEGylation of native disulfide bonds in proteins*. *Nature Protocols*, 2006. **1**(5): p. 2241-2252.
4. Pfisterer, A., et al., *Bioactive unnatural somatostatin analogues through bioorthogonal iodo- and ethynyl-disulfide intercalators*. *Chemistry*, 2011. **17**(35): p. 9697-707.
5. Castaneda, L., et al., *Acid-cleavable thiomaleamic acid linker for homogeneous antibody-drug conjugation*. *Chem Commun (Camb)*, 2013. **49**(74): p. 8187-9.
6. Badescu, G., et al., *A new reagent for stable thiol-specific conjugation*. *Bioconjug Chem*, 2014. **25**(3): p. 460-9.
7. McDowall, L. and M.H. Stenzel, *Disulfide bridge based conjugation of peptides to RAFT polymers*. *Polymer Chemistry*, 2014. **5**(5): p. 1772-1781.
8. Viktor A. Zapol'skii, J.C.N., Mimoza Gjikaj, and Dieter E. Kaufmann, *Chemistry of polyhalogenated nitrobutadienes, 4: reactions of mono-, bis-, and tris(4-tolylthio) derivatives of 2-nitroperchloro-1,3-butadiene with α,β -bifunctional nucleophiles*. *ARKIVOC*, 2007: p. (i) 76-93.
9. Koichi Matsumura, O.M., Hiroshi Shimadzu, and Maoto Hashimoto, *Studies of Nitriles. X 1) Synthesis and Reactions of 2-acylamino-3,3-bis-(substituted mercapto)acrylonitriles and their derivatives. A new Synthesis of 2-substituted-5-(substituted mercapto)oxazole-4-carbonitriles and their derivatives*. *Chem. Pharm. Bull.*, 1976. **24**(5): p. 948-959.
10. A. N. Kornienko, S.G.P.o., V. M. Prokopenko, and V. S. Brovarets, *Synthesis of 2-Aryl-4-cyano-1,3-oxazole-5-sulfonyl Chlorides and N-Substituted Sulfonamides*. *Russian Journal of General Chemistry*, 2012. **Vol. 82, No. 11**: p. 1855–1858.
11. Davis, F.F., *Commentary - The origin of pegnology*. *Advanced Drug Delivery Reviews*, 2002. **54**(4): p. 457-458.
12. Varsha Gandhi, K.M., Rajesh Grover, Sen Pathak, Bharat B. Aggarwal *Multi-Targeted Approach to Treatment of Cancer*. Springer Book 2015.

13. Nucci, M.L., R. Shorr, and A. Abuchowski, *The Therapeutic Value of Poly(Ethylene Glycol)-Modified Proteins*. *Advanced Drug Delivery Reviews*, 1991. **6**(2): p. 133-151.
14. Harris, J.M., N.E. Martin, and M. Modi, *Pegylation - A novel process for modifying pharmacokinetics*. *Clinical Pharmacokinetics*, 2001. **40**(7): p. 539-551.
15. Lee, H., et al., *N-terminal site-specific mono-PEGylation of epidermal growth factor*. *Pharmaceutical Research*, 2003. **20**(5): p. 818-825.
16. Goodson, R.J. and N.V. Katre, *Site-Directed Pegylation of Recombinant Interleukin-2 at Its Glycosylation Site*. *Bio-Technology*, 1990. **8**(4): p. 343-346.
17. Yamasaki, N., A. Matsuo, and H. Isobe, *Novel Polyethylene-Glycol Derivatives for Modification of Proteins*. *Agricultural and Biological Chemistry*, 1988. **52**(8): p. 2125-2127.
18. Marbach, P., M. Neufeld, and J. Pless, *Clinical-Applications of Somatostatin Analogs*. *Advances in Experimental Medicine and Biology*, 1985. **188**: p. 339-353.
19. Wang, J.W., et al., *Clinical applications of somatostatin analogs for growth hormone-secreting pituitary adenomas*. *Patient Preference and Adherence*, 2014. **8**: p. 43-51.
20. Novartis,
https://www.pharma.us.novartis.com/sites/www.pharma.us.novartis.com/files/sandostatin_inj.pdf. 2016.
21. Na, D.H. and P.P. DeLuca, *PEGylation of octreotide: I. Separation of positional isomers and stability against acylation by poly(D,L-lactide-co-glycolide)*. *Pharm Res*, 2005. **22**(5): p. 736-42.
22. Na, D.H., K.C. Lee, and P.P. DeLuca, *PEGylation of octreotide: II. Effect of N-terminal mono-PEGylation on biological activity and pharmacokinetics*. *Pharmaceutical Research*, 2005. **22**(5): p. 743-749.
23. Pfisterer, A., *Ortsgerichtete Modifikationen von Somatostatin-14 zur Darstellung von maßgeschneiderten Biohybridkonjugaten*. Dissertation, MPIP Mainz, 2012.
24. Greenfield, N.J., *Using circular dichroism spectra to estimate protein secondary structure*. *Nature Protocols*, 2006. **1**(6): p. 2876-2890.
25. Brabant, G., *Insulin-like growth factor-I: marker for diagnosis of acromegaly and monitoring the efficacy of treatment*. *Eur J Endocrinol*, 2003. **148 Suppl 2**: p. S15-20.

26. Caliceti, P., *Pharmacokinetic and biodistribution properties of poly(ethylene glycol)–protein conjugates*. *Advanced Drug Delivery Reviews*, 2003. **55**(10): p. 1261-1277.
27. Freidel, C., S. Kaloyanova, and K. Peneva, *Chemical tags for site-specific fluorescent labeling of biomolecules*. *Amino Acids*, 2016.
28. Folling, J., et al., *Fluorescence nanoscopy by ground-state depletion and single-molecule return*. *Nature Methods*, 2008. **5**(11): p. 943-945.
29. Heilemann, M., et al., *Subdiffraction-resolution fluorescence imaging with conventional fluorescent probes*. *Angewandte Chemie-International Edition*, 2008. **47**(33): p. 6172-6176.
30. Kaloyanova, S., et al., *Water-Soluble NIR-Absorbing Rylene Chromophores for Selective Staining of Cellular Organelles*. *J Am Chem Soc*, 2016. **138**(9): p. 2881-4.
31. Lukinavicius, G., et al., *A near-infrared fluorophore for live-cell super-resolution microscopy of cellular proteins*. *Nature Chemistry*, 2013. **5**(2): p. 132-139.
32. Luo, S.L., et al., *A review of NIR dyes in cancer targeting and imaging*. *Biomaterials*, 2011. **32**(29): p. 7127-7138.
33. Wuts, P.G.M.G., T. W., *Protective Groups in Organic Synthesis*. John Wiley & Sons, Inc.: Hoboken, NJ, 2006: p. 696-926.
34. Schlage, P., et al., *Anthracycline-GnRH derivative bioconjugates with different linkages: synthesis, in vitro drug release and cytostatic effect*. *J Control Release*, 2011. **156**(2): p. 170-8.
35. Pandya, H. and W. Debinski, *Toward Intracellular Targeted Delivery of Cancer Therapeutics Progress and Clinical Outlook for Brain Tumor Therapy*. *Biodrugs*, 2012. **26**(4): p. 235-244.
36. Minotti, G., et al., *Anthracyclines: molecular advances and pharmacologic developments in antitumor activity and cardiotoxicity*. *Pharmacol Rev*, 2004. **56**(2): p. 185-229.
37. Nadas, J. and D.X. Sun, *Anthracyclines as effective anticancer drugs*. *Expert Opinion on Drug Discovery*, 2006. **1**(6): p. 549-568.
38. He, S., et al., *Comparison of active and passive targeting of doxorubicin for somatostatin receptor 2 positive tumor models by octreotide-modified HPMA copolymer-doxorubicin conjugates*. *Drug Delivery*, 2016. **23**(1): p. 285-296.

39. F. Kratz, A.W., B. Schmid, D.- E. Chung and M. Gitzel *Prodrugs of Anthracyclines in Cancer Chemotherapy*. *Curr Med Chem*, 2006. **13**:477–523.
40. Geisow, M.J. and W.H. Evans, *Ph in the Endosome - Measurements during Pinocytosis and Receptor-Mediated Endocytosis*. *Experimental Cell Research*, 1984. **150**(1): p. 36-46.
41. Jin, Y., et al., *A peptide-based pH-sensitive drug delivery system for targeted ablation of cancer cells*. *Chem Commun (Camb)*, 2015. **51**(77): p. 14454-14457.
42. Amherdt, M., Y.C. Patel, and L. Orci, *Binding and Internalization of Somatostatin, Insulin, and Glucagon by Cultured Rat Islet Cells*. *Journal of Clinical Investigation*, 1989. **84**(2): p. 412-417.
43. Brocchini, C.G.a.S., *PEGylation and its impact on the design of new protein-based medicines*. 2014.
44. Luxon, B.A., et al., *Pegylated interferons for the treatment of chronic hepatitis C infection*. *Clin Ther*, 2002. **24**(9): p. 1363-83.
45. Alconcel, S.N.S., A.S. Baas, and H.D. Maynard, *FDA-approved poly(ethylene glycol)-protein conjugate drugs*. *Polymer Chemistry*, 2011. **2**(7): p. 1442-1448.

5 Doxorubicin-Indole conjugates as anticancer agents

Nowadays, there are many established approaches to treat cancer such as surgical excision, irradiation, drug therapy, and chemotherapy, respectively. [1] In recent years, research has been focused on the treatment of cancer by finding chemotherapeutic agents that defeat cancer completely, among others by increasing the toxicity of the drugs and a targeted therapy. A widely discussed subclass of these agents is the group of cytotoxic antibiotics that inhibit cell growth or cell division. [2]

Doxorubicin, also known as Adriamycin or 14-hydroxydaunomycin, belongs to the class of anthracycline antibiotics and was discovered by isolation from the pigment-producing *Streptomyces peucetius* in the early 1960s. [3] This drug is still frequently used in cancer therapy and belongs to the most effective agents with a broad scope of application against a multitude of tumors such as breast cancer, small cell lung bronchial carcinoma and malignant lymphoma. [3, 4] Chemically the framework of doxorubicin consists of a four ring structure that is linked *via* a glycoside bond to a daunosamine shown on (Figure 57, A-D). [3] [5] Although doxorubicin has been used for more than 40 years in chemotherapy, the exact mechanism of action is still unclear. [4, 6] Nevertheless, a variety of characteristics are known which are responsible for the cytotoxic action of doxorubicin.

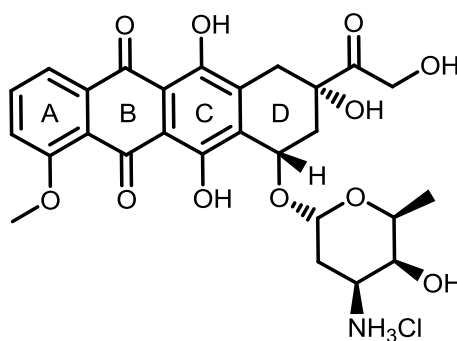


Figure 57: Doxorubicin as hydrochloric acid salt

One of the molecular targets of doxorubicin is considered to be DNA intercalation and inhibition of DNA topoisomerases enzyme, mainly type 2, as confirmed by Cummings *et al.* [7] The enzymes catalyze the concerted breakage and rejoining of DNA strands during DNA replication and transcription. [8] The exact mechanism of topoisomerase inhibition was discussed by Topcu *et al.* and modelling DNA intercalation of anthracyclines was performed by Moro *et al.* [9] [10] Doxorubicin impedes the progression of this enzyme which relaxes

supercoils in DNA for transcription. [6, 11] Thereby, the process of replication and macromolecular biosynthesis is stopped. [9] [7] The interaction of the drug to DNA is either based on DNA intercalation or on the binding to the minor groove of the DNA. [12] The non-covalent binding between the drug and DNA is described to be highly efficient (binding affinity: $0.13 - 0.16 * 10^6 \text{ M}^{-1}$). [13]

Another important mechanism is based on the formation of oxygen derived free radicals by anthracyclines resulting in the peroxidation of lipid biomembranes and disruption of cellular organelle structure and function. [14] These free radicals can either be formed by the enzymatic reduction of the anthracycline ring producing a free hydroxyl radical or nonenzymatically from the conjugation between the anthracycline's hydroquinone portions with intracellular ferric iron. In the 1970s, Lown *et al.* showed the potential of these radicals to induce DNA breaks resulting in cell death.

Additional action mechanisms of doxorubicin were also described in the review of Minotti *et al.* [4] that confirm anticancer activity, but with less support for experimental data. DNA interaction is supposed to be the main intracellular target for doxorubicin and the cytotoxicity is mediated *via* stabilization of a topoisomerase 2 cleavage complexes. However, the drug itself can also dissociate from the DNA and the enzyme is no longer inhibited. Thus, higher binding-affinities of the cytostatic agent are a valuable approach to increase the toxicity. [15, 16]

5.1 Design and Synthesis of Doxorubicin-Indole conjugates

The conjugation of doxorubicin with other DNA binding molecules is an appropriate strategy to increase the DNA binding affinity of the drug. Bis-intercalating doxorubicin dimers have already been reported in literature to have higher binding constants towards DNA compared to single doxorubicin. [17-19] An alternative would be to couple minor groove binders to doxorubicin. Minor grooves as well as major grooves are naturally formed cavities alternating the DNA backbone. They exist due to the fact that DNA molecules form a double helix by the creation of hydrogen bonds between the different base pairs attached to the sugar-phosphate backbone (Figure 58). [20] Minor groove binders are suitable candidates and are well known as strong DNA-binding ligands such as the dyes Hoechst 33258 and DAPI, which are used for DNA staining. In addition, Baraldi *et al.* reported on different classes of DNA minor groove binders as potential antitumor and antimicrobial agents. [21]

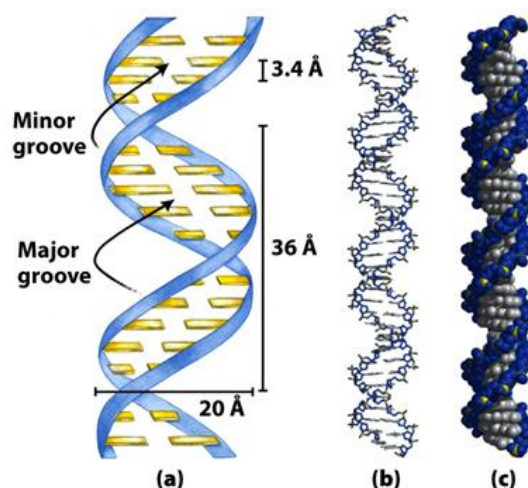


Figure 58: Schematic overview of the DNA helix and the formation of minor and major grooves (Figure 8-13 from Lehninger Principles of Biochemistry, Fifth Edition, © 2008 W.H. Freeman and Company)

Specifically, several synthetic and natural indole derivatives have shown significant DNA binding ability as well as DNA sequence specificity. Gupta *et al.* concretized this possibility and described indole derivatives as DNA minor groove binders and thus anticancer agents. [22] Furthermore, Zhao *et al.* have used bis-indolyl moieties coupled to the DNA alkylating agent cyclopropabenzindole (CBI) to increase the affinity towards DNA due to the additional binding of the indole units to the DNA minor groove. [23] The aforementioned studies emphasized the high potential of DNA groove binders to increase the DNA binding affinity of different compounds, especially in the field of anticancer therapy.

The motivation of this work is to combine both modes of DNA binding, DNA intercalation and minor groove binding in one molecule (Figure 59). The synthesis of these new molecules would result in a new class of anticancer agents that are previously unreported. Doxorubicin was used as a DNA intercalation substrate, which was functionalized at its daunosamine moiety with an indole derivative. Modeling systems of doxorubicin and DNA have already proven that the sugar part of doxorubicin is directed to the minor groove, while the anthracene part intercalates between the DNA base pairs *via* π -stacking. Furthermore, indole is known as a minor groove binder, which has already been demonstrated by different research groups. [9, 23]

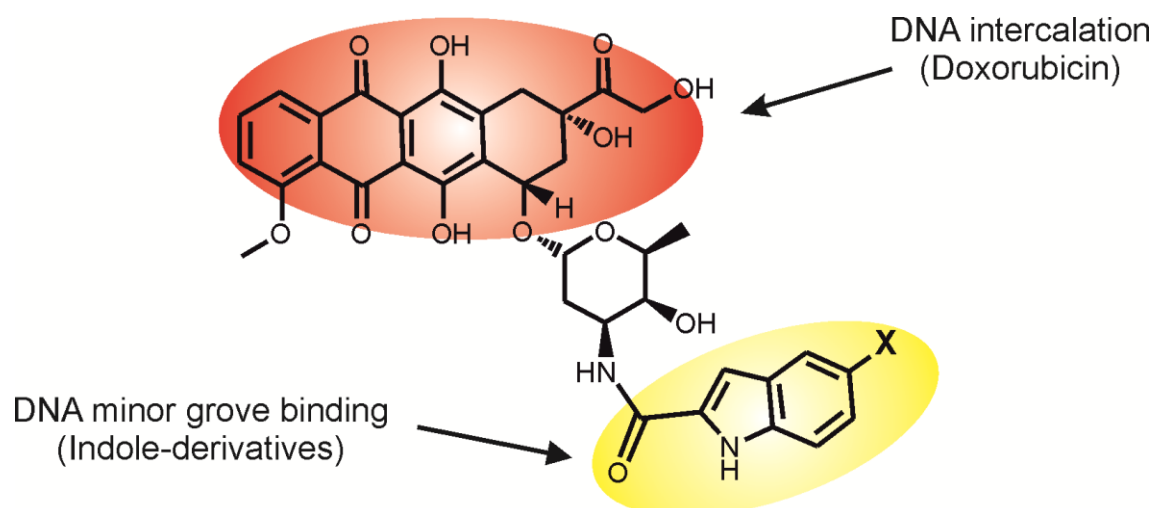


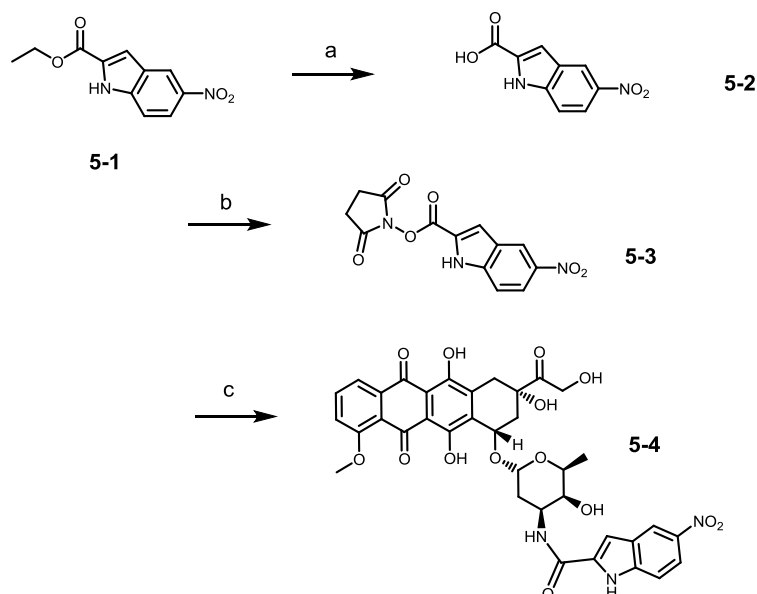
Figure 59: Schematic overview of doxorubicin-indole derivative, the position of the different functional groups tested at the indole is marked with X

By adding the indole to the sugar of doxorubicin, the final molecule would be capable of intercalating and binding into the minor groove of the DNA. Thus, the final molecules were expected to possess a higher binding affinity to DNA that could result in a higher toxicity compared to doxorubicin or indole derivatives alone. Therefore, it is a valuable approach to increase the cytotoxic capacity of doxorubicin. [15, 16] Binding affinities of these molecules with DNA were determined by means of MST and the toxicity was investigated by cytotoxicity *in vitro* assays.

In the following sections, the syntheses of different doxorubicin-indole conjugates are described. Those conjugates mainly differ in the functional group at the indole moiety and the number of indole units, which are coupled to doxorubicin.

5.1.1 Synthesis of doxorubicin-indole-NO₂ conjugate (Doxind-NO₂)

The first modification of doxorubicin with an indole unit was performed using an ethyl 5-nitroindole-2-carboxylate. In the first step the ester of the indole derivative **5-1** was hydrolyzed to the free acid, which was converted to the activated NHS-ester **5-3** to react with the free amine of the doxorubicin molecule in the next step (Scheme 16). As the indole-derivative was used in excess, no native doxorubicin could be detected after 4 hours as monitored by analytical HPLC, which simplified the following purification step of **5-4**. This was achieved by preparative HPLC yielding the final Doxind-NO₂ conjugate as a red powder.



Scheme 16: (a) THF/MeOH/1M NaOH (1:1:1), 24 h, r.t., 96%. (b) *N*-hydroxysuccinimide (1.15 eq), *N,N'*-Diisopropylcarbodiimide (1.2 eq), dry dichloromethane, argon, overnight, r.t., 92%. (c) Doxorubicin hydrochloride (0.9eq), DIPEA (1.2 eq), dry DMF, argon, 4 h, r.t., 55%

In addition to HPLC and MALDI-TOF MS, NMR spectroscopy was used to analyze the structure of **5-4** as shown on Figure 60 together with the peak assignment. The ^1H NMR spectrum supported the proposed structure and also proved the purity of the compound. The spectrum exhibits signals from the indole as well as doxorubicin and the signal of the formed amide bond is detected at 8.29 ppm (peak *p*). 2D NMR experiments additionally proved the formation of the desired compound by showing the expected interactions of the different protons, for instance the crosspeaks of *p* and *l* verify the existence of the conjugated product.

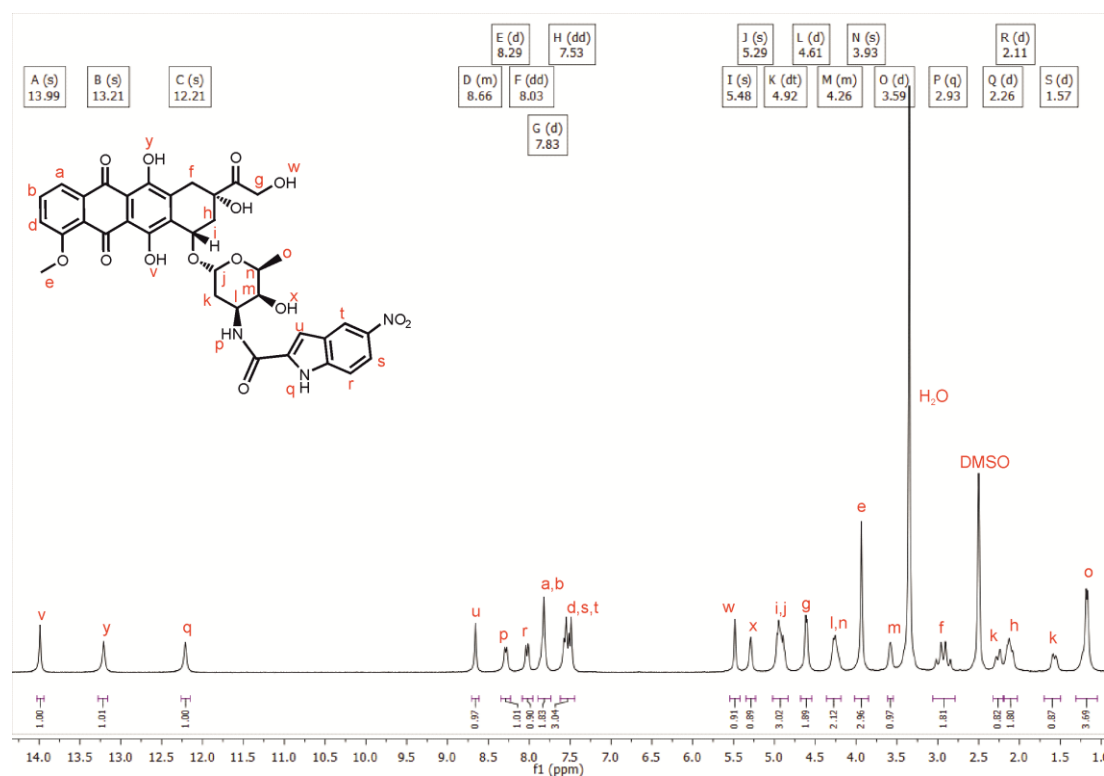
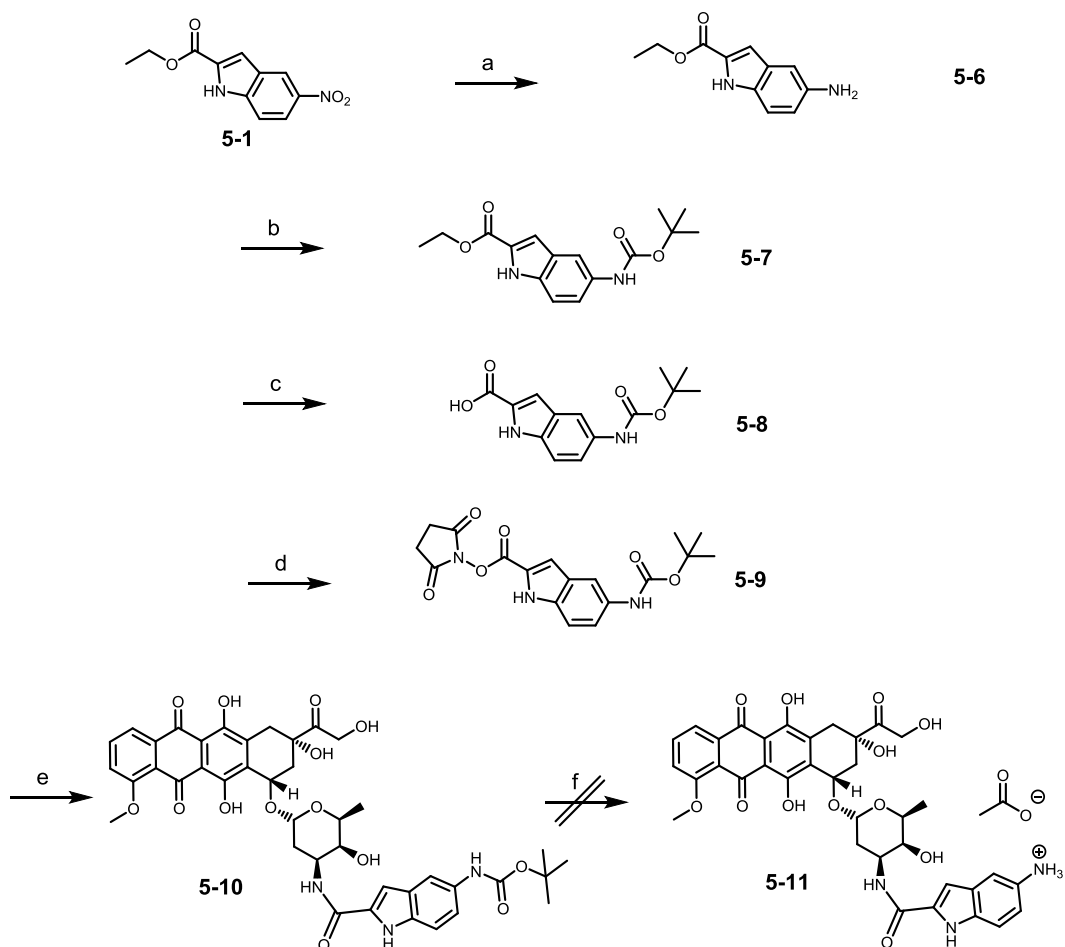


Figure 60: ¹H-NMR spectrum of compound **5-4** in DMSO-d₆ (700 MHz)

5.1.2 Synthesis of doxorubicin-indole NH₂ conjugate (Doxind-NH₂)

The next indole derivative possesses an amine functional group (Scheme 17). Therefore, the nitro group of the starting material **5-1** was reduced in the first step. Afterwards, the amine was protected with a tert-butyloxycarbonyl protecting group **5-7** (Boc-group), which was necessary to prevent side reactions in the following steps. Afterwards, the ester of **5-7** was hydrolyzed to the free acid, which was converted to the activated NHS-ester. Crosslinking of the indole moiety **5-9** and doxorubicin was achieved by amide bond formation between the activated acid and the free amine of the drug. This more elaborate synthesis pathway had to be chosen, as neither a direct reduction of **5-4** nor **5-3** was possible under the tested conditions, which would have simplified the synthesis of **5-11**. The ¹H NMR and ¹³C NMR spectra as well as the MALDI MS support the proposed structures of the compounds **5-6** - **5-9**.



Scheme 17: a) dioxane, NaHCO_3 (10 eq), $\text{Na}_2\text{S}_2\text{O}_4$ (7 eq), argon, 1h, r.t., 59%. b) di-tert-butyl dicarbonate (1 eq), THF, argon, overnight, 70°C , 95%. c) THF/MeOH/1M NaOH (1:1:1), 24 h, r.t., 96%. d) *N*-hydroxysuccinimide (1.15 eq), *N,N'*-Diisopropylcarbodiimide (1.2 eq), dry dichloromethanol, argon, overnight, r.t., 92%. e) doxorubicin hydrochloride (0.9eq), DIPEA (1.2 eq), dry DMF, argon, 4 h, r.t., 77 %. f) not possible

However, the final selective cleavage of the Boc-group failed, although different methods were tested. The limiting factor is the instability of doxorubicin in presence of either heat or acids, which are commonly used to cleave the Boc-group. Finally, with a ratio of 10% TFA in DCM it was possible to detect the desired molecule by means of MALDI-TOF MS (Figure 61) next to different side products, but the desired target-molecule could not be purified either by silica column chromatography or by preparative HPLC.

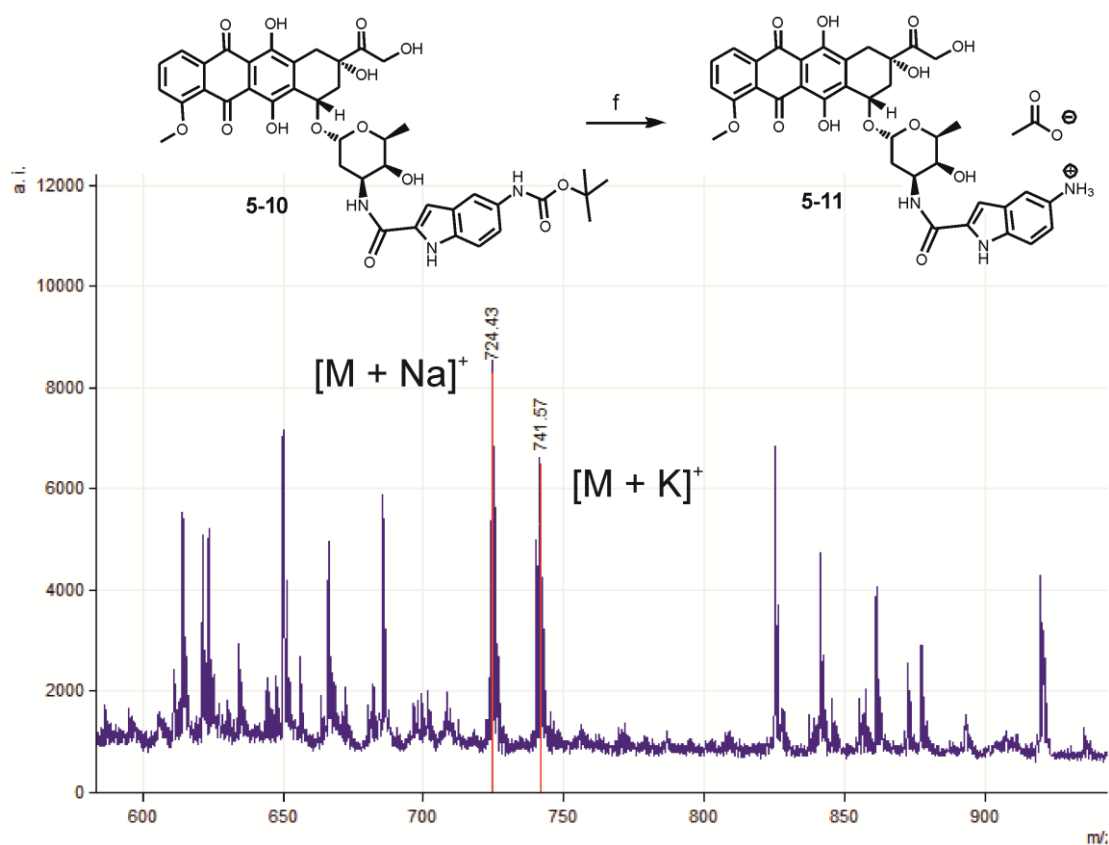
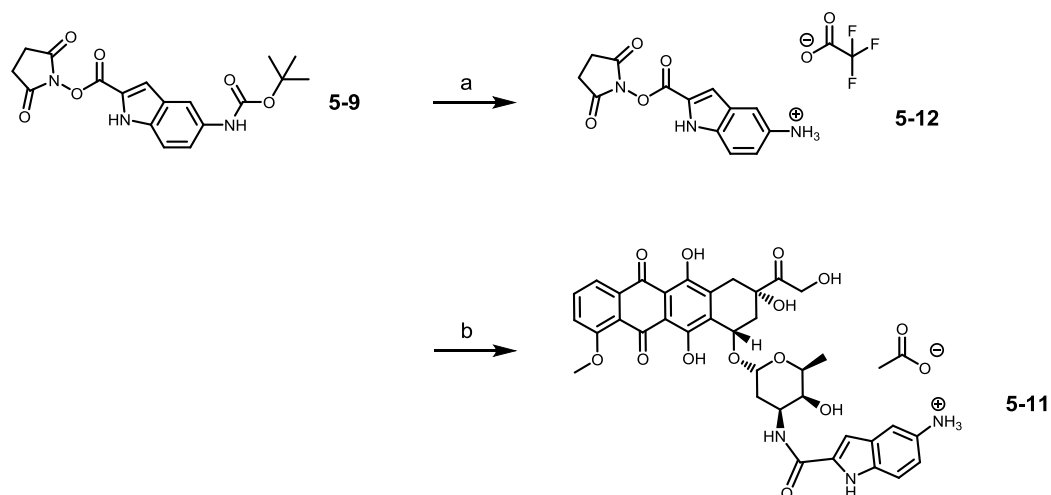


Figure 61: MALDI-TOF MS obtained from the reaction mixture during the preparation of **5-11** (matrix: α -CHCA)

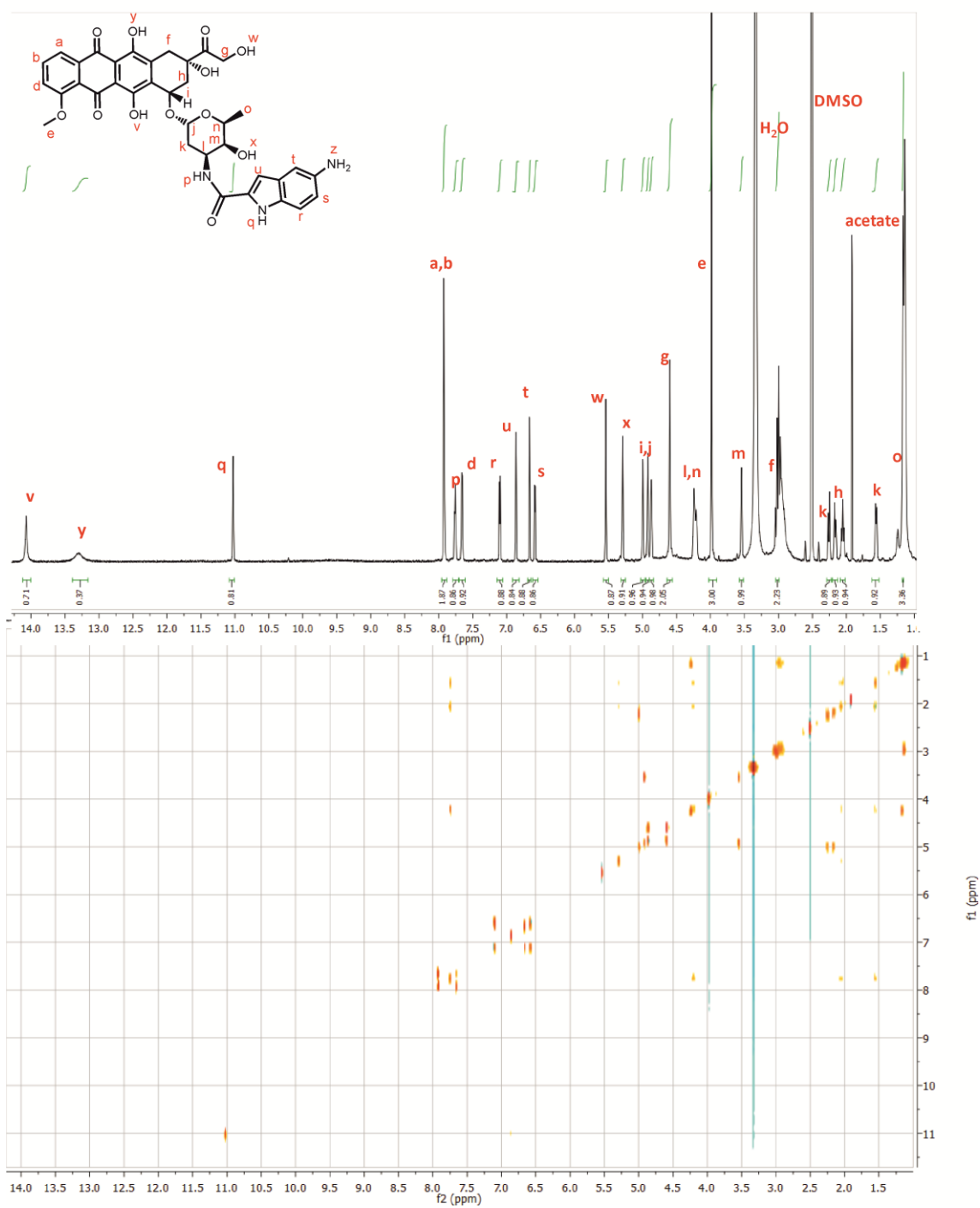
As the cleavage of the Boc-group in presence of doxorubicin was not possible, the synthesis plan was changed as depicted in Scheme 18. The main difference is the cleavage step of the Boc-protecting group after the formation of the NHS-indole derivative **5-9**. The reaction process of the cleavage step was checked continuously by TLC to identify the optimal reaction time. Finally, after 30 min no starting material **5-9** was left and only a single fluorescent spot on the starting line could be detected under the UV lamp. After removal of the solvents under reduced pressure to guarantee that no TFA is left, the resulting compound was dissolved in DMF. The pH was adjusted to $pH = 7/8$ with DIPEA to neutralize unreacted TFA from the previous step, which could not be completely removed under the reduced pressure. Consequently, this solution was added to doxorubicin. The reaction process was monitored as well as purified by means of HPLC to obtain the final pure doxorubicin-indole NH_2 derivate in 60% yield. The stability of this compound was investigated by means of NMR. The chemical shifts did not change within 10 days in DMSO giving a first hint for the stability of the compound. Furthermore, the compound was dissolved in MilliQ water and incubated for 14 days at room temperature to control the stability within aqueous solutions by means of HPLC. The retention times of the product did

not change and no additional products arose within this time period, which shows that the doxorubicin-indole NH_2 compound is a stable compound.



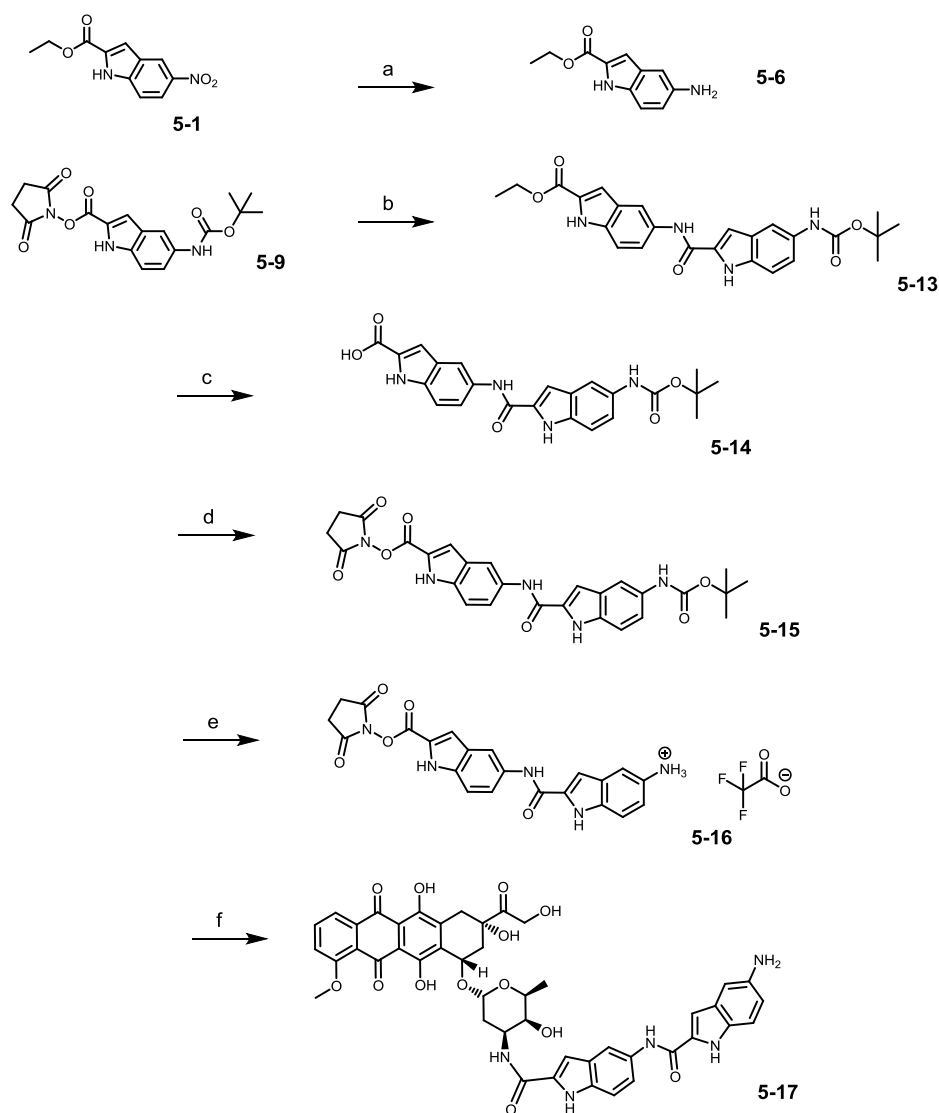
Scheme 18: a) dry DCM/TFA (1:1), 1h, r.t., argon, quant. yield b) doxorubicin hydrochloride (0.9eq), DIPEA, dry DMF, argon, 4 h, r.t., 60 %.

The existence of **5-11** was shown by MALDI MS and the structural confirmation was achieved by NMR spectroscopy. The corresponding H-H TOCSY spectrum is shown on Figure 62. As already discussed for **5-4**, the NMR spectrum exhibits clearly assignable signals and their intensity ratios of all peaks agree with the theoretically expected ones. In total the integration of the downfield part gives eleven protons in total, in which five at a time can be assigned to the drug and the indole (including the hydroxyl and amine protons). Additionally, the H-H interaction in the TOCSY between *l* and *p* proves the formation of the amide bond between doxorubicin and the indole derivative, thus the last left downfield proton can be assigned to the amide proton.

Figure 62: H-H TOCSY spectrum of compound **5-11** in DMSO d⁶ (700 MHz)

5.1.3 Synthesis of doxorubicin-indole-indole-NH₂ conjugate (Doxindind-NH₂)

In order to investigate the influence of the number of indole moieties on the binding affinity to DNA, a doxorubicin conjugate containing two indole units was prepared (Scheme 19). We hypothesized that the introduction of another indole unit would additionally increase the binding as already shown by Zhao *et al.* for DNA alkylating agents carrying different indole derivatives. [23]



Scheme 19: a) dioxane, NaCHO₃ (10 eq), Na₂S₂O₄ (7 eq), argon, 1h, r.t., 59%. b) dry DCM/TFA (1:1), 1h, r.t., argon, quant. yield, **5-6** (0.9 eq), dry DMF, argon, r.t., 4 h, 72%. c) THF/MeOH/1M NaOH (1:1:1), 24 h, r.t., 92%. d) *N*-hydroxysuccinimide (1.15 eq), *N,N'*-Diisopropylcarbodiimide (1.4 eq), dry DCM, argon, overnight, r.t., 75%. e) dry DCM/TFA (1:1), 1h, r.t., argon, quant. f) doxorubicin hydrochloride (0.9eq), DIPEA, dry DMF, argon, 4 h, r.t., 41 %.

The final synthesis of the bis-indole was accomplished *via* an amide bond formation between the previously described compounds **5-6** and **5-9**. Afterwards, the ester group of **5-13** was hydrolyzed to the free acid, which was converted to the activated NHS-ester, analogously to the synthesis pathway to **5-4** and **5-11** (Scheme 16 and Scheme 18). After purification by preparative HPLC the product **5-17** was obtained as a red powder. The final conjugate was amongst others analyzed by MALDI-TOF MS as depicted in Figure 63, showing the detection of the sodium as well as the potassium adduct of **5-17**.

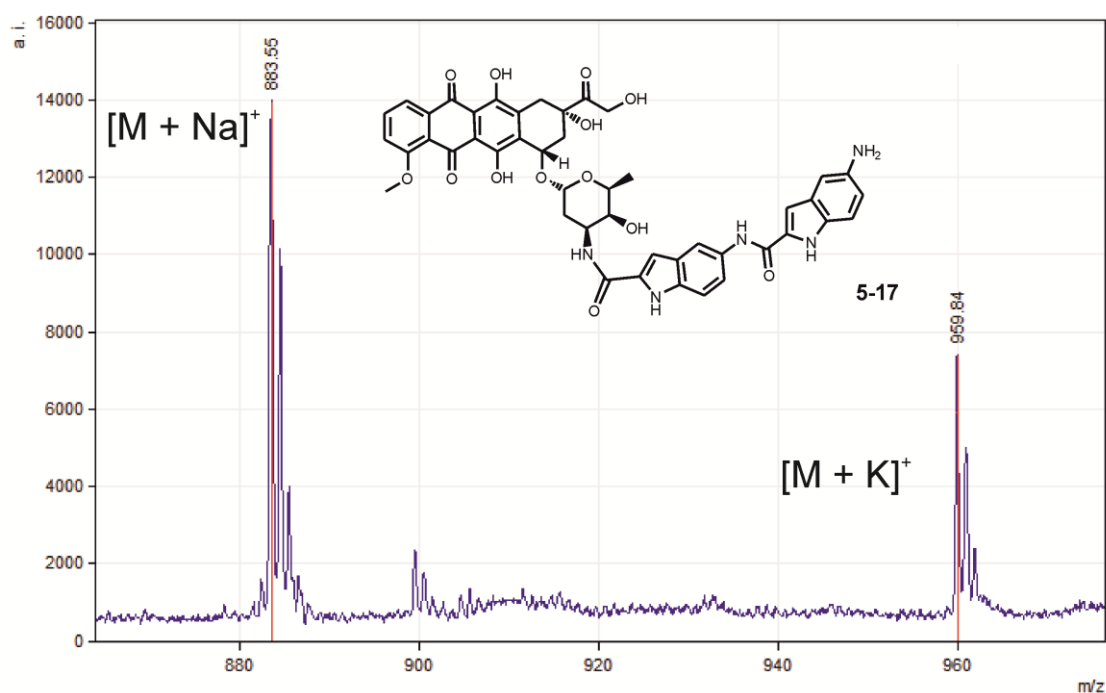


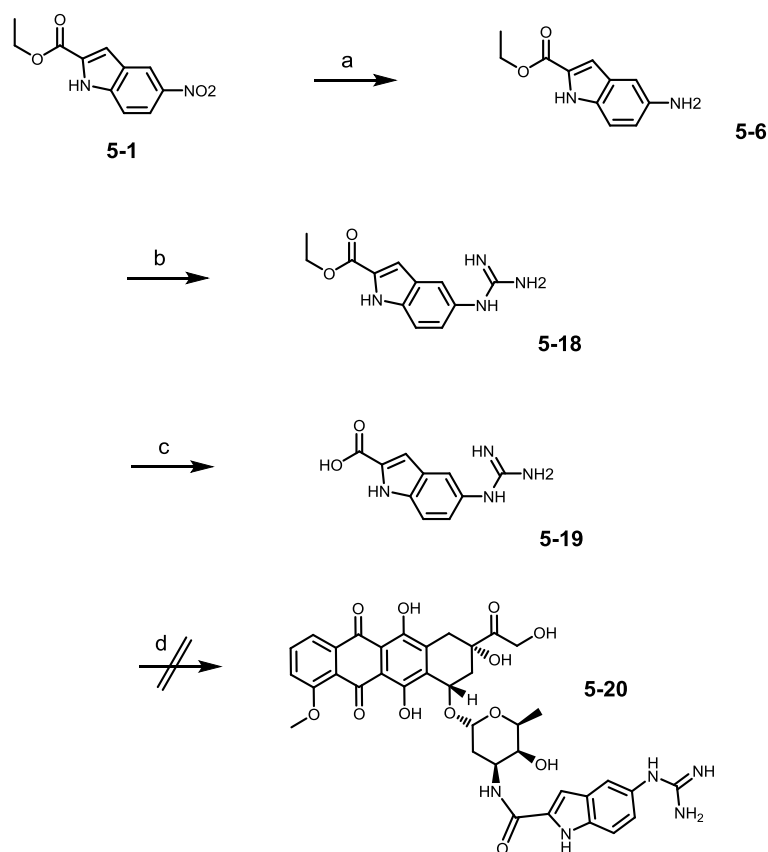
Figure 63: MALDI-TOF MS spectrum of the isolated doxorubicin-indole-indole NH_2 conjugate **5-17** (matrix α -CHCA)

5.1.4 Synthesis of doxorubicin-indole guanidyl conjugate (Doxind-G)

Nature uses distinct functional groups to recognize and bind phosphate anions in the minor groove at the DNA backbone like the guanidine group. This group is a part of the side chain of arginine and remains charged over a wide pH range, which is reflected in the high pK_a value (12.48) of its protonated counterpart. [24] Therefore, it possesses many structural features that make it a versatile moiety for molecular binding to DNA, like its ability to form up to five hydrogen bonds with nucleic acids. A binding mode in which it bridges two phosphates and establishes distinct additional interactions with a guanosine in the minor groove has been reported. [25] This part focused on the synthesis of another doxorubicin-indole conjugate, possessing a guanidine group attached to the indole (Scheme 20). Thereby, the binding affinity of the final conjugate to dsDNA was expected to be higher compared to the conjugates synthesized so far.

After the reduction of the nitro group, the aromatic amine of **5-6** was converted into a guanidine group (compound **5-18**). Saponification of **5-18** was accomplished with 1M NaOH to obtain the free acid, as proven by ¹H NMR, ¹³C NMR and MALDI-TOF MS. The final coupling to doxorubicin was tested with different coupling reagents as *N,N,N',N'*-Tetramethyl-O-(*N*-succinimidyl)uronium tetrafluoroborate (TSTU), 1-Ethyl-3-(3dimethylaminopropyl)-carbodiimide (EDC), *N,N'*-Diisopropylcarbodiimide (DIC) and 1-[Bis(dimethylamino)-methylene]-1*H*-1,2,3-triazolo[4,5-*b*]pyridinium3-oxid hexafluorophosphate (HATU) using DMF, DMSO or a mixture of both as the solvent and DIPEA as a base to obtain a slightly basic pH value. In all cases the reaction process was monitored by analytical HPLC. However, none of the tested coupling reagents yielded the expected product **5-20** (Scheme 20).

A possible explanation for the failure of this final reaction is probably the solubility of **5-19**, as this compound was only soluble in DMF and DMSO at high dilution ratios (0.5 mg/ml). The reason for this is the strong intermolecular interaction due to π - π stacking and the mutual attraction of the negatively charged carboxylic group and the positively charged guanidine group (zwitterion). Thereby it is assumed that the carboxylic group is not activated and thus no amide formation can occur.



Scheme 20: a) dioxane, NaCHO_3 (10 eq), $\text{Na}_2\text{S}_2\text{O}_4$ (7 eq), argon, 1h, r.t., 59%. b) p-Toluenesulfonic acid (1.1 eq), cyanamide (1.2 eq), dioxane, argon, 90°C , overnight, 55%. c) MeOH/1M NaOH (1:1), argon, r.t., overnight, 78%. d) not possible

Alternative reaction pathways to obtain the final desired compound **5-19** as the guanidylation of **5-11** or **5-12** were tried but are not accomplishable, as the required heating during this reaction either destroyed doxorubicin or the NHS-ester of **5-12**. An additional reaction pathway could be the protection of the guanidyl amines of **5-18** with a tert-butyloxycarbonyl group in the first step. This would be similar to the use of Boc-protected arginine amino acids in the peptide synthesis also avoiding possible side reactions. Afterwards the procedure would be similar to the synthesis of **5-11**, meaning saponification, NHS-ester formation, Boc-cleavage at the guanidyl and finally the coupling to doxorubicin.

5.2 Binding affinity measurements using Microscale Thermophoresis

In this work Microscale Thermophoresis (MST) was used as the method of choice to determine binding affinities between different molecules, and to confirm the desired higher binding affinity of the novel synthesized doxorubicin-indole conjugates towards dsDNA. The advantage of this relatively new technique compared to other techniques such as isothermal titration calorimetry (ITC), electrophoretic mobility shift assay (EMSA) or surface plasmon resonance (SPR) based techniques are the easy handling, small sample amount, short measuring time without complex method set-ups, and the fact that there is almost no limitation of molecule size or molecular weight. [26] Furthermore, this technique enables the measurement of a wide range of biomolecular interactions under close-to-native conditions. [26, 27]

MST is based on the fact that molecules move within a microscopic temperature gradient, which is called thermophoresis (Figure 64). The movement of the molecules depends on a number of factors including hydration shell, charge and size of the molecule. Any change of these factors results in a relative change of the molecule's movement and concentration along the temperature gradient. MST uses fluorescence to follow the thermophoretic movement of the molecules and to monitor the distribution inside a capillary. This fluorescence can either be intrinsic to the molecule or an attached dye. [26] [27]

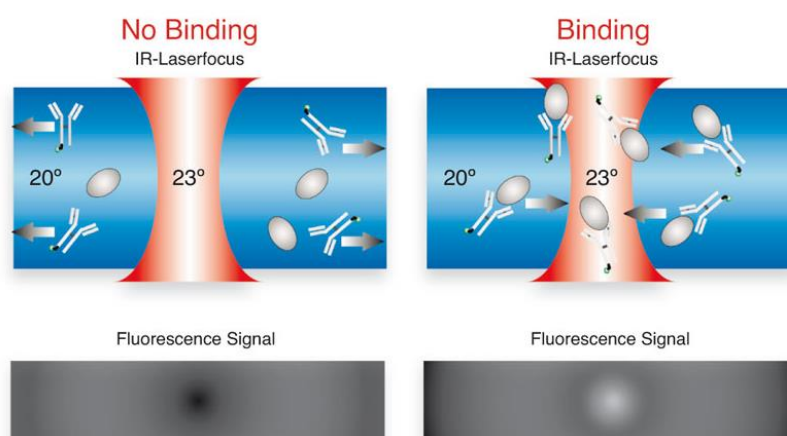


Figure 64: Moving of particles in cases of binding or no binding, molecules will move from warm to cold (no binding) or the reverse (binding) [27] (from <http://www.nanotemper-technologies.com/technologies/mst-technology/>)

The thermophoresis of a single fluorescently labeled molecule M typically differs significantly from the thermophoresis of a bound molecule $B-M$ after a binding event between two components due to even minute changes in the previously mentioned three factors. [26]

The temperature gradient is induced by an IR-Laser, which is focused into the capillary (Figure 64). Before the laser is switched on ($t = 5s$), the molecules are initially distributed equally in solution. Due to the strong absorption of the laser, the aqueous solution in the laser spot is raised between 1-6 °C, depending on the intensity chosen by the operator. The temperature jump is kept constant for around 30 seconds and induces the thermophoretic movement of the molecules inside the capillary, causing a decrease of fluorescence. Unbound molecules will move from warm to cold areas due to the diffusion of the solvent molecules to balance the temperature differences, whereas bound molecules will move the reverse way. [28] Within the heated region the local concentration of molecules decreases until it reaches a steady-state distribution, in which the thermo-diffusion is equal to the mass-diffusion. After 30 seconds the laser is switched off again and the original fluorescence signal F_{norm} will be reached due to the back diffusion of the molecules. The change of fluorescence in such a MST experiment is directly correlated with the thermophoretic characteristic of the molecule used. Any binding process causes a change of parameters as size, charge or solvation entropy of the fluorescent molecule, which is detected by the system. Finally, the binding affinity is quantified based on the measured differences in the MST fluorescence signal. [29]

A serial dilution of the binding substrate is used to detect quantitative binding parameters. The typical sigmoidal binding curve is obtained by plotting F_{norm} against the logarithm of the different concentrations of the dilution series. Finally the dissociation constant k_D as the result of the MST experiment is directly deduced by fitting this binding curve with the nonlinear solution of the law of mass action (Figure 65). A detailed description of the derivation of the dissociation constant calculation is given in the appendix 9.

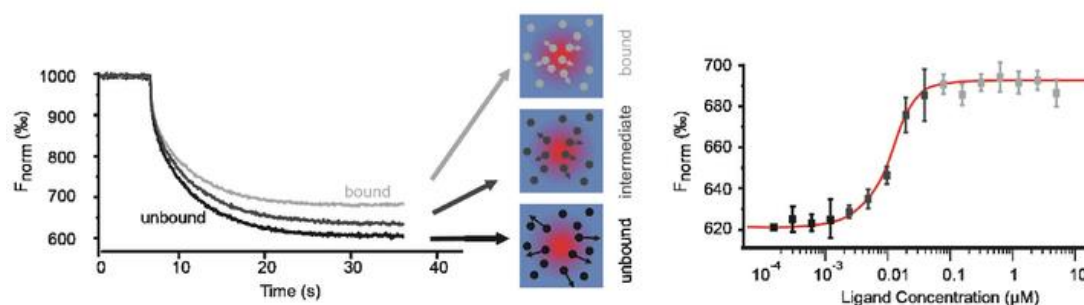


Figure 65: Example for fluorescent measurement and final plotting against the concentration [30]

The left part shows the plotting of the normalized fluorescence in three different sample capillaries with different concentrations against the time. It illustrates the different MST signals due to the thermophoretic movements of the bound (grey) and unbound (black) molecules. The obtained normalized fluorescent signal of the fully bound and unbound samples is around 100% for both until the temperature gradient is induced by switching on the laser at $t = 5$ s. Afterwards both samples show different thermophoresis due to the different sizes upon binding and led to different normalized fluorescent signals.

The right part is a plot of the normalized fluorescence points of all different sample capillaries against the concentration contained in the capillary, which results in the shown binding curve used for the final binding affinity calculations. Every capillary contains a different amount of ligand, but the same amount of fluorophore, and is measured as shown of the left side. Each single measurement results in one of the points used for the fitting as highlighted on the right side. The concentration of the fluorescent components is kept constant, whereas the concentration of the ligand is increased in each capillary until the saturation of the binding is achieved.

The capability of Microscale Thermophoresis to measure binding affinities between small molecules or polymers and fluorescently labelled nucleic acids has already been proven by our group in different studies. [19, 24, 31] The simple set up of MST allows for the determination of affinities in a timely manner making it the method of choice for the analysis of small molecules binding to DNA and, therefore, was used in this work.

5.2.1 Doxorubicin – DNA intercalation

To simulate the binding of the different doxorubicin-indole conjugates towards dsDNA, a Cy5 labelled model dsDNA (12 base pairs) was used. The plotting of the measured fluorescent signal of the different prepared capillaries against the doxorubicin-derivative concentrations was performed for varying concentrations of the drug in each sample ($c = 7812.5 - 7.6$ nM) and a constant concentration of 50 nM Cy5 labelled DNA. For example, Figure 66 shows the obtained binding curve of **5-17** that can be used to calculate the binding affinity constant. Similar curves could be measured for doxorubicin, doxorubicin – indole NO₂ (**5-4**) and doxorubicin – indole NH₂ (**5-11**) as summarized in

Table 4.

Table 4: Binding affinity constants between a 12 base pair long DNA and doxorubicin as well as **5-4**, **5-11** and **5-17**

Molecule	Binding affinity K_a in $10^6 * M^{-1}$
Doxorubicin	0.37
Doxorubicin – Indole NO ₂ (5-4)	2.35
Doxorubicin – Indole NH ₂ (5-11)	8.13
Doxorubicin – Indole-Indole NH ₂ (5-17)	27.03

The measured binding affinities confirm the expectation that the synthesized doxorubicin-indole conjugates have a stronger binding towards dsDNA compared to doxorubicin alone, based on the additional minor groove binding of the introduced indole. Whereas **5-4** already shows a 7 times ($K_a = 2.35 * 10^6 M^{-1}$) stronger binding affinity compared to single doxorubicin, **5-11** as well as **5-17** show almost 20 times ($K_a = 8.13 * 10^6 M^{-1}$), respectively 70 times ($K_a = 27.03 * 10^6 M^{-1}$), stronger binding affinities. By interpreting the values given in

Table 4, it can be stated that the amount of indole units as well as the functional group attached to the indole have an influence on the binding affinity towards the dsDNA. As already shown by Zhao and co-workers, two indole molecules have the ideal size for dsDNA minor groove binding. [32] Nevertheless, we can prove that one indole unit attached to doxorubicin also increases the dsDNA binding significantly. Concerning the utilized functional groups, amino- versus nitro-group, it can be declared that the increased binding affinity of **5-11** with an amino group is not only caused by the formation of more hydrogen bonds to the DNA backbone, but also due to improved water solubility. Figure 66 is an example for plotting the thermophoresis data of the measured fluorescent signal against the concentration of the doxorubicin-indole derivative. The corresponding figures of doxorubicin, **5-4** as well as **5-11** are given in the appendix (appendix 9).

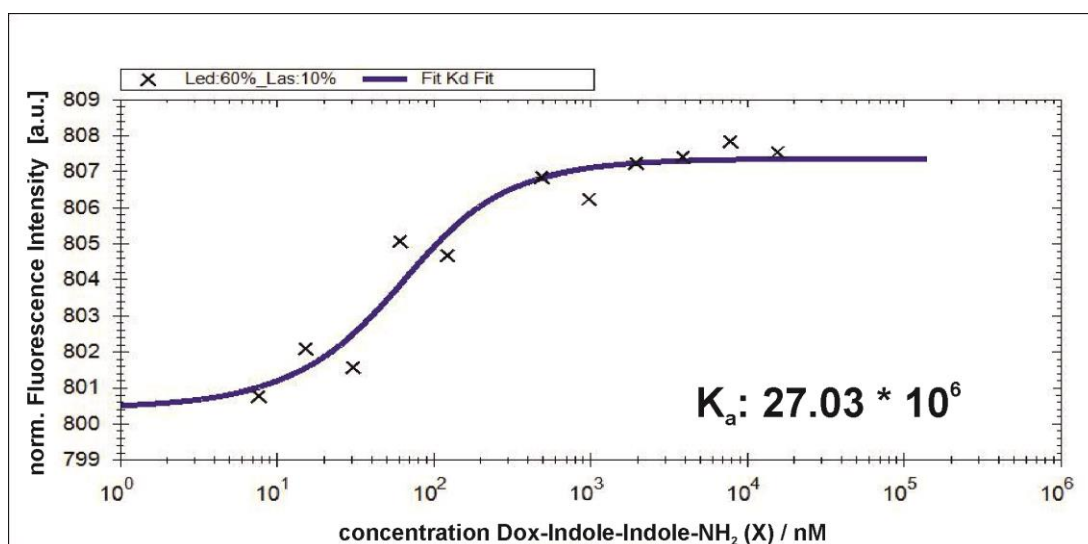


Figure 66: Thermophoresis data compound **5-17**, plotting of the measured fluorescent signal against the doxorubicin-indole-indole NH₂ (**5-17**) concentration of each sample prepared (c (**5-17**) = 7812.5 – 7.6 nM) at a constant concentration of 50 nM Cy5 labelled DNA (12 base pairs) in each sample. Settings used are LED 60% and LAS 10%, Buffer MST, Absorption red – Emission red

5.3 Toxicity studies of the doxorubicin-indole conjugates

The cytotoxicity of conjugate **5-11** was investigated on three different cell lines: the wild type and doxorubicin resistant neuroblastoma tumor cell lines (Kelly wt and Kelly ADR) as well as the breast cancer cell line MCF7. The IC₅₀ values were determined by a luminescence-based cell viability assay. Compared to the binding affinity calculations by means of MST, the determined IC₅₀ values (Table 5) showed a lower toxicity compared to doxorubicin alone (IC₅₀ = 0.5 μM). Nevertheless, compound **5-11** showed higher efficiency against the wild type neuroblastoma cell line in comparison with the resistant type and the MCF7 cell line.

The lower toxicity values could be explained by the lower cellular uptake of the doxorubicin-indole conjugate compared to doxorubicin. In order to perform the cell tests, all tested conjugates had to be initially dissolved in DMSO and were then diluted with MilliQ water to reduce the DMSO content to 10%. Otherwise the conjugates were almost insoluble in water. Solubility tests in water already showed the poorer solubility of the doxorubicin-indole conjugates compared to doxorubicin, which can be explained by the fact that the aromatic amine of the indole is less basic and, thus, probably not charged at pH 7 compared to the aliphatic amine of doxorubicin. Furthermore, the possibility of aggregation in solution

due to π - π stacking is increased by the introduction of the indole part and further reduces the water solubility.

However, in order to circumvent this problem of poor water solubility of compound **5-11**, the counter ion acetate was substituted by either chlorine or sulfonate, but in both cases the determined IC_{50} values did not change significantly. Therefore, additional cytotoxicity test for **5-4** and **5-17** were not performed, as both compounds even showed lower water solubility.

Table 5: IC_{50} values of doxorubicin-indole NH_2 (**5-11**) for different cell lines

Cell line	IC_{50} [μM]
MCF7	12.65
Kelly Wt	9.77
Kelly ADR	17.19

In contrast to doxorubicin, the anticancer drug paclitaxel (taxol) has relatively poor water solubility, but still possesses high toxicity, which qualifies it to be used to treat different cancer types such as ovarian, breast or lung cancer. A similar behavior has been expected for the doxorubicin-indole derivative. However, in the end it has to be stated that the toxicity studies could not confirm our hypothesis of a higher toxicity of the novel conjugates compared to doxorubicin, although the MST results were still very promising.

There are many factors that can influence cell cytotoxicity like solubility, side of action, bio distribution, or plasma stability. The results presented herein satisfied the expectations of creating conjugates combining DNA intercalation and minor groove binding with binding affinities towards DNA stronger than doxorubicin. However, the limiting factor in this study is the poor cytotoxicity influenced by the low water solubility of the conjugates compared to native doxorubicin. A better water solubility is supposed to lead to higher intracellular concentrations and therefore lower IC_{50} values.

Although **5-20** (doxorubicin-indole with guanidine group) could not yet be synthesized successfully it is assumed that this molecule would have had the highest water solubility and toxicity of the synthesized conjugates, as the guanidine group is charged around pH 7. Although this remains to be proven, the synthesis of **5-20** is highly attractive towards finding novel and powerful anticancer agents.

Unfortunately, even when we have an excellent idea in hand we often encounter problems due to the complexity of biological systems that we cannot always predict, yet this experience helps us to move forward in creating more efficient anticancer agents. One way to do so is to find suitable delivery systems such as cell-penetrating peptides or water soluble polymers for these proposed conjugates. A second possibility would be to introduce other functional groups to the indole to form a sulfonate- or phosphate-esters possessing higher water solubility.

5.4 References

1. Dale, H.P.R.M.M., *Rang and Dale's Pharmacology*. Elsevier Churchill Livingstone, 2012. **seventh edition**.
2. Waksman, S.A. and H.B. Woodruff, *Bacteriostatic and bactericidal substances produced by a soil actinomyces*. Proceedings of the Society for Experimental Biology and Medicine, 1940. **45**: p. 609-614.
3. Weiss, R.B., *The Anthracyclines - Will We Ever Find a Better Doxorubicin*. Seminars in Oncology, 1992. **19**(6): p. 670-686.
4. Minotti, G., et al., *Anthracyclines: Molecular advances and pharmacologic developments in antitumor activity and cardiotoxicity*. Pharmacological Reviews, 2004. **56**(2): p. 185-229.
5. Arcamone, F., et al., *Adriamycin (14-Hydroxydaunomycin) a Novel Antitumor Antibiotic*. Tetrahedron Letters, 1969(13): p. 1007-&.
6. Gewirtz, D.A., *A critical evaluation of the mechanisms of action proposed for the antitumor effects of the anthracycline antibiotics Adriamycin and daunorubicin*. Biochemical Pharmacology, 1999. **57**(7): p. 727-741.
7. Cummings, J. and C.S. McArdle, *Studies on the in vivo disposition of adriamycin in human tumours which exhibit different responses to the drug*. Br J Cancer, 1986. **53**(6): p. 835-8.
8. Champoux, J.J., *DNA topoisomerases: Structure, function, and mechanism*. Annual Review of Biochemistry, 2001. **70**: p. 369-413.
9. Moro, S., et al., *Interaction model for anthracycline activity against DNA topoisomerase II*. Biochemistry, 2004. **43**(23): p. 7503-7513.
10. Topcu, Z., *DNA topoisomerases as targets for anticancer drugs*. J Clin Pharm Ther, 2001. **26**(6): p. 405-16.
11. Nadas, J. and D.X. Sun, *Anthracyclines as effective anticancer drugs*. Expert Opinion on Drug Discovery, 2006. **1**(6): p. 549-568.
12. Capranico, G., et al., *A protein-mediated mechanism for the DNA sequence-specific action of topoisomerase II poisons*. Trends in Pharmacological Sciences, 1997. **18**(9): p. 323-329.
13. Schneider, Y.J., et al., *DNA-Binding Parameters of Daunorubicin and Doxorubicin in the Conditions Used for Studying the Interaction of Anthracycline-DNA Complexes with Cells Invitro*. Cancer Chemotherapy and Pharmacology, 1979. **2**(1): p. 7-10.
14. Dorr, R.T., *Cytoprotective agents for anthracyclines*. Seminars in Oncology, 1996. **23**(4): p. 23-34.

15. Chaires, J.B., et al., *Structure-based design fill of a new bisintercalating anthracycline antibiotic*. Journal of Medicinal Chemistry, 1997. **40**(3): p. 261-266.
16. Portugal, J., et al., *A new bisintercalating anthracycline with picomolar DNA binding affinity*. Journal of Medicinal Chemistry, 2005. **48**(26): p. 8209-8219.
17. Phillips, D.R., et al., *Bis-Daunomycin Hydrazones - Interactions with DNA*. Investigational New Drugs, 1992. **10**(2): p. 79-88.
18. Leng, F.F., W. Priebe, and J.B. Chaires, *Ultratight DNA binding of a new bisintercalating anthracycline antibiotic*. Biochemistry, 1998. **37**(7): p. 1743-1753.
19. M. Lelle, C.F., S. Kaloyanova, I. Tabujew, A. Schramm, M. Musheev, C. Niehrs, K. Müllen, K. Peneva, *Overcoming drug resistance by cell-penetrating peptide-mediated delivery of a doxorubicin dimer with high DNA-binding affinity*. European Journal of Medicinal Chemistry, 2017. **130**: p. 336-345.
20. David L. Nelson, M.M.C., *Lehninger Principles of Biochemistry, 6th edition*. 2012.
21. Baraldi, P.G., et al., *DNA minor groove binders as potential antitumor and antimicrobial agents*. Medicinal Research Reviews, 2004. **24**(4): p. 475-528.
22. Gupta, S.P., et al., *Indole Derivatives as DNA Minor Groove Binders*. Chemistry of Phytopotentials: Health, Energy and Environmental Perspectives, 2012: p. 149-153.
23. Zhao, R.Y., et al., *Synthesis and Biological Evaluation of Antibody Conjugates of Phosphate Prodrugs of Cytotoxic DNA Alkylators for the Targeted Treatment of Cancer*. Journal of Medicinal Chemistry, 2012. **55**(2): p. 766-782.
24. Tabujew, I., et al., *The Guanidinium Group as a Key Part of Water-Soluble Polymer Carriers for siRNA Complexation and Protection against Degradation*. Macromolecular Rapid Communications, 2014. **35**(13): p. 1191-1197.
25. Perreault, D.M., L.A. Cabell, and E.V. Anslyn, *Using guanidinium groups for the recognition of RNA and as catalysts for the hydrolysis of RNA*. Bioorganic & Medicinal Chemistry, 1997. **5**(6): p. 1209-1220.
26. Jerabek-Willemsen, M., et al., *Molecular Interaction Studies Using Microscale Thermophoresis*. Assay and Drug Development Technologies, 2011. **9**(4): p. 342-353.
27. GmbH, N., *Microscale thermophoresis - Background*. 2016.

28. Zillner, K., et al., *Microscale Thermophoresis as a Sensitive Method to Quantify Protein: Nucleic Acid Interactions in Solution*. Functional Genomics: Methods and Protocols, Second Edition, 2012. **815**: p. 241-252.
29. Seidel, S.A.I., et al., *Microscale thermophoresis quantifies biomolecular interactions under previously challenging conditions*. Methods, 2013. **59**(3): p. 301-315.
30. Baaske, P., et al., *Optical Thermophoresis for Quantifying the Buffer Dependence of Aptamer Binding*. Angewandte Chemie-International Edition, 2010. **49**(12): p. 2238-2241.
31. Lelle, M., et al., *Octreotide-Mediated Tumor-Targeted Drug Delivery via a Cleavable Doxorubicin-Peptide Conjugate*. Mol Pharm, 2015. **12**(12): p. 4290-300.
32. Zhao, R.Y., et al., *Synthesis and biological evaluation of antibody conjugates of phosphate prodrugs of cytotoxic DNA alkylators for the targeted treatment of cancer*. J Med Chem, 2012. **55**(2): p. 766-82.

6 Summary and Perspective

Disulfide-intercalating agents belong to a relatively young subclass of bioorthogonal coupling reagents, which is gaining interest in the field of bioconjugate chemistry as they enable the site-selective modification of complex peptides and proteins without changing their structure or function. This work was focused on the design and synthesis of two novel disulfide intercalating systems for such modification purposes. Depending on the different application either drugs, chromophores or polymers were successfully attached to octreotide. Furthermore, novel doxorubicin derivatives combining DNA intercalation as well as DNA minor groove binding have been developed and their binding to DNA was compared to doxorubicin using microscale thermophoresis.

In [Chapter 3](#), the development of a novel cross linker reagent, which is based on the amino acid cysteine was described. It is similar to the bis-disulfide linker system introduced previously in our group, whereupon the number of atoms which are intercalating between the disulfide bridge during the reaction was significantly reduced. This is an important aspect that can greatly influence the function of peptides upon modification ([Figure 67](#): structure **left**). In addition, this linker system can be cleaved under reductive conditions unlike previous analogues.

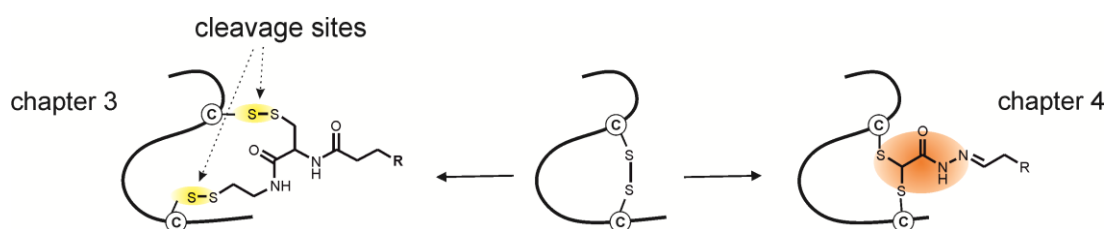


[Figure 67](#): Schematic overview of the two different novel approaches in the field of disulfide intercalation reagents, the structure **left** shows the disulfide based linker system described in [Chapter 3](#), whereas the structure **right** shows the novel linker system based on 3,3-dichloroacrylic acid discussed in [Chapter 4](#)

The somatostatin analogue octreotide was chosen as the model peptide, because of its high affinity towards somatostatin receptors 2 and 5, which are overexpressed on various tumor cells and primary tumor tissues such as human pancreatic carcinoid BON cells or non-small cell lung cancer. [1] Based on this interaction, a targeted delivery of a perylene chromophore and chemotherapeutic drug towards tumor cells was accomplished, as proven by microscopy and cell toxicity experiments. Thereby, higher toxicity values for the doxorubicin-octreotide

conjugate could be achieved compared to the literature, mainly because the drug was attached *via* a hydrazone bond instead of an oxime bond as previously reported. The difference between both groups is the stability at acidic pH. Whereas the oxime bond is stable at acidic pH and does not enable the drug to release inside the cell, the aforementioned hydrazone bond undergoes hydrolysis in an acidic environment like within an endosome to free doxorubicin inside the cellular organelles and the cytoplasm of tumor cells (Figure 68). [2] Different cleavage studies in the presence of glutathione or at acidic pH proved the formation of the expected cleavage products. Furthermore, by the addition of different functional groups to the linker system and, thus, to octreotide (e.g. ethynyl-, iodo-, hydroxylamine, hydrazine, amine – and carboxylic acid group), a new platform was created that enable a high portfolio of chemical modification reactions to be performed on octreotide.

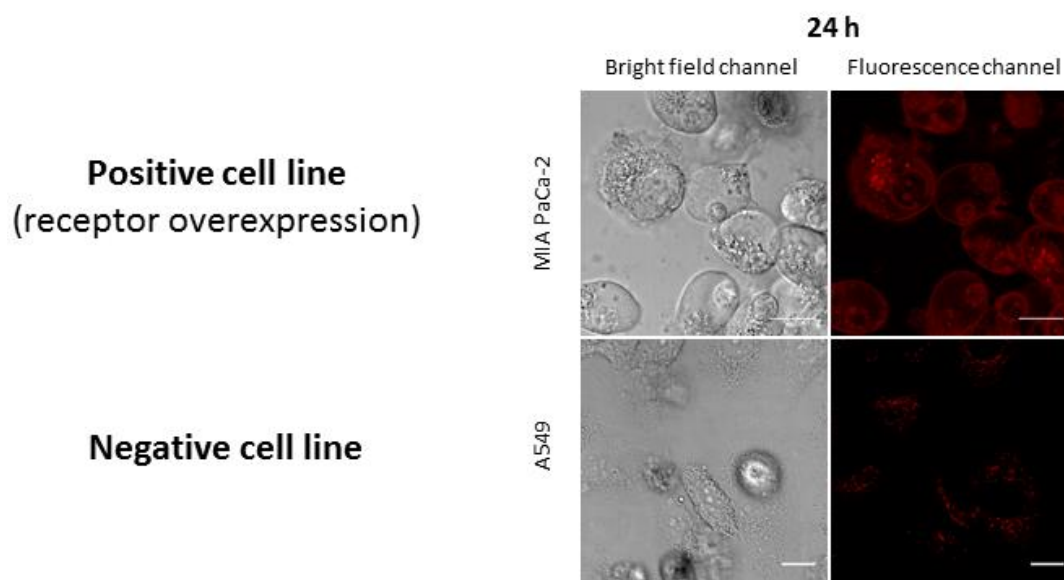


Figure 68: Microscopy images (bright field as well as fluorescence channel) of the doxorubicin-octreotide conjugate described in Chapter 3 for a targeted delivery of doxorubicin towards MIA PaCa-2 cell lines, which have an overexpression of somatostatin receptors, proving the receptor mediated uptake of the synthesized conjugates. In contrast, there is almost no uptake in A549 cells, which are lacking the corresponding receptor. Scale bar 15 μ m, red fluorescence color is caused by the intrinsic fluorescence of doxorubicin

The drawback of conventional chemical techniques, which often result in heterogeneous product mixtures due to the poor selectivity of the chosen functional groups, was discussed in [Chapter 4](#). The primary aim in this part was to prepare the smallest cross-linker possible to avoid any disturbance on the structure of the peptide. Therefore, the synthetic approach presented focused on the modification of peptides and proteins at the disulfide bond by a

novel class of intercalating agents based on 3,3-dichloroacrylic acid, the smallest possible conjugate to modify disulfide bonds (Figure 67: structure **right**). This technique was successfully established for the modification of octreotide by PEGylation, a novel NIR absorbing perylene-monoimide dye (Figure 69) and the anticancer drug doxorubicin.

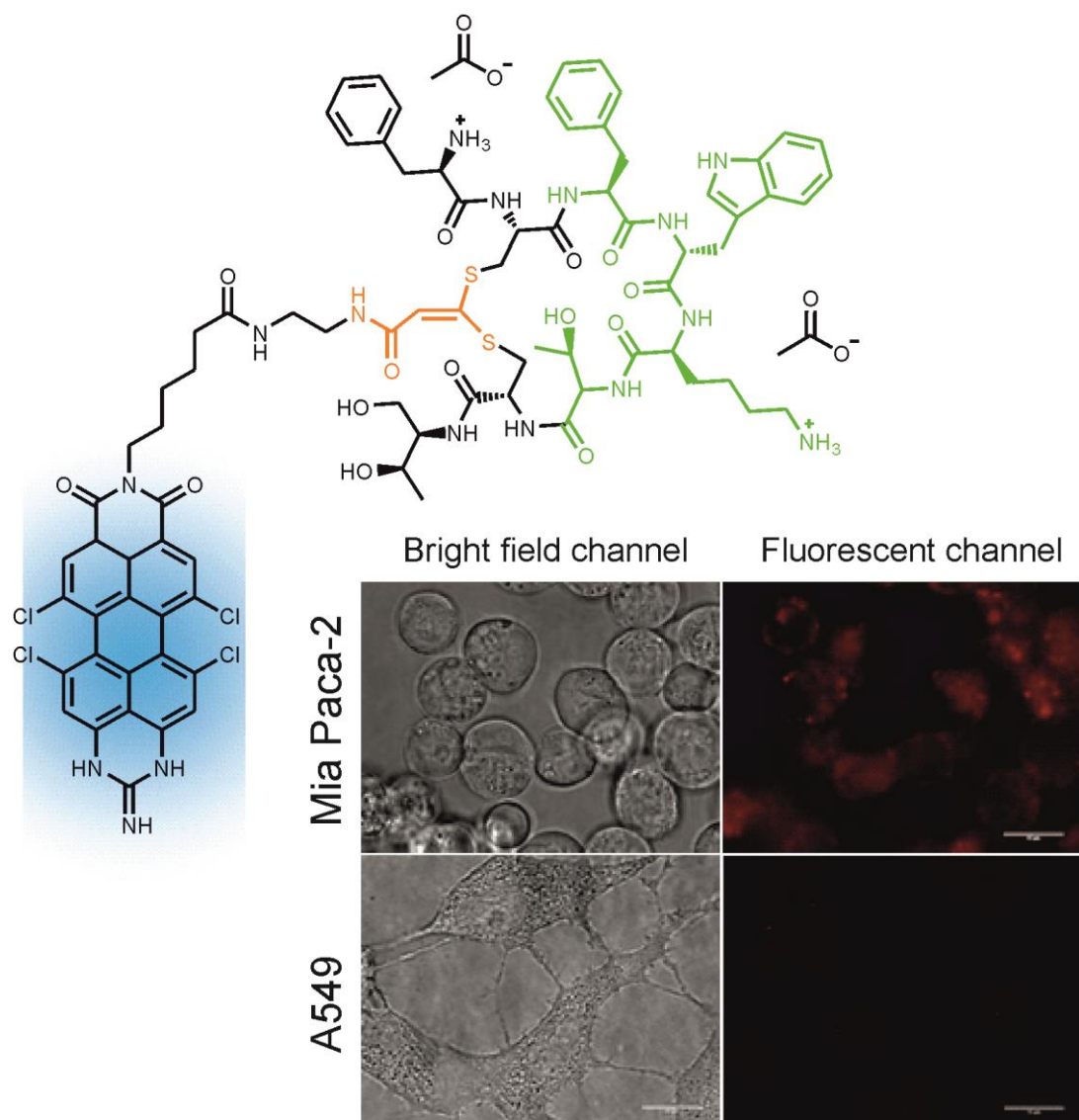
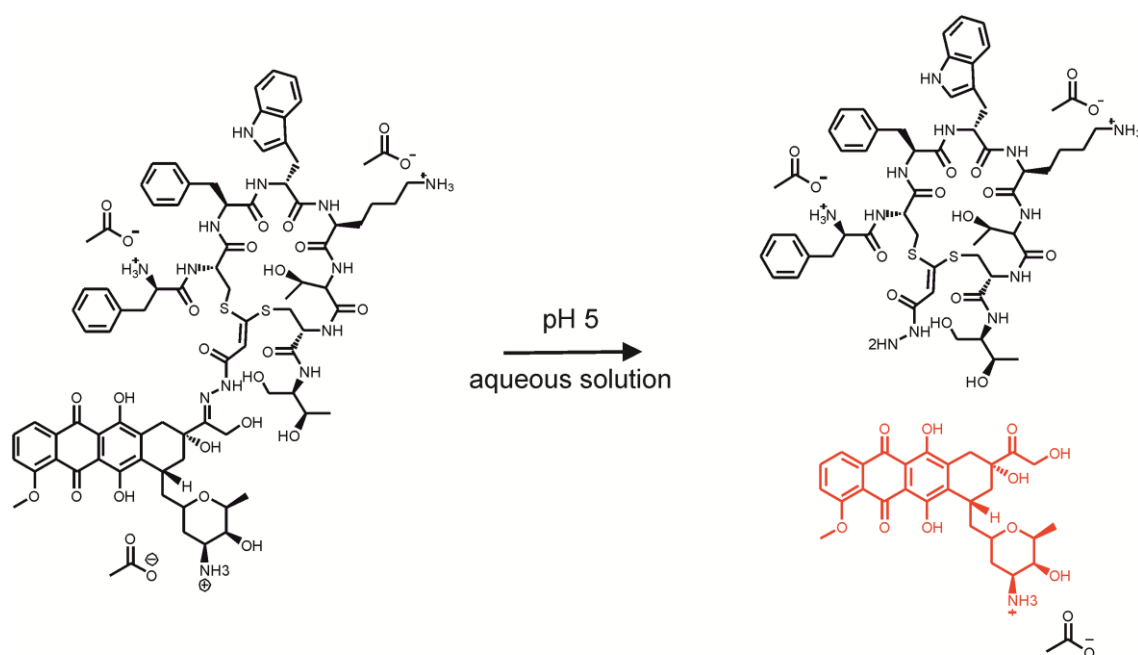


Figure 69: Chemical structure of the PMI-octreotide conjugate (blue: PMI dye, orange: disulfide intercalating system, green: receptor binding motif of octreotide responsible for the receptor interaction); microscopy images (bright field as well as fluorescence channel) again prove the receptor mediated uptake of the conjugates towards Mia PaCa-2 cells only, indicated by the red fluorescent dots representing PMI fluorescence, scale bar 15 μm

After computational calculations and circular dichroism studies were carried out, the complete spatial structure recovery was proven by the successful interaction of the novel synthesized octreotide conjugates with the corresponding somatostatin receptors. Coupling

of a novel synthesized NIR dye to octreotide based on this disulfide-intercalation linker showed high potential in trafficking studies of tumor cells which overexpress somatostatin receptors 2 and 5. Finally, doxorubicin was coupled to octreotide to realize a targeted delivery to the tumor site based on the receptor mediated cell uptake of the conjugate. First cleavage studies were carried out under conditions which mimic the low pH of the endolysosomal environment in cells, and the successful release of doxorubicin due to the introduced hydrazone bond was demonstrated. The targeted cytotoxic effects of the conjugate were stronger by a factor of 7 for the positive MIA Paca-2 cells compared to the negative A549 cells (Figure 70).



Compound	IC ₅₀ MIA Paca-2 cell line (μM)	IC ₅₀ A549 cells line (μM)
Doxorubicin-Octreotide conjugate (4-26)	2.29 ± 0.21	14.35 ± 1.89

Figure 70: Schematic overview on the general cleavage principle of the synthesized doxorubicin-octreotide conjugate at acidic pH enabling the native drug to be released. The table proves the targeted delivery of the drug-peptide conjugates towards MIA PaCa-2 cells, which overexpress cell surface somatostatin receptors.

Due to the selective tumor targeting based on the attached octreotide, higher doses of the drug-peptide conjugate could be applied in contrast to doxorubicin, which is lacking the targeting effect and, therefore, causing almost the same toxicity to every cell line. In addition to this, doxorubicin is known to suffer from multidrug resistance (MDR), which means that the therapeutic efficacy of the anticancer drug is limited. The mechanism related to this drug inefficiency typically involves membrane proteins (e.g. P-glycoproteins) that belong to the

ATP-binding cassette transporter superfamily. [3-5] Therefore, further studies, especially cell toxicity tests, should focus on the cytotoxic effect of the drug-peptide conjugate on drug sensitivity as well as doxorubicin-resistant cancer cells to evaluate if drug resistance can be overcome.

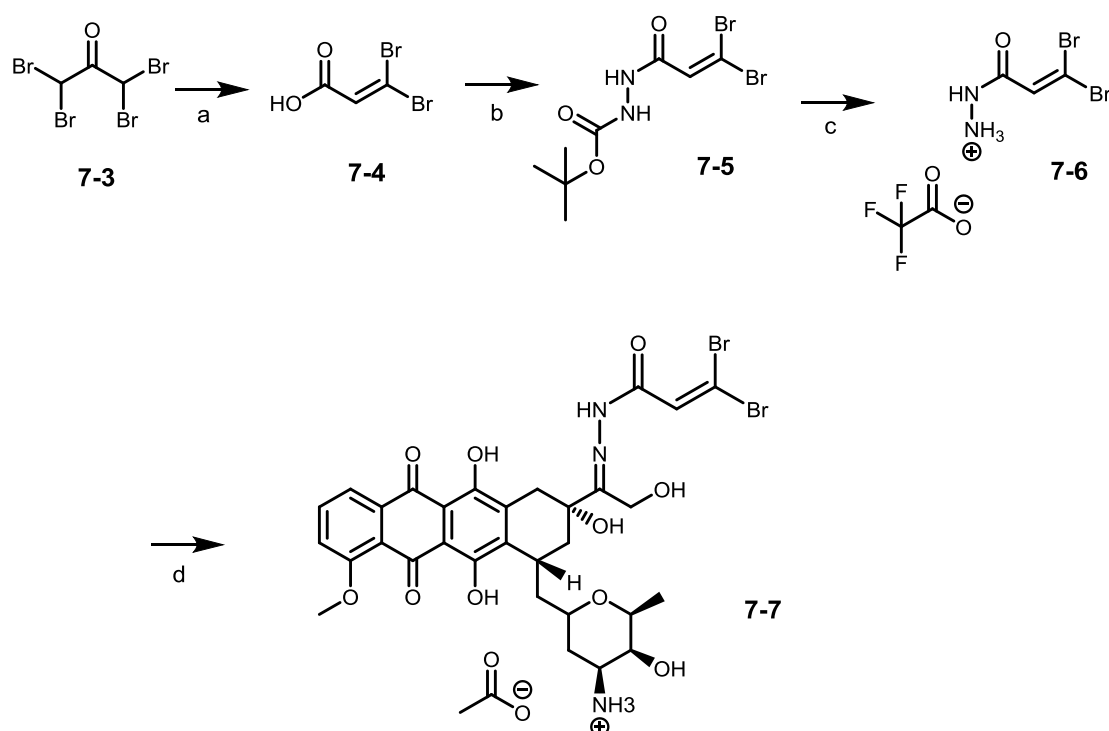
The crucial advantage of the novel linker system is in addition to fast coupling reactions with high yields and the low number of reaction steps to obtain the final conjugate, that only one carbon atom is introduced between the initial disulfide bonds, properties which could not be achieved so far. In addition, 3,3-dichloroacrylic acid is commercially available, which means the molecule can directly be used for the conjugation of cargo and peptide.

Future work should have a closer look at the possibility to use the novel small linker system for the modification of bigger peptides and proteins possessing accessible disulfide bonds as interferons or interleukins. The same is true for the disulfide based crosslinker described in Chapter 3, although 3,3-dichloroacrylic acid is expected to be more successful due to the introduction of only one atom between the sulfur atoms of the initial disulfide bond. For instance, the novel systems can be used for the PEGylation of diverse peptides suffering from short plasma half-life or instability due to the enzymatically digestion.

Due to its small size, its proven stability and the possibility to introduce cleavable functional groups, the novel developed 3,3-dichloroacrylamide based linker offers great potential for the modification of various biomolecules in future applications.

Additionally, the novel conjugation system could be further improved in future by the substitution of the chlorine atoms with bromine, as those are more reactive in the described doubled addition-elimination process with the sulfhydryl groups of the reduced peptide. As 3,3-dibromoacrylic acid is not commercially available compared to 3,3-dichloroacrylic acid, it was already synthesized successfully using one step only starting from 1,1,3,3-tetrabromoacetone (compound **7-3**). A Favorsky rearrangement of the tetra halo ketone dissolved in an aqueous sodium carbonate solution yielded the expected Favorsky product 3,3-dibromoacrylic acid **7-4** (Scheme 21). [6] Coupling reactions with dyes, chromophores and polymers could be accomplished as described in Chapter 4. Initial tests have already been performed by the coupling of the doxorubicin-dibromo-linker **7-7** to octreotide, indicating that the final peptide modification is possible *in situ*, which means that the peptide does not need to be purified after the reduction with TCEP before coupling. In contrast, coupling reactions with the linker systems described herein in Chapter 3 and Chapter 4 were

always performed after an additional purification step of the peptide after the successful reduction, in order to avoid any side reaction with the reducing agent.



Scheme 21: Synthesis pathway of the novel Doxorubicin-dibromo-linker **7-7**, experimental conditions are given in appendix 10.

Compared to the modification of peptides described in the previous chapters, [Chapter 5](#) concentrated on the modification of the anticancer drug doxorubicin, with the intention to increase its binding affinity towards dsDNA and, thus, enable higher cell toxicity. Doxorubicin was used as the DNA intercalation substrate and was functionalized at its sugar amine with different indole derivatives which are known to be DNA minor groove binders (Figure 71 and Figure 72).

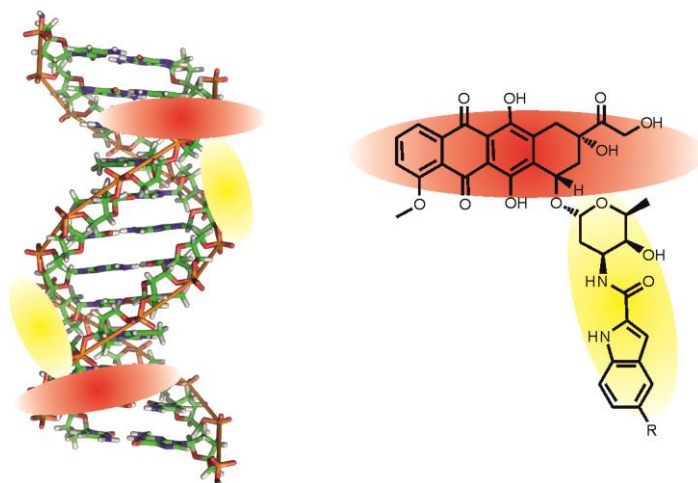


Figure 71: Schematic overview of a doxorubicin-indole conjugate as well as the expected DNA binding that combines DNA intercalation and minor groove binding

Binding affinity studies *via* Microscale Thermophoresis confirmed our expectations. All synthesized conjugates had a significantly stronger binding towards DNA compared to doxorubicin. However, final toxicity tests showed the opposite result as expected based on a lower toxicity compared to doxorubicin, which is assumed to be caused by the poor water solubility of the conjugates.

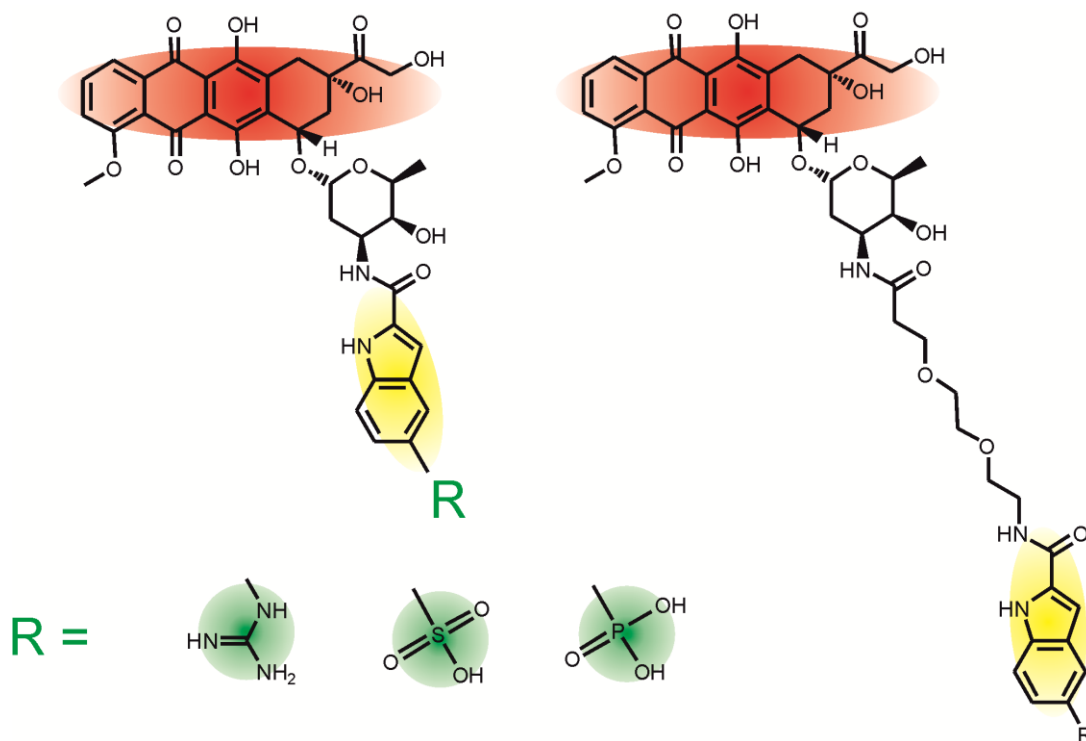


Figure 72: Alternative doxorubicin-indole conjugates with an optimized performance concerning improved water solubility

Unfortunately, even when we have an excellent idea to counter such challenges we often encounter problems due to the complexity of biological systems that we cannot always predict, but, nevertheless, this experience helps us to move forward in creating more efficient anticancer agents. One way to do so is to find suitable delivery systems such as cell-penetrating peptides or water soluble polymers for these proposed conjugates like liposomal formulations. A second possibility would be the introduction of additional functional groups to the indole to form a sulfonate- or phosphate-esters.

In the end, we can admit that the chemical approaches and results presented in this work can find widespread application in the modification of therapeutic proteins.

But for sure, coming back to the introduction of this thesis, we are by far not at the end of the journey of taking advantage of bioconjugation to create novel tools for research, diagnostics, and therapeutics.

6.1 References

1. Sun, L.C. and D.H. Coy, *Somatostatin receptor-targeted anti-cancer therapy*. *Curr Drug Deliv*, 2011. **8**(1): p. 2-10.
2. Lelle, M., et al., *Octreotide-Mediated Tumor-Targeted Drug Delivery via a Cleavable Doxorubicin-Peptide Conjugate*. *Mol Pharm*, 2015. **12**(12): p. 4290-300.
3. Nadas, J. and D.X. Sun, *Anthracyclines as effective anticancer drugs*. *Expert Opinion on Drug Discovery*, 2006. **1**(6): p. 549-568.
4. Dean, M., Y. Hamon, and G. Chimini, *The human ATP-binding cassette (ABC) transporter superfamily*. *Journal of Lipid Research*, 2001. **42**(7): p. 1007-1017.
5. Leslie, E.M., R.G. Deeley, and S.P.C. Cole, *Multidrug resistance proteins: role of P-glycoprotein, MRP1, MRP2, and BCRP (ABCG2) in tissue defense*. *Toxicology and Applied Pharmacology*, 2005. **204**(3): p. 216-237.
6. Rappe, C. and Andersso.K, *Favorsky Rearrangements .15. Products and by-Products from Rearrangement of Tetrahalo Ketones*. *Acta Chemica Scandinavica*, 1969. **23**(8): p. 2839-&.

7 Experimental part

7.1 General methods

7.1.1 Chemicals and solvents

Solvents, chemicals and reagents were bought from commercial sources (Acros Organics, Alfa Aesar, AppliChem, ABCR, Deutero, Fisher Scientific, Fluka, Merck, Rapp Polymere and Sigma Aldrich) and used without further purification. Doxorubicin hydrochloride and octreotide diacetate were purchased from Ontario Chemicals, Inc. (Guelph, Ontario, Canada). Cell viability was determined using CellTiter-Glo® Assay (Promega Corporation) according to the manufacturer's instructions. WST-1 colorimetric cell viability assay was ordered from Roche Molecular Biochemicals (Mannheim, Germany).

5' labelled oligo DNA with Cy5 (12 bp DNA: sequence 5' - CGCGCGCGCGCG - 3', 36 bp DNA: 5'-TCGACCGTTCTGCCACGTGATATCTGAGTCAGCTTA - 3') was purchased by the company Thermo Fisher Scientific GmbH. Labeled siRNA was provided by the group of Prof. Dr. Helm (JGU Mainz).

7.1.2 Chromatography

Preparative column chromatography was performed on silica gel from Macherey Nagel with a grain size of 0.063 – 0.200 mm (silica gel) or 0.04 – 0.063 (flash silica gel).

For analytical thin layer chromatography (TLC), silica gel coated aluminum foils (ALUGRAM® SIL G/UV₂₅₄) were used. Compounds were detected by fluorescence quenching at 254 nm, self-fluorescence at 366 nm and staining with potassium permanganate or ninhydrin. For eluents, analytically pure solvents (p.a. or technical grade) were distilled prior to use. Corresponding mix ratios of the solvents are listed in the synthesis part.

7.1.3 Inert Atmosphere

Oxygen or moisture sensitive reactions were carried out under argon atmosphere (grade 4.8, Westfalen AG). Reactions were degassed by purging a stream of argon through the reaction mixture.

7.2 Analytical Techniques

7.2.1 RP-HPLC

RP-HPLC was conducted on a Jasco LC-2000Plus system (Groß-Umstadt, Germany), with appropriate diode array detector (MD-2015), solvent delivery pumps (PU-2086) and columns. Analytical RP-HPLC was carried out with a ReproSil 100 C18 (250 x 4.6 mm) column from Jasco with 5 μm particle size as a stationary phase and a flow rate of 1 ml/min. Purification of the products was performed on a Jasco ReproSil 100 C18 (250 x 20 mm) column with a flow rate of 15 ml/min and 5 μm silica as stationary phase. The applied eluents were 25 mM triethylammonium acetate buffer (pH 7) [A] and acetonitrile [B] with a linear gradient.

RP-HPLC-MS studies were conducted on a Jasco LC- 2000Plus System and analyzation was performed with an Agilent 1290 UHPLC system equipped with a Agilent 6490 triple quadrupole mass spectrometer.

7.2.2 Mass spectrometry

Matrix-assisted laser desorption ionization time-of-flight (MALDI-TOF) mass spectrometry was performed on a Bruker Reflex II TOF spectrometer equipped with a 337 nm nitrogen laser. 2,5-Dihydroxybenzoic acid or α -cyano-4-hydroxycinnamic acid (peptidic sample) were utilized as matrix.

FD mass spectra were obtained on a VG Instruments ZAB 2-SE-FPD (8 kV) spectrometer and electrospray ionization (ESI) mass spectrometry was carried out on a Waters/Micromass QToF Ultima spectrometer.

7.2.3 NMR spectroscopy

The NMR experiments were performed on an Bruker Avance III 250, AMX 300, Bruker DRX 500, Bruker Avance III 700 and Bruker WB 850 (Bruker Avance III) spectrometer, as well as on an Avance-III 600 MHz spectrometer (Bruker, Rheinstetten, Germany) equipped with a TCI cryoprobe using standard pulse sequences from the Bruker library provided with TopSpin 3.5 pl2. For DOSY experiments an Avance-III HD 400 MHz (Bruker, Rheinstetten, Germany) equipped with a BBFO-Smart probe was used. The ^1H and ^{13}C chemical shifts were referenced to the residual solvent signal (DMSO- d_6 : $\delta\text{H} = 2.50$ ppm, DMSO- d_6 : $\delta\text{C} =$

39.52 ppm), (CD_2HOD : $\delta\text{H} = 3.31$ ppm, CD_3OD : $\delta\text{C} = 49.00$ ppm) and the ^{15}N chemical shifts are given relative to liquid ammonia ($\text{NH}_3(\text{aq})$: $\delta\text{N} = 0.0$ ppm). Coupling constants (J) are given in Hz.

7.2.4 Microscale Thermophoresis

Measurements were performed on a NanoTemper Monolith NT.115 instrument using the red filter (absorption: 600-650 nm, emission: 675 – 690 nm) for excitation and detection of fluorescence. The measurement was performed in standard capillaries at different LED and IR-Laser intensities with Laser-On time 30 sec between Laser-Off time 5 sec in the beginning and the end. To determine the affinity of a binding reaction, a titration series of one binding partner was performed while the fluorescent binding partner (siRNA or labeled DNA) was kept at a constant concentration.

Binding of the polymer particles to fluorescently labeled siRNA was quantified in phosphate buffered saline (PBS, pH 7.4, purchased from life TechnologiesTM). The ratio of polymer-particle to siRNA was varied from 1 to 250. After mixing both components the samples were incubated for 20 minutes at ambient temperature for complexation.

Binding of doxorubicin and doxorubicin-derivatives to Cy5-labeled DNA was quantified in a special prepared buffer (50 mM TRIS Puffer (pH 6.5), 15 mM sodium chloride, 10 mM magnesium chloride, 0.05 % Tween 20).

Analysis and fitting of the detected signals was performed with the software NT Analysis 1.4.27 based on the theoretic calculations described by Jerabek-Willemsen *et al.* and Baaske *et al.*^[3, 4]

7.2.5 SDS-PAGE

SDS-PAGE was carried out with NuPAGE[®] Novex[®] 16 % Tricine Gels (1.0 mm, 12 well) and NuPAGE Tricine SDS Buffer Kit from Invitrogen. Appropriate staining of the peptide bands upon SDS-PAGE was accomplished with Coomassie Brilliant Blue and a 5% - barium iodine solution as well as 0.1 M iod solution was used for PEG staining. The obtained bands were compared to the Kaleidoscope Prestained Standard (Catalog number 161-0324) and the polypeptide SDS-PAGE Molecular Weight Standard (Catalog Number 161-0326).

7.2.6 Circular dichroism spectroscopy

The ECD and UV spectra were recorded on a J-815 circular dichroism spectropolarimeter (Jasco, Tokyo, Japan) using a quartz glass cuvette with a path length of 1 mm and a spectral range of 300–180 nm. The scan speed was set to 20 nm/min and the number of repetitions to 8. An aqueous 10 mM phosphate buffer at pH 7.6 was used as solvent during all measurements. The concentration was about 0.08 mmol/L. The baseline was corrected by subtraction of a solvent spectrum obtained with the same parameters.

7.2.7 pH dependent cleavage studies

A 0.5 mM solution of the dye or doxorubicin conjugate either in Dulbecco's phosphate-buffered saline (DPBS) or in a phosphate buffer with pH 5 was incubated at 37 °C in an Eppendorf Thermomixer compact (300 rpm). The stability of the conjugate was monitored by RP-HPLC on a Jasco LC - 2000Plus System for 24 h. The degradation products were analyzed by comparison with reference compounds.

7.2.8 GPC

All polymers were characterized using gel permeation chromatography (GPC) with dimethylformamide (DMF) as eluent. GPC in DMF was performed at 60°C. The columns used were PSS GRAM 100 and PSS GRAM 1000 (particle size: 10 µm, porosity: 100 and 1000 Å, PSS Mainz). A refractive index detector (SECurity RID, PSS) and a UV Detector (SECurity VWD, wavelength: 270 nm, PSS) were used to detect the polymer. Molecular weights were calculated using a calibration performed with PEO standards (Polymer Standards Services GmbH, Mainz).

7.2.9 Cell cultures

Human pancreatic carcinoma cells MIA PaCa-2 were purchased from DSMZ (German Collection of Microorganisms and Cell Cultures, Braunschweig, Germany) and cultured in Dulbecco's Modified Eagle Medium (DMEM) supplemented with 10% heat-inactivated fetal bovine serum (FBS), 2.5% heat-inactivated horse serum and 1% Penicillin/Streptomycin antibiotics (**Life Technologies**, Darmstadt, Germany). The human lung carcinoma cells A549

(ATCC CCL-185) were grown in F-12K medium (Kaighn's modification of Ham's F-12 medium) supplemented with 10% fetal calf serum (FCS) and 100 units/mL penicillin as well as

100 µg/mL streptomycin. Cells did not exceed passage 14 and were cultured in DMEM supplemented with 10% FCS, 2 mM glutamine and 10^5 IU/l Penicillin-Streptomycin. The above-mentioned cells were maintained at 37°C and 5% CO₂ in a humidified incubator and were subcultured every 3-4 days with 0.25% trypsin. Cell culture materials were from Life Technologies, Nunc and Sigma Aldrich.

7.2.10 Cell viability assay

The cytotoxic effects of doxorubicin, octreotide and the hybrid on MIA PaCa-2 and A549 cells were investigated with the CellTiter-Glo cell proliferation assay according to manufacturer's instructions. Briefly, cells were seeded into 96-well plates with a density of 3×10^3 cells per well in 100 µl medium and incubated to allow attachment. After 24 h the medium was removed and Doxorubicin or the Doxorubicin derivative was added at various concentrations from 0.1-50 µM in 100 µl serum free medium. The cells were incubated for 24 h and 72h with the drugs added directly into the cell culture medium. Cell viability was determined 24h and 72h after treatment with the compounds based on quantitation of ATP by the CellTiter-Glo luminescent cell viability assay. The evolved luminescence was measured on a Tecan plate reader (Grödig, Austria) to quantify the viability of the cells in each well. Wells without drug treatment were used to obtain 100% cell viability and blank wells with medium only were subtracted from sample wells and control cells. Drug concentrations were transformed into a logarithmic scale prior to analysis and the obtained data from the survival curves were expressed as IC₅₀ values in µM. Every experiment was performed in independent triplicates. The viability of AtT-20 cells was determined in a similar manner 72 h after treatment with the compounds using the WST-1 colorimetric assay at 450 nm (Roche Molecular Biochemicals).

7.2.11 Fluorescence Microscopy

For fluorescence microscopy imaging, cells were seeded at a concentration of 1×10^4 cells per well in 200 μL of cell culture medium without phenol red and grown for 24 h. 8-well chambered cover glasses with a polymer bottom were used (μ -Slide 8 Well, IbiTreat, ibidi). A 1 mM solution of the respective compound was prepared in DMSO and diluted to the indicated concentration. Stock solutions were prepared direct prior being used.

The subcellular localization of the respective conjugate was tested in different cell lines with live cells at 37°C and 5% CO_2 . Widefield images were obtained with a 60x/1.4 oil immersion objective on an inverse Olympus microscope (IX70) using following filters: for perylene monoimide derivatives - BP 628/40, BP 692/40.

Fluorescence confocal laser scanning microscopy (CLSM) images were acquired with a TCS SP5 (Leica) equipped with a 63x/1.4 and 100x/1.4 oil objective and an incubation chamber for live cell imaging (37°C, 5 % CO_2). The respective PMI conjugate was excited by an argon laser at $\lambda_{ex} = 633$ nm (power set to 10 %) and the emission range was set to $\lambda_{em} = 680$ -760 nm. Dox-containing conjugate was excited at 488 nm (power set to 15 %) and the emission range was set to $\lambda_{em} = 540$ -640 nm. Staining of the nucleus was obtained via DRAQ5 (2.5 μM final concentration, Thermo Fisher Scientific) excited with HeNe laser (633 nm, power set to 15 %) and detected at 680-760.

7.2.12 Determination of adrenocorticotrophic hormone (ACTH) secretion

The ACTH secretion of AtT-20 cells was determined by a radioimmunoassay as previously described by Stalla *et al.*, and the obtained values were normalized with the cell viability results from the WST-1 assay. The ACTH antisera were produced in rabbits using a synthetic βM -23-corticotropin-amide-bovine thyroglobulin conjugate. For the ACTH RIA, we used the antibody AC2-VII with a working dilution of 1:10.000. As tracer we used ACTH 1-39 (Bachem) labeled with 125J (PerkinElmer, Waltham, MA) with the chloramine-T method. One-hundred microliters of the diluted supernatants were incubated with 100 μL of the primary antibody plus 100 μL of tracer (20.000 cpm/100 μL) for 24 h at +4 °C. The day after, 100 μL of secondary goat antirabbit (1:50, Upstate) was added and incubated for 1 h at room temperature. After washing with 6% polyethylene glycol 6000 (Merck) twice, radioactivity was measured in the gamma counter (PerkinElmer, Waltham, MA). Final ACTH values are presented as (pg/mL)/OD450 nm.

7.2.13 Computational details

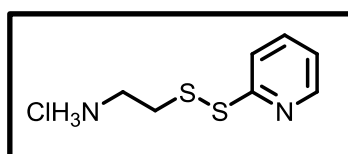
The UFF, AM1 and PM6 calculations were performed using Gaussian 09 (Rev. D.01).¹ DFT calculations were performed using the Orca 3.0.3 program package.² The B3LYP³ and B2GP-PLYP⁴ functionals were used together with the def2-TZVPP or def2-QZVPP basis sets, respectively.⁵ The RIJCOSX approximation was used in combination with the corresponding auxiliary basis sets.⁶ The D3BJ empirical dispersion correction was included.⁷ Tight SCF and geometry optimization convergence criteria were used together with the following grid settings: Grid4 FinalGrid5 GridX4. The one- and two-dimensional surface scans were performed using step sizes of 10° for the corresponding dihedral angles. The stationary points were reoptimized without constraints and identified as local minima by calculation of the full exact hessian (yielding no imaginary frequency).

7.3 Organic synthesis

7.3.1 Compounds part 3:

2-(2-pyridyldithio)ethylamine hydrochloride

(3-2)



2,2-Dithiodipyridine (2 g, 17.61 mmol) was dissolved in 50 ml methanol and degassed in an ultrasonic bath for 30 minutes. To this solution 2-mercaptoethylamine hydrochloride (23 g, 105.63 mmol, **3-1**) was slowly added within one hour. Afterwards, the flask was sealed with a septum and the reaction mixture was stirred overnight at room temperature under argon. The yellow solution was precipitated twice in cold diethyl ether and the product was obtained as a colorless crystalline solid.

Yield

3.92 g, 17.61 mmol, quantitative yield

MS

m/z (MALDI-TOF) 187.00 [M+H]⁺;

¹H-NMR (300 MHz, DMSO-*d*₆, 298 K)

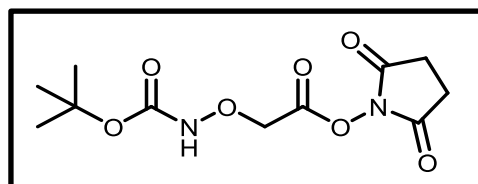
δ (ppm) = 8.56-8.46 (m, 1H), 8.30 (s, 3H), 7.88-7.80 (m, 1H), 7.76 (d, 1H), 7.34-7.25 (m, 1H), 3.17-3.01 (m, 4H);

¹³C-NMR (75 MHz, DMSO-*d*₆, 298 K)

δ (ppm) = 158.09, 149.80, 137.89, 121.59, 120.00, 37.65, 34.74

2,5-Dioxopyrrolidin-1-yl-2-(tert-butoxycarbonyl)aminoxyacetat

(3-4)



Initially, a slurry of *N*-hydroxysuccinimide (189.62 mg, 1.65 mmol) and (*Boc*-aminoxy)acetic acid (300 mg, 1.57 mmol, **3-3**) in 10 ml dry dichloromethane (DCM) was prepared. Under argon *N,N'*-diisopropylcarbodiimide (22.74 mg, 282,56 μ l, 1.80 mmol) was added and the clear solution was stirred for 4 h. Afterwards, the precipitated urea was filtered off and washed with a small amount of DCM. The obtained solution was diluted with 100 ml DCM and washed four times with brine. The organic layer was dried with magnesium sulfate and the solvent was removed *in vacuo* to obtain the product as a colorless solid.

Yield

0.420 mg, 1.46 mmol, 93%

MS

m/z (MALDI-TOF) 357.04 $[M+3Na]^+$

¹H-NMR (300 MHz, DMSO-*d*₆, 298 K)

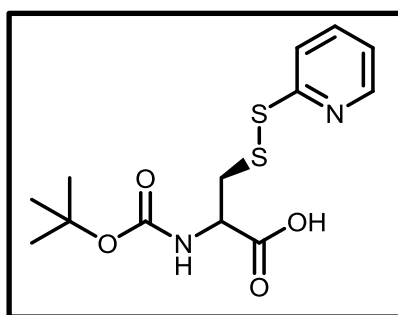
δ (ppm) = 10.36 (s, 1H), 4.82 (s, 2H), 2.84 (s, 4H), 1.42 (s, 9H)

¹³C-NMR (75 MHz, DMSO-*d*₆, 298 K)

δ (ppm) = 169.95, 165.14, 156.57, 80.60, 69.90, 27.93, 25.47

N-(*tert*-butoxycarbonyl)-*S*-(pyridin-2-ylthio)cysteine

(3-6)



2,2-Dithiodipyridine (11.95 g, 54.23 mmol) was dissolved in 50 ml methanol and degassed in an ultrasonic bath for 30 minutes. To this solution *Boc*-cysteine (2 g, 9.04 mmol, **3-5**) was slowly added within one hour. Afterwards, the flask was sealed with a septum and the reaction mixture was stirred overnight at room temperature under argon. Afterwards the solvent was removed *in vacuo*, the yellow oil was again dissolved in acetone and precipitated three times in cold hexane. The product was obtained as a colorless crystalline solid.

Yield

2.99 g, 9.04 mmol, quantitative yield

MS

m/z (ESI-TOF) 331.4 $[M+H]^+$, 353.8 $[M+Na]^+$, 369.1 $[M+K]^+$

 1H -NMR (300 MHz, DMSO- d_6 , 298 K)

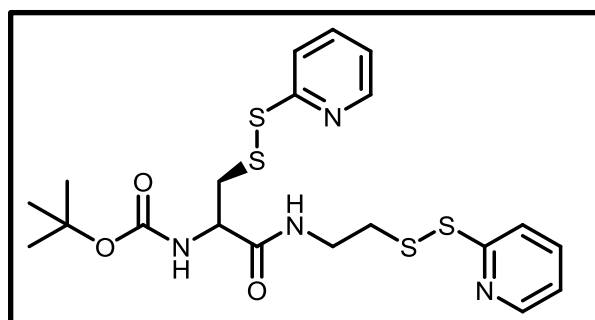
δ (ppm) = 12.88 (s, 1H), 8.47 (d, 2H), 7.78 (m, 3H), 7.39 (d, 2H), 7.25 (m, 2H), 4.16 (m, 1H), 3.13 (m, 2H), 1.39 (s, 9H)

 ^{13}C -NMR (75 MHz, DMSO- d_6 , 298 K)

δ (ppm) = 172.16, 158.76, 155.35, 149.16, 137.79, 121.26, 119.31, 78.33, 52.73, 39.97, 28.15

tert-butyl (1-oxo-3-(pyridin-2-yl)disulfanyl)-1-((2-(pyridin-2-yl)disulfanyl)ethyl)amino)propan-2-yl)carbamate

(3-7)



The Boc protected cysteine derivative (2 g mg, 6.05 mmol, **3-6**), *N,N,N,N*-tetramethyl-*O*-(*N*-succinimidyl)uronium tetrafluoroborate (2 g, 6.86 mmol) and **3-2** (1.47 g, 6.86 mmol) were dissolved in 20 ml dry *N,N*-dimethylformamide (DMF). *N,N*-diisopropylethylamine (DIPEA) (4.22 ml, 24.21 mmol) was added and the solution was stirred in an argon atmosphere for 4 h at room temperature. Subsequently, 350 ml ethyl acetate was added and the solution was washed three times with brine. The organic layer was dried with magnesium sulfate and the solvent was removed *in vacuo*. Afterwards, the residue was purified by silica gel column chromatography (ethyl acetate) to obtain the product as yellow oil.

Yield

2.62 g, 5.25 mmol, 86%

MS

m/z (ESI-TOF) 499.13 $[M+H]^+$, 521.11 $[M+Na]^+$, 537.08 $[M+K]^+$

m/z (HR ESI-TOF) 499.0987 $[M+H]^+$ (calc. 499.0966)

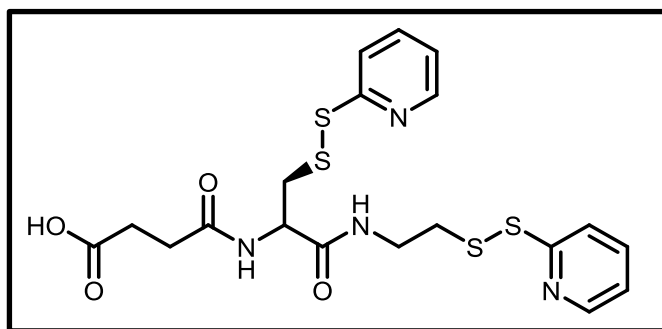
¹H-NMR (500 MHz, DMSO-*d*₆, 298 K)

δ (ppm) = 8.48 – 8.44 (m, 2H), 8.27 (t, J = 5.8 Hz, 1H), 7.83 – 7.78 (m, 2H), 7.77 – 7.60 (m, 2H), 7.30 – 7.26 (m, 1H), 7.24 (ddt, J = 7.2, 4.7, 1.5 Hz, 2H), 4.16 (m, J = 8.7, 4.6 Hz, 1H), 3.37 (m, J = 12.9, 6.6 Hz, 1H), 3.29 (m, J = 13.4, 6.4 Hz, 1H), 3.14 (dd, J = 13.4, 4.8 Hz, 1H), 3.08 – 2.99 (m, 1H), 2.92 – 2.84 (m, 2H), 1.37 (d, 9H)

¹³C-NMR (125 MHz, DMSO-*d*₆, 298 K)

δ (ppm) = 170.09, 158.99, 157.33, 155.22, 149.65, 137.95, 121.82, 119.34, 78.44, 53.66, 40.94, 37.89, 37.26, 28.17.

4-oxo-4-((1-oxo-3-(pyridin-2-yl)disulfanyl)-1-((2-(pyridin-2-yl)disulfanyl)ethyl)amino)propan-2-yl)amino)butanoic acid

(3-9)

The modified Boc-cysteine derivate (500 mg, 1,00 mmol, **3-7**) was dissolved in 10 ml dry DCM and 5 ml of trifluoroacetic acid (TFA) was added. This solution was stirred for 1 h at room temperature followed by removal of solvent and reagent under reduced pressure. The obtained oil was dissolved in 5 ml dry NMP and consecutively DIPEA (776.09 mg, 1.05 ml, 6 mmol) and succinic anhydride (600.9 mg, 6 mmol) was added. Subsequently, the reaction mixture was stirred under argon for 2 h at room temperature. Afterwards, the solution was diluted with 250 ml ethyl acetate, washed three times with brine and dried over magnesium sulfate. The solvent was removed *in vacuo* to obtain the product as yellow oil.

Yield

341 mg, 683.85 μ mol, 68%

MS

m/z (MALDI-TOF) 520.82 $[M+Na]^+$, 542.77 $[M+2Na]^+$

¹H-NMR (500 MHz, DMSO-*d*₆, 298 K)

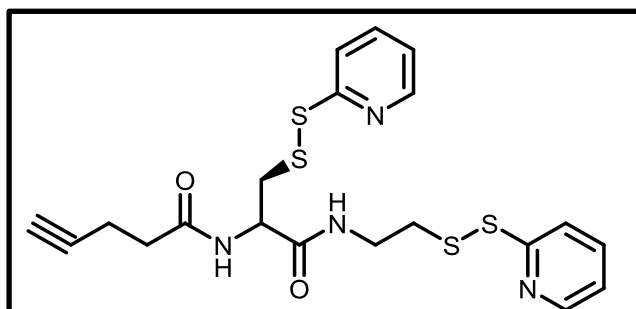
δ (ppm) = 12.15 (s, 1H), 8.52 – 8.43 (m, 2H), 8.36 (d, J = 8.0 Hz, 1H), 8.23 (t, J = 5.7 Hz, 1H), 7.81 (m, J = 9.8, 7.1, 4.7, 2.1 Hz, 2H), 7.75 (m, J = 8.1, 4.7, 1.1 Hz, 2H), 7.31 – 7.21 (m, 2H), 4.47 (td, J = 8.0, 5.2 Hz, 1H), 3.34 (m, 1H), 3.21 – 3.13 (m, 1H), 3.04 – 2.96 (m, 1H), 2.88 (m, 1H), 2.49 – 2.40 (m, 4H)

¹³C-NMR (125 MHz, DMSO-*d*₆, 298 K)

δ (ppm) = 173.57, 171.31, 169.74, 159.00, 149.56, 137.82, 121.16, 119.25, 52.09, 40.71, 38.06, 37.12, 28.78, 28.65

***N*-(1-oxo-3-(pyridin-2-yl)disulfanyl)-1-((2-(pyridin-2-yl)disulfanyl)ethyl)amino)propan-2-yl)pent-4-ynamide**

(3-10)



The modified Boc-cysteine derivative (100 mg, 200.52 μ mol, **3-7**) was dissolved in 10 ml dry DCM and 5 ml of trifluoroacetic acid (TFA) was added. This solution was stirred for 1 h at room temperature followed by removal of solvent and reagent under reduced pressure. The obtained oil was dissolved in 2 ml dry DMF and consecutively added to a solution of DIPEA (31.62 mg, 42.61 μ l, 244.65 μ mol), HATU (77.32 mg, 203.87 μ mol) and 4-pentynoic acid (20 mg, 203.87 μ mol) in 3 ml DMF. Subsequently, the reaction mixture was stirred under argon for 2 h at room temperature. Afterwards, the solution was diluted with 250 ml ethyl acetate, washed three times with brine and dried over magnesium sulfate. The solvent was removed *in vacuo* and the residue was purified by silica gel column chromatography (ethyl acetate) to obtain the product as yellow oil.

Yield

85 mg, 177.58 μ mol, 87%

MS

m/z (MALDI-TOF) 479.69 $[M+H]^+$, 501.65 $[M+Na]^+$

¹H-NMR (500 MHz, DMSO-*d*₆, 298 K)

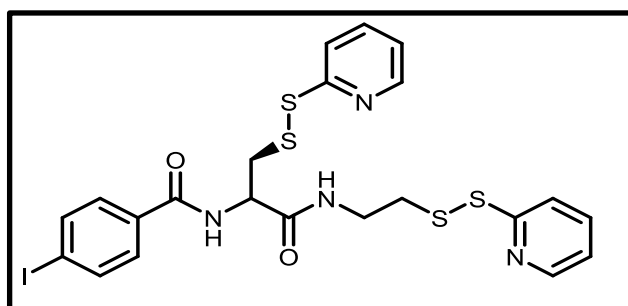
δ (ppm) = 8.48 – 8.43 (m, 2H), 8.37 (d, J = 8.1 Hz, 1H), 8.30 (t, J = 5.7 Hz, 1H), 7.81 (m, J = 8.1, 7.3, 3.1, 1.8 Hz, 2H), 7.75 (m, J = 8.1, 2.8, 1.0 Hz, 2H), 7.24 (ddd, J = 7.3, 4.8, 1.1 Hz, 2H), 4.50 (td, J = 8.4, 5.4 Hz, 1H), 3.39 – 3.34 (m, 1H), 3.16 (dd, J = 13.4, 5.3 Hz, 1H), 2.99 (dd, J = 13.4, 8.6 Hz, 1H), 2.88 (t, J = 6.9 Hz, 2H), 2.76 (q, J = 1.6, 1.1 Hz, 1H), 2.37 – 2.33 (m, 4H)

¹³C-NMR (125 MHz, DMSO-*d*₆, 298 K)

δ (ppm) = 170.48, 169.62, 158.97, 149.59, 137.80, 121.19, 119.24, 71.34, 51.94, 40.70, 38.03, 37.14, 34.02, 14.02.

4-iodo-*N*-(1-oxo-3-(pyridin-2-yl)disulfanyl)-1-((2-(pyridin-2-yl)disulfanyl)ethyl)amino)propan-2-yl)benzamide

(3-11)



The modified Boc-cysteine derivate (105 mg, 210.55 μ mol, **3-7**) was dissolved in 10 ml dry DCM and 5 ml of trifluoroacetic acid (TFA) was added. This solution was stirred for 1 h at room temperature followed by removal of solvent and reagent under reduced pressure. The obtained oil was dissolved in 2 ml dry DMF and consecutively added to a solution of DIPEA (34.39 mg, 46.35 μ l, 266.11 μ mol), HATU (96.72 mg, 255.02 μ l) and 4-iodobenzoic acid (55 mg, 221.76 μ mol) in 3 ml DMF. Subsequently, the reaction mixture was stirred under argon for 2 h at room temperature. Afterwards, the solution was diluted with 250 ml ethyl acetate, washed three times with brine and dried over magnesium sulfate. The solvent was removed *in vacuo* and the residue was purified by silica gel column chromatography (ethyl acetate) to obtain the product as yellow oil.

Yield

110 mg, 175 μ mol, 79%

MS

m/z (MALDI-TOF) 627.04 [M+H]⁺, 649.02 [M+Na]⁺

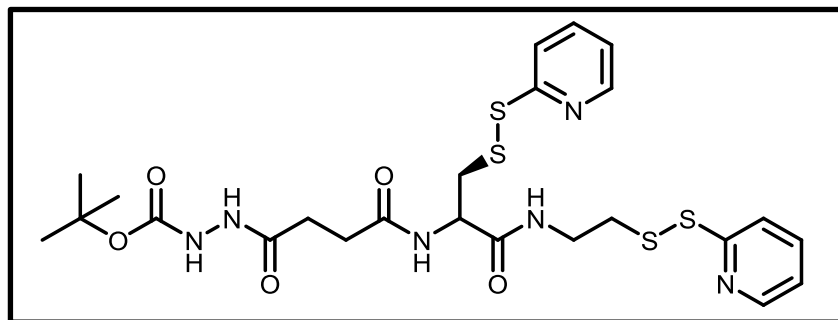
¹H-NMR (500 MHz, DMSO-*d*₆, 298 K)

δ (ppm) = 8.85 (d, *J* = 8.0 Hz, 1H), 8.51 – 8.39 (m, 2H), 8.37 (t, *J* = 5.7 Hz, 1H), 7.96 – 7.86 (m, 2H), 7.83 – 7.77 (m, 1H), 7.76 – 7.71 (m, 2H), 7.70 – 7.60 (m, 2H), 7.31 – 7.16 (m, 2H), 4.68 (m, *J* = 9.9, 7.9, 4.6 Hz, 1H), 3.31 – 3.26 (m, 1H), 3.23 – 3.13 (m, 1H), 2.93 – 2.85 (m, 2H)

¹³C-NMR (125 MHz, DMSO-*d*₆, 298 K)

δ (ppm) = 169.71, 165.82, 158.94, 149.56, 137.76, 137.13, 133.23, 129.50, 121.18, 119.26, 99.16, 52.72, 40.29, 38.11, 37.16

tert-butyl 2-(4-oxo-4-((1-oxo-3-(pyridin-2-yl)disulfanyl)-1-((2-(pyridin-2-yl)disulfanyl)-ethyl)amino)propan-2-yl)amino)butanoyl)hydrazine-1-carboxylate

(3-12)

Compound **3-9** (300 mg, 601.63 μmol) was dissolved in 3 ml of dry DMF and flushed with argon. DIPEA (93.31 mg, 125.75 μl, 721.95 μmol) was added dropwise and the reaction solution was stirred for 5 minutes. Afterwards HATU (1-[Bis(dimethylamino)methylene]-1H-1,2,3-triazolo[4,5-b]pyridinium 3-oxid hexafluorophosphate, 273.46 mg, 691.87 μmol), dissolved in 2 ml of dry DMF, was added dropwise and stirring was continued for 10 min until tert-butyl carbazate (87.46 mg, 661.79 μmol) was added. Subsequently the reaction mixture was stirred under argon for 1.5 h at room temperature. Afterwards, the solution was diluted with 250 ml ethyl acetate, washed three times with brine and dried over magnesium sulfate. The solvent was removed *in vacuo* and the residue was purified by silica gel column chromatography (ethyl acetate) to obtain the product as yellow oil.

Yield

312 mg, 509.14 μmol, 85%

MS

m/z (ESI-TOF) 613.16 [M+H]⁺; 635.14 [M+Na]⁺

m/z (HR ESI-TOF) 613.1395 [M+H]⁺ (calc. 613.1390)

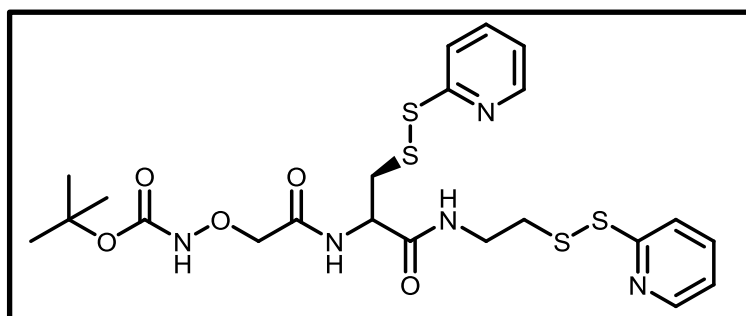
¹H-NMR (700 MHz, DMSO-*d*₆, 298 K)

δ (ppm) = 9.58 (s, 1H), 8.69 (d, J = 9.1 Hz, 1H), 8.45 (d, J = 4.8 Hz, 2H), 8.40 (d, J = 8.0 Hz, 1H), 8.26 (t, J = 5.6 Hz, 1H), 7.81 (tt, J = 7.5, 2.5 Hz, 2H), 7.74 (dd, J = 8.1, 3.3 Hz, 2H), 7.23 (dd, J = 7.6, 4.6 Hz, 2H), 4.45 (m, J = 9.8, 9.1, 5.1 Hz, 1H), 3.37 (s, 2H), 3.20 – 3.13 (m, 1H), 3.00 (dd, J = 13.4, 9.0 Hz, 1H), 2.89 (s, 2H), 2.33 (d, J = 34.3 Hz, 4H), 1.39 (s, 9H)

¹³C-NMR (176 MHz, DMSO-*d*₆, 298 K)

δ (ppm) = 171.77, 170.24, 159.51, 150.00, 138.23, 121.63, 119.74, 79.50, 52.57, 51.82, 41.07, 38.58, 37.52, 28.52

tert-butyl (2-oxo-2-((1-oxo-3-(pyridin-2-yl)disulfanyl)-1-((2-(pyridin-2-yl)disulfanyl)ethyl)amino)propan-2-yl)amino)ethoxy)carbamate

(3-13)

The modified Boc-cysteine derivative (200 mg, 401.05 μ mol, **7**) was dissolved in 10 ml dry DCM and the identical amount of trifluoroacetic acid (TFA) was added. This solution was stirred for 1 h at room temperature followed by removal of solvent and reagent under reduced pressure. The obtained oil was dissolved in 5 ml dry DMF and consecutively DIPEA (257.8 mg, 347.4 μ l, 1.99 mmol) and the NHS-BOC-aminoxyacetic acid (138 mg, 478.7 μ mol, **3-4**) were added. Subsequently, the reaction mixture was stirred under argon for 3 h at room temperature. Afterwards, the solution was diluted with 250 ml ethyl acetate, washed three times with brine and dried over magnesium sulfate. The solvent was removed *in vacuo* and the residue was purified by silica gel column chromatography (ethyl acetate) to obtain the product as yellow oil.

Yield

115 mg, 201.1 μ mol, 50%

MS

m/z (ESI-TOF) 572.14 $[M+H]^+$; 594.12 $[M+Na]^+$; 1165.25 $[2M+Na]^+$;

m/z (HR ESI-TOF) 572.1130 $[M+H]^+$ (calc. 572.1124)

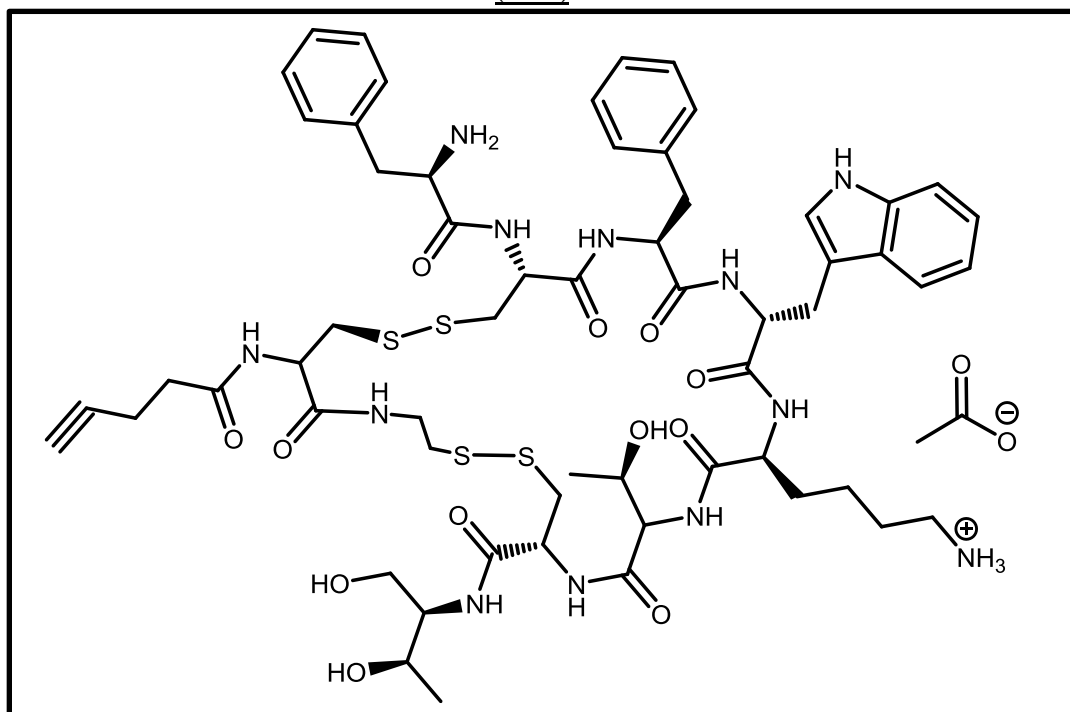
 $^1\text{H-NMR}$ (700 MHz, DMSO- d_6 , 298 K)

δ (ppm) = 10.31 (s, 1H), 8.45 (d, $J = 4.9$ Hz, 2H), 8.41 (t, $J = 5.7$ Hz, 2H), 7.81 (dddd, $J = 7.6, 5.5, 3.7, 1.9$ Hz, 2H), 7.74 (dd, $J = 8.0, 5.1$ Hz, 2H), 7.24 (dd, $J = 7.8, 4.6$ Hz, 2H), 4.58 (td, $J = 8.4, 5.0$ Hz, 1H), 4.31 – 4.15 (m, 2H), 3.35 (dp, $J = 26.7, 6.7$ Hz, 2H), 3.21 (dd, $J = 13.5, 5.2$ Hz, 1H), 3.03 (dd, $J = 13.6, 8.7$ Hz, 1H), 2.89 (t, $J = 6.8$ Hz, 2H), 1.40 (s, 9H)

 $^{13}\text{C-NMR}$ (176 MHz, DMSO- d_6 , 298 K)

δ (ppm) = 169.25, 168.20, 159.00, 156.89, 149.61, 137.82, 119.29, 80.67, 74.62, 51.48, 40.57, 38.12, 37.11, 27.98

4-((4R,10S,13R,16S,19R)-13-((1H-indol-3-yl)methyl)-19-((R)-2-amino-3-phenylpropanamido)-16-benzyl-4-(((2R,3R)-1,3-dihydroxybutan-2-yl)carbamoyl)-7-((R)-1-hydroxyethyl)-6,9,12,15,18,25-hexaoxo-24-(pent-4-ynamido)-1,2,21,22-tetrathia-5,8,11,14,17,26-hexaazacyclooctacosan-10-yl)butan-1-aminium acetate

(3-18)

Initially, octreotide acetate (28 mg, 25.94 μmol , **3-15**) was reduced under argon in a 4 ml phosphate buffer (pH 6.2) with *tris*(2-carboxyethyl)phosphine (TCEP) hydrochloride (29.75

mg, 103.77 μmol) for 60 min. The reduced peptide **3-17** was purified by RP-HPLC and the isolated fraction was added to **3-10** (25 mg, 52.23 μmol) dissolved in 10 ml DMF/phosphate buffer (1:1) – pH 7. Afterwards the reaction mixture was stirred for 1 h at room temperature in an argon atmosphere. Subsequently, the solution was purified by RP-HPLC and the solvent of the isolated fractions was removed *in vacuo*, whereby the product was obtained as a white solid.

Yield

51 mg, 38.13 μmol , 73%

MS

m/z (MALDI-TOF) 1278.23 $[\text{M}+\text{H}]^+$, 1300.22 $[\text{M}+\text{Na}]^+$

RP-HPLC

t_{R} = 30.89 min (280 nm),

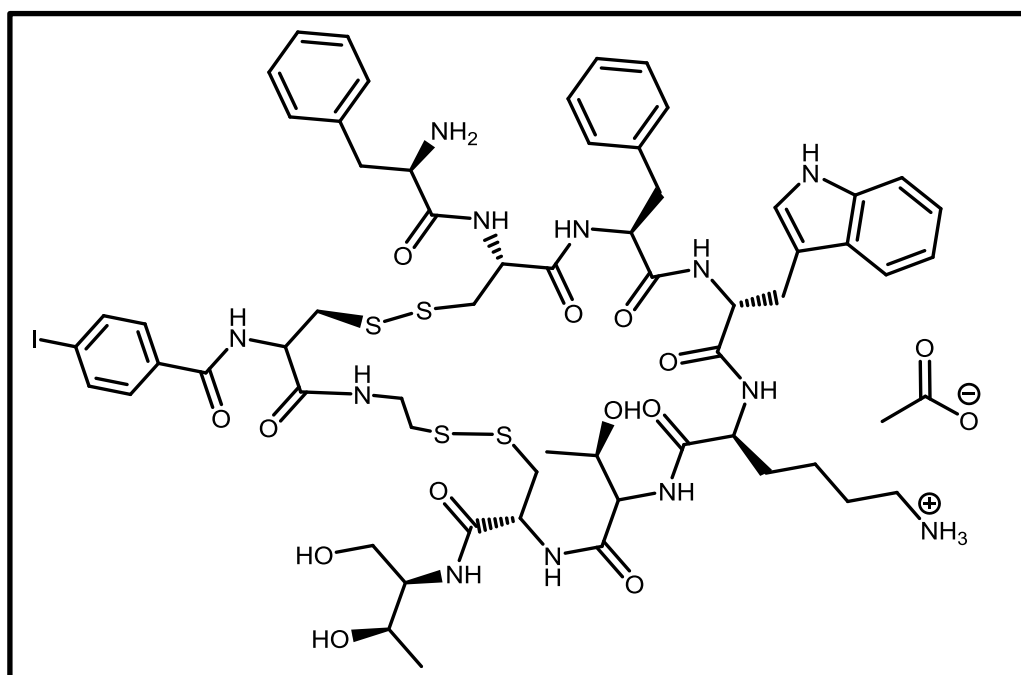
A: 25 mM triethylammonium acetate (TEAA) buffer (pH 7)

B: acetonitrile (ACN)

0 min 100% A – 40 min 30% A

4-((4R,10S,13R,16S,19R)-13-(((1H-indol-3-yl)methyl)-19-((R)-2-amino-3-phenylpropanamido)-16-benzyl-4-(((2R,3R)-1,3-dihydroxybutan-2-yl)carbamoyl)-7-((R)-1-hydroxyethyl)-24-(4-iodobenzamido)-6,9,12,15,18,25-hexaoxo-1,2,21,22-tetrathia-5,8,11,14,17,26-hexaazacyclooctacosan-10-yl)butan-1-aminium acetate

(3-19)



Initially, octreotide acetate (50 mg, 46.33 μmol , **3-15**) was reduced under argon in a 4 ml phosphate buffer (pH 6.2) with *tris*(2-carboxyethyl)phosphine (TCEP) hydrochloride (53.12 mg, 185.31 μmol) for 60 min. The reduced peptide **3-17** was purified by RP-HPLC and the isolated fraction was added to **3-11** (30 mg, 47.73 μmol) dissolved in 10 ml DMF/phosphate buffer (1:1) – pH 7. Afterwards the reaction mixture was stirred for 1 h at room temperature in an argon atmosphere. Subsequently, the solution was purified by RP-HPLC and the solvent of the isolated fractions was removed *in vacuo*, whereby the product was obtained as a white solid.

Yield

25 mg, 16.81 μmol , 35%

MS

m/z (MALDI-TOF) 1427.38 [M+H]⁺;) 1449.35 [M+Na]⁺

RP-HPLC

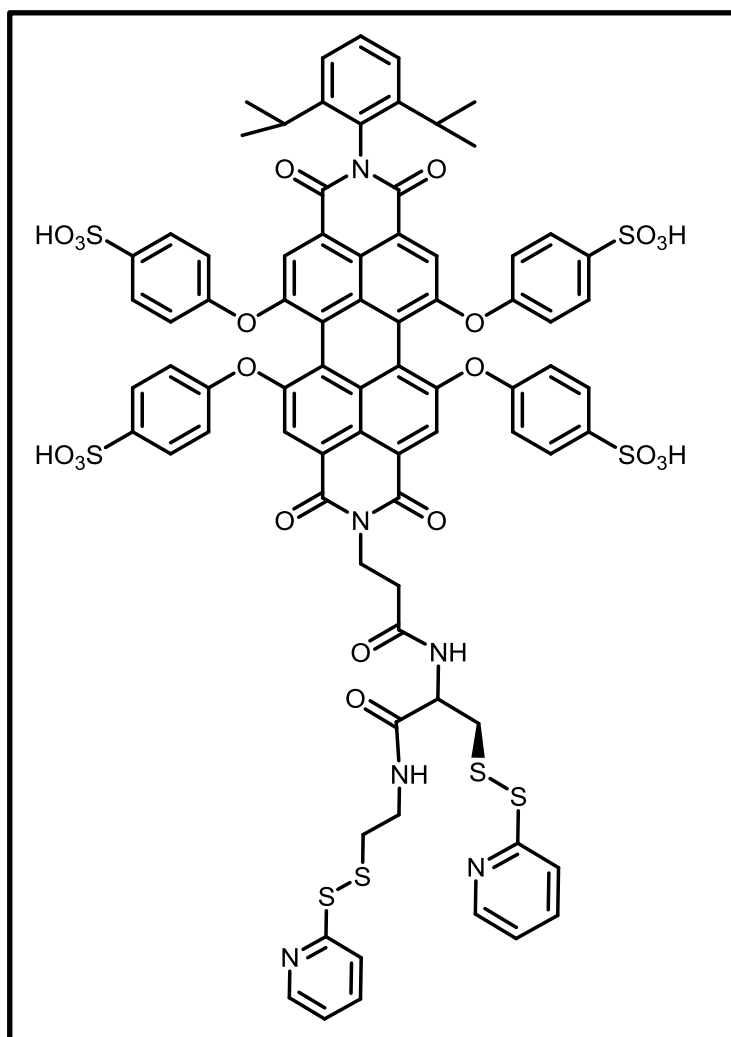
t_{R} = 35.00 min (280 nm)

A: 25 mM triethylammonium acetate (TEAA) buffer (pH 7)

B: acetonitrile (ACN)

0 min 100% A – 40 min 30% A

N-(2,6-diisopropylphenyl)-N'-((3-oxo-3-((1-oxo-3-(pyridin-2-yl)disulfaneyl)-1-((2-(pyridin-2-yl)disulfaneyl)ethyl)amino)propan-2-yl)amino)propyl)-1,6,7,12-tetra(4-sulfophenoxy)-perylene-3,4:9,10-tetracarboxydiimid
(3-22)



The modified Boc-cysteine derivate (21 mg, 41 μmol , **3-7**) was dissolved in 10 ml dry DCM and 5 ml of trifluoroacetic acid (TFA) was added. This solution was stirred for 1 h at room temperature followed by removal of solvent and reagent under reduced pressure. The obtained oil was dissolved in 2 ml dry DMF and consecutively added to a solution of DIPEA (22.18 mg, 29.89 μl , 171.59 μmol), HATU (15.62 mg, 41 μmol) and PDI-COOH (45 mg, 34.32 μmol , **3-22**) in 3 ml DMF. Subsequently, the reaction mixture was stirred under argon for 2 h at room temperature and was subsequently purified by reversed-phase high-performance liquid chromatography (RP-HPLC). The solvent of the isolated fractions was removed under reduced pressure, whereby the product was obtained as a violet solid.

Yield

61 mg, 29.09 μ mol, 85%

MS

m/z (ESI-TOF) 1691.21 [M+H]⁺,

m/z (HR ESI-TOF) 1691.1725 [M+H]⁺ (calc. 1691.1761)

¹H-NMR (500 MHz, DMSO-*d*₆, 298 K)

δ (ppm) = 8.87 (s, 5H), 8.41 (t, $J = 2.4$ Hz, 1H), 8.40 (d, $J = 4.0$ Hz, 1H), 8.37 (dd, $J = 4.8$, 1.7 Hz, 1H), 8.23 (t, $J = 5.7$ Hz, 1H), 7.89 (d, $J = 11.2$ Hz, 4H), 7.76 (td, $J = 7.8$, 1.9 Hz, 1H), 7.73 – 7.67 (m, 2H), 7.66 (d, $J = 8.5$ Hz, 4H), 7.62 – 7.59 (m, 4H), 7.41 (t, $J = 7.8$ Hz, 1H), 7.28 (d, $J = 7.8$ Hz, 2H), 7.18 (td, $J = 7.9$, 4.8 Hz, 2H), 6.99 (d, $J = 8.5$ Hz, 4H), 6.94 (d, $J = 8.3$ Hz, 4H), 4.41 (td, $J = 8.4$, 5.2 Hz, 1H), 4.21 (dq, $J = 24.9$, 6.7 Hz, 2H), 3.27 – 3.23 (m, 1H), 3.06 – 3.03 (m, 1H), 2.93 (dd, $J = 13.5$, 8.6 Hz, 1H), 2.81 (t, $J = 6.8$ Hz, 2H), 2.68 (p, $J = 6.8$ Hz, 2H), 2.54 (s, 1H), 1.01 (d, $J = 6.8$ Hz, 12H). TEAA: 21: 1.16 (t, 36H), 22: 3.09 (q, 24H), 23: 8.87 (s, 4H)

RP-HPLC

$t_R = 25.56$ min (560 nm),

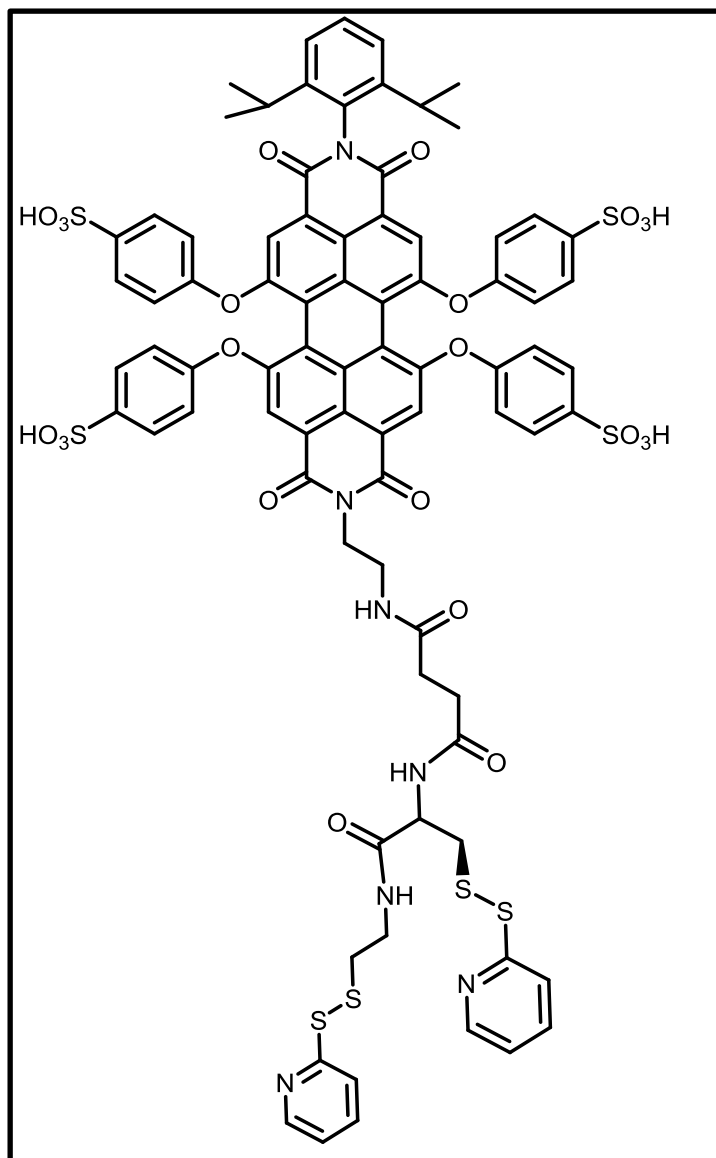
A: 25 mM triethylammonium acetate (TEAA) buffer (pH 7)

B: acetonitrile (ACN)

0 min 100% A – 40 min 30% A

N-(2,6-diisopropylphenyl)-N'-((3-oxo-3-((1-oxo-3-(pyridin-2-yl)disulfaneyl)-1-((2-(pyridin-2-yl)disulfaneyl)ethyl)amino)propan-2-yl)amino)propyl)-1,6,7,12-tetra(4-sulfophenoxy)-perylene-3,4:9,10-tetracarboxydiimide

(3-23)



The cysteine-acid derivative (35 mg, 70.19 μmol , **3-9**) was dissolved in 3 ml of dry DMF and flushed with argon. DIPEA (22.68 mg, 30.56 μl , 175.47 μmol) was added dropwise and the reaction solution was stirred for 5 minutes. Afterwards HATU (1-[Bis(dimethylamino)methylene]-1H-1,2,3-triazolo[4,5-b]pyridinium 3-oxid hexafluorophosphate, 31.94 mg, 84.22 μmol), dissolved in 2 ml of dry DMF, was added dropwise and stirring was continued for 10 min until the PDI-NH₂ dye (45 mg, 35.09 μmol , **3-21**) was added. Subsequently the reaction mixture was stirred under argon for 1 h at room temperature. Afterwards the solution was purified by RP-HPLC and the solvent of the isolated fractions was removed *in vacuo*, whereby the product was obtained as a violet solid.

Yield

68 mg, 29.83 μmol , 85%

MS

m/z (ESI-TOF) 1762.24 $[\text{M}+\text{H}]^+$

m/z (HR ESI-TOF) 1762.2080 $[\text{M}+\text{H}]^+$ (calc. 1762.2127)

$^1\text{H-NMR}$ (500 MHz, DMSO- d_6 , 298 K)

δ (ppm) = 8.88 (s, 4H), 8.43 – 8.40 (m, 1H), 8.40 – 8.35 (m, 2H), 8.27 (t, $J = 5.7$ Hz, 1H), 7.99 (t, $J = 6.1$ Hz, 1H), 7.92 (d, $J = 3.1$ Hz, 4H), 7.76 (dtd, $J = 9.6, 7.6, 1.9$ Hz, 2H), 7.71 (dd, $J = 7.6, 1.9$ Hz, 2H), 7.67 (d, $J = 8.3$ Hz, 4H), 7.60 (d, $J = 8.2$ Hz, 4H), 7.41 (t, $J = 7.8$ Hz, 1H), 7.28 (d, $J = 7.8$ Hz, 2H), 7.18 (ddd, $J = 9.1, 7.0, 4.5$ Hz, 2H), 6.99 (d, $J = 8.5$ Hz, 4H), 6.94 (d, $J = 8.4$ Hz, 4H), 4.38 (td, $J = 8.6, 4.7$ Hz, 1H), 4.13 – 3.97 (m, 2H), 3.29 (s, 2H), 3.16 (dt, $J = 6.8, 4.0$ Hz, 2H), 2.98 (dd, $J = 13.5, 9.3$ Hz, 1H), 2.86 (t, $J = 7.0$ Hz, 2H), 2.67 (h, $J = 7.1$ Hz, 2H), 2.26 (tt, $J = 20.2, 10.2$ Hz, 4H), 1.16 (t, $J = 7.2$ Hz, 41H), 1.01 (d, $J = 6.8$ Hz, 12H); TEAA: 26: 1.16 (t, 36H), 27: 3.08 (q, 24H), 28: 8.88 (s, 4H)

RP-HPLC

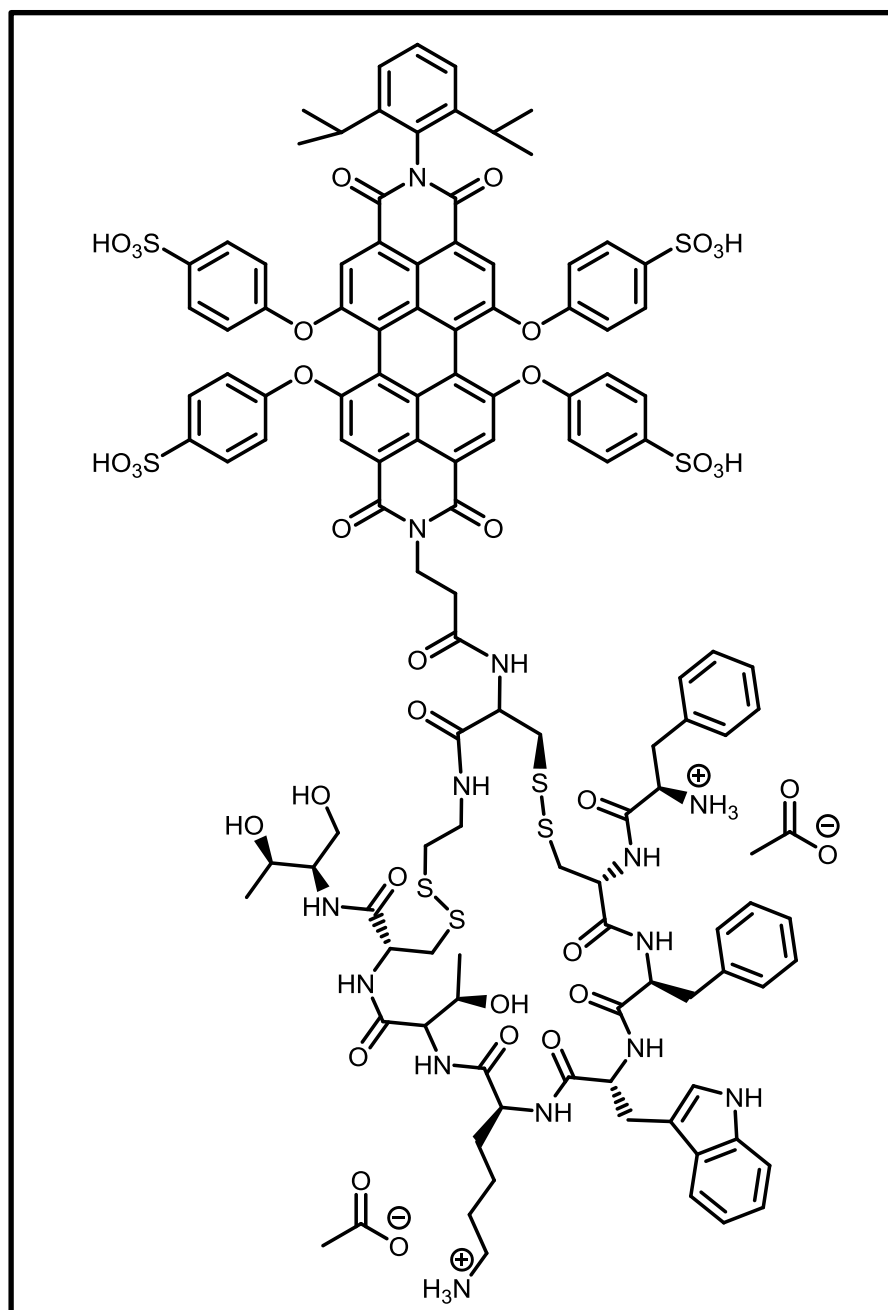
$t_{\text{R}} = 26.43$ min (560 nm),

A: 25 mM triethylammonium acetate (TEAA) buffer (pH 7)

B: acetonitrile (ACN)

0 min 100% A – 40 min 30% A

N-(2,6-diisopropylphenyl)-N'-(4-((4R,10S,13R,16S,19R)-13-((1H-indol-3-yl)methyl)-19-((R)-2-ammonio-3-phenylpropanamido)-16-benzyl-24-butyramido-4-((2R,3R)-1,3-dihydroxybutan-2-yl)carbamoyl)-7-((R)-1-hydroxyethyl)-6,9,12,15,18,25-hexaoxo-1,2,21,22-tetrathia-5,8,11,14,17,26-hexaazacyclooctacosan-10-yl)butan-1-aminiumacetate)-1,6,7,12-tetra(4-sulfophenoxy)-perylene-3,4:9,10-tetracarboxydiimide
(3-24)



Initially, octreotide acetate (20 mg, 18.53 μmol , **3-15**) was reduced under argon in a 4 ml phosphate buffer (pH 6.2) with *tris*(2-carboxyethyl)phosphine (TCEP) hydrochloride (21.25 mg, 74.12 μmol) for 60 min. The reduced peptide **3-17** was purified by RP-HPLC and the isolated fraction was added to the PDI-COOH dye derivative **3-22** (22 mg, 10.48 μmol)

dissolved in 10 ml DMF/phosphate buffer (1:1) – pH 7. Afterwards the reaction mixture was stirred for 1 h at room temperature in an argon atmosphere. Subsequently, the solution was purified by RP-HPLC and the solvent of the isolated fractions was removed *in vacuo*, whereby the product was obtained as a violet solid.

Yield

25 mg, 8.45 μmol , 80%

MS

m/z (MALDI-TOF) 2489.74 $[\text{M}+\text{H}]^+$; 2511.72 $[\text{M}+\text{Na}]^+$; 2527.69 $[\text{M}+\text{K}]^+$; 2533.71 $[\text{M}+2\text{Na}]^+$

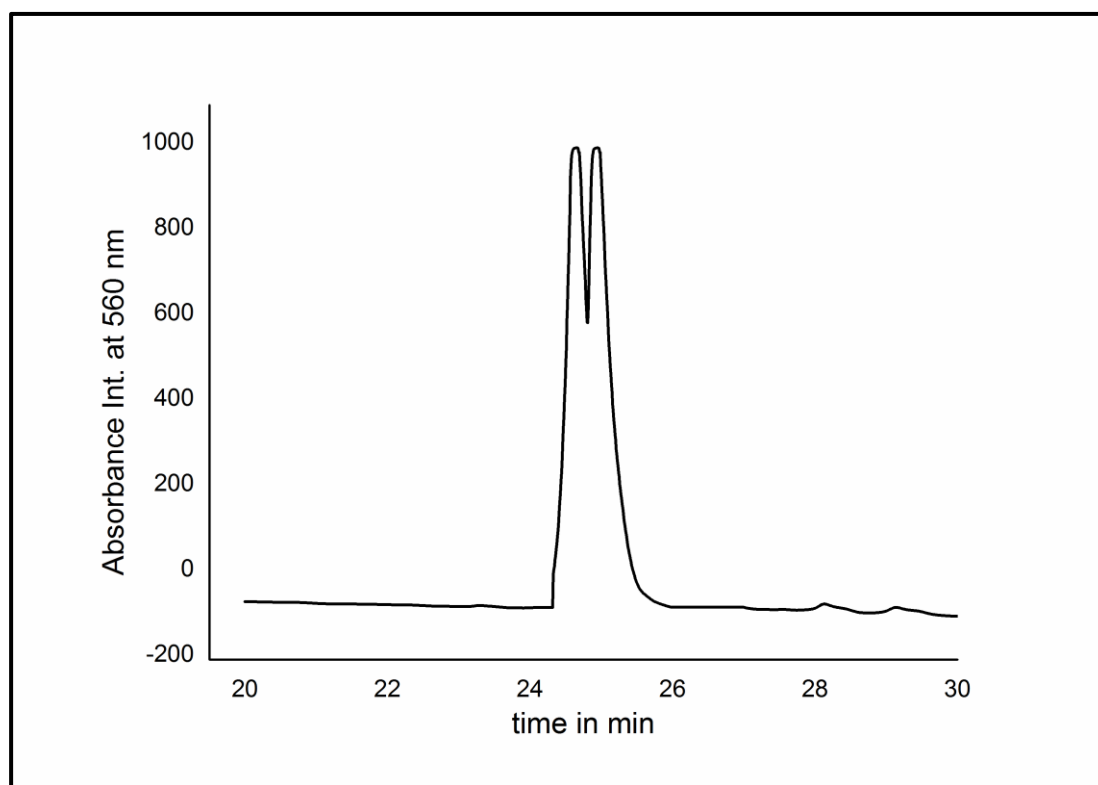
RP-HPLC

$t_{\text{R}} = 24.63 + 24.93$ min (isomers, 560 nm)

A: 25 mM triethylammonium acetate (TEAA) buffer (pH 7)

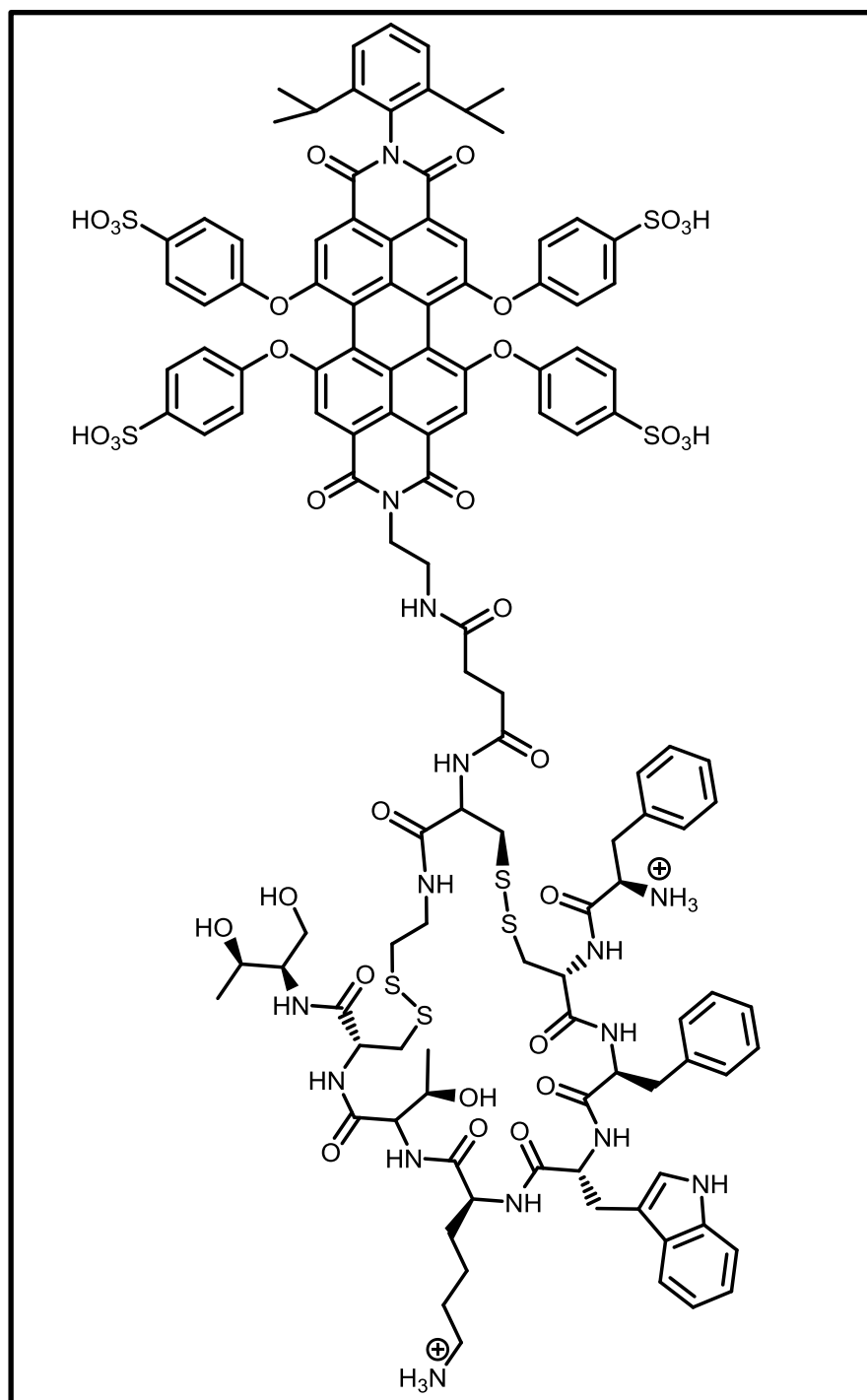
B: acetonitrile (ACN)

0 min 100% A – 40 min 30% A



N-(2,6-diisopropylphenyl)-N'-4-((4R,10S,13R,16S,19R)-13-((1H-indol-3-yl)methyl)-19-((R)-2-ammonio-3-phenylpropanamido)-16-benzyl-4-(((2R,3R)-1,3-dihydroxybutan-2-yl)carbamoyl)-7-((R)-1-hydroxyethyl)-6,9,12,15,18,25-hexaaxo-24-(4-oxo-4-(propylamino)butanamido)-1,2,21,22-tetrathia-5,8,11,14,17,26-hexaazacyclooctacosan-10-yl)butan-1-aminiumacetate)-1,6,7,12-tetra(4-sulfophenoxy)-perylene-3,4:9,10-tetracarboxydiimide

(3-25)



Initially, octreotide acetate (15 mg, 13.9 μmol , **3-15**) was reduced under argon in a 4 ml phosphate buffer (pH 6.2) with *tris*(2-carboxyethyl)phosphine (TCEP) hydrochloride (15.94 mg, 55.59 μmol) for 60 min. The reduced peptide **3-17** was purified by RP-HPLC and the isolated fraction was added to (20 mg, 9.23 μmol , **3-23**) dissolved in 10 ml DMF/phosphate buffer (1:1) – pH 7. Afterwards the reaction mixture was stirred for 1 h at room temperature in an argon atmosphere. Subsequently, the solution was purified by RP-HPLC and the solvent of the isolated fractions was removed *in vacuo*, whereby the product was obtained as a violet solid.

Yield

21 mg, 6.93 μmol , 76%

MS

m/z (MALDI-TOF) 2560.97 $[\text{M}+\text{H}]^+$; 2582.95 $[\text{M}+\text{Na}]^+$; 2604.94 $[\text{M}+2\text{Na}]^+$; 2626.93 $[\text{M}+3\text{Na}]^+$

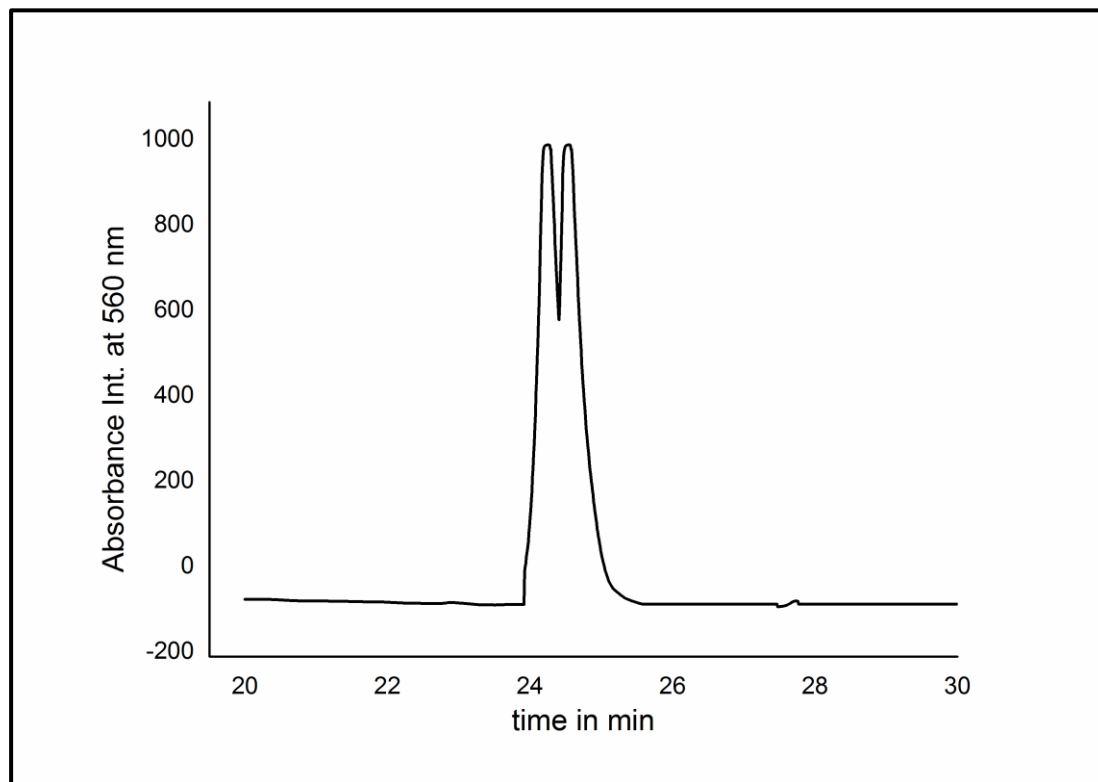
RP-HPLC

$t_{\text{R}} = 24.00 + 24.27$ min (isomers, 560 nm)

A: 25 mM triethylammonium acetate (TEAA) buffer (pH 7)

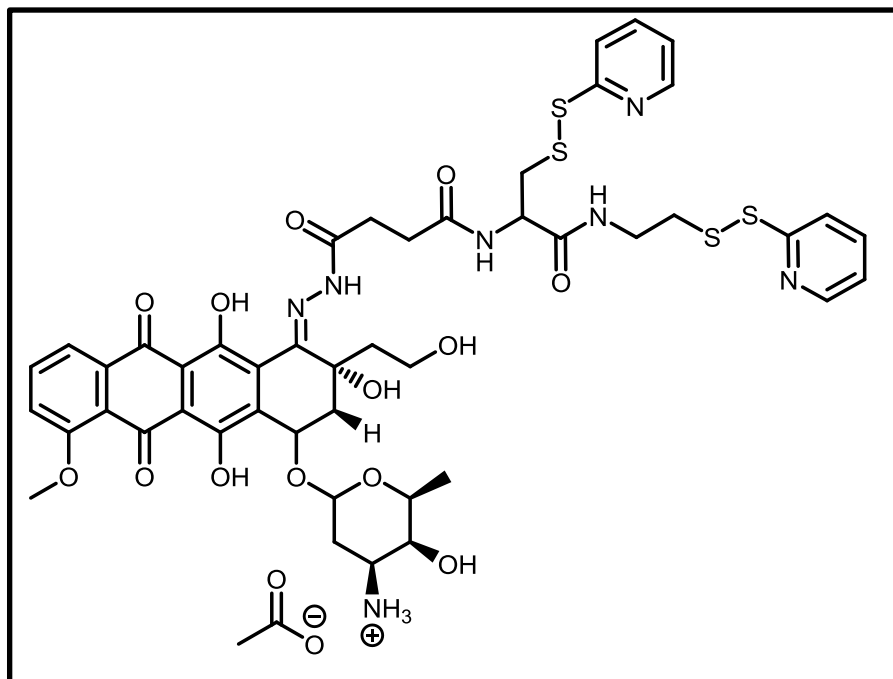
B: acetonitrile (ACN)

0 min 100% A – 40 min 30% A



(2S,3S,4S)-3-hydroxy-2-methyl-6-(((3R,Z)-3,5,12-trihydroxy-3-(2-hydroxyethyl)-10-methoxy-6,11-dioxo-4-(2-(4-oxo-4-((1-oxo-3-(pyridin-2-yl)disulfaneyl)-1-((2-(pyridin-2-yl)disulfaneyl)ethyl)amino)propan-2-yl)amino)butanoyl)hydrazineylidene)-1,2,3,4,6,11-hexahydrotetracen-1-yl)oxy)tetrahydro-2H-pyran-4-aminiumacetate

(3-26)



Compound **3-12** (150 mg, 244.78 μmol) was gradually dissolved in 5 ml dry DCM and 1.5 ml of TFA was added. The solution was vigorously stirred for 30 min at room temperature and the solvent and reagent were removed under reduced pressure. Doxorubicin hydrochloride (212 mg, 365.73 μmol) was dissolved in 4 ml DMF/sodium acetate buffer (1:1) – pH 5.0 and was added to the oily residue. Afterwards, the reaction mixture was stirred for 48 h at room temperature and was subsequently purified by reversed-phase high-performance liquid chromatography (RP-HPLC). The solvent of the isolated fractions was removed under reduced pressure, whereby the product was obtained as a red solid.

Yield

110 mg, 105 μmol , 43%

MS

m/z (MALDI-TOF) 1060.50 $[\text{M}+\text{H}]^+$

¹H-NMR (500 MHz, DMSO-*d*₆, 298 K)

δ (ppm) = 10.84 + 10.46 (2x s, 1H), 8.48 + 8.36 (d, *J* = 7.8 Hz, 1H), 8.45 – 8.38 (m, 2H), 8.26 + 8.15 (2x t, *J* = 5.9 Hz, 1H), 7.87 (m, *J* = 5.2 Hz, 2H), 7.79 – 7.73 (m, 2H), 7.73 – 7.66 (m, 2H), 7.61 (d, 2H), 7.19 (m, *J* = 5.9 Hz, 2H), 5.22 (d, *J* = 3.5 Hz, 1H), 5.05 + 4.95 (d, *J* = 6.1 Hz, 1H), 4.52 + 4.42 – 4.32 (m, 1H), 4.44 (d, *J* = 6.5 Hz, 2H), 4.14 – 3.99 (m, 1H), 3.97 (d, *J* = 2.0 Hz, 3H), 3.35 (s, 1H), 3.32 (dd, *J* = 10.2, 6.1 Hz, 2H), 3.17 (d, *J* = 1.8 Hz, 2H), 3.12 (d, *J* = 4.9 Hz, 1H), 2.97 (d, *J* = 4.4 Hz, 1H), 2.96 – 2.88 (m, 1H), 2.86 (t, *J* = 6.7 Hz, 2H), 2.71 – 2.53 (m, 1H), 2.43 (d, *J* = 7.2 Hz, 1H), 2.33 (dd, *J* = 16.4, 7.3 Hz, 1H), 2.24 (dd, *J* = 13.8, 4.7 Hz, 1H), 1.82 (d, *J* = 1.8 Hz, 3H), 1.68 (td, *J* = 12.8, 3.6 Hz, 1H), 1.53 (dd, *J* = 12.6, 4.3 Hz, 1H), 1.19 – 1.10 (m, 3H);

RP-HPLC

*t*_R = 19.17 (494 nm)

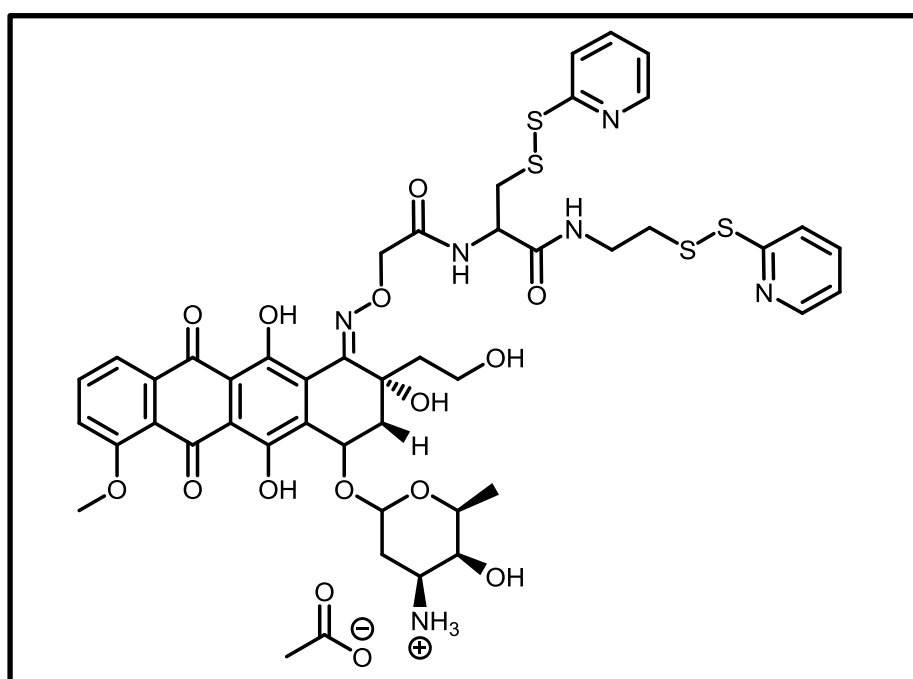
A: 25 mM triethylammonium acetate (TEAA) buffer (pH 7)

B: acetonitrile (ACN)

0 min 75% A – 30 min 40% A

(2S,3S,4S)-3-hydroxy-2-methyl-6-(((3R,Z)-3,5,12-trihydroxy-3-(2-hydroxyethyl)-10-methoxy-6,11-dioxo-4-((2-oxo-2-((1-oxo-3-(pyridin-2-yl)disulfaneyl)-1-((2-(pyridin-2-yl)disulfaneyl)ethyl)amino)propan-2-yl)amino)ethoxy)imino)-1,2,3,4,6,11-hexahydrotetracen-1-yl)oxy)tetrahydro-2H-pyran-4-aminiumacetate

(3-27)



Compound **3-13** (140 mg, 244.86 μmol) was gradually dissolved in 10 ml dry DCM and the identical amount of TFA was added. The solution was vigorously stirred for 1 h at room temperature and the solvent and reagent were removed under reduced pressure. Doxorubicin hydrochloride (169.71 mg, 292.6 μmol) was dissolved in 7 ml DMF/sodium acetate buffer (1:1) – pH 4.8 and was added to the oily residue. Afterwards, the reaction mixture was stirred for 48 h at room temperature and was subsequently purified by reversed-phase high-performance liquid chromatography (RP-HPLC). The solvent of the isolated fractions was removed under reduced pressure, whereby the product was obtained as a red solid.

Yield

182 mg, 182.52 μmol , 75%

MS

m/z (MALDI-TOF) 1019.35 $[\text{M}+\text{Na}]^+$

 $^1\text{H-NMR}$ (500 MHz, DMSO- d_6 , 298 K)

δ (ppm) = 8.40 (t, 1H), 8.39 (m, 2H), 8.34 (dd, 1H), 7.91 – 7.83 (m, 2H), 7.87 (m, 2H), 7.73 (m, 3H), 7.61 (d, 2H), 7.16 (dddd, $J = 17.7, 7.3, 4.8, 1.0$ Hz, 2H), 5.21 (d, $J = 3.6$ Hz, 1H), 4.93 (t, $J = 4.6$ Hz, 1H), 4.54 – 4.45 (m, 1H), 4.49 (d, 2H), 4.43 (d, $J = 12.4$ Hz, 1H), 4.33 (d, $J = 12.4$ Hz, 1H), 4.09 (q, $J = 6.5$ Hz, 1H), 3.96 (s, 3H), 3.35 (s, $J = 2.8$ Hz, 1H), 3.29 (m, $J = 13.2, 6.9$ Hz, 2H), 3.16 (m, 1H), 3.08 (d, $J = 6.4$ Hz, 1H), 3.02 (d, $J = 2.6$ Hz, 1H), 2.97 (m, $J = 15.9, 7.4, 4.1$ Hz, 2H), 2.83 (t, $J = 6.8$ Hz, 2H), 2.46 – 2.39 (m, 1H), 2.18 (dd, $J = 14.4, 5.7$ Hz, 1H), 1.83 (s, 3H), 1.68 (td, $J = 12.7, 3.6$ Hz, 1H), 1.51 (dd, $J = 12.8, 4.5$ Hz, 1H), 1.14 (d, $J = 6.4$ Hz, 3H)

RP-HPLC

$t_R = 21.21$ (494 nm)

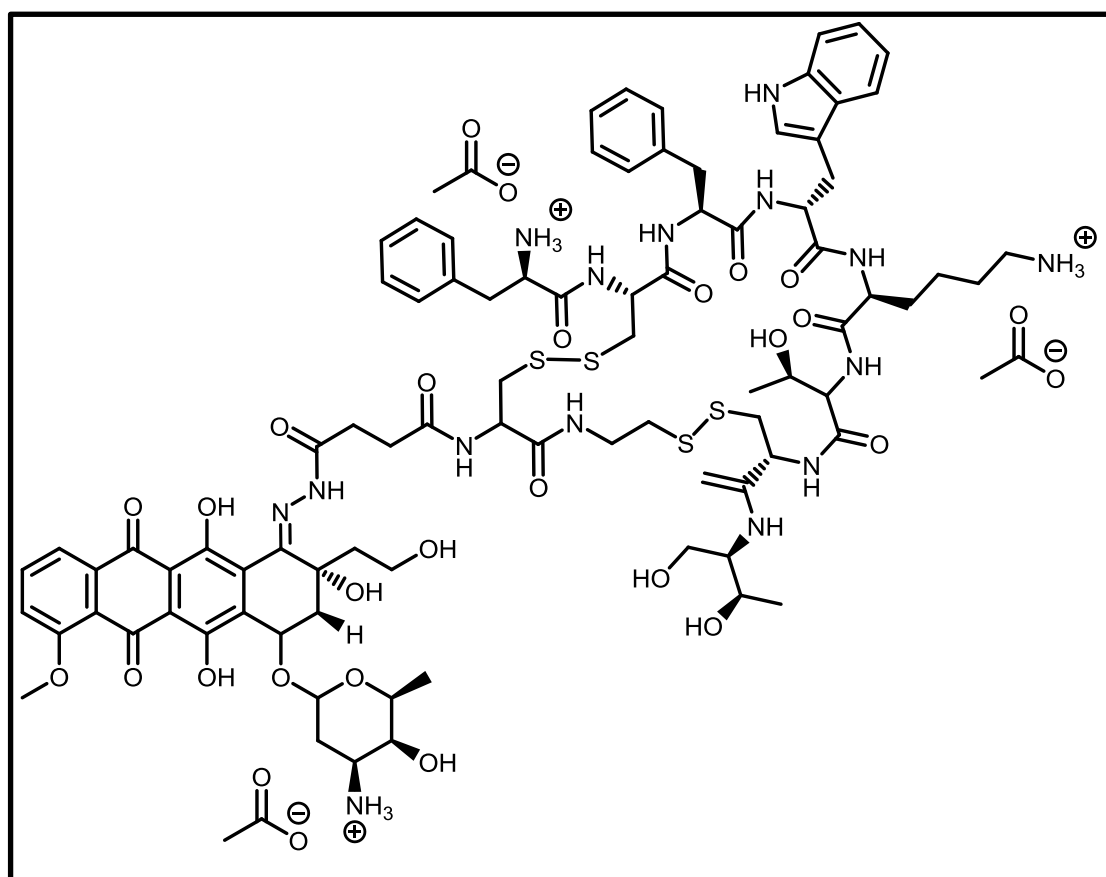
A: 25 mM triethylammonium acetate (TEAA) buffer (pH 7)

B: acetonitrile (ACN)

0 min 75% A – 30 min 40% A

(2S,3S,4S)-6-(((3R,Z)-4-(2-(4-(((4R,10S,13R,16S,19R)-13-((1H-indol-3-yl)methyl)-19-((R)-2-ammonio-3-phenylpropanamido)-10-(4-ammoniobutyl)-16-benzyl-4-(1-(((2R,3R)-1,3-dihydroxybutan-2-yl)amino)vinyl)-7-((R)-1-hydroxyethyl)-6,9,12,15,18,25-hexaoxo-1,2,21,22-tetrathia-5,8,11,14,17,26-hexaazacyclooctacosan-24-yl)amino)-4-oxobutanoyl)hydrazineylidene)-3,5,12-trihydroxy-3-(2-hydroxyethyl)-10-methoxy-6,11-dioxo-1,2,3,4,6,11-hexahydrotetracen-1-yl)oxy)-3-hydroxy-2-methyltetrahydro-2H-pyran-4-aminiumacetate

(3-28)



Initially, octreotide acetate (25 mg, 23 μmol , 0.9 eq, **3-15**) was reduced under argon in a 4 ml phosphate buffer (pH 6.2) with *tris*(2-carboxyethyl)phosphine (TCEP) hydrochloride (26.6 mg, 92.6 μmol) for 60 min. The reduced peptide **3-17** was purified by RP-HPLC and the isolated fraction was added to compound **3-26** (20 mg, 19.3 μmol) dissolved in 10 ml DMF/phosphate buffer (1:1) – pH 7. Afterwards the reaction mixture was stirred for 1 h at room temperature in an argon atmosphere. Subsequently, the solution was purified by RP-HPLC and the solvent of the isolated fractions was removed *in vacuo*, whereby the product was obtained as a red solid.

Yield25 mg, 13.61 μmol , 70%**MS** m/z (ESI-TOF) 919.28 $[\text{M}+2\text{H}]^{2+}$; 1836.63 $[\text{M}+\text{H}]^+$ m/z (ESI-TOF) 1836.6741 $[\text{M}+\text{H}]^+$ (calc. 1836.6782)**RP-HPLC** $t_R = 34.28 + 34.78$ (isomers, 480 nm)

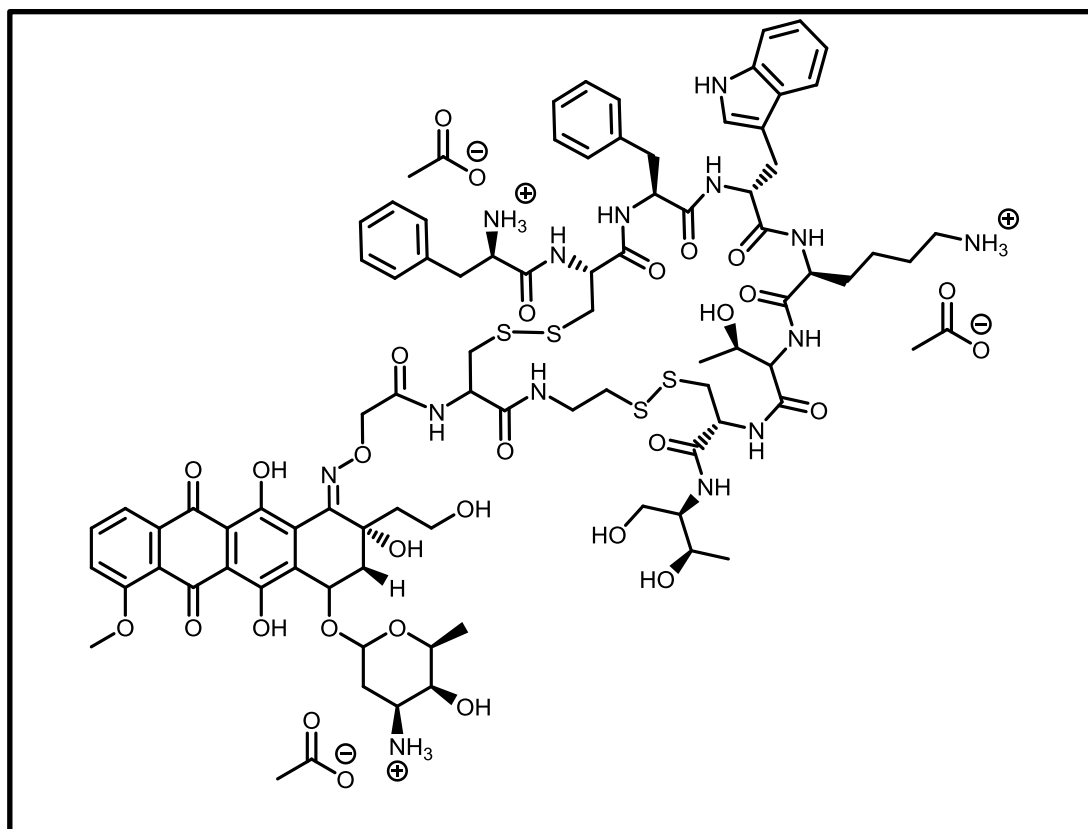
A: 25 mM triethylammonium acetate (TEAA) buffer (pH 7)

B: acetonitrile (ACN)

0 min 100% A – 40 min 30% A

(2S,3S,4S)-6-(((3R,Z)-4-((2-(((4R,10S,13R,16S,19R)-13-((1H-indol-3-yl)methyl)-19-((R)-2-ammonio-3-phenylpropanamido)-10-(4-ammoniobutyl)-16-benzyl-4-(((2R,3R)-1,3-dihydroxybutan-2-yl)carbamoyl)-7-((R)-1-hydroxyethyl)-6,9,12,15,18,25-hexaoxo-1,2,21,22-tetrathia-5,8,11,14,17,26-hexaazacyclooctacosan-24-yl)amino)-2-oxoethoxy)imino)-3,5,12-trihydroxy-3-(2-hydroxyethyl)-10-methoxy-6,11-dioxo-1,2,3,4,6,11-hexahydrotetracen-1-yl)oxy)-3-hydroxy-2-methyltetrahydro-2H-pyran-4-aminiumacetate

(3-29)



Initially, octreotide acetate (30 mg, 27.8 μmol , 0.9 eq, **3-15**) was reduced under argon in a 4 ml phosphate buffer (pH 6.2) with *tris*(2-carboxyethyl)phosphine (TCEP) hydrochloride (31.9 mg, 111 μmol , 4 eq) for 60 min. The reduced peptide **3-17** was purified by RP-HPLC and the isolated fraction was added to compound **3-27** (30 mg, 28.4 μmol) dissolved in 10 ml DMF/phosphate buffer (1:1) – pH 7. Afterwards the reaction mixture was stirred for 1 h at room temperature in an argon atmosphere. Subsequently, the solution was purified by RP-HPLC and the solvent of the isolated fractions was removed *in vacuo*, whereby the product was obtained as a red solid.

Yield

40 mg, 21.6 μmol , 76%

MS

m/z (MALDI-TOF) 1795.51 $[\text{M}+\text{H}]^+$; 1817.53 $[\text{M}+\text{Na}]^+$; 1833.49 $[\text{M}+\text{H}]^+$

RP-HPLC

t_{R} = 32.83 + 33.96 min (isomers, 480 nm)

A: 25 mM triethylammonium acetate (TEAA) buffer (pH 7)

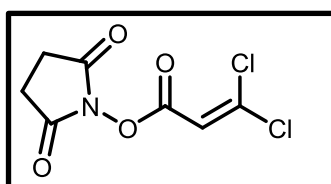
B: acetonitrile (ACN)

0 min 100% A – 40 min 30% A

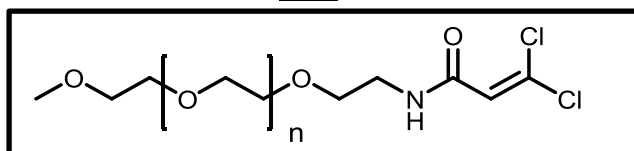
7.3.2 Compounds part 4:

3,3-dichloroacrylicacid *N*-hydroxysuccinimide ester

(4-6)



Initially, a slurry of *N*-hydroxysuccinimide (128.6 mg, 1.12 mmol) and 3,3-dichloroacrylic acid (150 mg, 1.06 mmol, **4-5**) in 20 ml dry dichloromethane (DCM) was prepared. Under argon *N,N'*-diisopropylcarbodiimide (147.74 mg, 183.3 μl , 1.17 mmol) was added and the clear solution was stirred for 4 h. Afterwards, the precipitated urea was filtered off and washed with a small amount of DCM. The obtained solution was diluted with 200 ml DCM and washed four times with water. The organic layer was dried with magnesium sulfate and the solvent was removed *in vacuo* to obtain the product as a colorless solid.

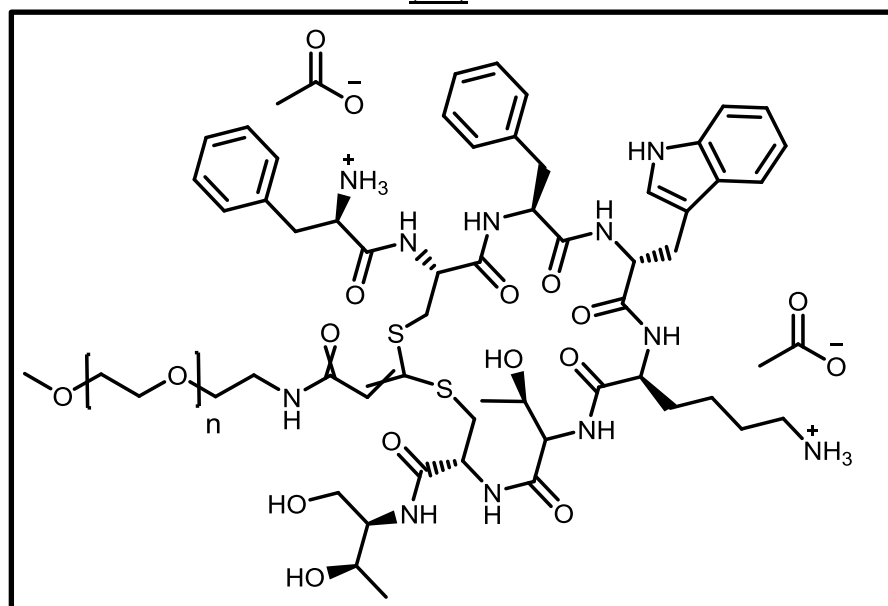
Yield225 mg, 945.3 μmol , 88%**MS** m/z (ESI-TOF) 572.14 $[\text{M}+\text{H}]^+$; 594.12 $[\text{M}+\text{Na}]^+$; 1165.25 $[2\text{M}+\text{Na}]^+$; m/z (HR ESI-TOF) 572.1130 $[\text{M}+\text{H}]^+$ (calc. 572.1124) **^1H -NMR (500 MHz, DMSO- d_6 , 298 K)** δ (ppm) = 7,38 (s, 1H), 2.84 (s, 4H) **^{13}C -NMR (125 MHz, DMSO- d_6 , 298 K)** δ (ppm) = 170.43, 158.60, 142.67, 115.67, 25.99**PEG-(5000)- dichloroacrylamide****(4-7)**

PEG5000-NH₂ (200 mg, 0.04 mM, 1 eq) was dissolved in 3 ml of dry DMF and flushed with argon. DIPEA (25,83 mg, 24,8 μL , 2 mM, 5 eq) was added dropwise and the reaction solution was stirred for 15 minutes. Afterwards compound **4-6** (38.1 mg, 16 mM, 4 eq), which was dissolved in 2 ml of dry DMF, was added within 10 minutes. This solution was stirred for 24 h at room temperature followed by removal of solvent and reagent under reduced pressure. The obtained white residue was dissolved in 4 ml MilliQ water and was purified by size exclusion chromatography (P2 gel) to obtain the product as a colorless powder.

Yield

150 mg, 73 %

Analysis: appendix 1

PEG5000 – Octreotide conjugate**(4-8)**

Initially, octreotide diacetate (30 mg, 29.3 μmol , **3-15**) was reduced under argon in 6 ml phosphate buffer (pH 6.2) with *tris*(2-carboxyethyl)phosphine (TCEP, **3-16**) hydrochloride (39.8 mg, 139 μmol) for 60 min. The reduced peptide **3-17** was purified by RP-HPLC and the isolated fraction was lyophilized overnight. The white powder was dissolved in 5ml DMF/phosphate buffer (1:1) – pH 7, stirred on ice and degassed with argon, before KOH was added (4.4 mg, 78.6 μmol , 100mg KOH in 1ml methanol). Afterwards **4-7** (20 mg, 19.5 μmol) was dissolved in 4 ml DMF/phosphate buffer (1:1) – pH 7 and added dropwise to the reaction solution. The reaction mixture was stirred for 24 h at room temperature in an argon atmosphere. Subsequently, the solvent was removed under reduced pressure. The obtained white residue was dissolved in 4 ml MilliQ water and was purified by size exclusion chromatography (P10 gel) to obtain the product as a colorless powder.

Yield

25 mg, 70 %

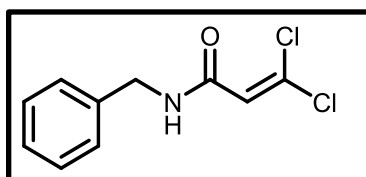
RP-HPLC $t_{\text{R}} = 34 \text{ min}$ (280 nm)

A: 25 mM triethylammonium acetate (TEAA) buffer (pH 7)

B: acetonitrile (ACN)

0 min 100% A – 40 min 30% A.

Analysis: appendix 2

N-benzyl-3,3-dichloroacrylamide**(4-9)**

3,3-dichloroacrylic acid (250 mg, 1.77 mmol, 1 eq, **4-5**) was dissolved in 3 ml of dry DMF and flushed with argon. DIPEA (298.02 mg, 401.65 μ l, 2.31 mmol, 1.3 eq) was added dropwise and the reaction solution was stirred for 5 minutes. Afterwards HATU (1-[Bis(dimethylamino)methylene]-1H-1,2,3-triazolo[4,5-b]pyridinium 3-oxid hexafluorophosphate, 841.27 mg, 2.13 mmol, 1.2 eq), dissolved in 2 ml of dry DMF, was added dropwise and stirring was continued for 10 min until benzylamine (180.56 mg, 1.69 mmol, 0.95) was added. Subsequently the reaction mixture was stirred under argon for 1 h at room temperature. Afterwards the solution was diluted with 250 ml ethyl acetate, washed three times with brine and dried over magnesium sulfate. The solvent was removed *in vacuo* and the residue was purified by silica gel column chromatography (ethyl acetate – methanol 7:3) to obtain the product as colorless oil.

Yield

230 mg, 56%

MS m/z (MALDI-TOF) 230.22 [M+H]⁺**¹H-NMR (500 MHz, DMSO-*d*₆, 298 K)** δ (ppm) = 8.71 (1H), 7.27 (2H), 7.27 (1H), 7.23 (1H), 6.73 (1H), 4.32 (2H)**¹³C-NMR (125 MHz, DMSO-*d*₆, 298 K)** δ (ppm) = 160.97, 138.64, 128.73, 128.33, 127.36, 126.96, 124.08, 42.15**RP-HPLC** t_R = 33 min (260 nm)

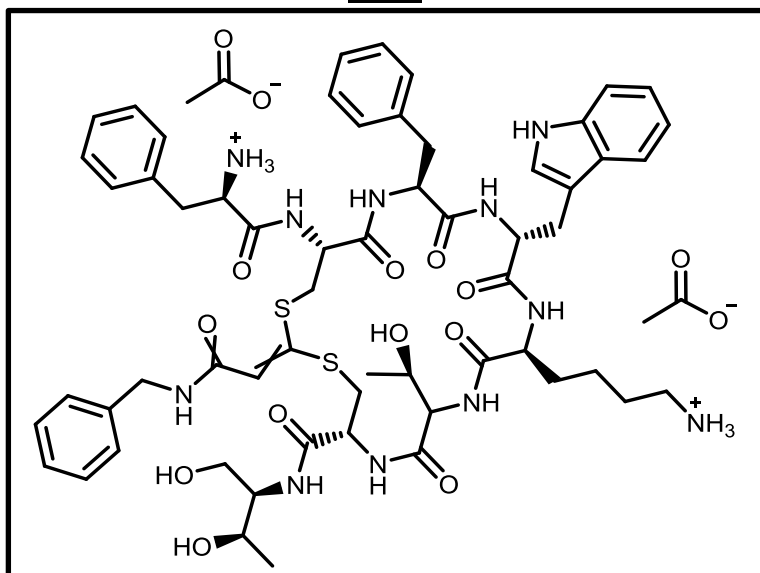
A: 25 mM triethylammonium acetate (TEAA) buffer (pH 7)

B: acetonitrile (ACN)

0 min 100% A – 40 min 30% A

4-((5R,11S,14R,17S,20R)-14-((1H-indol-3-yl)methyl)-20-((R)-2-ammonio-3-phenylpropanamido)-17-benzyl-2-(2-(benzylamino)-2-oxoethylidene)-5-(((2R,3R)-1,3-dihydroxybutan-2-yl)carbamoyl)-8-((R)-1-hydroxyethyl)-7,10,13,16,19-pentaoxo-1,3-dithia-6,9,12,15,18-pentaazacyclohencicosan-11-yl)butan-1-aminiumacetate

(4-10)



Initially, octreotide diacetate (65 mg, 60.2 μmol , **3-15**) was reduced under argon in 4 ml phosphate buffer (pH 6.2) with *tris*(2-carboxyethyl)phosphine (TCEP, **3-16**) hydrochloride (62.05 mg, 240.9 μmol) for 60 min. The reduced peptide **3-17** was purified by RP-HPLC and the isolated fraction was lyophilized overnight. The white powder was dissolved in 5ml DMF/phosphate buffer (1:1) – pH 7, stirred on ice and degassed with argon, before KOH was added (14.6 mg, 260.77 μmol , 100mg KOH in 1ml methanol). Afterwards **4-9** (10 mg, 43.5 μmol) was dissolved in 4 ml DMSO/phosphate buffer (1:1) – pH 7 and added dropwise to the reaction solution. The reaction mixture was stirred for 24 h at room temperature in an argon atmosphere. Subsequently, the solution was purified by RP-HPLC and the solvent of the isolated fractions was removed *in vacuo*, whereby the product was obtained as colorless solid.

Yield41 mg, 33.10 μmol , 76%**MS** m/z (MALDI-TOF) 1178 $[\text{M}+\text{H}]^+$, 1200 $[\text{M}+\text{Na}]^+$ **NMR:** appendix 3**RP-HPLC** t_{R} = 33.16 min (280 nm)

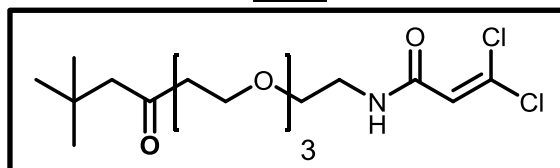
A: 25 mM triethylammonium acetate (TEAA) buffer (pH 7)

B: acetonitrile (ACN)

0 min 100% A – 40 min 30% A

3,3-dichloro-N-(2-(2-(2-((5,5-dimethyl-3-oxohexyl)oxy)ethoxy)ethoxy)ethyl)acrylamide

(4-12)



3,3-dichloroacrylic acid (200 mg, 1.42 mmol, 1 eq, **4-5**) was dissolved in 3 ml of dry DMF and flushed with argon. DIPEA (256.76 mg, 346.03 μ l, 1.99 mmol, 1.4 eq) was added dropwise and the reaction solution was stirred for 5 minutes. Afterwards HATU (1-[Bis(dimethylamino)methylene]-1*H*-1,2,3-triazolo[4,5-*b*]pyridinium 3-oxid hexafluorophosphate, 701.05 mg, 1.77 mmol, 1.25), dissolved in 2 ml of dry DMF, was added dropwise and stirring was continued for 10 min until *tert*-Butyl 12-amino-4,7,10-trioxadecanoate, compound **4-11**, (354.21 mg, 336.70 μ l, 1.28 mmol, 0.95) was added. Subsequently the reaction mixture was stirred under argon for 1 h at room temperature. Afterwards the solvent was removed *in vacuo* and the residue was purified by silica gel column chromatography (ethyl acetate – methanol 7:3) to obtain the product as colorless oil.

Yield

342 mg, 60%

MS

m/z (MALDI-TOF) 421.9 [M+Na]⁺

¹H-NMR (500 MHz, DMSO-*d*₆, 298 K)

δ (ppm) = 8.28 (1H), 6.69 (1H), 3.58 (2H), 3.49 (8H), 3.43 (2H), 3.25 (2H), 2.41 (2H), 1.39 (9H)

¹³C-NMR (125 MHz, DMSO-*d*₆, 298 K)

δ (ppm) = 170.38, 160.97, 128.65, 124.03, 79.67, 69.70, 69.69, 69.65, 69.59, 68.77, 66.22, 39.35, 35.82, 27.74

RP-HPLC

t_R = 32.09 min (230 nm)

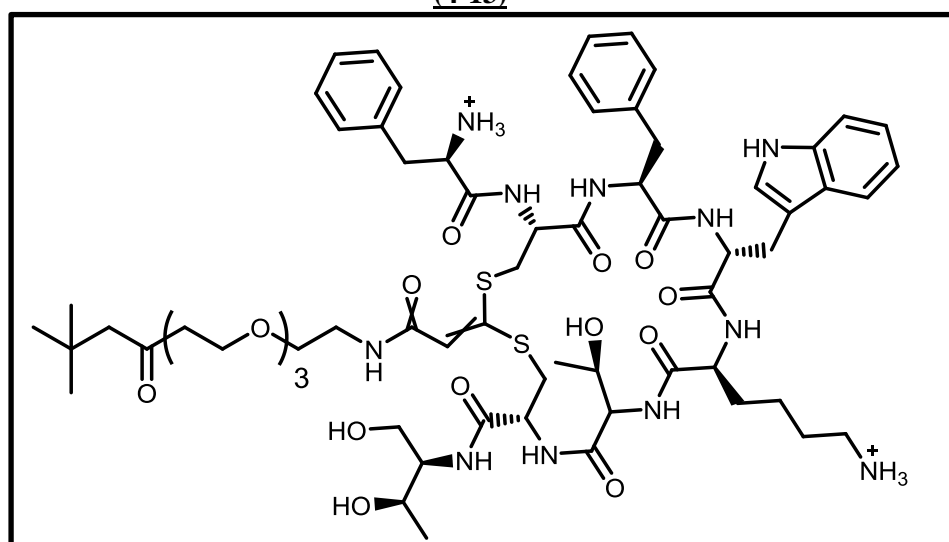
A: 25 mM triethylammonium acetate (TEAA) buffer (pH 7)

B: acetonitrile (ACN)

0 min 100% A – 40 min 30% A

4-((5R,11S,14R,17S,20R)-14-(((1H-indol-3-yl)methyl)-20-((R)-2-ammonio-3-phenylpropanamido)-17-benzyl-5-(((2R,3R)-1,3-dihydroxybutan-2-yl)carbonyl)-2-(17,17-dimethyl-2,15-dioxo-6,9,12-trioxa-3-azaoctadecylidene)-8-((R)-1-hydroxyethyl)-7,10,13,16,19-pentaoxo-1,3-dithia-6,9,12,15,18-pentaazacycloheneicosan-11-yl)butan-1-aminiumacetate

(4-13)



Initially, octreotide diacetate (65 mg, 60.22 μmol , **3-15**) was reduced under argon in 6 ml phosphate buffer (pH 6.2) with *tris*(2-carboxyethyl)phosphine (TCEP, **3-16**) hydrochloride (69.05 mg, 240.90 μmol) for 60 min. The reduced peptide **3-17** was purified by RP-HPLC and the isolated fraction was lyophilized overnight. The white powder was dissolved in 5ml DMF/phosphate buffer (1:1) – pH 7, stirred on ice and degassed with argon, before KOH was added (11.2 mg, 199.85 μmol , 100mg KOH in 1ml methanol). Afterwards **4-12** (15 mg, 37.47 μmol) was dissolved in 3 ml DMF/phosphate buffer (1:1) – pH 7 and added dropwise to the reaction solution. The reaction mixture was stirred for 24 h at room temperature in an argon atmosphere. Subsequently, the solution was purified by RP-HPLC and the solvent of the isolated fractions was removed *in vacuo*, whereby the product was obtained as a colorless solid (50 mg, 35.49 μmol , 71%). m/z (MALDI-TOF) 1348 $[\text{M}+\text{H}]^+$, 1670 $[\text{M}+\text{Na}]^+$; RP-HPLC t_{R} = 34.5 min (280 nm), A: 25 mM triethylammonium acetate (TEAA) buffer (pH 7), B: acetonitrile (ACN), 0 min 100% A – 40 min 30% A. Complete assignment of all NMR signal for both possible isomers is shown in the SI in detail.

Yield

50 mg, 35.49 μmol , 71%

MS

m/z (MALDI-TOF) 1348 $[\text{M}+\text{H}]^+$, 1670 $[\text{M}+\text{Na}]^+$

NMR: appendix 4

RP-HPLC

t_R = 34.5 min (280 nm)

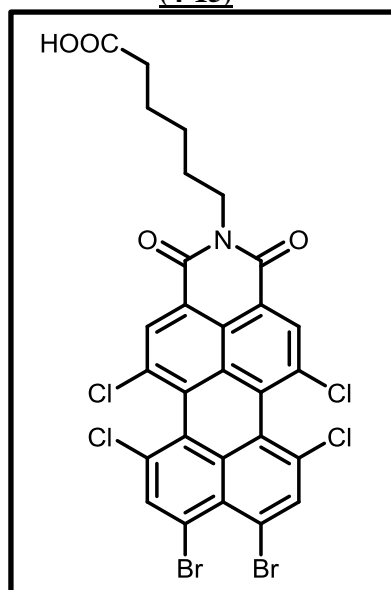
A: 25 mM triethylammonium acetate (TEAA) buffer (pH 7)

B: acetonitrile (ACN)

0 min 100% A – 40 min 30% A

6-(8,9-dibromo-5,6,11,12-tetrachloro-1,3-dioxo-1H-benzo[10,5]anthra[2,1,9-def]isoquinolin-2(3H)-yl)hexanoic acid

(4-15)



6-(8,9-dibromo-5,6,11,12-tetrachloro-1,3-dioxo-1H-benzo[5,10]anthra[2,1,9-def]isoquinolin-2(3H)-yl)hexanoic acid (**4-15**) was obtained from **4-14** (500 mg, 0.80 mmol) and 1.1 fold excess of 6-aminohexanoic acid (117 mg, 0.89 mmol) by heating in 6 ml mixture of NMP-CH₃COOH (2:1) at 100-105°C. After 2.5 hours the reaction mixture was cooled down, poured into water, acidified with HCl acid, the resulting precipitate was filtered off and the product was purified by column chromatography (CH₂Cl₂-CH₃OH 10:1).

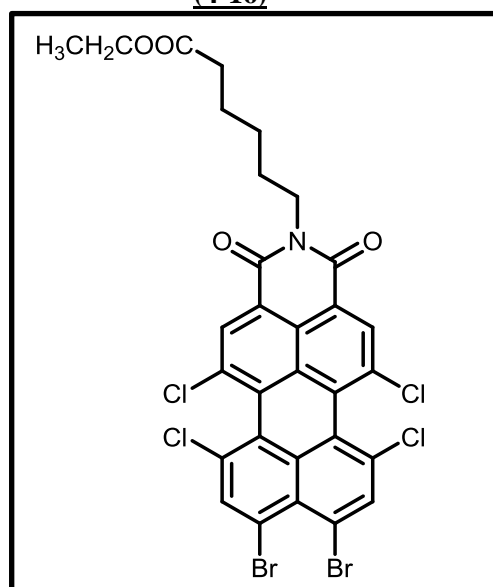
Yield

120 mg, 51 %

MSFD: m/z (%) = 731.5 (%) $[M]^+$ (calc. 731.04) **$^1\text{H-NMR}$ (300 MHz, DMSO- d_6 , 298 K)**

δ (ppm) = 12.00 (brs, 1H, COOH); 8.48 (s, 2H); 8.44 (s, 2H) 4.05 (t, $J = 7.0$ Hz, 2H); 2.22 (t, $J = 7.3$ Hz 2H); 1.70-1.50 (m, 4H); 1.41-1.32 (m, 2H).

ethyl 6-(8,9-dibromo-5,6,11,12-tetrachloro-1,3-dioxo-1H-benzo[10,5]anthra[2,1,9-def]isoquinolin-2(3H)-yl)hexanoate

(4-16)

Ethyl 6-(8,9-dibromo-5,6,11,12-tetrachloro-1,3-dioxo-1H-benzo[5,10]anthra[2,1,9def]isoquinolin-2(3H)-yl)hexanoate (**4-16**): 260 mg of **4-15** (0.35 mmol) were dissolved in 10 ml ethanol and 0.5 ml acetyl chloride was added. The reaction mixture was heated and stirred at 80°C for 3 hours. The solvent was evaporated and product was purified by column chromatography (CH₂Cl₂-CH₃OH 25:1).

Yield

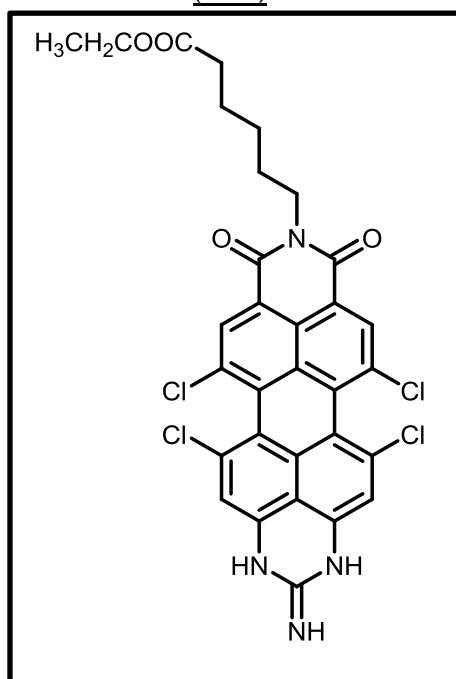
207 mg, 77 %

MSFD: m/z (%) = 759.5 (%) $[M]^+$ (calc. 759.1) **$^1\text{H-NMR}$ (300 MHz, DMSO- d_6 , 298 K)**

δ (ppm) = 8.27 (s, 2H); 7.39 (s, 2H); 7.06 (s, 2H); 4.02 (q, $J = 7.1$ Hz, 2H); 2.28 (t, $J = 7.3$ Hz, 2H); 1.66-1.51 (m, 4H); 1.38-1.3 (m, 2H); 1.14 (t, $J = 7.1$ Hz, 3H)

ethyl 6-(5,6,12,13-tetrachloro-2-imino-8,10-dioxo-1,3,8,10-tetrahydropyrido[3',4',5':6,7]phenaleno[1,2,3-gh]perimidin-9(2H)-yl)hexanoate

(4-17)



Ethyl 6-(5,6,12,13-tetrachloro-2-imino-8,10-dioxo-2,3-dihydropyrido[3',4',5':6,7]phenaleno[1,2,3-gh]perimidin-9(1H,8H,10H)-yl)hexanoate (**4-17**): 207 mg of **4-16** (0.27 mmol), 31 mg of guanidine hydrochloride (0.33 mmol) and 57 mg of K_2CO_3 (0.41 mmol) were suspended in 5 ml DMF. The resulting mixture was stirred and heated at $110^\circ C$ for 1.5 hours. The solvent was evaporated and the product was purified by column chromatography (CH_2Cl_2 - CH_3OH 10:1).

Yield

86 mg, 48 %

MS

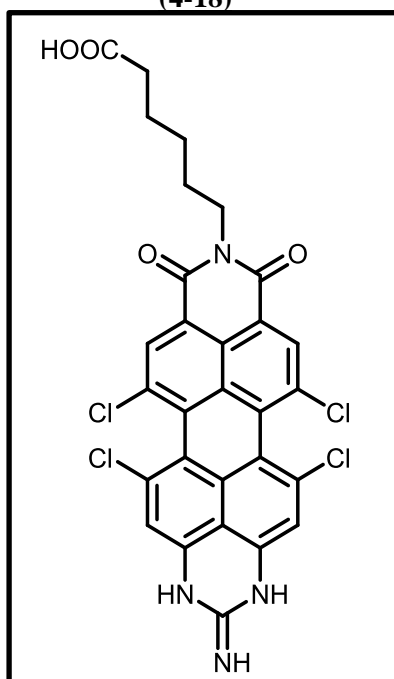
FD: m/z (%) = 759.5 (%) $[M]^+$ (calc. 759.1)

1H -NMR (300 MHz, $DMSO-d_6$, 298 K)

δ (ppm) = 8.27 (s, 2H); 7.39 (s, 2H); 7.06 (s, 2H); 4.02 (q, $J = 7.1$ Hz, 4H); 2.28 (t, $J = 7.3$ Hz, 2H); 1.66-1.51 (m, 4H); 1.38-1.3 (m, 2H); 1.14 (t, $J = 7.1$ Hz, 3H).

6-(5,6,12,13-tetrachloro-2-imino-8,10-dioxo-1,3,8,10-tetrahydropyridof[3',4',5':6,7]phenaleno[1,2,3-gh]perimidin-9(2H)-yl)hexanoic acid

(4-18)



86 mg of **4-17** (0,131 mmol) were suspended in 5 ml of ethanol (0,086 mol), 4 mg NaOH (0,1 mol) was added and the reaction mixture was heated up to 60°C for 10 minutes and stirred by room temperature for 1h. The progress of reaction was followed by TLC (CH₂Cl₂-CH₃OH 10:1). The solvent was evaporated, 50 ml of water were added, the solution was acidified with HCl (35%) and the resulting solid was filtered and dried.

Yield

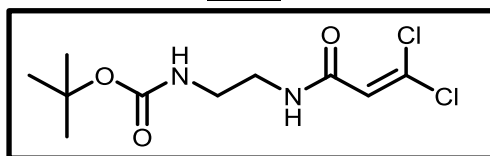
44 mg, 53 %

MS

m/z (MALDI-TOF) 663.63 [M+K]⁺

¹H-NMR (300 MHz, DMSO-*d*₆, 298 K)

δ (ppm) = 8.28 (s, 2H), 7.19 (brs, 2H), 7.09 (s, 2H), 4.05 (t, *J* = 6.9 Hz, 2H), 2.22 (t, *J* = 7.2 Hz, 2H), 1.66-1.50 (m, 4H), 1.39-1.30 (m, 2H).

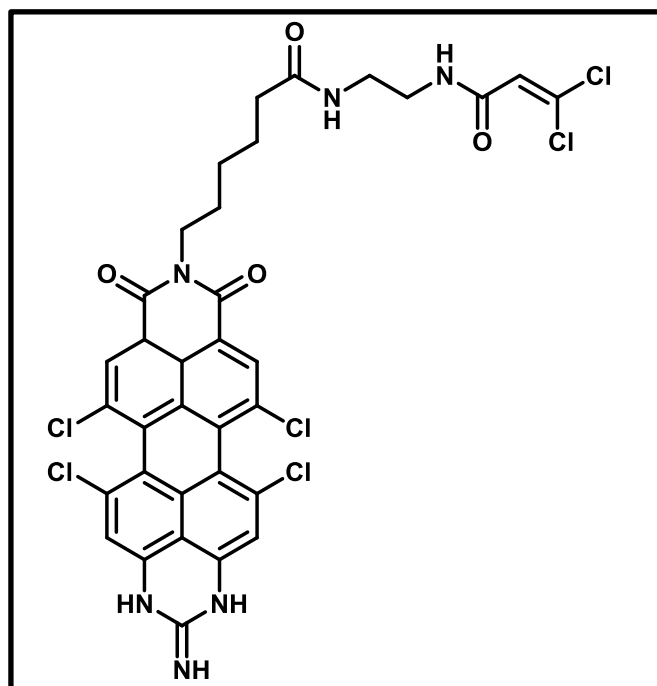
tert-butyl (2-(3,3-dichloroacrylamido)ethyl)carbamate**(4-19)**

3,3-dichloro acrylic acid (293.2 mg, 2.08 mmol, **4-5**) was dissolved in 15 ml DMF and degassed with argon. To this solution DIPEA (322.68 mg, 2.50 mmol, 434.9 μ l) was slowly added and stirred for 5 minutes. Afterwards, HATU ([Bis(dimethylamino)methylene]-1*H*-1,2,3-triazolo[4,5-*b*]pyridinium 3-oxid hexafluorophosphate, 945.66 mg, 2.39 mmol) was dissolved in 5 ml DMF and added dropwise to the first solution. The reaction mixture was stirred for another 5 minutes at room temperature, before N-Boc-ethylenediamine (300 mg, 1.87 mmol, 296.44 μ l) was added dropwise in a 4 ml DMF solution. After stirring for 2h at room temperature the solvent was removed *in vacuo* to obtain a yellow solid. Afterwards, the residue was purified by silica gel column chromatography (ethyl acetate – hexane 1:1) to obtain the product as yellow solid.

Yield

281 mg, 0.992 mmol, 48 %

MS m/z (ESI-TOF) 283.09 [M + H]⁺, 305.09 [M + Na]⁺, 321.04 [M + K]⁺**¹H-NMR (500 MHz, DMSO-*d*₆, 298 K)** δ (ppm) = 8.23 (1H), 6.82 (1H), 6.64 (1H), 3.12 (2H), 2.99 (2H), 1.37 (9H)**¹³C-NMR (125 MHz, DMSO-*d*₆, 298 K)** δ (ppm) = 161.05, 155.58, 128.47, 124.22, 77.68, 39.35, 38.66, 28.22

PMI – Linker conjugate**(4-20)**

4-18 (50 mg, 79.58 μmol , 1 eq) was dissolved in 3 ml of dry DMF and flushed with argon. DIPEA (15.43 mg, 20.79 μl , 119.37 μmol , 1.5 eq) was added dropwise and the reaction solution was stirred for 5 minutes. Afterwards HATU (1-[Bis(dimethylamino)methylene]-1*H*-1,2,3-triazolo[4,5-*b*]pyridinium 3-oxid hexafluorophosphate, 36.17 mg, 91.52 μmol , 1.15 eq), dissolved in 2 ml of dry DMF, was added dropwise and stirring was continued for 10 min until the Boc-protected compound **4-19** (20.39 mg, 111.41 μmol , 1.4 eq) was added. Subsequently the reaction mixture was stirred under argon for 1 h at room temperature. Afterwards the solvent was removed *in vacuo* and the residue was purified by silica gel column chromatography (MeOH – DCM 1:10) to obtain the product as dark blue powder.

Yield

51 mg, 81 %

MS m/z (MALDI-TOF) 791.75 $[\text{M}+\text{H}]^+$, 813.79 $[\text{M}+\text{Na}]^+$ **$^1\text{H-NMR}$ (700 MHz, DMSO- d_6 , 298 K)** δ (ppm) = 11.85, 8.3, 8.23, 7.82, 7.34, 7.07, 6.61, 4.04, 3.12, 3.1, 2.07, 1.62, 1.54, 1.31 **$^{13}\text{C-NMR}$ (176 MHz, DMSO- d_6 , 298 K)** δ (ppm) = 172.70, 162.72, 161.50, 134.16, 131.48, 129.02, 124.63, 124.33, 111.71, 111.71, 40.02, 38.87, 38.41, 35.75, 27.75, 26.67, 25.42.

dropwise to the reaction solution. The reaction mixture was stirred for 24 h at room temperature in an argon atmosphere. Subsequently, the solution was purified by RP-HPLC and the solvent of the isolated fractions was removed *in vacuo*, whereby the product was obtained as colorless solid.

Yield

55 mg, 30.53 μmol , 80.7%

MS

m/z (MALDI-TOF) 1738.62 $[\text{M}+\text{H}]^+$, 1760.63 $[\text{M}+\text{Na}]^+$

NMR: appendix 5

RP-HPLC

t_{R} = 33.93 min (716 nm)

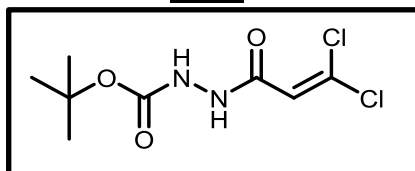
A: 25 mM triethylammonium acetate (TEAA) buffer (pH 7)

B: acetonitrile (ACN)

0 min 80% A – 40 min 10% A

tert-butyl 2-(3,3-dichloroacryloyl)hydrazine-1-carboxylate

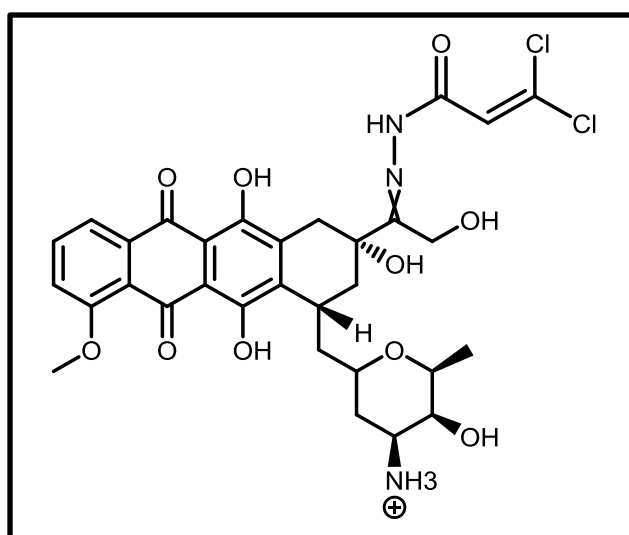
(4-22)



3,3-dichloro acrylic acid (489 mg, 3.18 mmol, **4-5**) was dissolved in 15 ml DMF and degassed with argon. To this solution DIPEA (494 mg, 3.82 mmol) was slowly added and stirred for 5 minutes. Afterwards, HATU (-[Bis(dimethylamino)methylene]-1*H*-1,2,3-triazolo[4,5-*b*]pyridinium 3-oxid hexafluorophosphate) was dissolved in 5 ml DMF and added dropwise to the first solution. The reaction mixture was stirred for another 5 minutes at room temperature, before *tert*-butyl carbazate (400 mg, 3.02 mmol) was added dropwise in a 4 ml DMF solution. After stirring for 2h at room temperature the solvent was removed *in vacuo* to obtain a yellow solid. Afterwards, the residue was purified by silica gel column chromatography (ethyl acetate – hexane 1:1) to obtain the product as yellow solid.

Yield

360 mg, 1.418 mmol, 46 %

MS m/z (ESI-TOF) 254.02 [M]⁺¹H-NMR (300 MHz, DMSO-*d*₆, 298 K) δ (ppm) = 9.87 (s, 1H), 8.93 (s, 1H), 6.63 (s, 1H), 1.40 (s, 9H)¹³C-NMR (75 MHz, DMSO-*d*₆, 298 K) δ (ppm) = 161.15, 155.44, 121.27, 79.91, 28.38.**(3,3-dichloroacryloyl)hydrazone carrying doxorubicin****(4-23)**

4-22 (52 mg, 203.8 μmol) was gradually dissolved in 5 ml dry DCM and the identical amount of TFA was added. The solution was vigorously stirred for 1 h at room temperature and the solvent and reagent were removed under reduced pressure. Doxorubicin hydrochloride (100 mg, 172.4 μmol) was dissolved in 40 ml dry methanol and was added to the oily residue. Afterwards, the reaction mixture was stirred for 48 h at room temperature and was subsequently purified by reversed-phase high-performance liquid chromatography (RP-HPLC). The solvent of the isolated fractions was removed under reduced pressure, whereby the product was obtained as a red solid.

Yield70 mg, 102.87 μmol , 60%

MS

m/z (MALDI-TOF) 791.75 [M+H]⁺, 813.79 [M+Na]⁺

¹H-NMR (650 MHz, DMSO-*d*₆, 298 K)

δ (ppm) = 6.98 (1H), 7.91 (1H), 7.81 (1H), 7.54 (1H), 5.47 (1H), 5.01 (1H), 4.62 + 4.66 (2H), 4.20 (1H), 4.01 (3H), 3.65 (1H), 3.51 (1H), 2.90 + 3.34 (2H), 2.31 + 2.52 (2H), 1.90 + 2.00 (2H), 1.32 (3H).

¹³C-NMR (151 MHz, DMSO-*d*₆, 298 K)

δ (ppm) = 188.4, 188.2, 164.7, 162.5, 155.8, 157.9, 156.0, 137.3, 137.2, 136.5, 136.5, 135.1, 120.5, 120.5, 121.6, 120.3, 112.4, 112.2, 101.2, 74.2, 73.8, 68.4, 68.1, 59.0, 57.1, 48.5, 40.5, 34.9, 29.9, 17.1

RP-HPLC

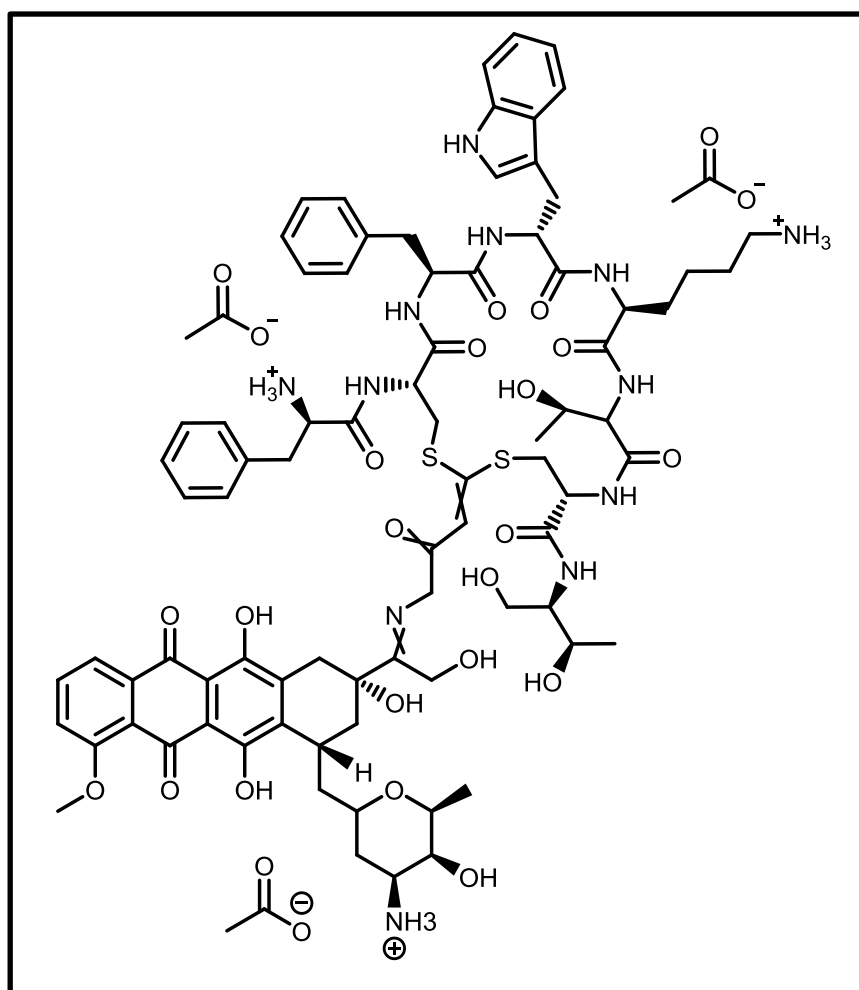
t_R = 30.9 min (480 nm)

A: 25 mM triethylammonium acetate (TEAA) buffer (pH 7)

B: acetonitrile (ACN)

0 min 100% A – 40 min 30% A;

For further analysis: appendix 6

Doxorubicin-octreotide hybrid**(4-26)**

Initially, octreotide diacetate (62 mg, 57.44 μmol , **3-15**) was reduced under argon in 6 ml phosphate buffer (pH 6.2) with *tris*(2-carboxyethyl)phosphine (TCEP) hydrochloride (82.3 mg, 287.2 μmol , **3-16**) for 60 min. The reduced peptide **3-17** was purified by RP-HPLC and the isolated fraction was lyophilized overnight. The white powder was dissolved in 2ml DMF/phosphate buffer (1:1) – pH 7, stirred on ice and degassed with argon, before KOH was added (6.6 mg, 117,6 μmol , 100 mg KOH in 1ml methanol). Afterwards **4-23** was dissolved in 2 ml DMF/phosphate buffer (1:1) – pH 7 and added dropwise to the reaction solution. The reaction mixture was stirred for 1 h at room temperature in an argon atmosphere. Subsequently, the solution was purified by RP-HPLC and the solvent of the isolated fractions was removed *in vacuo*, whereby the product was obtained as a red solid.

Yield13 mg, 7.98 μmol , 27%

MS

m/z (MALDI-TOF) 1628.6 $[M+H]^+$, 1650.6 $[M+Na]^+$

$^1\text{H-NMR}$ (650 MHz, DMSO- d_6 , 298 K) and $^{13}\text{C-NMR}$ (151 MHz, DMSO- d_6 , 298 K)

appendix 7

RP-HPLC

t_R = 32 min (480 nm)

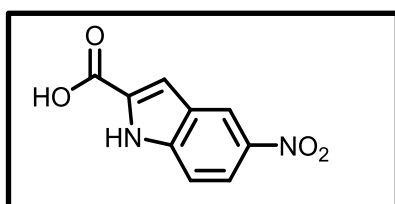
A: 25 mM triethylammonium acetate (TEAA) buffer (pH 7)

B: acetonitrile (ACN)

0 min 100% A – 40 min 30% A;

7.3.3 Compounds part 5:**5-nitro-1H-indole-2-carboxylic acid**

(5-2)



Compound **5-1** (2.5 g, 10,67 mmol) was dissolved in 50 mL THF:MeOH (1:1) and mixed with 4 g NaOH in 30 mL water. The reaction solution was stirred for 24 h until no starting compound was left and added to 300 mL water. Afterwards the pH was adjusted to pH 1 with HCl (35%). The precipitated product was collected by vacuum filtration, redissolved in THF and dried with MgSO_4 . Solvents were removed under high vacuum to yield the brown product (**5-2**).

Yield

2.12g, 10.28 mmol, 96 %

MS

m/z (MALDI-TOF) 229.01 $[M+Na]^+$, 244.98 $[M+K]^+$

$^1\text{H-NMR}$ (300 MHz, DMSO- d_6 , 298 K)

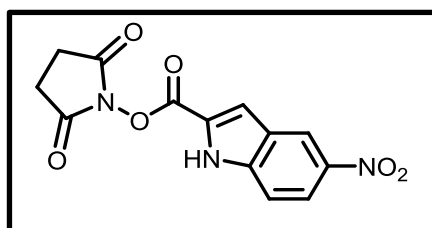
δ (ppm) = 13.34 (s, 1H), 12.53 – 12.37 (m, 1H), 8.69 (d, J = 2.2 Hz, 1H), 8.09 (dd, J = 9.1, 2.3 Hz, 1H), 7.57 (dt, J = 9.1, 0.7 Hz, 1H), 7.36 (dd, J = 2.1, 0.9 Hz, 1H).

^{13}C -NMR (75 MHz, DMSO- d_6 , 298 K)

δ (ppm) = 162.11, 141.30, 139.90, 132.05, 125.88, 119.55, 119.13, 113.08, 109.74.

2,5-dioxopyrrolidin-1-yl 5-nitro-1H-indole-2-carboxylate

(5-3)



Compound **5-2** (500 mg, 2.43 mmol) and 1-hydroxypyrrolidine-2,5-dione (293.09 mg, 2.55 mmol) were dissolved in 15 mL THF. DIC (N,N'-diisopropylcarbodiimide, 321.39 mg, 394.35 μl , 2.55 mol) was added and the reaction was stirred under argon for 3h. The solvent was removed under vacuum, the remaining product was redissolved in EtOAc (400 mL) and washed with saturated NaCl solution (3x 200 mL). The organic layer was dried with MgSO_4 and the solvent removed under vacuum to yield the product (**5-3**).

Yield

653 mg, 2.15 mmol, 89 %

MS

m/z (MALDI-TOF) 342.29 $[\text{M}+\text{K}]^+$

^1H -NMR (300 MHz, DMSO- d_6 , 298 K)

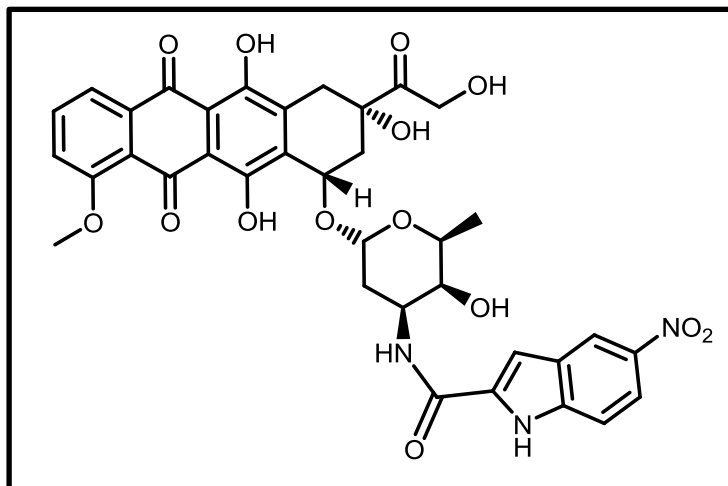
δ (ppm) = 13.34 – 12.91 (m, 1H), 8.82 (d, J = 2.2 Hz, 1H), 8.21 (dd, J = 9.2, 2.2 Hz, 1H), 7.85 – 7.78 (m, 1H), 7.67 (d, J = 9.2 Hz, 1H), 2.93 (s, 4H).

^{13}C -NMR (75 MHz, DMSO- d_6 , 298 K)

δ (ppm) = 170.23, 156.51, 142.04, 140.93, 125.65, 124.60, 120.79, 120.43, 113.99, 113.70, 25.57.

N-((2S,3S,4S,6R)-3-hydroxy-2-methyl-6-(((1S,3S)-3,5,12-trihydroxy-3-(2-hydroxyacetyl)-10-methoxy-6,11-dioxo-1,2,3,4,6,11-hexahydrotetracen-1-yl)oxy)tetrahydro-2H-pyran-4-yl)-5-nitro-1H-indole-2-carboxamide

(5-4)



Compound **5-3** (150 mg, 494.67 μmol) and Doxorubicin (260.82 mg, 449.71 μmol) were dissolved in 20 mL DMF and stirred for 2 h under argon after the addition of DIPEA (87.19 mg, 114.72 μL , 674.6 μmol). Solvent was removed under reduced pressure. The product was purified by column chromatography ($\text{CHCl}_3/\text{MeOH}$ 20:1). After removal of the solvents under vacuum, the remaining product was redissolved in THF, precipitated in hexane, filtered off and dried under high vacuum to yield the red product **5-4**.

Yield

182 mg, 248.8 μmol , 55 %

MS

m/z (MALDI-TOF) 754.25 $[\text{M}+\text{Na}]^+$, 770.24 $[\text{M}+\text{Na}]^+$

 $^1\text{H-NMR}$ (500 MHz, $\text{DMSO-}d_6$, 298 K)

δ (ppm) = 13.99 (s, 1H), 13.21 (s, 1H), 12.21 (s, 1H), 8.70 – 8.62 (m, 1H), 8.29 (d, $J = 7.9$ Hz, 1H), 8.03 (dd, $J = 9.2, 2.4$ Hz, 1H), 7.83 (d, $J = 7.1$ Hz, 2H), 7.53 (dd, $J = 19.2, 9.3$ Hz, 3H), 5.48 (s, 1H), 5.29 (s, 1H), 4.92 (dt, $J = 17.9, 5.9$ Hz, 3H), 4.61 (d, $J = 5.8$ Hz, 2H), 4.36 – 4.19 (m, 2H), 3.93 (s, 3H), 3.59 (d, $J = 5.2$ Hz, 1H), 2.93 (q, $J = 18.3$ Hz, 2H), 2.26 (d, $J = 14.0$ Hz, 1H), 2.11 (d, $J = 14.0$ Hz, 2H), 1.57 (d, $J = 12.2$ Hz, 1H), 1.17 (d, $J = 6.1$ Hz, 3H).

 $^{13}\text{C-NMR}$ (125 MHz, $\text{DMSO-}d_6$, 298 K)

δ (ppm) = 213.78, 186.26, 160.65, 159.46, 156.07, 154.42, 141.10, 139.16, 136.03, 135.38, 135.13, 134.47, 133.99, 126.24, 119.80, 119.05, 118.97, 118.86, 118.24, 112.71, 110.62,

110.49, 105.38, 100.41, 74.87, 70.00, 67.84, 66.60, 63.69, 56.46, 45.84, 36.56, 31.99, 29.45, 17.00.

RP-HPLC

$t_R = 40.05$ min

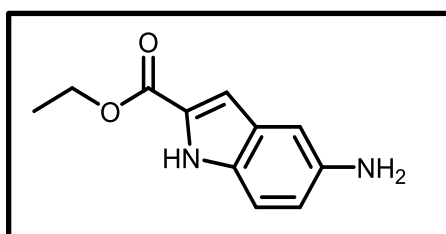
A: 25 mM triethylammonium acetate (TEAA) buffer (pH 7)

B: acetonitrile (ACN)

0 min 100% A – 40 min 30% A;

ethyl 5-amino-1H-indole-2-carboxylate

(5-6)



5-Nitro-indole-2-carboxylic acid (500 mg, 2.13 mmol, **5-1**) was dissolved in 100 mL dioxane. Sodium dithionite (2.23 g, 12.81 mmol) as well as NaHCO_3 (1.79 g, 21.35 mmol) were dissolved in water and added to the dioxane solution stepwise and the reaction was stirred under argon for 1 h. Afterwards the precipitate was filtered off and the brown solution was added to 300 mL 1M NaHCO_3 . The aqueous solution was washed five times with DCM (150 mL). The organic phases were collected and dried with MgSO_4 . The solvents were evaporated under vacuum to yield the brown product ethyl 5-aminoindole-2-carboxylate (**5-6**).

Yield

170 mg, 38%

MS

m/z (MALDI-TOF) 205.08 $[\text{M}+\text{H}]^+$, 227.12 $[\text{M}+\text{Na}]^+$

m/z (ESI-TOF) 205.11 $[\text{M}+\text{H}]^+$, 245.12 $[\text{M}+\text{K}]^+$

$^1\text{H-NMR}$ (500 MHz, $\text{DMSO-}d_6$, 298 K)

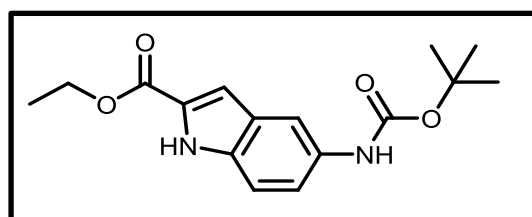
δ (ppm) = 11.38 (s, 1H), 7.15 (d, $J = 8.0$ Hz, 1H), 6.83 (d, $J = 2.2$ Hz, 1H), 6.69 (d, $J = 8.0$ Hz, 2H), 4.64 (s, 2H), 4.29 (q, $J = 7.0$ Hz, 2H), 1.31 (t, $J = 7.0$ Hz, 3H).

¹³C-NMR (125 MHz, DMSO-*d*₆, 298 K)

δ (ppm) = 161.39, 142.22, 131.51, 127.73, 126.60, 116.59, 112.67, 106.00, 102.87, 66.34, 60.03, 14.34.

ethyl 5-((*tert*-butoxycarbonyl)amino)-1H-indole-2-carboxylate

(5-7)



5-aminoindole-2-carboxylate (**5-6**) (700 mg, 3.43 mmol) and di-*tert*-butyl dicarbonate (748 mg, 3.43 mmol) were dissolved in 50 mL THF, refluxed for 24 h until no starting compound was left. The reaction solution was added to 300 mL 1M NaHCO₃ and the product was extracted from the aqueous solution by DCM (5x 150 mL). The organic phases were collected and dried with MgSO₄. The solvents were evaporated under vacuum to yield the brown product ethyl 5-((*tert*-butoxycarbonyl)amino)-indole-2-carboxylate (**5-7**).

Yield

880 mg, 85%

MS

m/z (MALDI-TOF) 305.72 [M+H]⁺, 327.68 [M+Na]⁺

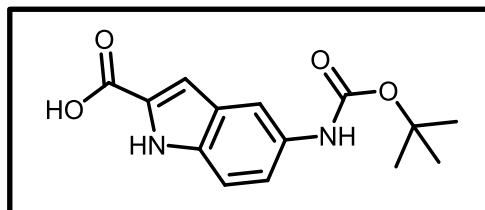
m/z (ESI-TOF) 327.68 [M+Na]⁺, 631.28 [2*M+Na]⁺

¹H-NMR (300 MHz, DMSO-*d*₆, 298 K)

δ (ppm) = 11.72 (s, 1H), 9.17 (s, 1H), 7.81 (s, 1H), 7.32 (d, J = 8.8 Hz, 1H), 7.26 (d, J = 8.8 Hz, 1H), 7.05 (d, J = 2.2 Hz, 1H), 4.32 (q, J = 7.1 Hz, 2H), 1.48 (s, 9H), 1.33 (t, J = 7.1 Hz, 3H).

¹³C-NMR (75 MHz, DMSO-*d*₆, 298 K)

δ (ppm) = 161.23, 153.10, 133.73, 132.49, 127.61, 126.68, 112.40, 107.33, 78.56, 60.31, 28.22, 14.29.

5-((tert-butoxycarbonyl)amino)-1H-indole-2-carboxylic acid**(5-8)**

Compound **5-7** (850 mg, 2.79 mmol) was dissolved in 20 mL THF:MeOH (1:1) and mixed with 1g NaOH in 10 mL water. The reaction solution was stirred for 20 h until no starting compound was left and added to 500 mL water. Afterwards the pH was adjusted to pH 1 with HCl (35%). The precipitated product was collected by vacuum filtration, redissolved in THF and dried with MgSO₄. Solvents were removed under high vacuum to yield the brown product 5-((tert-butoxycarbonyl)amino)-indole-2-carboxylic acid (**5-8**).

Yield

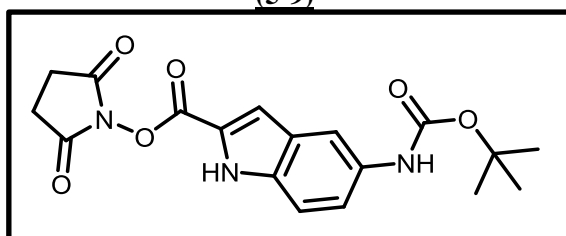
750mg, 96%

¹H-NMR (300 MHz, DMSO-*d*₆, 298 K)

δ (ppm) = 12.86 (s, 1H), 11.58 (s, 1H), 9.16 (s, 1H), 7.77 (s, 1H), 7.45 – 7.16 (m, 2H), 6.98 (d, $J = 2.0$ Hz, 1H), 1.48 (s, 9H).

¹³C-NMR (75 MHz, DMSO-*d*₆, 298 K)

δ (ppm) = 162.68, 153.08, 133.58, 132.27, 126.77, 112.27, 106.95, 78.49, 66.97, 28.12, 25.08.

2,5-dioxopyrrolidin-1-yl 5-((tert-butoxycarbonyl)amino)-1H-indole-2-carboxylate**(5-9)**

Compound **5-8** and 1-hydroxypyrrolidine--2,5-dione were dissolved in 20 mL THF. DIC (N,N'-diisopropylcarbodiimide) was added and the reaction was stirred under argon for 3h. The solvent was removed under vacuum, the remaining product was redissolved in

EtOAc (400 mL) and washed with saturated NaCl solution (3x 200 mL). The organic layer was dried with MgSO₄ and the solvent removed under vacuum to yield the product 2,5-dioxopyrrolidin-1-yl 5-((*tert*-butoxycarbonyl)amino)-indole-2-carboxylate (**5-9**).

Yield

530 mg, 79%

MS

m/z (MALDI-TOF) 374.22 [M+H]⁺

m/z (ESI-TOF) 769.26 [2*M+Na]⁺

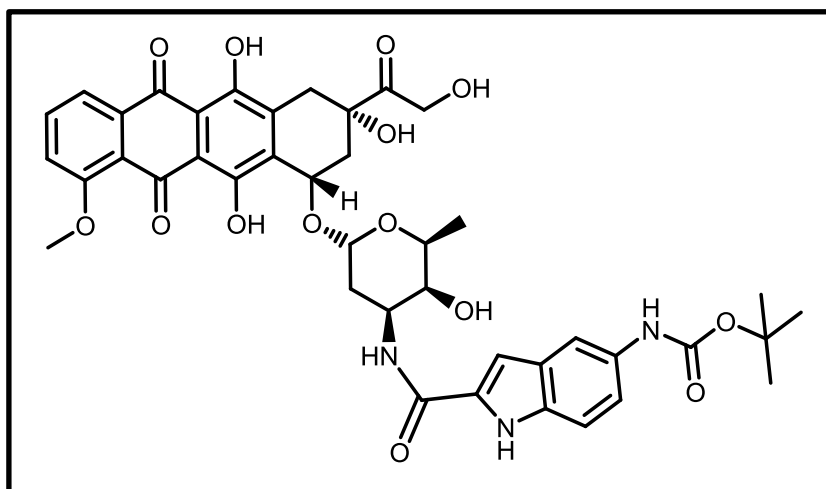
¹H-NMR (700 MHz, DMSO-*d*₆, 298 K)

δ (ppm) = 12.28 (d, *J* = 2.2 Hz, 1H), 9.30 (s, 1H), 7.93 (s, 1H), 7.44 (d, *J* = 2.0 Hz, 1H), 7.38 (d, *J* = 2.0 Hz, 2H), 4.03 (q, *J* = 7.1 Hz, 2H), 2.90 (s, 4H), 1.49 (s, 9H).

¹³C-NMR (176 MHz, DMSO-*d*₆, 298 K)

δ (ppm) = 170.43, 156.80, 153.06, 135.01, 133.25, 126.60, 121.21, 112.70, 111.17, 78.77, 28.17, 25.52.

***tert*-butyl (2-(((2*S*,3*S*,4*S*,6*R*)-3-hydroxy-2-methyl-6-(((1*S*,3*S*)-3,5,12-trihydroxy-3-(2-hydroxyacetyl)-10-methoxy-6,11-dioxo-1,2,3,4,6,11-hexahydrotetracen-1-yl)oxy)tetrahydro-2*H*-pyran-4-yl)carbamoyl)-1*H*-indol-5-yl)carbamate**

(5-10)

Compound **5-9** (230 mg, 670 μmol) and doxorubicin (400 mg, 737 μmol) were dissolved in 20 mL DMF and stirred for 2 h under argon after the addition of DIPEA (0.18 mL, 1 mmol).

The solution was added to 300 mL EtOAc and washed 3x with saturated NaCl. The organic layer was dried with MgSO₄ and the solvent was removed under vacuum. During the work up a second product arises, which could be separated by column chromatography (CHCl₃/MeOH 20:1). After removal of the solvents under vacuum, the remaining product was redissolved in THF, precipitated in Hexane, filtered off and dried under high vacuum to yield the red product (**5-10**).

Yield

100 mg, 20%

MS

m/z (MALDI-TOF) 824.29 [M+Na]⁺, 1625.59 [2M+Na]⁺

m/z (FD) 802.7

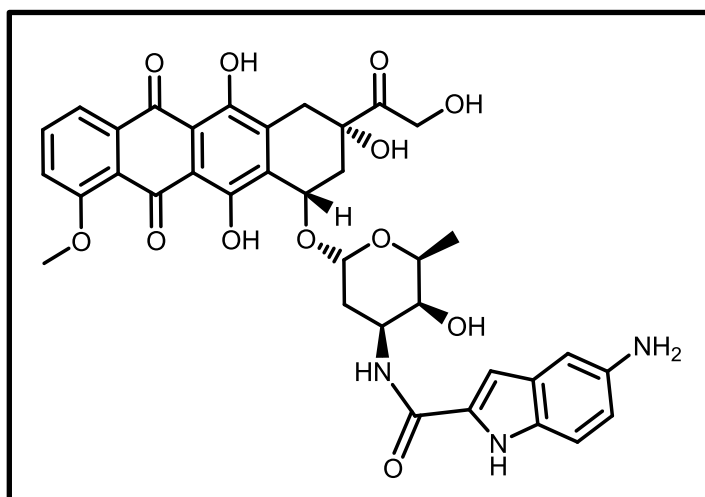
¹H-NMR (700 MHz, DMSO-*d*₆, 298 K)

δ (ppm) = 14.02 (s, 1H), 13.25 (s, 1H), 11.34 (s, 1H), 9.08 (s, 1H), 7.93 – 7.82 (m, 3H), 7.72 (s, 1H), 7.61 (dt, J = 6.4, 4.1 Hz, 1H), 7.25 (d, J = 8.8 Hz, 1H), 7.15 (d, J = 8.8 Hz, 1H), 7.06 (d, J = 2.2 Hz, 1H), 5.50 (s, 1H), 5.35 – 5.23 (m, 1H), 5.00 – 4.91 (m, 2H), 4.87 (t, J = 6.1 Hz, 1H), 4.65 – 4.54 (m, 2H), 4.24 (p, J = 9.3, 7.9 Hz, 2H), 3.96 (s, 3H), 3.55 (d, J = 5.1 Hz, 1H), 3.00 (d, J = 18.1 Hz, 1H), 2.93 (d, J = 18.0 Hz, 1H), 2.25 (d, J = 14.4 Hz, 1H), 2.14 (dd, J = 14.3, 5.7 Hz, 1H), 2.11 – 2.04 (m, 1H), 1.57 (dd, J = 12.4, 4.5 Hz, 1H), 1.47 (s, 9H), 1.17 (d, J = 6.6 Hz, 3H).

¹³C-NMR (176 MHz, DMSO-*d*₆, 298 K)

δ (ppm) = 214.24, 186.97, 186.86, 161.22, 160.72, 156.59, 154.95, 153.60, 136.63, 135.99, 135.09, 134.56, 133.21, 132.50, 127.39, 120.44, 120.16, 119.42, 112.50, 111.23, 111.10, 103.36, 100.92, 78.90, 75.43, 70.51, 68.50, 67.18, 64.16, 57.00, 46.02, 40.49, 37.18, 32.55, 30.14, 28.69, 17.53.

5-amino-*N*-((2*S*,3*S*,4*S*,6*R*)-3-hydroxy-2-methyl-6-(((1*S*,3*S*)-3,5,12-trihydroxy-3-(2-hydroxyacetyl)-10-methoxy-6,11-dioxo-1,2,3,4,6,11-hexahydrotetracen-1-yl)oxy)tetrahydro-2*H*-pyran-4-yl)-1*H*-indole-2-carboxamide
(5-11)



5-9 (30 mg, 90.01 μmol) was gradually dissolved in 5 ml dry DCM and the identical amount of TFA was added. The solution was vigorously stirred for 1 h at room temperature and the solvent and reagent were removed under reduced pressure. Doxorubicin hydrochloride (57.42 mg, 99.01 μmol) was dissolved in 5 ml dry DMF and was added to the oily residue. DIPEA (13.96 mg, 18.81 μL , 108.01 μmol) was used to make the pH basic. Afterwards, the reaction mixture was stirred for 4 h at room temperature and was subsequently purified by reversed-phase high-performance liquid chromatography (RP-HPLC). The solvent of the isolated fractions was removed under reduced pressure, whereby the product was obtained as a red solid (**5-11**).

Yield

38 mg, 54.16 μmol , 60 %

MS

m/z (MALDI-TOF) 724.43 $[\text{M}+\text{Na}]^+$, 741.57 $[\text{M}+\text{K}]^+$

m/z (ESI-TOF) 724.22 $[\text{M}+\text{Na}]^+$, 1403.47 $[2\text{M}+\text{H}]^+$, 1425.44 $[2\text{M}+\text{Na}]^+$

¹H-NMR (700 MHz, DMSO-*d*₆, 298 K)

δ (ppm) = 14.07 (s, 1H), 13.30 (s, 1H), 11.07 – 10.96 (m, 1H), 7.95 – 7.88 (m, 2H), 7.76 (t, J = 6.9 Hz, 1H), 7.68 – 7.63 (m, 1H), 7.10 (dd, J = 8.7, 3.3 Hz, 1H), 6.91 – 6.82 (m, 1H), 6.66 (t, J = 2.7 Hz, 1H), 6.58 (dt, J = 6.7, 2.2 Hz, 1H), 5.54 (t, J = 2.5 Hz, 1H), 5.29 (d, J = 3.6 Hz, 1H), 5.00 (t, J = 4.2 Hz, 1H), 4.92 (t, J = 5.5 Hz, 1H), 4.87 (q, J = 5.6 Hz, 1H), 4.60 (d, J = 4.9 Hz, 2H), 4.22 (ddt, J = 23.2, 9.2, 4.9 Hz, 2H), 3.98 (d, J = 2.7 Hz, 3H), 3.57 – 3.51 (m,

1H), 3.00 (t, $J = 16.1$ Hz, 2H), 2.29 – 2.14 (m, 2H), 2.10 – 2.02 (m, 1H), 1.92 (d, $J = 3.5$ Hz, 2H), 1.61 – 1.51 (m, 1H), 1.17 (dd, $J = 6.5, 4.0$ Hz, 3H).

¹³C-NMR (176 MHz, DMSO-*d*₆, 298 K)

δ (ppm) = 187.07 (d, $J = 17.3$ Hz), 161.28, 160.93, 156.62, 154.98, 142.23, 136.70, 136.09, 135.21, 134.63, 131.58, 130.91, 128.40, 120.56, 120.22, 119.49, 115.39, 112.84, 111.33, 111.19, 103.05, 102.21, 100.91, 75.47, 70.56, 68.53, 67.21, 64.14, 57.08, 46.06, 37.29, 32.59, 30.18, 17.56

RP-HPLC

$t_R = 33.37$ min

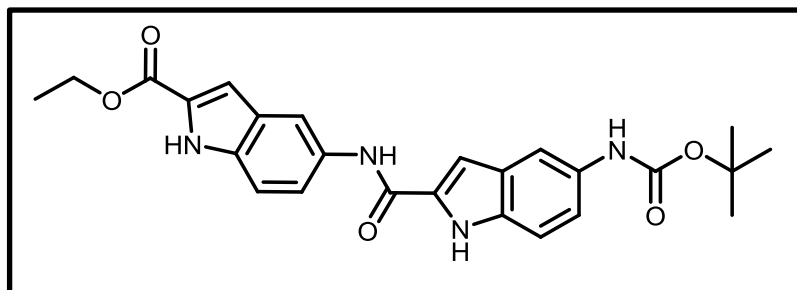
A: 25 mM triethylammonium acetate (TEAA) buffer (pH 7)

B: acetonitrile (ACN)

0 min 100% A – 40 min 30% A;

ethyl 5-(5-((tert-butoxycarbonyl)amino)-1H-indole-2-carboxamido)-1H-indole-2-carboxylate

(5-13)



5-7 (100 mg, 489.65 μmol) was gradually dissolved in 10 ml dry DCM and the identical amount of TFA was added. The solution was vigorously stirred for 1 h at room temperature and the solvent and reagent were removed under reduced pressure (as an easier and conventional alternative **5-6** can be used directly). **5-9** (164.5 mg, 440.68 μmol) was dissolved in 5 ml dry DMF and was added to the oily residue. DIPEA was used to make the pH basic. Afterwards, the reaction mixture was stirred for 4 h under argon at room temperature and was subsequently added to 200 ml EtOAc and brine (3x 150 ml) was used for washing. The organic phases were collected, dried with MgSO_4 and purified by column chromatography (EtOAc/Hex 3:2). The solvent of the isolated fractions was removed under reduced pressure, whereby the product was obtained as a brown solid (**5-13**).

Yield

121 mg, 261,62 μmol , 53 %

MS

m/z (MALDI-TOF) 462.65 $[\text{M}+\text{H}]^+$, 484.58 $[\text{M}+\text{Na}]^+$

m/z (FD) 462.1

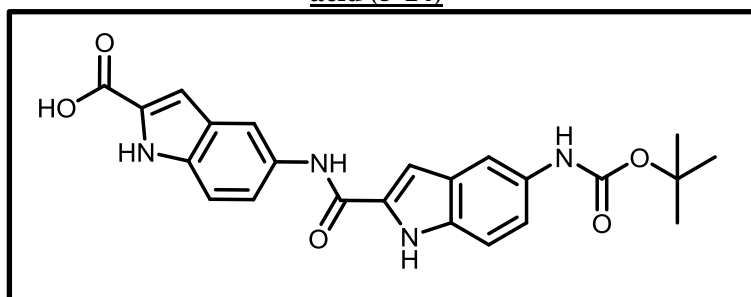
 $^1\text{H-NMR}$ (700 MHz, DMSO- d_6 , 298 K)

δ (ppm) = 11.87 (s, 1H), 11.56 (s, 1H), 10.11 (s, 1H), 9.15 (s, 1H), 8.13 (d, $J = 1.9$ Hz, 1H), 7.79 (s, 1H), 7.59 (dd, $J = 9.0, 2.0$ Hz, 1H), 7.44 (d, $J = 8.9$ Hz, 1H), 7.37 – 7.26 (m, 2H), 7.22 (dd, $J = 8.9, 2.0$ Hz, 1H), 7.16 (d, $J = 2.0$ Hz, 1H), 4.35 (q, $J = 7.1$ Hz, 2H), 1.49 (s, 9H), 1.17 (t, $J = 7.1$ Hz, 3H).

 $^{13}\text{C-NMR}$ (176 MHz, DMSO- d_6 , 298 K)

δ (ppm) = 161.22, 159.54, 153.11, 134.50, 133.12, 132.26, 132.20, 131.82, 127.93, 127.06, 126.58, 120.01, 117.43, 113.10, 112.50, 112.20, 107.71, 103.21, 78.46, 60.36, 28.17, 14.25.

5-((*tert*-butoxycarbonyl)amino)-1*H*-indole-2-carboxamido)-1*H*-indole-2-carboxylic acid (5-14)



Compound **5-13** (100 mg, 216.21 μmol) was dissolved in 8 mL dioxane:MeOH (1:1) and mixed with 1g NaOH in 8 mL water. The reaction solution was stirred for 24 h until no starting compound was left and added to 500 mL water. Afterwards the pH was adjusted to pH 1 with HCl (35%). The precipitated product was collected by vacuum filtration to yield the brown product (**5-14**).

Yield

85 mg, 195,65 μmol , 90 %

MS

m/z (MALDI-TOF) 436.26 $[\text{M}+\text{Na}]^+$

¹H-NMR (700 MHz, DMSO-*d*₆, 298 K)

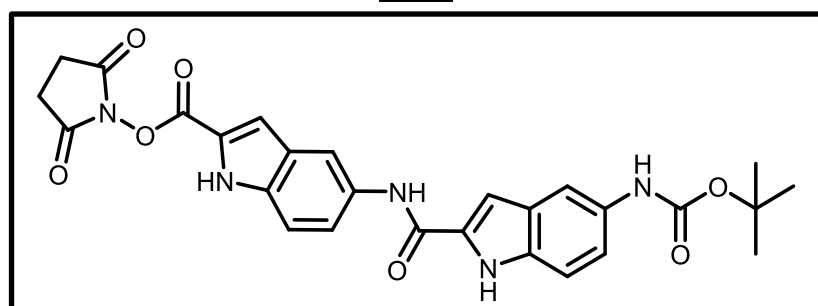
δ (ppm) = 12.93 (s, 1H), 11.74 (d, J = 2.2 Hz, 1H), 11.56 (d, J = 2.2 Hz, 1H), 10.10 (s, 1H), 9.15 (s, 1H), 8.13 (d, J = 1.9 Hz, 1H), 7.80 (s, 1H), 7.57 (dd, J = 8.9, 2.0 Hz, 1H), 7.47 – 7.38 (m, 1H), 7.38 – 7.27 (m, 2H), 7.23 (dd, J = 8.8, 2.0 Hz, 1H), 7.10 (dd, J = 2.2, 0.9 Hz, 1H), 1.49 (s, 9H).

¹³C-NMR (176 MHz, DMSO-*d*₆, 298 K)

δ (ppm) = 162.69, 159.43, 153.12, 134.29, 133.04, 132.20, 131.58, 129.01, 127.00, 126.67, 119.57, 112.95, 112.39, 112.09, 107.29, 103.09, 78.46, 28.16.

2,5-dioxopyrrolidin-1-yl 5-(5-((*tert*-butoxycarbonyl)amino)-1H-indole-2-carboxamido)-1H-indole-2-carboxylate

(5-15)



Compound **5-14** (22 mg, 50.64 μ mol) and 1-hydroxypyrrolidine--2,5-dione (6.12 mg, 53.17 μ mol) were dissolved in 5 mL dry THF. DIC (*N,N'*-diisopropylcarbodiimide, 6.71 mg, 8.23 μ l, 53.17 μ mol) was added and the reaction was stirred under argon for 3h. The solvent was removed under vacuum and the remaining product was redissolved in EtOAc (50 mL) and washed with saturated NaCl solution (5x 50 mL). The organic layer was dried with MgSO₄ and the solvent removed under vacuum to yield the product (**5-15**).

Yield

20 mg, 37.63 μ mol, 74 %

MS

m/z (MALDI-TOF) 532.74 [M+Na]⁺, 553.63 [M+K]⁺

¹H-NMR (700 MHz, DMSO-*d*₆, 298 K)

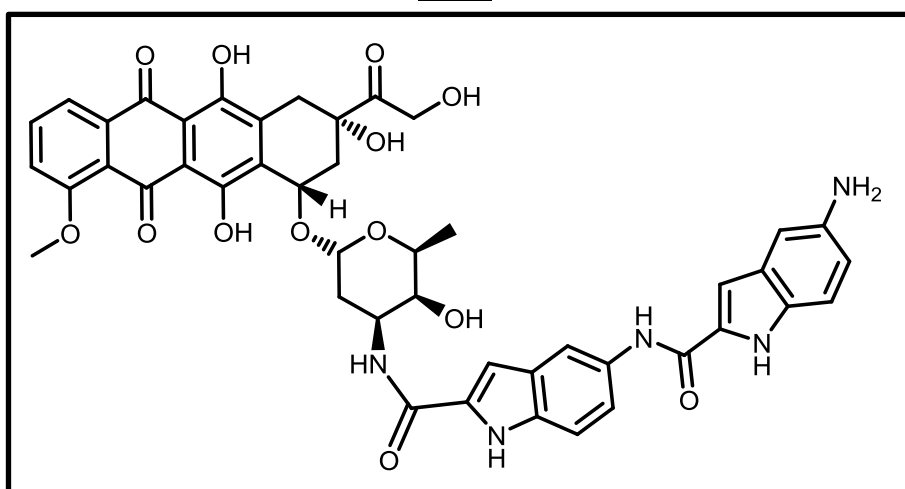
δ (ppm) = 12.45 (d, *J* = 2.2 Hz, 1H), 11.84 (d, *J* = 2.2 Hz, 1H), 10.48 (s, 1H), 9.17 (s, 1H), 8.32 (d, *J* = 1.9 Hz, 1H), 7.83 – 7.76 (m, 2H), 7.54 – 7.48 (m, 2H), 7.38 – 7.32 (m, 2H), 7.25 (d, *J* = 8.8 Hz, 1H), 2.92 (s, 4H), 1.48 (s, 9H).

¹³C-NMR (176 MHz, DMSO-*d*₆, 298 K)

δ (ppm) = 170.45, 162.32, 159.46, 156.82, 153.16, 135.70, 133.13, 132.71, 132.10, 126.93, 126.42, 121.73, 121.39, 112.87, 112.14, 111.49, 104.05, 78.51, 35.75, 30.78, 25.55.

5-amino-*N*-(2-(((2*S*,3*S*,4*S*,6*R*)-3-hydroxy-2-methyl-6-(((1*S*,3*S*)-3,5,12-trihydroxy-3-(2-hydroxyacetyl)-10-methoxy-6,11-dioxo-1,2,3,4,6,11-hexahydrotetracen-1-yl)oxy)tetrahydro-2*H*-pyran-4-yl)carbamoyl)-1*H*-indol-5-yl)-1*H*-indole-2-carboxamide

(**5-17**)



5-15 (40 mg, 75 μmol) was gradually dissolved in 3 ml dry DCM and the identical amount of TFA was added. The solution was vigorously stirred for 1 h at room temperature and the solvent and reagent were removed under reduced pressure. Doxorubicin hydrochloride (47.84 mg, 82.49 μmol) was dissolved in 3 ml dry DMF and was added to the oily residue. DIPEA was used to make the pH basic. Afterwards, the reaction mixture was stirred for 24 h at room temperature and was subsequently purified by reversed-phase high-performance liquid chromatography (RP-HPLC). The solvent of the isolated fractions was removed under reduced pressure, whereby the product was obtained as a red solid (**5-17**).

Yield

31 mg, 23.26 μmol, 48 %

MS

m/z (MALDI-TOF) 883.55 [M+K]⁺

¹H-NMR (700 MHz, DMSO-*d*₆, 298 K)

δ (ppm) = 14.05 (d, J = 3.8 Hz, 1H), 13.28 (s, 1H), 12.04 (s, 1H), 11.54 (s, 1H), 10.28 (s, 1H), 10.07 (d, J = 61.0 Hz, 3H), 8.08 (s, 1H), 8.05 – 7.98 (m, 1H), 7.89 (d, J = 4.4 Hz, 2H), 7.67 (s, 1H), 7.66 – 7.60 (m, 1H), 7.60 – 7.50 (m, 2H), 7.47 (s, 1H), 7.40 (dd, J = 9.0, 3.8 Hz, 1H), 7.20 (d, J = 15.0 Hz, 2H), 5.55 (s, 1H), 5.30 (s, 1H), 4.98 (s, 2H), 4.62 (d, J = 4.0 Hz, 2H), 4.25 (dd, J = 16.7, 8.4 Hz, 2H), 3.97 (d, J = 3.8 Hz, 3H), 3.58 (s, 1H), 3.10 – 3.03 (m, 3H), 3.02 – 2.93 (m, 3H), 2.27 (d, J = 14.1 Hz, 1H), 2.16 (d, J = 13.6 Hz, 1H), 2.13 – 2.06 (m, 1H), 1.60 (d, J = 12.5 Hz, 1H), 1.19 (t, J = 6.6 Hz, 3H).

¹³C-NMR (176 MHz, DMSO-*d*₆, 298 K)

δ (ppm) = 214.27, 187.01, 186.91, 161.24, 160.68, 159.49, 156.62, 154.97, 136.67, 136.03, 135.96, 135.13, 134.61, 134.23, 134.03, 132.85, 131.69, 127.48, 127.27, 120.47, 120.19, 119.45, 119.02, 118.97, 113.93, 113.31, 112.60, 111.26, 111.13, 103.93, 103.81, 100.93, 75.45, 70.56, 68.52, 67.20, 64.17, 57.06, 46.14, 45.90, 42.58, 40.90, 37.23, 32.57, 30.15, 17.57.

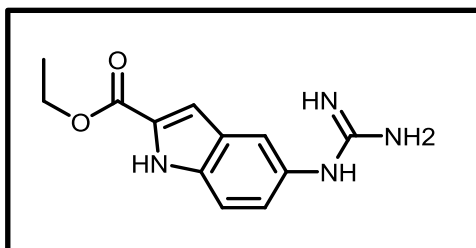
RP-HPLC

t_R = 37.84 min

A: 25 mM triethylammonium acetate (TEAA) buffer (pH 7)

B: acetonitrile (ACN)

0 min 100% A – 40 min 30% A;

Ethyl 5-guanidino-1*H*-indole-2-carboxylate (5-18)

Compound **5-6** (200 mg, 979.29 μ mol), p-toluenesulfonic acid (185.50 mg, 1.08 μ mol) and cyanamide (49.40 mg, 1.18 μ mol) were dissolved in 30 ml dioxane and the solution was stirred after flushing with argon for 10 min for 2 h at 110 °C until everything was diluted and at 90 °C overnight. The solvent was removed under vacuum and the remains were

subsequently purified by reversed-phase high-performance liquid chromatography (RP-HPLC) to yield a brown powder (**5-18**).

Yield

180 mg, 730.91 μmol , 75 %

MS

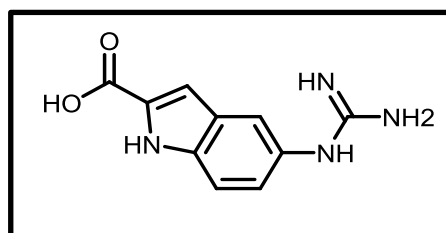
m/z (MALDI-TOF) 245.86 $[\text{M}+\text{H}]^+$, 268.83 $[\text{M}+\text{Na}]^+$, 288.92 $[\text{M}+\text{K}]^+$

 $^1\text{H-NMR}$ (300 MHz, DMSO- d_6 , 298 K)

δ (ppm) = 12.03 (s, 1H), 7.48 (s, 4H), 7.48 (m, $J = 8.0$ Hz, 2H), 7.15 (d, $J = 2.2$ Hz, 1H), 7.09 (d, $J = 8.0$ Hz, 1H), 4.64 (s, 2H), 4.34 (q, $J = 7.0$ Hz, 2H), 1.34 (t, $J = 7.0$ Hz, 3H).

 $^{13}\text{C-NMR}$ (75 MHz, DMSO- d_6 , 298 K)

δ (ppm) = 172.87, 161.09, 142.22, 131.51, 127.73, 126.60, 116.59, 112.67, 60.51, 45.47, 66.34, 14.34.

5-guanidino-1H-indole-2-carboxylic acid (5-19)

Compound **5-18** (215 mg, 873.03 μmol) was dissolved in 6 ml MeOH and mixed with 1g NaOH in 6 mL water. The reaction solution was stirred for 24 h until no starting compound was left and subsequently purified by reversed-phase high-performance liquid chromatography (RP-HPLC) to yield a brown powder (**5-19**).

Yield

170 mg, 782.66 μmol , 90 %

MS

m/z (MALDI-TOF) 218.85 $[\text{M}+\text{H}]^+$, 241.79 $[\text{M}+\text{Na}]^+$

 $^1\text{H-NMR}$ (300 MHz, DMSO- d_6 , 298 K)

δ (ppm) = 11.22 (s, 1H), 7.92 (s, 4H), 7.39 (d, $J = 8.3$ Hz, 2H), 7.01 – 6.86 (m, 1H), 6.71 (s, 1H).

 $^{13}\text{C-NMR}$ (75 MHz, DMSO- d_6 , 298 K)

δ (ppm) = 172.14, 157.03, 148.36, 134.81, 127.81, 126.38, 120.47, 118.16, 112.97, 103.37.

Acknowledgements

Mein ganz besonderer Dank gilt [REDACTED] und [REDACTED], die es mir ermöglicht hat, diese faszinierende Arbeit am Max-Planck-Institut für Polymerforschung durchführen zu können.

Ein herzlicher Dank gebührt dabei besonders [REDACTED], die mir immerzu die nötigen Freiräume gewährt hat, um die in dieser Dissertation vorliegenden Ergebnisse zu verwirklichen. Eine Vielzahl der hier erreichten Resultate wäre ohne ihre stets motivierende und ermutigende Einstellung sowie konstruktive Kritik nicht möglich gewesen.

Ich danke meinen Labor- und Bürokollegen [REDACTED] für die vielen interessanten Gespräche fachlicher und privater Natur. Die zahlreichen Gelegenheiten zum Ideenaustausch haben die Forschungsprojekte maßgeblich vorangetrieben und die lockeren Plaudereien gestalteten die Zeit stets kurzweilig.

Meinem Vorgänger [REDACTED] danke ich besonders für seine engagierte und gute Unterstützung bei meinem Start ins MPIP-Leben sowie vielen nützlichen Diskussionen zu verschiedenen Themen dieser Arbeit.

[REDACTED] danke ich für die vielen interessanten Gespräche und Lektionen über die Möglichkeiten der NMR sowie unvergesslichen Momenten des Triumphes auf dem Fußballplatz.

Allen Kooperationspartnern des Instituts für Molekulare Biologie, der Universitätsmedizin sowie der Arbeitsgruppe von [REDACTED], insbesondere [REDACTED], der Johannes Gutenberg-Universität Mainz und der Arbeitsgruppe von [REDACTED] des Max-Planck-Institut für Psychiatrie München bin ich aufgrund der ertragreichen Zusammenarbeit ebenfalls zu Dank verpflichtet.

Des Weiteren gilt mein Dank all jenen, die mich bei der Analyse und Charakterisierung der isolierten Substanzen unterstützt haben. Hierbei sind besonders zu nennen: [REDACTED], für die Aufnahme der Fluoreszenzspektren; [REDACTED] und [REDACTED] der Massenspektrometrie-Abteilung; [REDACTED], [REDACTED] und [REDACTED], der NMR-Abteilung, sowie [REDACTED] vom IMB Mainz für die sehr gute Zusammenarbeit bei verschiedenen HPLC-MS Studien.

Herzlich danke ich auch allen Mitgliedern dieses Arbeitskreises für die wunderbare gemeinsame Zeit, den guten Zusammenhalt und die vielen schönen gemeinsamen Erlebnissen.

Schließlich danke ich von ganzen Herzen meinen Eltern, meinen Geschwistern und meinen Freunden, die stets an mich geglaubt und mich immer mit allen Kräften unterstützt haben.

List of publications

1. “Octreotide-Mediated Tumor-Targeted Drug Delivery via a Cleavable Doxorubicin-Peptide Conjugate”
Marco Lelle, Stefka Kaloyanova, **Christoph Freidel**, Marily Theodoropoulou, Michael Musheev, Christof Niehrs, Guenter Stalla, Kalina Peneva; From *Molecular Pharmaceutics* (2015), 12(12), 4290- 4300
2. “The guanidinium group as a key part of water-soluble polymer carriers for siRNA complexation and protection against degradation”
Ilja Tabujew, **Christoph Freidel**, Bettina Krieg, Mark Helm, Kaloian Koynov, Klaus Muellen, Kalina Peneva; From *Macromolecular Rapid Communications* (2014), 35(13), 1191-1197
3. “Chemical tags for site-specific fluorescent labeling of biomolecules”
Christoph Freidel, Stefka Kaloyanova, Kalina Peneva; *Amino Acids*. 2016 Jun; 48(6):1357-72
4. “Overcoming drug resistance by cell-penetrating peptide-mediated delivery of a doxorubicin dimer with high DNA-binding affinity”
Marco Lelle, **Christoph Freidel**, Stefka Kaloyanova, Ilja Tabujew, Alexander Schramm, Michael Musheev, Christof Niehrs, Klaus Müllen, Kalina Peneva; *Eur J Med Chem*. 2017 Apr 21;130:336-345
5. “Site-Selective Modification of Peptides and Proteins with Minimal Structural Alteration “
Christoph Freidel, Lars Andernach, Stefka Kaloyanova, Marco Lelle, Marily Theodoropoulou, Günter Stalla, Till Opatz, Klaus Müllen, Kalina Peneva
in preparation
6. “Octreotide-Mediated Tumor-Targeted Doxorubicin and PDI-dye Delivery via novel Cleavable linker systems”
Christoph Freidel, Ilja Tabujew, Stefka Kaloyanova, Marco Lelle, Klaus Müllen, Kalina Peneva
in preparation

Appendix

Appendix 1 (4-7)

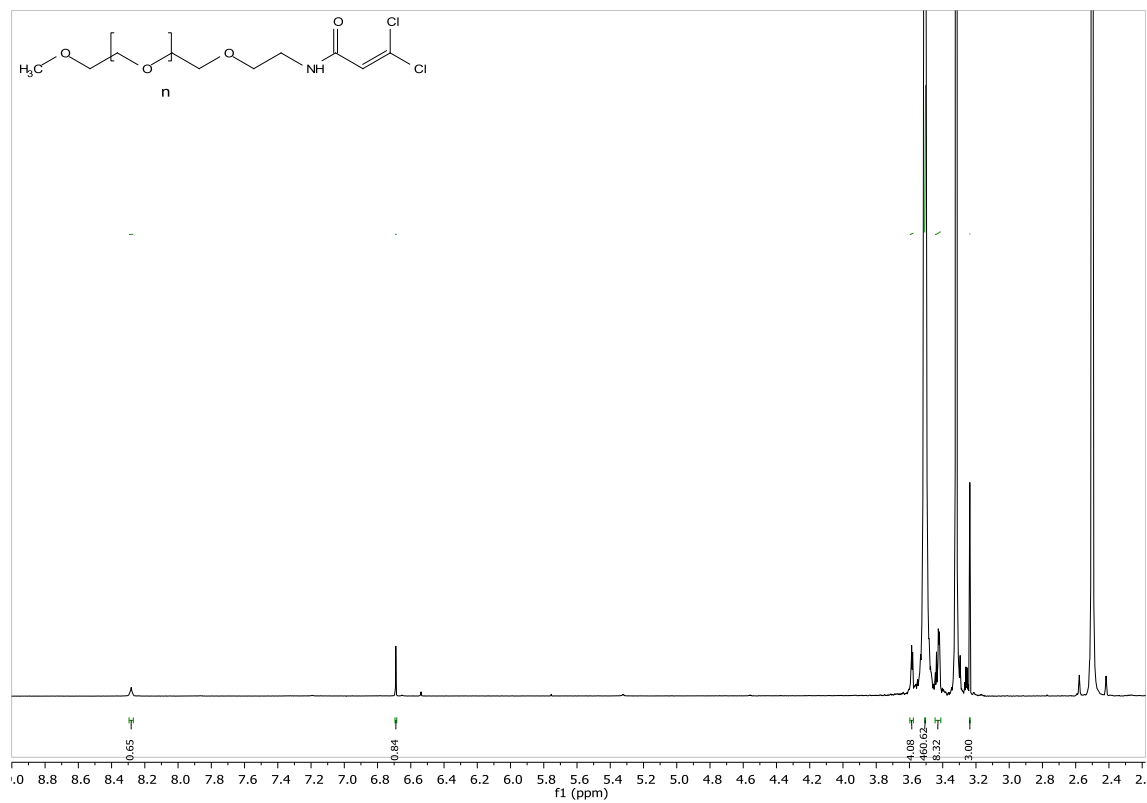


Figure 73: ¹H NMR of compound 4-7 (300 MHz, DMSO-d₆, 298 K)

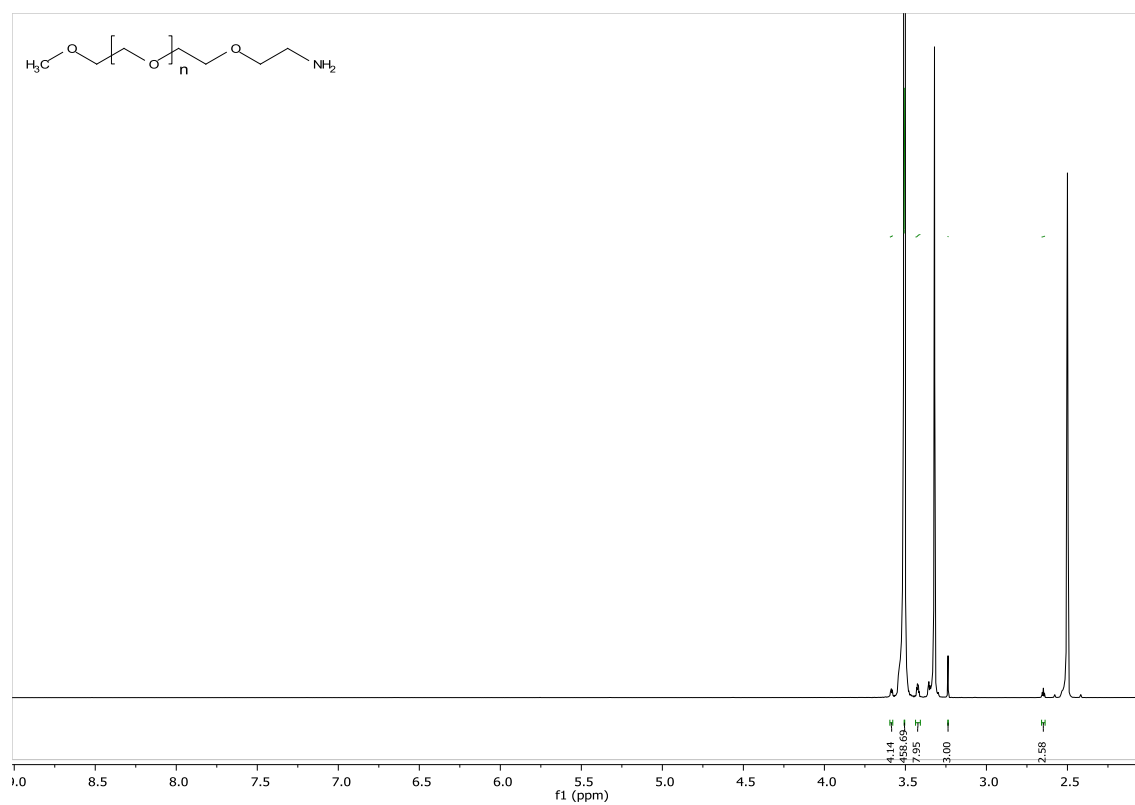


Figure 74: ^1H NMR of PEG-(5000)- NH_2 (300 MHz, $\text{DMSO-}d_6$, 298 K)

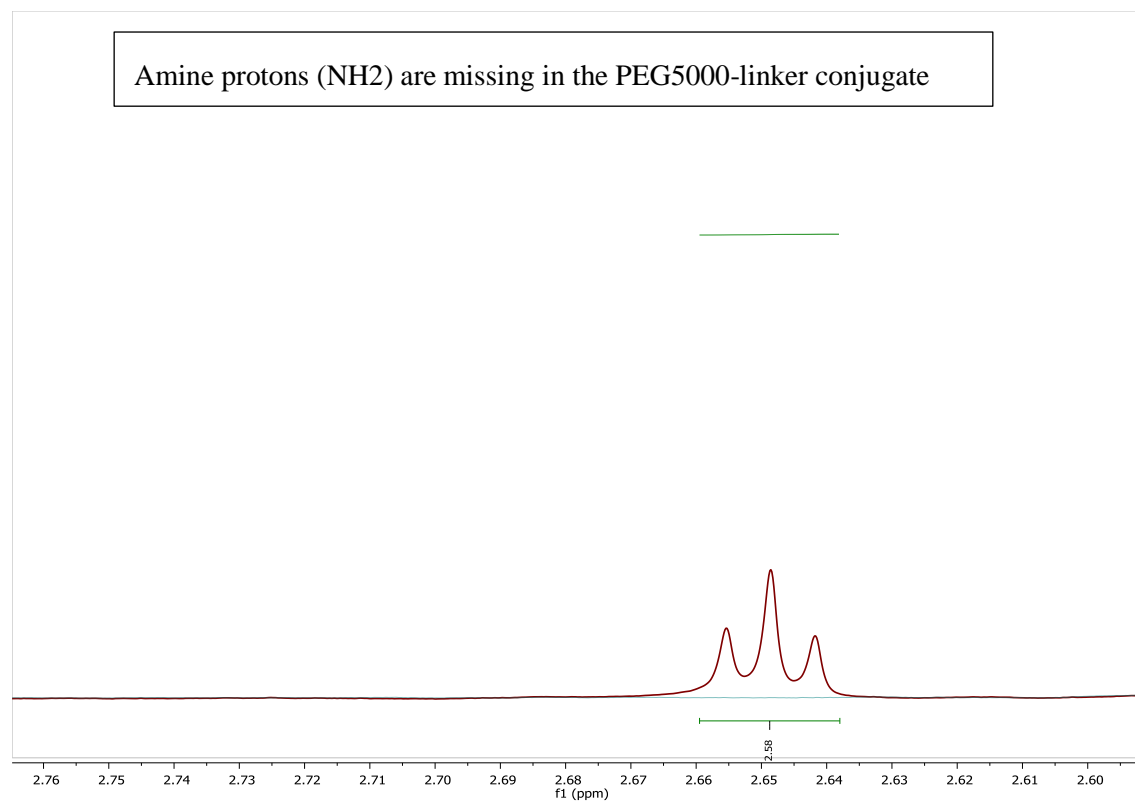


Figure 75: ^1H NMR overlay of compound **4-7** and PEG-(5000)- NH_2 (300 MHz, $\text{DMSO-}d_6$, 298 K)

Furthermore, two new peaks (NH and acrylic H) can be found in the PEG5000-linker conjugate spectrum

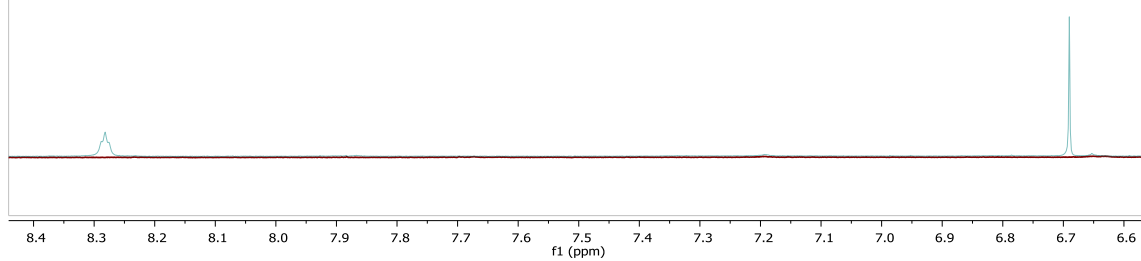
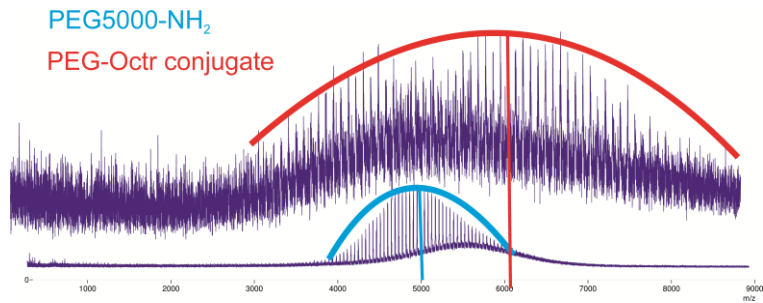


Figure 76: ^1H NMR overlay of compound **4-7** and PEG-(5000)- NH_2 (300 MHz, $\text{DMSO}-d_6$, 298 K)

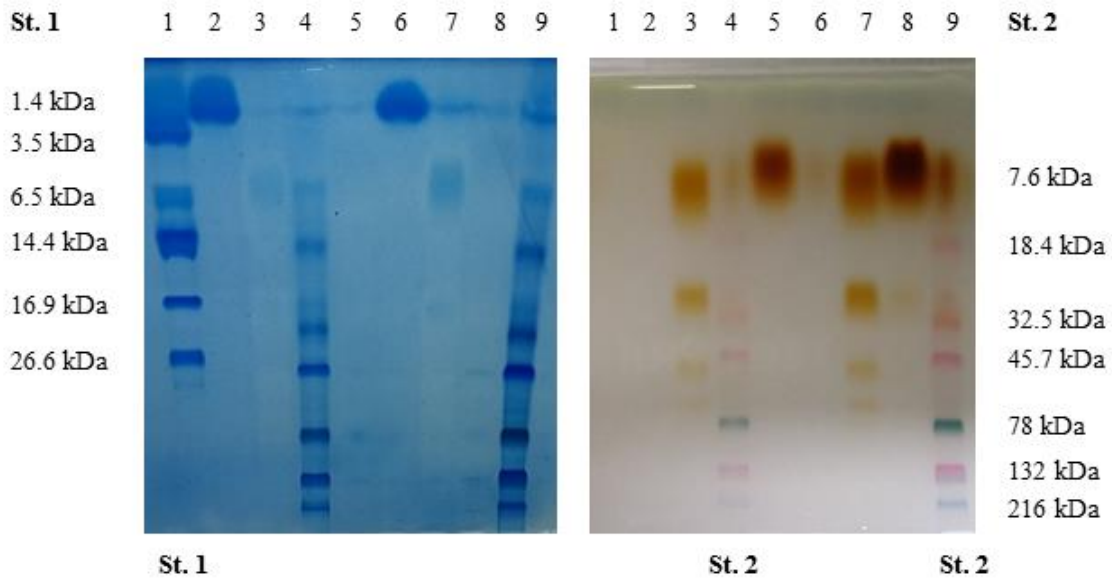
Appendix 2 (4-8)

MALDI-TOF



SDS-PAGE

Compound	line
Octreotide:	2, 6
PEG(5000)-NH ₂ :	5, 8
4-8:	3, 7
Standard 1:	1
Standard 2:	4, 9



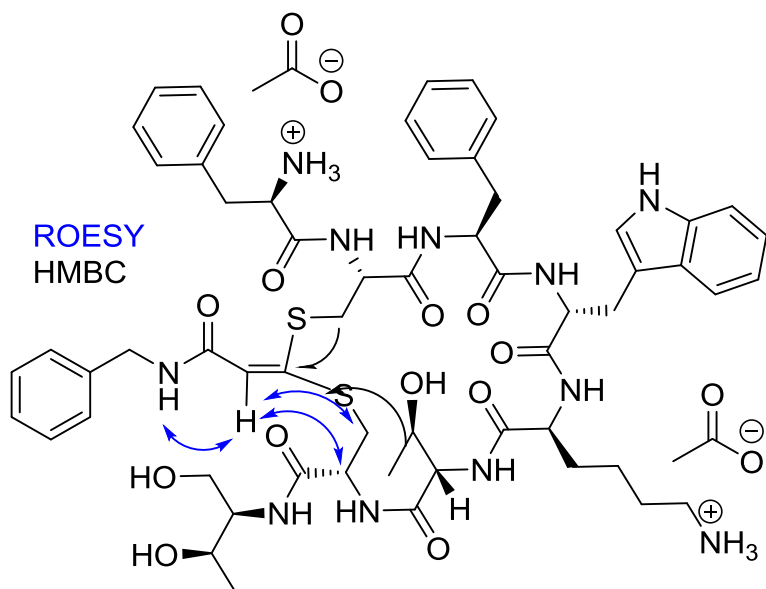
GPC Results:Table 6: Gel permeation chromatography of PEG-5000-NH₂, 4-7 and 4-8

Sample	Molecular weight	PDI	Conditions
PEG-5000	4930,12	1,04	Calibration: peodmf18.CAL Eluent: DMF Flow rate: 1,0 ml/min Pump: PSS SECcurity Inj.vol.: 100,00 Column1: PSS GRAM 100 Column2: GRAM 1000 Column3: Gram 1000 Temp.: 60,00 °C Detector: SECcurity VWD (270mm) Detector: SECcurity RID
4-7	5021,88	1,04	
4-8	5823,88	1,04	

Appendix 3 (4-10)

HMBC and ROESY key relations for Benzylamin – Octreotide

(4-10) towards **Thr**



HMBC and ROESY key relations for Benzylamin – Octreotide

(4-10) towards **Phe**

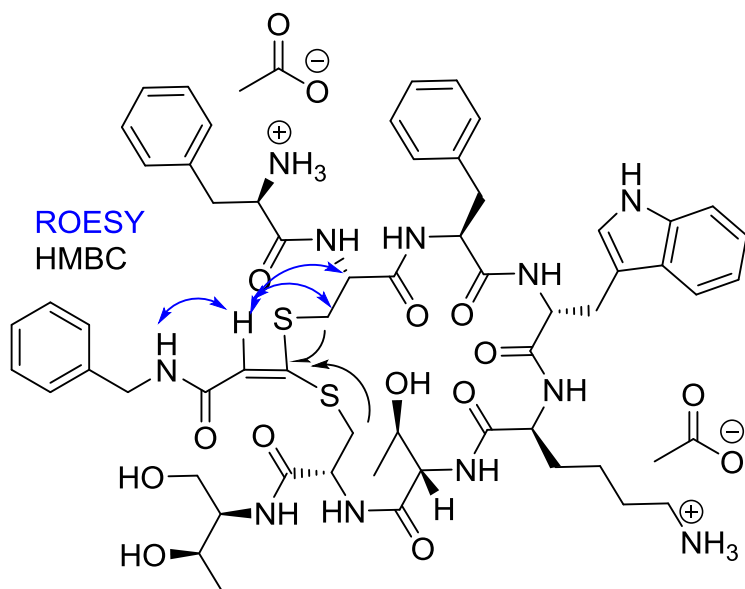


Table 7: ¹H NMR (650 MHz, DMSO-*d*₆, 298 K) and ¹³C-NMR (650 MHz, DMSO-*d*₆, 298 K) of (4-10)

Benzylamin – Octreotide (4-10) assignment towards Thr-ol					
	Proton/Carbon Chemical Shift (ppm)				
Residue	NH	C ^α H	C ^β H	others	Amid C
D-Phe 1	-	3.40/56.0	2.98+2.51/40.9	138.9; 7.20/129.4 7.24/128.1 7.17/126.1	174.7
Cys 2	-	4.53/51.6	3.15+3.28/33.5	-	169.6
Phe 3	8.15	4.50/54.2	2.73+2.81/37.5	137.4 6.97/129.3 7.09/128.0 7.10/126.2	170.5
D-Trp 4	8.47/120.6 11.0/130.4	4.36/54.5	2.87+3.07/27.4	109.8 7.14/123.9 136.2 7.32/111.4 7.06/120.9 7.00/118.3 7.59/118.4 127.1	172.0
Lys 5	8.49/118.5	4.16/53.2	1.47+1.61/31.1	1.11/22.2 (γ) 1.36/29.4 (δ) 2.56/39.7 (ε)	171.9
Thr 6	7.84/108.3	4.19/58.7	4.03/66.0	1.03/19.1	169.8
Cys 7	8.62/117.9	4.56/51.4	3.16+3.35/36.0	-	169.3
Thr(ol) 8	7.64/112.6	3.62/56.0	3.83/64.3	3.46+3.0/60.2 3.83/64.3 0.98/19.9	
Benzylacrylamid-	8.30/116.4	-	-	7.22/127.4; 7.27/128.3; 7.22/127.4 139.6 4.23/42.0; 164.1; 5.96/113.5 149.1	-

Table 8: ^1H NMR (650 MHz, $\text{DMSO-}d^6$, 298 K) and ^{13}C -NMR (650 MHz, $\text{DMSO-}d^6$, 298 K) of (4-10)

Benzylamin – Octreotide (4-10) assignment towards Phe					
Residue	Proton/Carbon Chemical Shift (ppm)				
	NH	C^αH	C^βH	others	Amid C
D-Phe 1	-	3.41/56.0	2.94+2.53/40.8	138.7; 7.19/129.4 7.23/128.2 7.16/126.1	174.7
Cys 2	-	4.67/51.2	2.99+3.20/36.3	-	168.9
Phe 3	8.41	4.63/53.8	2.70+2.81/37.9	137.3 7.02/129.2 7.13/128.0 7.13/126.3	170.5
D-Trp 4	8.57/122.1 11.0/130.3	4.39/54.3	2.81+3.05/27.3	109.7 7.07/123.7 136.2 7.32/111.4 7.06/120.9 6.98/118.3 7.55/118.3 127.2	171.5
Lys 5	8.30/118.7	4.14/52.9	1.41+1.61/31.1	1.02/22.1 (γ) 1.32/29.4 (δ) 2.55/39.7 (ϵ)	171.7
Thr 6	7.79/108.7	4.17/58.6	3.99/66.3	1.01/19.6	169.7
Cys 7	8.40	4.61/52.8	3.18/34.7	-	169.4
Thr(ol) 8	7.52/113.7	3.62/56.0	3.86/64.1	3.31+3.45/60.3 3.86/64.1 0.98/20.0	
Benzylacrylamid-	8.30/116.4	-	-	7.22/126.8; 7.30/128.3; 7.26/127.4 139.3 4.29/42.1; 164.2; 6.23/119.4 147.1	-

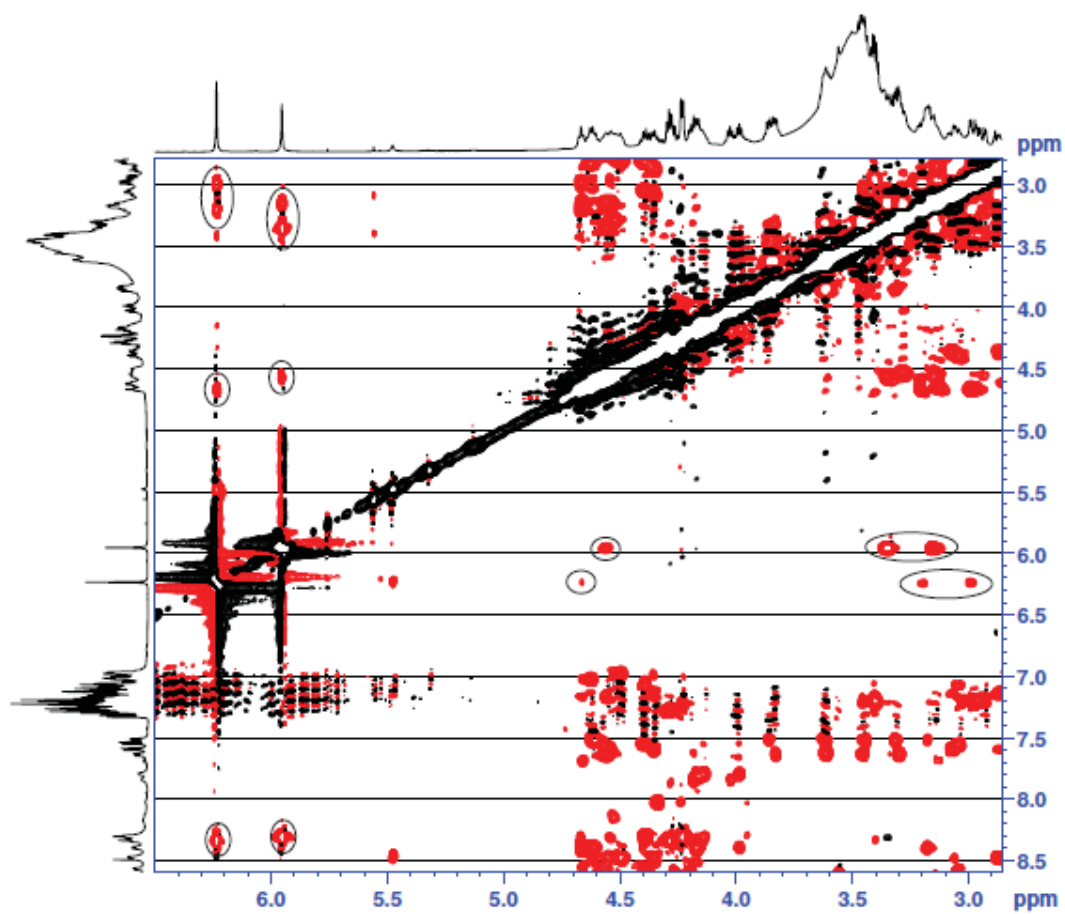
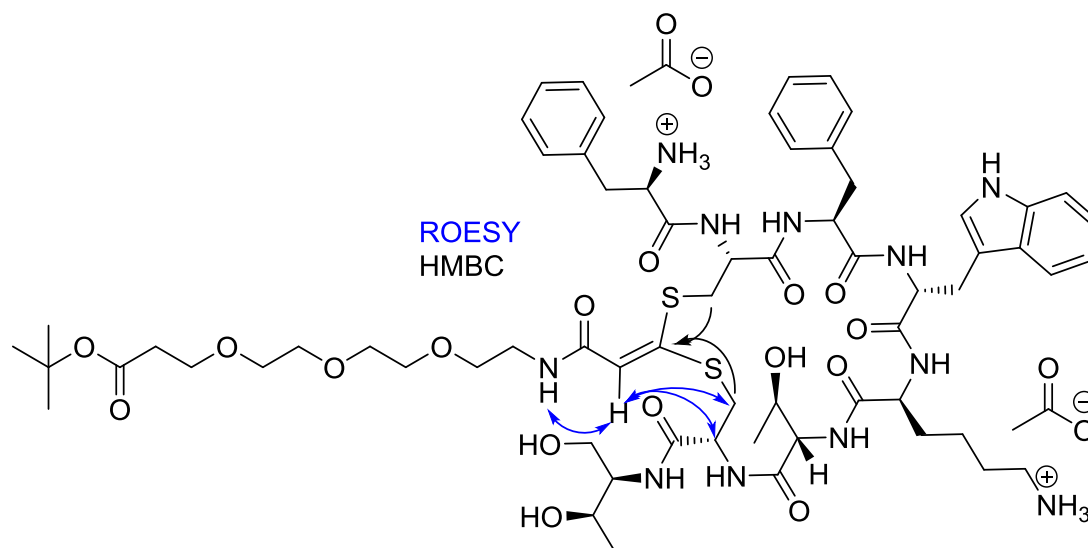


Figure 77: Part of the ROESY spectrum of **4-10** (crosspeaks between olefinic protons and cysteines as well as amide protons marked)

Appendix 4 (4-13)

HMBC and ROESY key relations for Short PEG – Octreotide (4-13) towards

Thr



HMBC and ROESY key relations for Short PEG – Octreotide (4-13) towards

Phe

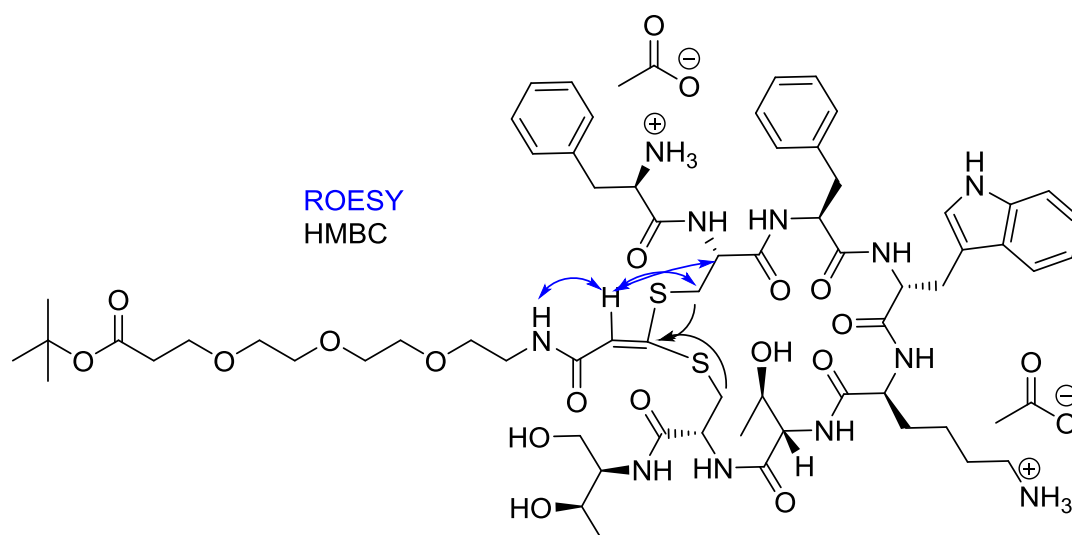


Table 9: ¹H NMR (650 MHz, DMSO-*d*₆, 298 K) and ¹³C-NMR (650 MHz, DMSO-*d*₆, 298 K) of **4-13**

Short PEG – Octreotide (4-13) assignment towards Thr-ol					
	Proton/Carbon Chemical Shift (ppm)				
Residue	NH	C ^α H	C ^β H	others	Amid C
D-Phe 1	-	3.40/56.0	2.51+2.98/40.9	138.9 7.20/129.4 7.25/128.2 7.17/126.2	174.7
Cys 2	-	4.53/51.5	3.15+3.26/33.5	-	169.7
Phe 3	8.14/114.6	4.49/54.2	2.73+2.82/37.5	137.4 6.96/129.3 7.09/128.0 7.12/126.3	170.5
D-Trp 4	8.48/120.8 (Indol) 10.94/130.4	4.33/54.6	2.87+3.07/27.3	109.8 7.13/123.9 136.2 7.33/111.4 7.07/121.0 7.01/118.3 7.58/118.3 127.1	172.0
Lys 5	8.42/118.4	4.16/53.2	1.46+1.63/31.1	1.10/22.3 (γ) 1.36/29.4 (δ) 2.56/39.9 (ε)	172.0
Thr 6	7.77/108.5	4.18/58.8	4.02/66.0	1.04/19.3	169.8
Cys 7	8.47/117.9	4.58/51.4	3.13+3.33/36.2	-	169.3
Thr(ol) 8	7.57/112.5	3.63/56.2	3.86/64.2	1.00/20.0 3.30+3.44/60.2	-
Short PEGamid-	7.88			1.38/27.8 79.8 170.5 2.40/35.9 3.57/66.3 3.47/69.7 3.36/69.3 3.17/38.4 5.92/113.6	164.3

Table 10: ^1H NMR (650 MHz, $\text{DMSO-}d_6$, 298 K) and ^{13}C -NMR (650 MHz, $\text{DMSO-}d_6$, 298 K) of **4-13**

Short PEG – Octreotide (4-13) assignment towards Phe					
Residue	Proton/Carbon Chemical Shift (ppm)				Amid C
	NH	C^αH	C^βH	others	
D-Phe 1	-	3.41/56.0	2.53+2.95/40.9	138.7 7.20/129.4 7.25/128.1 7.12/126.1	174.4
Cys 2	-	4.67/51.2	2.98+3.18/36.3	-	168.9
Phe 3	8.14/114.6	4.62/53.8	2.70+2.81/37.9	137.2 7.01/129.2 7.13/128.0 7.17/126.2	170.5
D-Trp 4	8.57/122.2 (Indol) 10.92/130.3	4.37/54.4	2.82+3.04/27.3	109.7 7.06/123.7 136.2 7.33/111.4 7.07/120.9 6.98/118.3 7.54/118.3 127.1	171.6
Lys 5	8.24/118.6	4.15/52.9	1.42+1.62/31.2	1.03/22.0 (γ) 1.32/29.5 (δ) 2.55/39.9 (ϵ)	171.7
Thr 6	7.73/108.7	4.16/58.6	3.98/66.3	1.01/19.7	169.7
Cys 7	8.36/119.1	4.61/52.8	3.16/39.7	-	169.4
Thr(ol) 8	7.47/113.8	3.62/56.0	3.86/64.1	1.00/19.9 3.33+3.47/60.3	-
Short PEGamid-	7.92			1.38/27.8 79.8 170.5 2.40/35.9 3.57/66.3 3.47/69.7 3.40/69.2 3.22/38.5 6.20/119.6	164.2

Schematic overview of the following HMBC and ROESY spectra, which clearly proof that the interaction of the linker takes place at the two cysteine thiols forming two new thiol-ether bonds.

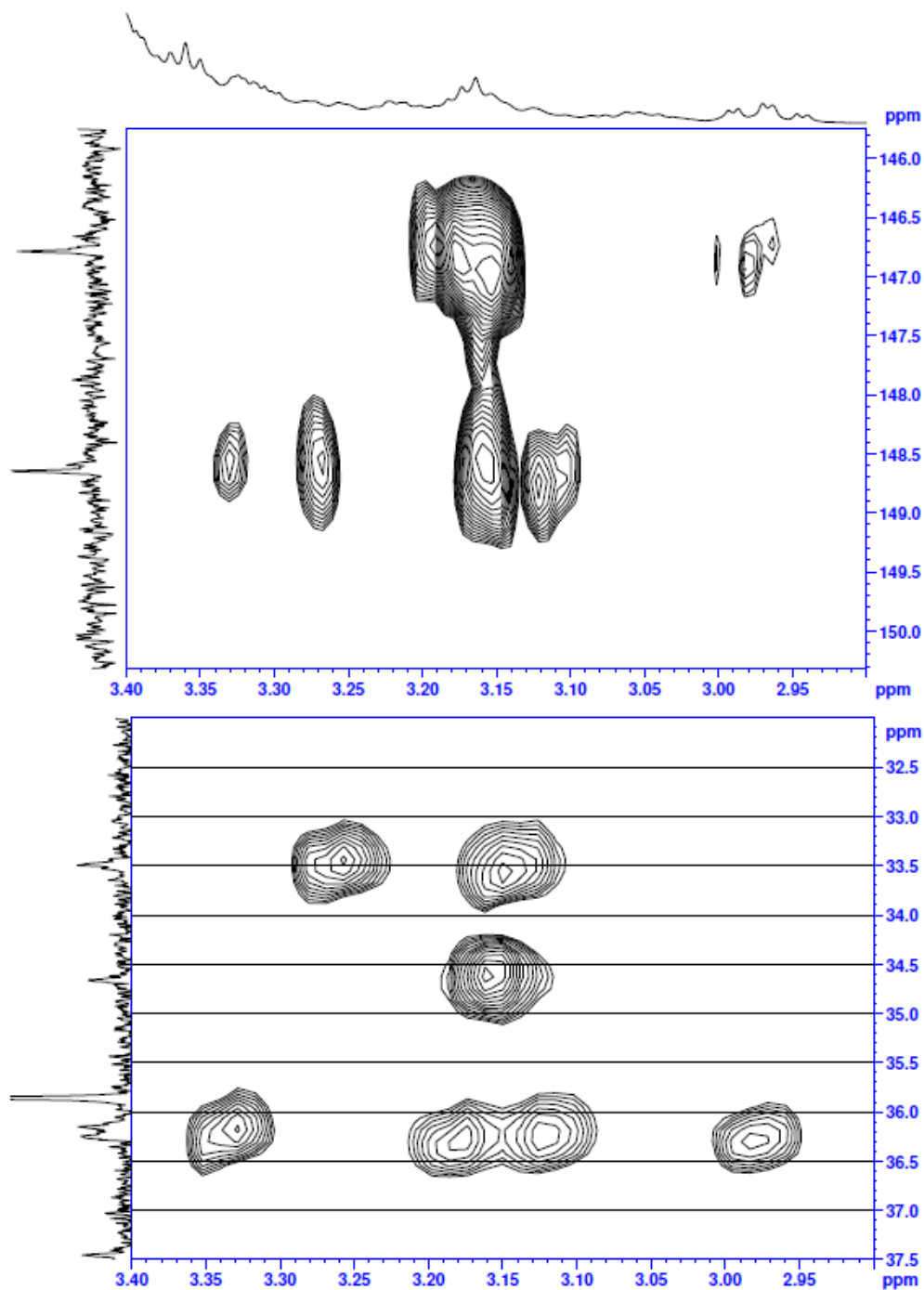


Figure 78: Part of the HMBC spectrum (top) showing ^1H - ^{13}C long range correlations to the olefinic carbon and GSQC spectrum (bottom) showing the methylene groups of the cysteines of the shortPEG-octreotide-conjugate **4-13**

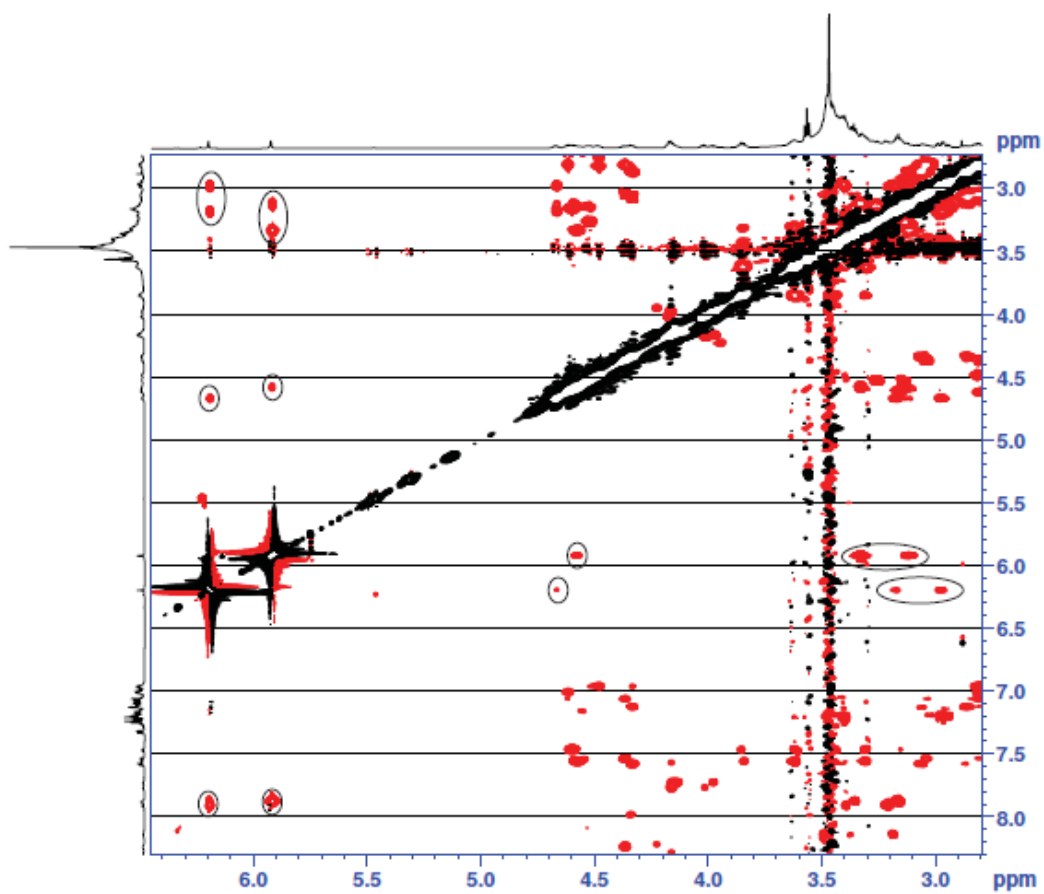
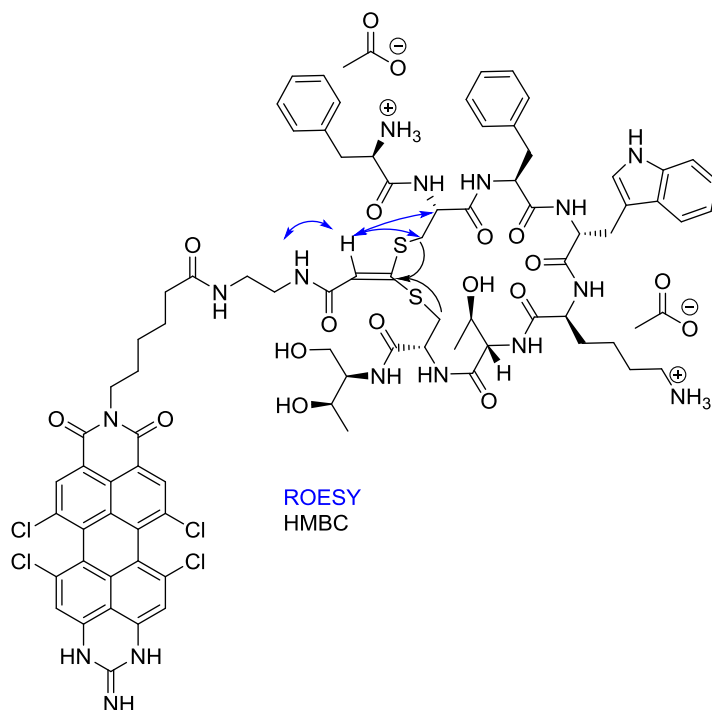


Figure 79: Part of the ROESY spectrum of **4-13** (crosspeaks between olefinic protons and cysteines as well as amide protons marked)

Appendix 5 (4-21)

HMBC and ROESY key relations for PMI – Octreotide (4-21) towards **Phe**



HMBC and ROESY key relations for PMI – Octreotide (4-21) towards **Thr**

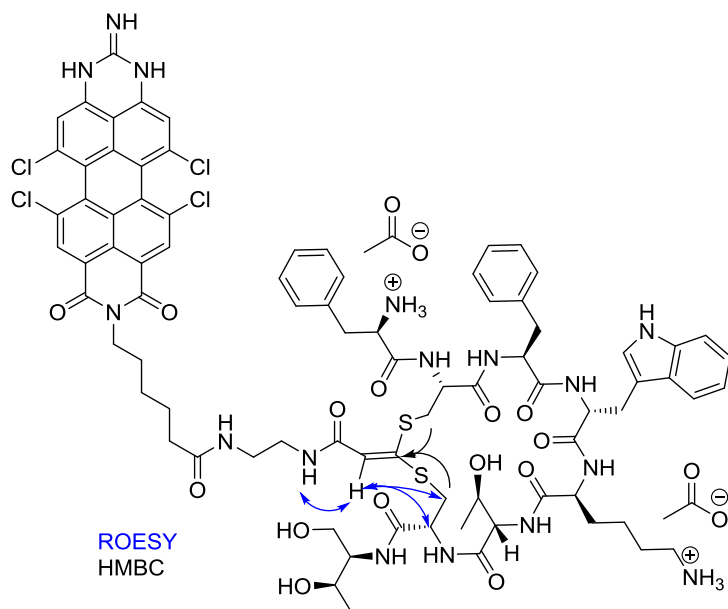


Table 11: ¹H NMR (650 MHz, DMSO-*d*₆, 298 K) and ¹³C-NMR (650 MHz, DMSO-*d*₆, 298 K) of 4-21

PMI – Octreotide (4-21) assignment towards Phe					
	Proton/Carbon Chemical Shift (ppm)				
Residue	NH	C ^α H	C ^β H	others	Amid C
D-Phe 1	-	3.43/56.0	2.54+2.96/40.8	138.6 7.19/129.4 7.23/128.2 7.15/126.2	174.4
Cys 2	-	4.67/51.3	3.20+2.99/36.4	-	168.9
Phe 3	8.30/118.9	4.60/53.9	2.70+2.80/37.4	137.2 6.99/129.2 7.10/128.1 7.11/126.3	170.6
D-Trp 4	8.59/122.3 Indol 10.87/130.0	4.36/54.4	2.82+3.07/27.1	109.7 7.12/123.8 136.2 7.32/111.4 7.07/121.0 6.99/118.3 7.53/118.4 127.1	171.6
Lys 5	8.18/118.4	4.18/52.7	1.42+1.66/31.0	1.03/21.9 (γ) 1.42/26.9 (δ) 2.65/38.8 (ε)	171.6
Thr 6	7.71/109.1	4.17/58.7	3.98/66.3	1.02/19.7	169.8
Cys 7	8.31	4.65/52.88	3.16/34.9	-	169.4
Thr(ol) 8	7.47/113.7	3.63/56.1	3.86/64.2	0.99/20.1 3.63/56.1 3.32+3.46/60.4	-
PMI-linker-amid-				PMI: 219.1 (NH) 163.1 (out) 6.61/82.3 (NH) 155.9 (out) 7.14/117.9 138.3 (Cl) 110.9 (in) 131.6 (in) 110.6 (out) 110.9 (out) 130.4 (Cl) 132.0 (in) 8.17/129.9 122.2 (out) 126.2 (in) 162.3 (=O)	Linker: 4.08/39.5 1.62/27.5 1.31/26.4 1.54/25.1 2.07/35.4 172.5 (=O) 7.88/112.6 (NH) 3.11/38.3 3.11/38.5 7.93/114.7 (NH) 164.4 (=O) 6.17/120.4 146.6

Table 12: ¹H NMR (650 MHz, DMSO-*d*₆, 298 K) and ¹³C-NMR (650 MHz, DMSO-*d*₆, 298 K) of 4-21

PMI – Octreotide (4-21) assignment towards Thr-ol					
Residue	Proton/Carbon Chemical Shift (ppm)				Amid C
	NH	C ^α H	C ^β H	others	
D-Phe 1	-	3.43/56.0	2.52+2.99/40.8	138.6 7.19/129.4 7.23/128.2 7.15/126.2	174.7
Cys 2	-	4.52/51.7	3.18+3.27/33.5	-	169.8
Phe 3	8.13/115.9	4.44/54.4	2.77+2.85/37.2	137.4 6.96/129.3 7.09/128.1 7.11/126.3	170.7
D-Trp 4	8.49/120.9 Indol 10.89+10.90/130.4	4.32	2.89+3.08/27.1	109.9 7.07/123.8 136.2 7.33/111.4 7.07/121.0 7.01/118.3 7.57/118.3 127.1	171.9
Lys 5	8.25/118.0	4.21/52.8	1.48+1.66/31.9	1.11/22.0 (γ) 1.42/26.9 (δ) 2.65/38.8 (ε)	171.8
Thr 6	7.74/109.1	4.15/59.1	3.99/66.1	1.05/19.6	170.0
Cys 7	8.34/118.2	4.64/51.4	3.09+3.32/36.2	-	169.4
Thr(ol) 8	7.50/112.5	3.63/56.1	3.86/64.2	0.99/20.0 3.63/56.1 3.32+3.46/60.4	-
PMI-linker-amid-				PMI: 219.1 (NH) 163.1 (out) 6.61/82.3 (NH) 155.9 (out) 7.14/117.9 138.3 (Cl) 110.9 (in) 131.6 (in) 110.6 (out) 110.9 (out) 130.4 (Cl) 132.0 (in) 8.17/129.9 122.2 (out) 126.2 (in) 162.3 (=O)	Linker: 4.08/39.5 1.62/27.5 1.31/26.4 1.54/25.1 2.07/35.4 172.4 (=O) 7.85/112.7 (NH) 3.06/38.5 3.06/38.3 7.89/112.6 (NH) 164.4 (=O) 5.89/114.1 148.6

Schematic overview of the following ROESY and HMBC spectra, which clearly proof that the interaction of the linker takes place at the two cysteine thiols forming to new thiol-ether bonds.

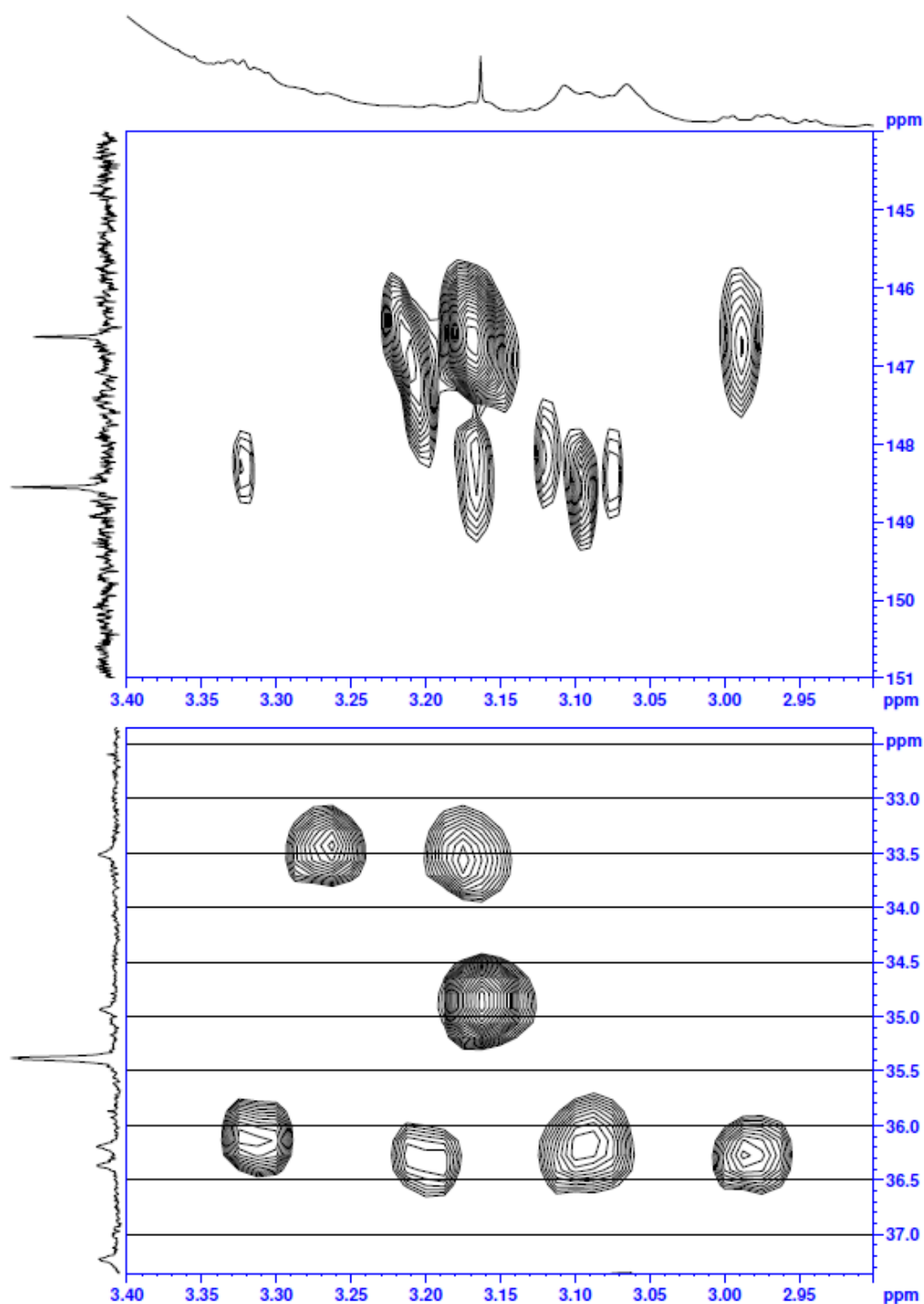


Figure 80: Part of the HMBC spectrum (top) showing ^1H - ^{13}C long range correlations to the olefinic carbon and GSQC spectrum (bottom) showing the methylene groups of the cysteines of the dye-octreotide-conjugate **4-21**

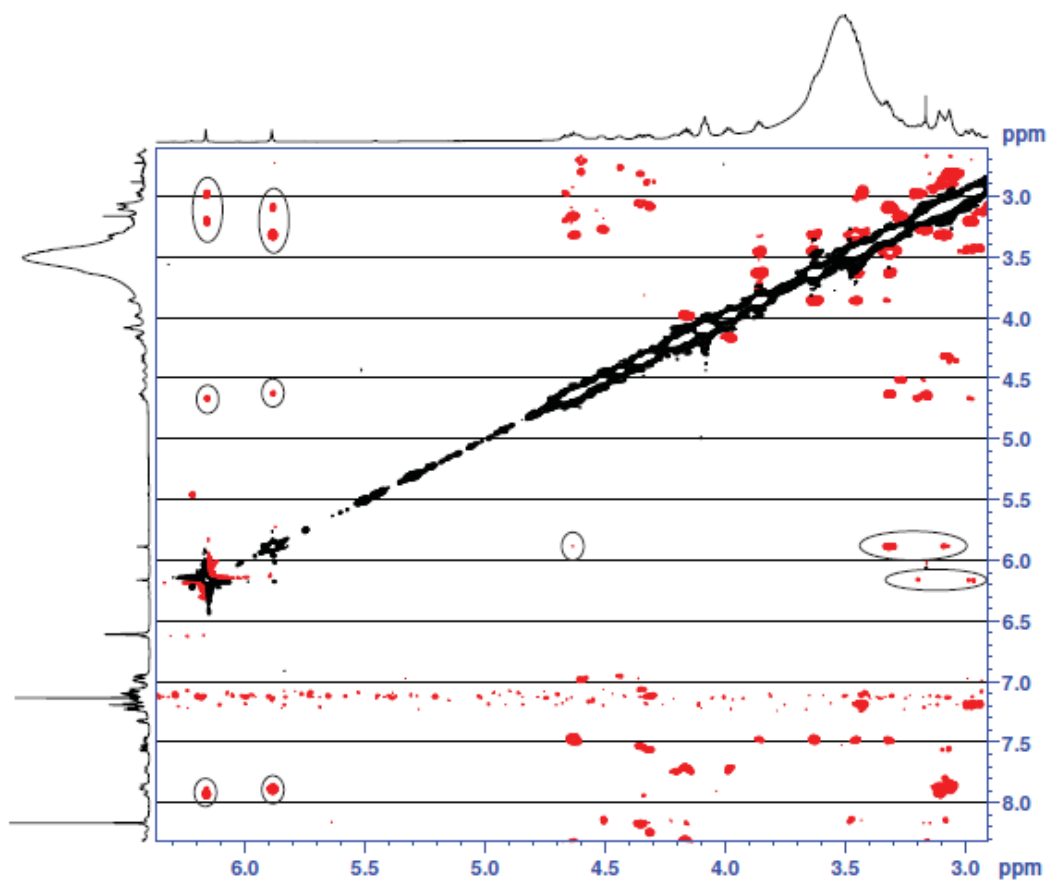


Figure 81: Part of the ROESY spectrum of **4-21** (crosspeaks between olefinic protons and cysteines as well as amide protons marked)

Appendix 6 (4-23)

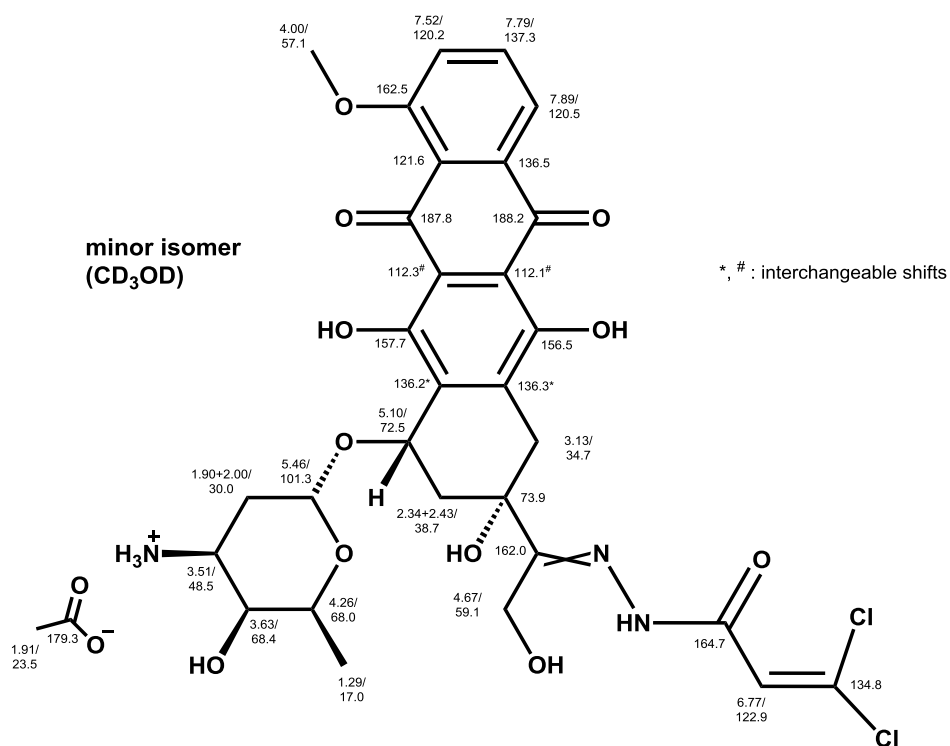
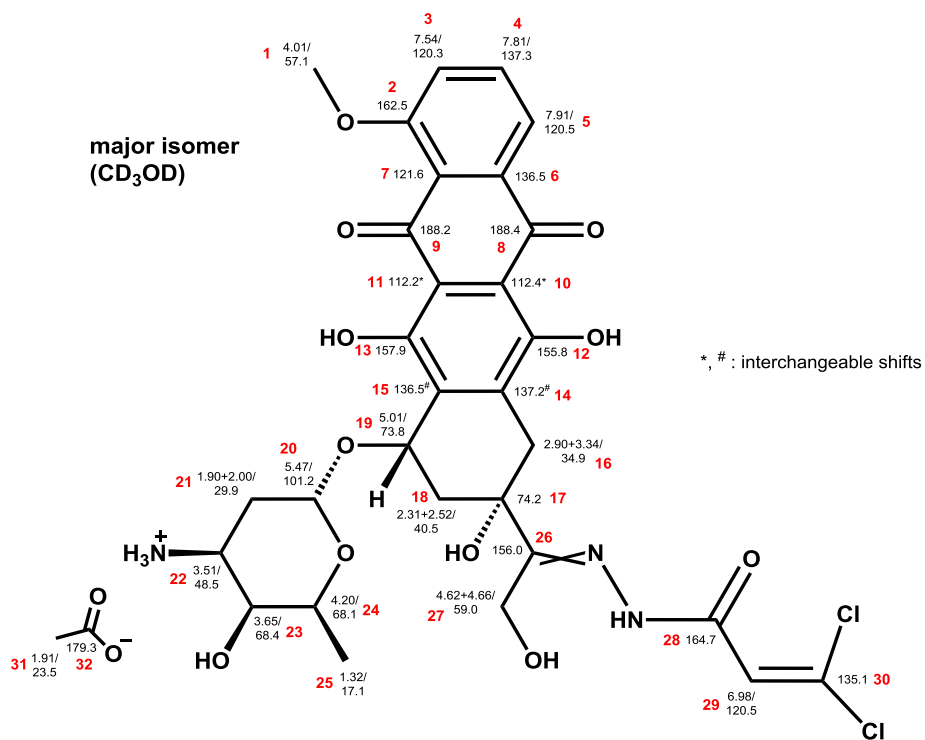


Table 13: ^1H and ^{13}C NMR signal assignment of compound **4-23**, the structure is shown on the following page. The table shows the chemical shifts of the **major isomer** in CD_3OD .

	Chemical shift ^1H (ppm)	Chemical shift ^{13}C (ppm)
Proton (600 MHz)/Carbon Chemical (151 MHz) Shift (ppm)		
1	4.01	57.1
2	-	162.5
3	7.54	120.3
4	7.81	137.3
5	7.91	120.5
6	-	136.5
7	-	121.6
8	-	188.4
9	-	188.2
10	-	112.4
11	-	112.2
12	-	155.8
13	-	157.9
14	-	137.2
15	-	136.5
16	2.90 + 3.34	34.9
17	-	74.2
18	2.31 + 2.52	40.5
19	5.01	73.8
20	5.47	101.2
21	1.90 + 2.00	29.9
22	3.51	48.5
23	3.65	68.4
24	4.20	68.1
25	1.32	17.1
26	-	156.0
27	4.62 + 4.66	59.0
28	-	164.7
29	6.98	120.5
30	-	135.1

Appendix 7

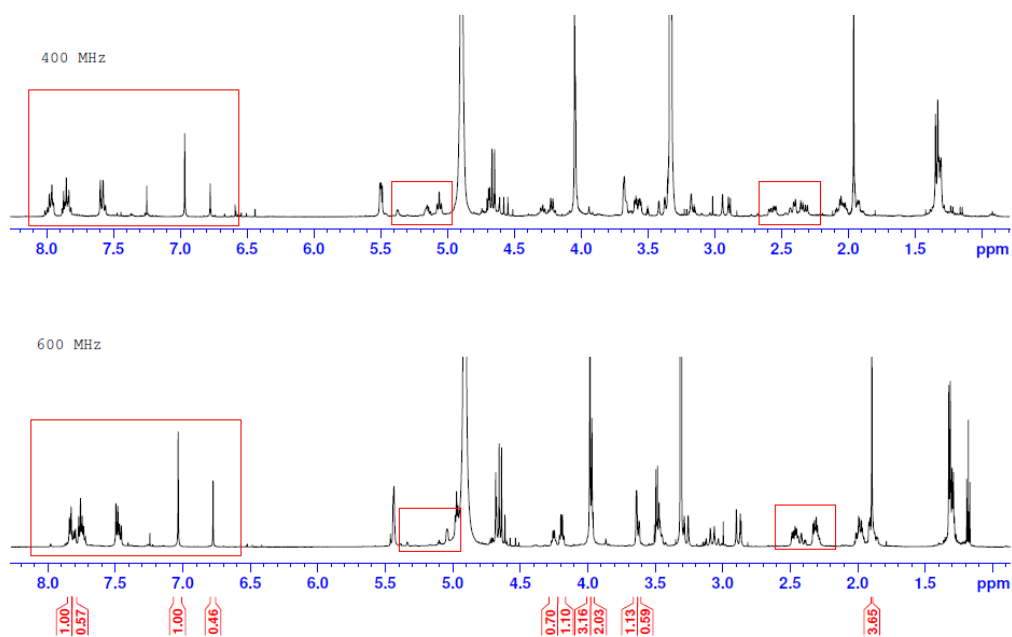


Figure 82: ^1H NMR spectrum of compound **4-23** at 400 MHz as well as 600 MHz in CD_3OD to see peak differences in dependence of the field strength

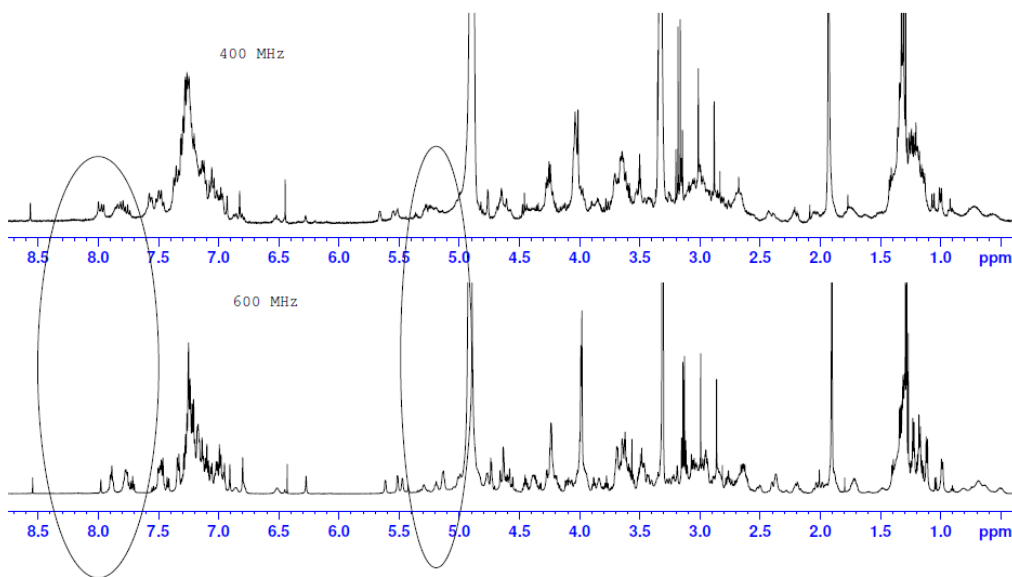


Figure 83: ^1H NMR spectrum of **4-26** at 400 MHz as well as 600 MHz in CD_3OD to see peak differences in dependence of the field strength

As it was not possible to assign all measured signals to the atoms as up to four different isomers can be formed during the reaction, the covalent attachment of doxorubicin and octreotide was also verified by DOSY NMR.

Analysis of three characteristic signals from doxorubicin-part (8.00-7.78 [aromatic protons], 5.67-5.49 [acetalic position] and 4.06-4.00 ppm [methoxy group]) and octreotide-part (7.30-7.22 [phenyls from Phe], 5.31-5.27 [α -protons of Cys] and 0.77-0.65 ppm [γ -protons of Lys]) showed the same diffusion constants $2.735 \times 10^{-10} \text{ m}^2/\text{s}$. These diffusion constants are different from the diffusion constants found for octreotide $3.665 \times 10^{-10} \text{ m}^2/\text{s}$ (7.39-7.23 [phenyls from Phe], 5.31-5.22 [α -protons of Cys] and 0.65-0.51 ppm [γ -protons of Lys]) and doxorubicin-linker $4.182 \times 10^{-10} \text{ m}^2/\text{s}$ (7.96-7.78 [aromatic protons], 5.50-5.46 [acetalic position] and 4.06-4.00 ppm [methoxy group]).

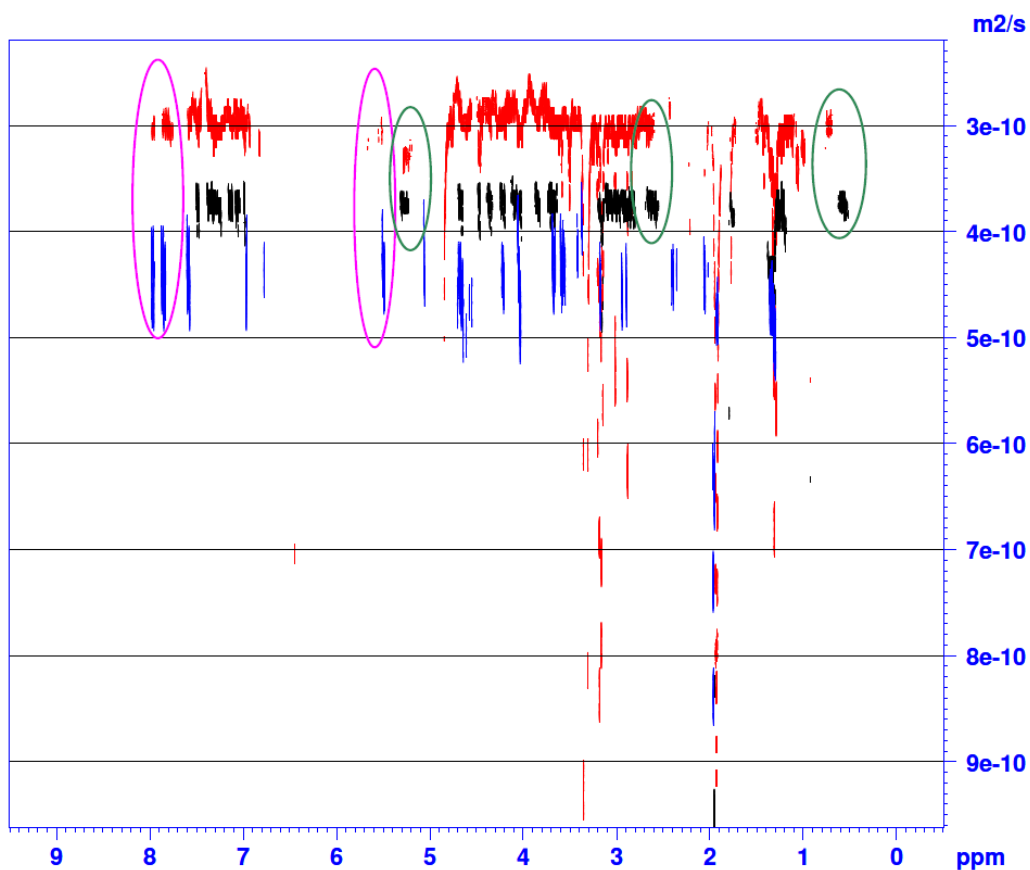
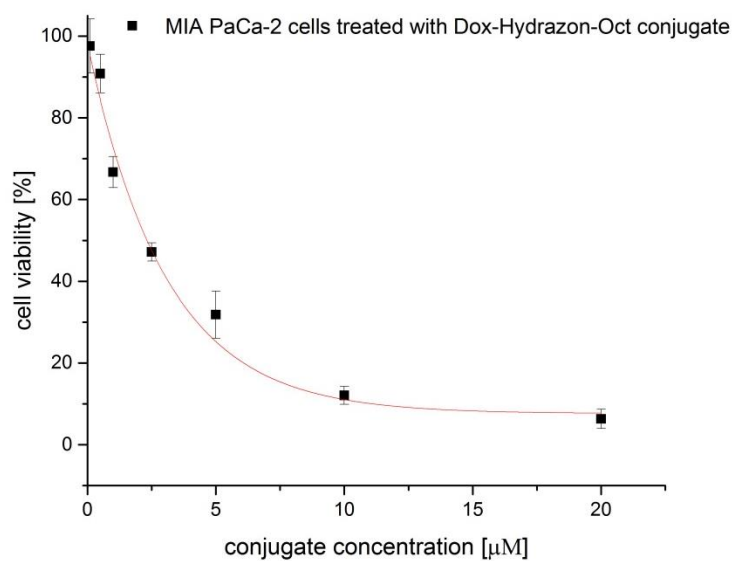


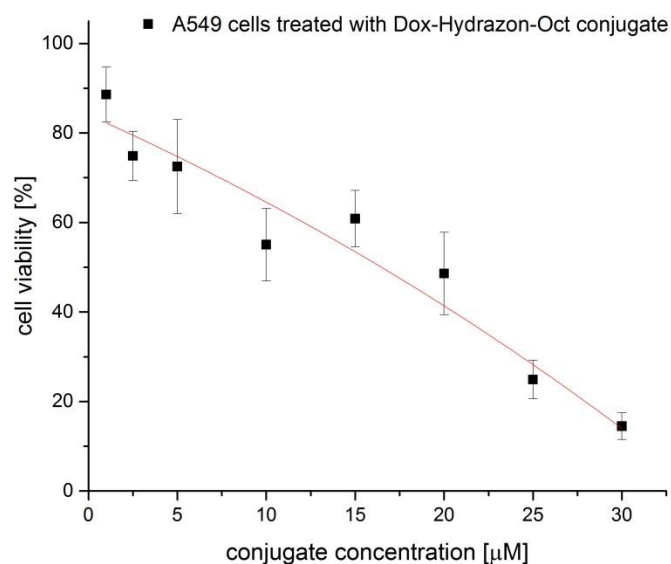
Figure 84: DOSY NMR of **3-26** (blue), **3-24** (black) and **octreotide 3-15** (blue) in CD_3OD

Appendix 8

Cell viability 4-26



A



B

Figure 85: Determination of the antiproliferative activity of the Doxorubicin-Hydrzone-Octreotide hybrid **4-26** with the CellTiter-Glo cell viability assay. **A.** MIA PaCa-2 cells treated with different concentrations of Dox-Hydrzone-Oct conjugate for 72h at 37°C **B.** A549 cells treated with different concentrations of Dox-Hydrzone-Oct conjugate for 72h at 37°C.

Appendix 9

Derivation of the Dissociation Constant Calculation

Based on the work of Seidel, S.A.I., *et al.*, *Microscale thermophoresis quantifies biomolecular interactions under previously challenging conditions*. Methods, 2013. **59**(3): p. 301-315

Calculation of the binding affinity based on the previously described measurements is correspondingly done by use of the Soret coefficient S_T , which determines the steady state concentration change under a temperature difference ΔT and is shown in equation (1). The derivation of this equation from the thermal diffusion coefficients is explained by Seidel *et al.*

$$\frac{c_{hot}}{c_{cold}} = \exp(-S_T * \Delta T) \quad (1)$$

For small temperature and concentration changes as it is the case in MST experiments, the above mentioned equation, which describes the concentration change due to thermophoresis, can be approximated by linearization:

$$\frac{c_{hot}}{c_{cold}} = 1 - \left(S_T - \frac{\delta F}{\delta T} \right) * \Delta T \quad (2)$$

Additionally, the fluorescence depends on the concentration as described in equation (3). The higher the concentration of the fluorophore, the higher is the detected signal.

$$\frac{F_1}{F_0} = \frac{c_{hot}}{c_{cold}} \quad (3)$$

Since relative fluorescence is used to quantify binding via MST, while F_{norm} corresponds to S_t and the concentrations described in equations (2) and (3) can be summarized to equation (4), which also considers the additional fluorescence change due to the fluorophore's temperature dependence $\frac{\delta F}{\delta T}$,

$$F_{norm} = \frac{F_1}{F_0} = \frac{c_{hot}}{c_{cold}} = 1 - \left(S_T - \frac{\delta F}{\delta T} \right) * \Delta T \quad (4)$$

The binding affinity can be quantified by analyzing the change in F_{norm} as a function of the concentration of the titrated binding partner. The bound fraction is described by equation (5) as the thermophoretic movement of bound and unbound state superpose linearly.

$$(5) \quad F_{norm} = (1 - x)F(A)_{norm}(unbound) + xF(AT)_{norm}(bound)$$

With

- F_{norm} : measured fluorescence after subtraction of the fluorescence baseline signal
- $F(A)_{norm}$ as the contribution of the unbound fluorescent molecule A
- $F(AT)_{norm}$ as the contribution of the fluorescent molecule A and its interacting titrant T
- x as the fraction of fluorescent molecules that formed the complex

Finally, the unknown parameter x (fraction of bound molecules), respectively the amount of unbound molecules can be calculated from the normalized fluorescence F_{norm} as shown by Seidel *et al.* F_{norm} is plotted against the concentration of the non-fluorescent molecule, which results in a binding curve with two plateaus. From this curve the dissociation constant can be derived, calculated from the mass of action, which is used a simple model of the binding event (equation 6).

$$K_d = [A] * \frac{[T]}{[AT]} \quad (6)$$

The dissociation constant K_d is the reciprocal value of the affinity constant K_a , which means that low K_d values indicate a strong binding affinity between the tested molecules. In the following chapters the binding affinity will be described by the affinity constants, although plotting and fitting of the intensities against the concentrations results in the automatically calculated dissociation constant K_d .

MST data plotting of doxorubicin and the synthesized conjugates 5-4, 5-11 and 5-17

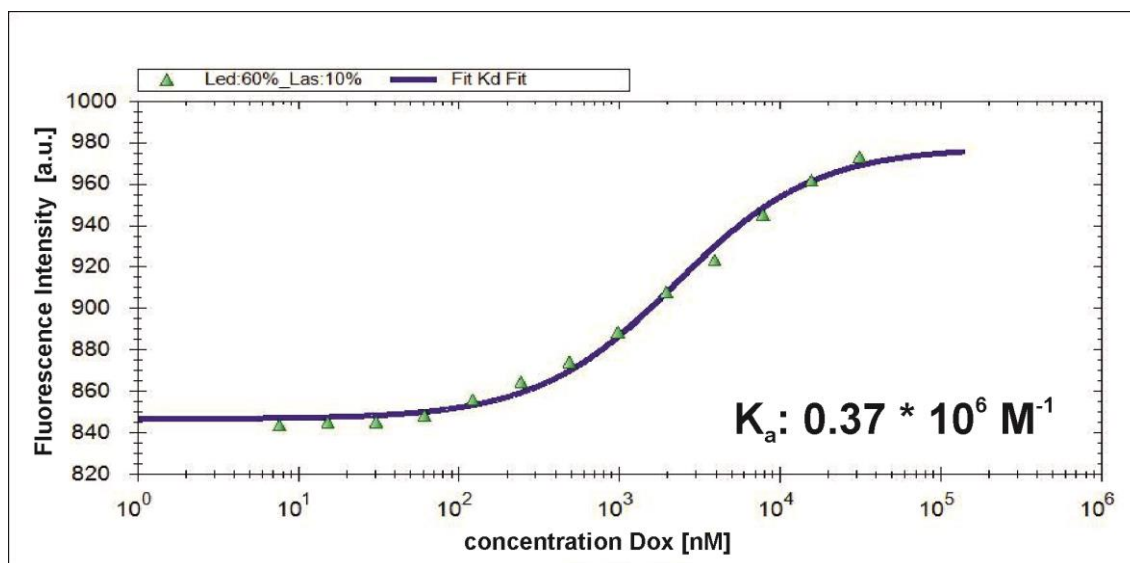


Figure 86: Thermophoresis data doxorubicin: plotting of the measured fluorescence signal against the doxorubicin concentration of each sample prepared ($c(\text{DOX}) = 31250 - 15.26 \text{ nM}$) at a constant concentration of 50 nM Cy5 labelled DNA (12 base pairs) in each sample. Settings used are LED 50% and LAS 10%, Buffer MST, Absorption red – Emission red

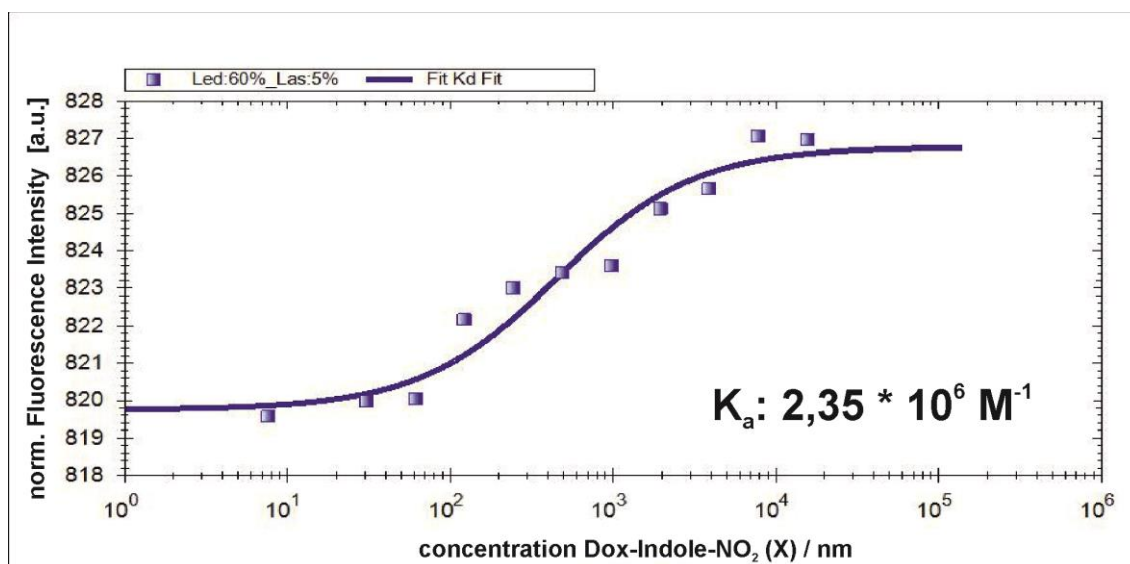


Figure 87: Thermophoresis data of compound 5-4: plotting of the measured fluorescent signal against the doxorubicin-indole NO_2 (5-4) concentration of each sample prepared ($c(\text{5-4}) = 7812.5 - 7.6 \text{ nM}$) at a constant concentration of 50 nM Cy5 labelled DNA (12 base pairs) in each sample. Settings used are LED 60% and LAS 10%, Buffer MST, Absorption red – Emission red

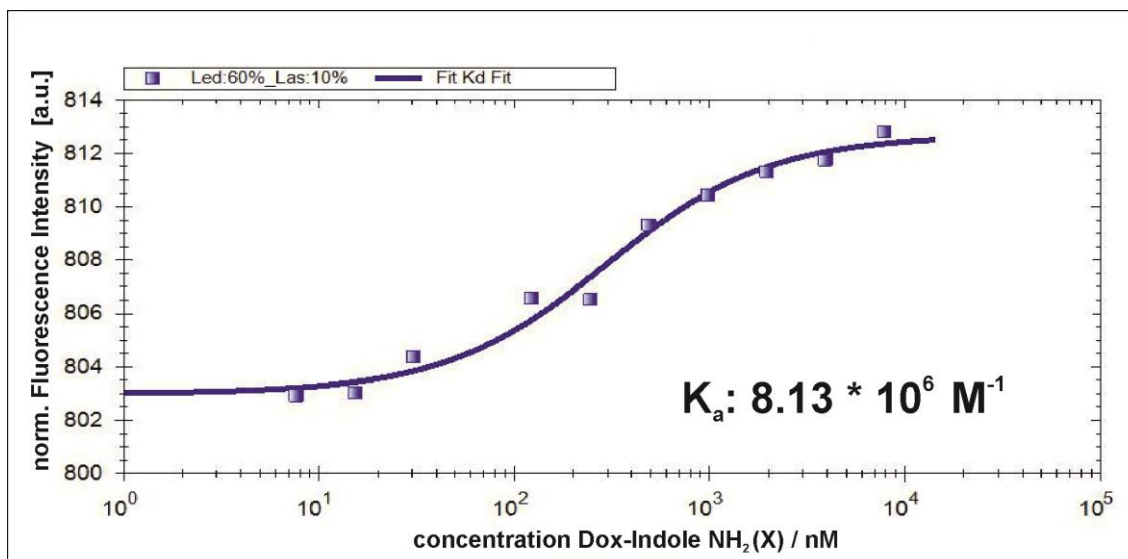


Figure 88: Thermophoresis data of compound **5-11**: plotting of the measured fluorescent signal against the doxorubicin-indole NH₂ (**5-11**) concentration of each sample prepared (c (**5-11**) = 7812.5 – 7.6 nM) at a constant concentration of 50 nM Cy5 labelled DNA (12 base pairs) in each sample. Settings used are LED 60% and LAS 10%, Buffer MST, Absorption red – Emission red

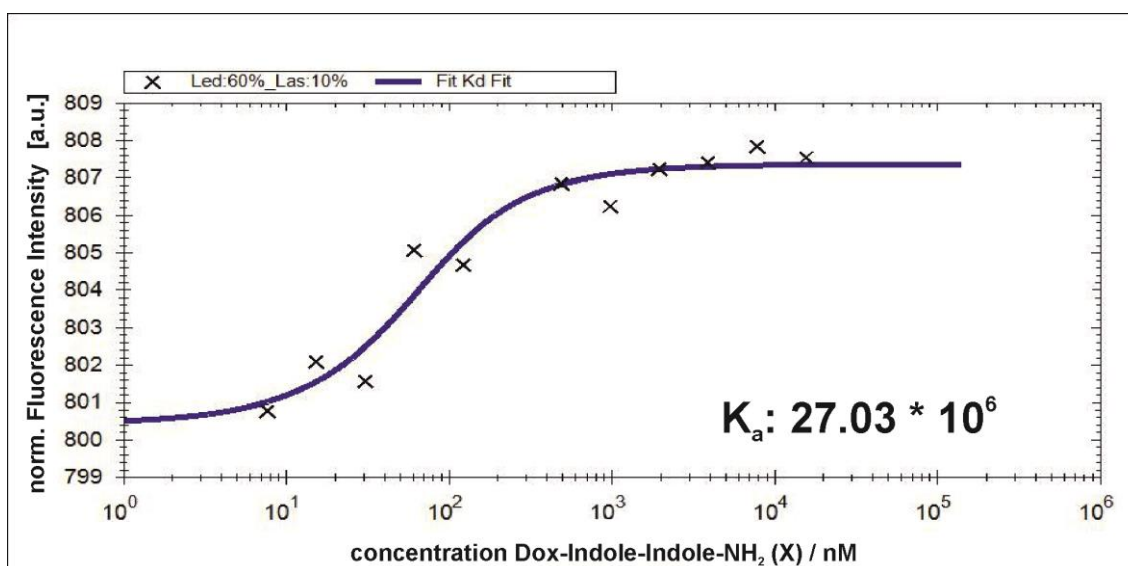


Figure 89: Thermophoresis data compound **5-17**, plotting of the measured fluorescent signal against the doxorubicin-indole-indole NH₂ (**5-17**) concentration of each sample prepared (c (**5-17**) = 7812.5 – 7.6 nM) at a constant concentration of 50 nM Cy5 labelled DNA (12 base pairs) in each sample. Settings used are LED 60% and LAS 10%, Buffer MST, Absorption red – Emission red

Appendix 10

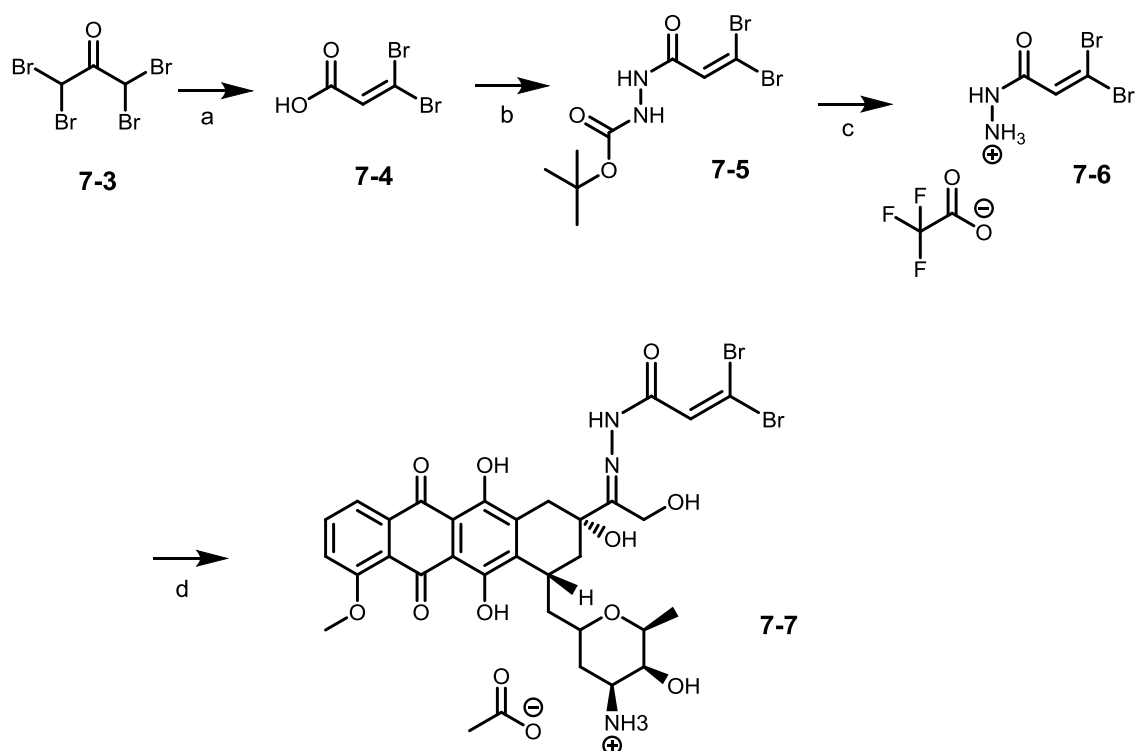


Figure 90: Synthesis of the Dox-dibromo-linker **7-7**. (a) 1,1,3,3-tetrabromoacetone, 10 eq NaHCO₃, MilliQ, argon, r.t., overnight, 60%; b) 1-[Bis(dimethylamino)methylene]-1H-1,2,3-triazolo[4,5-b]pyridinium 3-oxid hexafluorophosphate (1.15 eq), DIPEA (1.3 eq), tert-butyl carbazate (1.1 eq), DMF, argon, 2h, r.t., 46% (c) DCM/TFA (1:1), 1 h, r.t., quantitative yield; (d) doxorubicin hydrochloride, methanol, argon, 24h, r.t., 57%;